NOTE TO USERS

Page(s) missing in number only; text follows. Page(s) were scanned as received.

48, 76, 98, 168, 196

Page(s) not included in the original manuscript and are not available from the author or university. The manuscript was scanned as received.

This reproduction is the best copy available.

A MASS SPECTROMETRIC AND COMPUTATIONAL STUDY OF HYDROGEN TRANSFER REACTIONS IN RADICAL CATIONS

By

MOSCHOULA ANNA TRIKOUPIS, B. Sc.

A Thesis

Submitted to the School of Graduate Studies

In Partial Fulfillment of the Requirements

for the Degree

Doctor of Philosophy

McMaster University

A MASS SPECTROMETRIC AND COMPUTATIONAL STUDY OF HYDROGEN TRANSFER REACTIONS IN RADICAL CATIONS

HYDROGEN TRANSFER REACTIONS IN RADICAL CATIONS : A TANDEM MASS SPECTROMETRY STUDY

For my parents :

Thank You

DOCTOR OF PHILOSOPHY (2001)
(Chemistry)

McMaster University
Hamilton, Ontario

TITLE : A Mass Spectrometric and Computational Study of Hydrogen Transfer Reactions in Radical Cations

AUTHOR : Moschoula Anna Trikoupis (McMaster University)

SUPERVISOR : Dr. Johan K. Terlouw

NUMBER OF PAGES : xvii, 247

ABSTRACT

Hydrogen transfer reactions represent elementary chemical reactions of interest to both chemists and biochemists. In the context of the experimental work presented in this thesis, hydrogen transfers involved in both the unassisted and assisted isomerizations of several organic radical cations have been studied.

The structure characterization and reactivity of the ionic species were realized using a variety of tandem mass spectrometry based techniques. Not only conventional metastable ion (MI), collision-induced dissociation (CID) and neutralization-reionization (NR) were used but also the novel hybrid techniques CID/CID and NR/CID. The use of deuterium labelled isotopomers and quantum chemical calculations formed an essential component in the interpretation of the results.

Two of the simplest forms of hydrogen rearrangements are the 1,2- and 1,3-hydrogen shifts. It is well known that in the gas phase, pyridine radical cations can be readily differentiated from their ylide counterparts. The same holds true for both ionized acetone and acetamide, whose isomerization to their more stable enol counterparts is not observed because of a high energy barrier for the 1,3-hydrogen shift. However, it is shown that all three of these ions can be induced to rearrange into their more stable forms. This occurs through an ion-molecule interaction with an appropriate base molecule, under conditions of chemical ionization. For pyridine and acetone radical cations, the initially formed [pyridine$^{\bullet+}$•••base] and [acetone$^{\bullet+}$•••base] adduct ions isomerize by way of proton-transport catalysis to the stable complexes [α-pyridyl$^{\bullet+}$•••base] and [enol of acetone$^{\bullet+}$•••base] en route to their dissociation. However, multiple collision and deuterium labelling experiments on the [acetamide$^{\bullet+}$•••base] complex ion, indicate that unlike ionized acetone, which enolizes via a base catalyzed 1,3-proton shift, a different mechanism is operative in the acetamide system. *Ab initio* and density functional theory calculations support the experimental findings and reveal that this differing mechansim for ionized acetamide, can best be described as a consecutive $H^+/H^\bullet$ transfer between the substrate and base partners of the encounter complex.

Hydrogen transfer reactions also form the key pathway to the unimolecular dissociations of ionized dimethyl oxalate (DMO) and a series of ionized pentenyl methyl ethers. Prior to the expulsion of CO, ionized DMO undergoes intramolecular hydrogen bridging and subsequent C-C cleavage to generate the hydrogen bridged radical cation CH_2=O•••H•••O=C-$OCH_3^{\bullet+}$. Using the experimental results of vacuum ultraviolet photoionization and tandem mass spectrometry based experiments it is also shown that the measured appearance energy (AE) for the generation of the methoxycarbonyl cation, CH_3O-C=O^+ (10.5 eV), is not compatible with a simple bond cleavage involving the cogeneration of the radical CH_3O-C=O$^\bullet$. Collision-induced dissociative ionization experiments show that a consecutive two-step dissociation of low energy DMO ions into CO_2 and $CH_3^\bullet$, without the intermediacy of CH_3O-C=O$^\bullet$ occurs.

The dissociation chemistry of the low-energy $C_5H_9OCH_3^{\bullet+}$ ions generated from thirteen isomeric pentenyl methyl ethers derived from stable alkenols, was examined using metastable ion mass spectrometry characteristics. The experiments indicate that there is an influence of the position and substitution pattern of the double bond on the chemistry of ionic species. The closely similar reactions of C_2H_5CH=$CHCH_2OCH_3^{\bullet+}$, CH_2=$CHCH(CH_5)OCH_3^{\bullet+}$, and $CH_2CH(C_2H_5)CH_2OCH_3^{\bullet+}$ point to a common chemistry, which is rationalized in terms of facile 1,2-H and 1,2-C_2H_5 shifts via distonic ions. Each of the other isomers displays a distinct, though often related chemistry. These three ionic isomers also readily expel $C_2H_5^\bullet$ to give $C_4H_7^+$ ions of structure CH_2=CH-C^+(H)OCH_3. Elimination of CH_3OH is also significant for these ions and for $(CH_3)_2$C=$CHCH_2OCH_3^{\bullet+}$ and CH_3CH=$C(CH_3)CH_2OCH_3^{\bullet+}$.

In addition to the involvement of hydrogen transfers in dissociation reactions, additional ionic systems were studied. These studies involved the characterization of a number of H-shift isomers of the hydroxpyridines and pyridine N-oxide, the characterization of the isomeric dicoordinated borinium ions CH_3O-B-H^+ and CH_3-B-OH^+ and the iminothisulfine ion H-N≡C-S-$S^{\bullet+}$. Experiment and theory agree that each of the ions in these studies are stable species in the gas phase, however, much of the interesting chemistry lies with the isomerization and dissociation chemistry of some of the neutrals.

The final component of this work deals with the heat of formation of sulfine, CH_2=S=O. The value -30 ± 6 kJ/mol has been assigned to $\Delta H_f(CH_2=S=O)$, as determined by calculations at the CBS-QB3 level of theory. The derived value lies midway between two previously calculated values -9 ± 14 and -52 ± 10 kJ/mol. Our recommended value is evaluated against experimental observables, such as the measured proton affinity of sulfine and the appearance energy of $CH_2=S^+$-OH from dimethyl sulfoxide ions.

PREFACE

The larger part of this thesis describes the results obtained by the author during four years of experimental and computational research in gas phase ion chemistry. This field is ideally suited to the investigation by both experimental and theoretical methodologies. Indeed, the common set of conditions involved in mass spectrometric experiments and computational chemistry, i.e. the study of isolated particles, makes the two approaches complementary. Such investigations necessitate the collaboration of both experimental and theoretical chemists. Collaborative contributions from, Prof. Richard D. Bowen (Chapter 11), Prof. Chava Lifshitz (Chapter 6), Dr Pascal Gerbaux (Chapter 7), Prof. Robert Flammang (Chapter 7) and Dr Srinivas (Chapter 8 and 9) are greatly appreciated. The synthetic contributions of Mr. Simon Mandeville (Chapter 11) are also greatly appreciated. Finally, two individuals deserve special mention in the context of collaboration: Dr. Peter C. Burgers (Chapters 2 -6 and 10) and Prof. Paul J.A. Ruttink (Chapters 3-5 and 10). Their computational contributions, insights, suggestions and critical evaluations have significantly shaped the way that the results have been presented.

The permission of the American Chemical Society, Elsevier Science, the European Journal of Mass Spectrometry, and the Royal Chemical Society Publication Division to reproduce the data and text which has previously been published is also appreciated.

LIST OF PUBLICATIONS

1. M.A. Trikoupis, P.C. Burgers, P.J.A. Ruttink, J.K. Terlouw, Int. J. Mass Spectrom. (P. Longevialle Issue), in press.
Self-catalysis in the gas-phase: enolization of the acetone radical cation.

2. M.A. Trikoupis, P. Gerbaux, D.J. Lavorato, R. Flammang, J.K. Terlouw, Int. J. Mass Spectrom (P. Longevialle Issue), in press.
Hydrogen-shift isomers of ionic and neutral hydroxypyridines : a combined experimental and computational investigation

3. R.D. Bowen, M.A. Trikoupis, J.K. Terlouw, Eur. Mass Spectrom. in press.
Dissociation Reactions of Low-Energy Pentenyl Methyl Ether Radical Cations $C_5H_9OCH_3^{\bullet+}$

4. M.A. Trikoupis, P.C. Burgers, P.J.A. Ruttink, J.K. Terlouw, Int. J. Mass Spectrom. (Nico Nibbering Issue) (2001), *210/211*, 489.
The Benzonitrile Assisted Enolization of the Acetone and Acetamide Radical Cations : Proton-Transport Catalysis versus an Intermolecular $H^{+/\bullet}$ Transfer Mechanism.

5. P.J.A. Ruttink, P.C. Burgers, M.A. Trikoupis, J.K. Terlouw, Chem. Phys. Lett. (2001), *342*, 447.
The Heat of Formation of Sulfine, $CH_2=S=O$, revisited : a CBS-QB3 study.

6. R.D. Bowen, S. J. Mandeville, M.A. Trikoupis, J.K. Terlouw, Int. J. Mass Spectrom. (Nico Nibbering Issue) (2001), *210/211*, 489.
Dissociation Reactions of $CH_2=CHCH_2CH_2CH_2OCH_3^{\bullet+}$, Ionised Methyl Pent-4-enyl Ether.

7. S. Vivekananda, P. Raghunath, K. Bhanuprakash, R.Srinivas, M.A. Trikoupis, J.K. Terlouw, Chem. Phys. Lett. (2000), *332*, 251.
Characterization of Iminothiosulfine-type Ions $[HNCS_2]^{\bullet+/\bullet}$ and their Neutral Counterparts by Mass Spectrometry and Computational Chemistry.

8. R. Srinivas, S. Vivekanada, S.J. Blanksby, D. Schroder, M.A. Trikoupis, J.K. Terlouw, H. Schwarz, Int. J. Mass Spectrom. (2000), *202*, 315-322.
Generation and Characterization of Ionic and Neutral $(CH_3OBH)^{+/\bullet}$ and $(CH_3BOH)^{+/\bullet}$ in the Gas Phase by Tandem Mass Spectrometry.

9. S.J. Mandeville, R.D. Bowen, M.A. Trikoupis and J.K. Terlouw, Int. J. Mass Spectrom. (2000), *199*, 189-200.
The Effect of Variations of the Size and Structure of the Principal Alkyl Group on Alkene Elimination from the Immonium Ions $CH_3CH_2CH=N^+(CH_3)R$, $CH_3CH_2CH_2CH=N^+(CH_3)R$ and $CH_3CH_2CH_2CH_2CH=N^+(CH_3)R$.

10. L.M. Fell, P.J.A. Ruttink, P.C. Burgers, M.A. Trikoupis and J.K. Terlouw, Int. J. Mass Spectrom. (2000), *195/196*, 85-99.
The Dissociation Chemistry of the Hydrogen-Bridged Radical Cation [CH_2=O•••H•••O=C-OCH_3]$^{\bullet+}$: Proton Transport Catalysis and Charge Transfer.

11. M.A. Trikoupis, P.C. Burgers, P.J.A. Ruttink and J.K. Terlouw, Eur. Mass Spectrom. (1999), *5*, 431-439.
Lowering Large 1,2-H Shift Barriers by Proton-Transport Catalysis : The Challenging Case of the Pyridine Radical Cation.

12. S.J. Mandeville, R.D. Bowen, M.A. Trikoupis and J.K. Terlouw, Eur. Mass Spectrom. (1999), *5*, 339-351.
The Influence of the Size and Structure of a Spectator Alkyl Group on the Relative Rates of Competing Alkyl Radical Elimination from Ionised Tertiary Amines.

13. S.J. Mandeville, R.D. Bowen, M.A. Trikoupis and J.K. Terlouw, Chem. Comm. (1999), 2111-2112.
Water and Hydrogen Elimination From Ionised n-Propanol : Extraordinarily Large Kinetic Isotope Effects.

14. M.A. Trikoupis, J.K. Terlouw, P.C. Burgers, M.Peres and C. Lifshitz, J. Am. Soc. Mass Spectrom. (1999), *10*, 869-877.
How do Dimethyl Oxalate Ions Break in Half ? Loss of $CH_3^{\bullet}$ + CO_2 versus CH_3O-C=O$^{\bullet}$.

15. M.A. Trikoupis, P.C. Burgers and J.K. Terlouw, J. Am. Chem. Soc. (1998), *120*, 12131-12132.
Enolization of Gaseous Acetone Radical Cations: Catalysis by a Single Base Molecule.

ACKNOWLEDGMENTS

Many people have been a part of my graduate education, as teachers, colleagues and friends. Prof. Terlouw, first and foremost, is the best advisor and most enthusiastic teacher I could have wished for. He is actively involved in the work of all his students and always has their best interest in mind. Time after time, his easy grasp of chemistry, physics and mass spectrometry, at their most fundamental level, helped me in the struggle for my own understanding. Prof. Terlouw, thank you for believing in me !

I would also like to thank the members of my supervisory committee, Prof. John Brennan, and Prof. Brian McCarry, for their support, inspiration and positive outlook during my studies.

Many thanks are also extended to Dr. Peter Burgers and Prof. Paul Ruttink who have not only been of great help with my studies but who also did not hesitate to invite me into their homes during our trips to Europe. I appreciate their kindness immensely.

In my office in ABB, I was surrounded by my many knowledgeable and friendly people. My officemates Dave Lavorato, Tadek Olech, Kirk Green, Lorne Fell, Leah Allen, Suzanne Ackloo, Lisa Heydorn and George Timmins have been great sources of practical information and our late Friday afternoon discussions were always enjoyable.

I have been lucky to have the support of many good friends: Patti Rachiotis, Dalia Benjamin, Nada Reginato and Nadine Merkley. The members of the Death Machine and Power made the ultimate frisbee and soccer seasons not only great sources of relaxation but a lot of fun as well.

Most of all, I would like to thank those closest to me, whose presence helped make the completion of my graduate work possible ! I am thankful to Kris, my fiancé, and my future in-laws Jon, Lorna and George for their love and support. Special gratitude is devoted to my sister Evdoxia and my brother Nick, and especially my parents, Sousana and Ioannis, for their absolute confidence in me and their love and support. They have always encouraged me and guided me to independence, never trying to limit my aspirations.

TABLE OF CONTENTS

LIST OF FIGURES

LIST OF ABBREVIATIONS

AE	=	appearance energy
B	=	magnetic sector
B3LYP	=	hybrid Hartree-Fock/density functional theory
CA	=	collisional activation
CCSD(T)	=	coupled cluster singles doubles and triples
CE	=	charge exchange
CI	=	chemical ionization
CID	=	collision-induced dissociation
CIDI	=	collision-induced dissociative ionization
CP	=	cyclopropane
CR	=	charge reversal
CS	=	charge-stripping
CBS-QB3	=	DFT theoretical method
DFT	=	density functional theory
EI	=	electron ionization
ESA	=	electrostatic analyzer
eV	=	electron Volt (1 eV=23.061 kcal/mol or 96.487 kJ/mol)
ffr	=	field-free region
G2	=	Gaussian-2 theoretical method
ΔHf	=	enthalpy of formation
HF	=	Hartree-Fock
IE	=	ionization energy
KER	=	kinetic energy release
MI	=	metastable ion
MO	=	molecular orbital
MP	=	Moller-Plesset(perturbation theory)
MS	=	mass spectrometry
NDMA	=	N,N-dimethylaniline
m/z	=	mass to charge ration
NR(MS)	=	neutralization-reionization(mass spectrometry)
PA	=	proton affinity
q	=	charge
r,R	=	radius
SCF	=	self-consistent field
T	=	kinetic energy release (value)
TPEPICO	=	threshold photoelectron photoion coincidence
TS	=	transition state
ZAB-R	=	BEE three-sector mass spectrometer
ZPVE	=	zero-point vibrational energy

Chapter 1

1.1 Introduction, scope of this thesis

This thesis deals with studies in the field of gas-phase ion chemistry using a tandem magnetic deflection type mass spectrometer and computational chemistry as the major tools to probe the structure and reactivity of organic ions.

The studies focus on the chemistry of radical cations, that is the species $M^{\bullet+}$ obtained by ionization, with electrons or photons, of organic molecules M in the dilute gas-phase of the mass spectrometer. Such radical cations may have several stable isomers of unconventional structure, that is ions whose neutral counterpart is either very weakly bound or else represents an unstable molecule of only transient existence. These include distonic ions, ion-dipole complexes and the structurally related class of hydrogen-bridged radical cations. It is the key role that such ions (may) play in the chemistry of radical cations of conventional structure that forms the unifying theme of this thesis.

In this context, an important question of general interest concerns the role of a concept coined "proton-transport catalysis" in the encounter complex of a radical cation with a neutral molecule. This intriguing topic, which is briefly introduced in Section 1.4, is studied in Chapters 2-5.

The available methodology is not confined to the study of ionic species but can also be advantageously used to study elusive neutral species, as is illustrated by the short studies described in Chapters 8-10.

The results of the studies described in Chapters 2-11 of this thesis have all been reported in the scientific literature. Most of the work involves international collaborative research with various research groups. This mutually beneficial arrangement made it possible to address problems whose solution required complementary experimental and theoretical information - and expert intellectual input ! - from techniques and methodologies that are not available in our research group. However, the lion's share of the measurements of the

projects described in this thesis were performed (and interpreted) by the author using the "gas-phase ion and neutral chemistry laboratory" provided by the ZAB-R instrument at McMaster University. In addition, a significant part of the computational chemistry was also performed by the author, under the expert guidance of Prof. P.J.A. Ruttink, on the domestic computers.

To provide the non-expert reader of this thesis with some background information to the "research" Chapters, the following three topics will be briefly introduced and discussed. First, in Section 1.2, a brief overview will be given of the development of the mass spectrometer with the focus on the "gas-phase ion chemistry laboratory" of this study, the magnetic deflection type ZAB-R mass spectrometer. The field of mass spectrometry has grown spectacularly over the past decades and nowadays the term mass spectrometer clearly requires some further clarification and description: there is a bewildering array of conceptually quite different types of instruments on the market whose only common denominator is the separation of ion masses.

In the next Section, 1.3, the various experimental techniques used in this thesis will be briefly explained together with an even more concise description of the computational tools that have been used.

Finally, in Section 1.4, a brief introduction will be presented on radical cations of unconventional structure and their relationship to proton-transport catalysis.

1.2 The development of the mass spectrometer : from physics to physical chemistry to analytical chemistry

The development of mass spectrometry, or mass spectroscopy as it was originally called, can be traced back to the discovery by Goldstein (1886) of positive rays in a low-pressure electrical discharge tube. He observed, while using a perforated cathode, luminous streamers passing through the perforations or 'canals' into the space behind the cathode. He attributed this luminosity to rays of some sort which he called 'Kanalstrahlen'. These canal rays were subsequently deflected by Wien in magnetic and electric fields, and were shown thereby to be positively-charged particles.

J.J. Thomson (1897) had meanwhile demonstrated the existence of electrons, and had shown that cathode rays consist of streams of these particles. His attention was then drawn toward the counterpart of these cathode rays and, under his probing, positive rays began to reveal their remarkably complex character [1,2].

These discoveries and fundamental questions that had arisen regarding the precise mass and relative abundances of isotopes of the elements, led to the construction of a mass spectrograph by J.J. Thomson (1912), A.J. Dempster (1918) and F.W. Aston (1919).

During the following 40 years the concept of these early instruments was greatly improved by other experimental physicists and physical chemists, particularly A.O.C. Nier and J.H.E. Mattauch, and by 1960 several magnetic deflection type mass spectrometers became commercially available.

Thomson's mass spectrograph turned into a mass spectrometer when photographic detection was replaced by electric detection, e.g. with an electron multiplier, thus giving a direct record of ion abundance versus mass. Further, the discharge tube was split according to function into an ionization chamber and an analyzer tube, the permanent magnet was replaced by a powerful electromagnet and mass discrimination ("resolution") enhanced by using a huge curved capacitor, the electric sector (ESA), as a complementary ion imaging device, see Figure 1.1.

Apart from the spectacular improvements in resolution - from ~ 100 in the early instruments to 20 000 in one of the most popular instruments of the sixties, the AEI MS9 -, mass range and detection, one other factor has greatly contributed to the rapid acceptance of these mass spectrometers for the analysis of organic compounds : the molecules to be analyzed were not converted into ions in a discharge tube but rather by the interaction of a fast moving beam of electrons generated by a heated tungsten filament.

This ionization method, electron ionization (EI) with 50-100 eV electrons, of evaporated sample molecules at very low pressures (~ 10^{-7} Torr), converts a small fraction of the analyte into a mixture of ionized molecules (molecular ions, $M^{\bullet+}$) and structure characteristic ionic dissociation products, the fragment ions, with excellent reproducibility. In other words, EI mass spectra of organic compounds obtained under carefully controlled

conditions are very reproducible and contain a wealth of structure information. Some types of molecules may completely dissociate upon EI, but in such cases a complementary experiment with the same experimental set up can be used to protonate the molecule. The resulting $[M + H]^+$ ions are closed shell, even-electron cations and unlike the molecular ions $M^{\bullet+}$, which are open shell, odd-electron radical cations, they are far less prone to dissociation. Protonation can be readily achieved with reactant ions like CH_5^+ or H_3O^+, generated by EI of CH_4 and H_2O, respectively, at much higher pressures than those used in a routine EI experiment. The technique is called Chemical Ionization (CI), and following the pioneering work of Munson and Field, in the mid sixties, it rapidly became a routine method that has found many applications in organic analysis [3]. It also forms the basis of the experiments described in Chapters 2-5 for the generation of the ion-molecule encounter complexes studied in the context of proton-transport catalysis.

In the 1970's one of the major instrument developments concentrated on a direct coupling of the EI/CI mass spectrometers with the gas-chromatograph (GC) and in the beginning of the 1980's EI/CI GC/MS instruments, increasingly equipped with a (less expensive) quadrupole mass analyzer rather than a magnet and an electric sector, found widespread use in analytical chemistry.

Nevertheless, when, starting in the 1960's, the EI mass spectra of various classes of organic compounds were obtained, it was soon realized that the relationship between the structure of the neutral analyte molecule and the mass spectrum, that is the spectrum of the dissociation products generated from the ionized molecule, defied a straightforward interpretation in terms of simple bond cleavage reactions involving the loss of a radical. These do occur and in fact this is the most important reason that the structure information content of EI mass spectra remains vastly superior to that of any other ionization method. However, from the initial experiments, which were restricted to the use of isotopically labelled compounds and exact mass measurements of the fragment ions, it became readily clear that the initially generated molecular ions could extensively rearrange prior to dissociation, either by the loss of a radical or else by the loss of a molecule.

These intriguing observations attracted the interest of physical chemists and also increasingly theoretical chemists, since it was quickly realized that the study of the chemistry of solitary ions in the rarefied gas-phase of the mass spectrometer (where intermolecular reactions and solvation effects can be made completely absent) would also be relevant in understanding the chemistry of ions in condensed phases. This expectation has certainly proved to be correct. Following the seminal studies of the Beynon group at Purdue University on metastable ions [4] and the McLafferty Group at Cornell University on collisional activation [5], to mention just two of the pioneers in the field, the methodology that became available to probe the chemistry of ions in the gas-phase made a great leap forward. One landmark in instrument development was the VG ZAB-2F instrument, a high resolution magnetic deflection type instrument in which the magnetic sector (B) preceded the electric sector (E). This instrument became commercially available in 1977 and its BE geometry was ideally suited to the study of spontaneous and collision-induced dissociation of mass selected ions. Soon thereafter, it became clear that such instruments could also be used to study the structure and stability of (elusive) neutral species, by the technique of Neutralization-Reionization mass spectrometry (NRMS), see Section 1.3.3.

One of the greatest achievements of the use of these new methodologies in the study of the chemistry of radical cations was the discovery, in the beginning of the 1980's, of a new class of isomeric ions, the so-called distonic ions. The implication of this discovery will be discussed in some more detail in Section 1.4. Here we mention that it also marks the beginning of the increasingly important role of *ab initio* calculations in the field, which has greatly benefited from the seminal studies of the Radom group [6].

The development of magnetic deflection type instruments continued till the beginning of the 1990's and culminated in the construction of several three- and four-sector type instruments with various arrangements of magnetic and electric sectors. These instruments were used both in analytical mass spectrometry, analysis of peptides by MS/MS/MS experiments being one of the many applications, and also in gas-phase ion chemistry. The instrument used in this study, the ZAB-R, is such a multi-sector instrument, having a BEE geometry. A schematic diagram of this instrument is given in Figure 1.1.

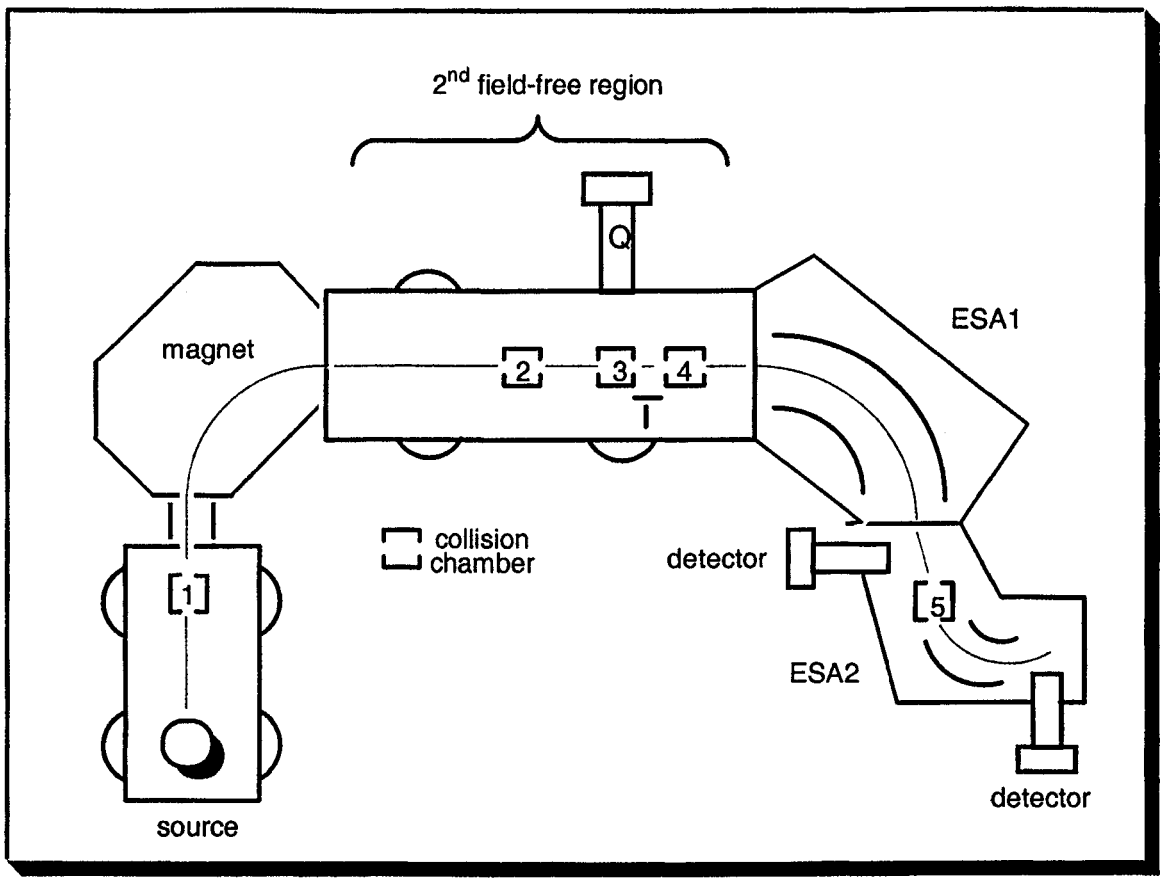

Figure 1.1. Schematic diagram of the VG Analytical ZAB-R instrument. The positive molecular and fragment ions generated in the ion source are extracted by means of a repeller electrode located in the ionization chamber which carries a small positive potential. Upon exiting the source, the ions are accelerated to 6-10 kilo-electron volts (keV) through a potential drop V and this fast moving beam of ions then enters a drift region preceding the magnet. This drift region is termed the first field free region (ffr) as it is free of any applied magnetic or electric fields. There are two additional field free regions in this instrument, the 2ffr and the 3ffr, located between the magnet and first electrostatic analyzer (ESA1) and between ESA1 and ESA2, respectively. It is within these field free regions where the reactivity and behaviour of the ions is explored

During the last decade the focus of instrument designers and manufacturers has shifted to the use of other types of mass analyzers in the construction of mass spectrometers. Apart from further developments of Fourier Transform Ion Cyclotron Resonance (FT-ICR), Ion Trap and Quadrupole based mass analyzers, a great deal of attention has been paid to achieve mass separation in time, rather than in space, as is done in a Time-of-Flight (TOF) mass analyzer.

The impetus for this shift in focus was provided by the introduction of ionization methods, in the beginning of the eighties, that can deal with highly polar and/or thermally labile biological substances (complex carbohydrates, peptides, glycopeptides, etc.) [7]. The extremely low volatility of such compounds makes them completely intractable by EI or CI but "soft ionization" methods like FAB (fast atom bombardment), ES (electrospray) or MALDI (matrix-assisted laser desorption/ionization) permit desorption/ejection of the sample molecules in ionic form directly from the condensed phase in which they are present, either as the free molecules themselves or in a suitably derivatized form. When dealing with mixtures, the separation method of choice is liquid chromatography and this technique is more readily combined with quadrupole mass analyzers than magnetic deflection type instruments. In the same vein, ionization by MALDI is eminently suited to mass analysis by time-of-flight and MALDI-TOF instruments now play a key role in the rapidly expanding use of mass spectrometry in the field of molecular biology and related disciplines.

Thus, while the last decade has not seen remarkable developments in the experimental tools available to gas-phase ion chemistry, a development in methodology and computing power short of a revolution is taking place in the use of computational chemistry in the field. Theoretical chemistry is ideally suited for the study of (ionic) reaction mechanisms in the gas-phase. The use of "chemistry by computer" has become so prevalent that theoretical results are usually presented in conjunction with experimental observations. These calculations are largely based upon *ab initio* molecular orbital (MO) and density functional (DF) theory, mathematical procedures that use no experimental information other than fundamental physical constants to calculate equilibrium geometries and their energies. These computational methods can be used to probe properties, such as the pathway between isomers, the relative energies of these species

and their corresponding ionic dissociation levels and are readily adapted to reactive (and therefore transient) gas-phase ions as easily as to their more stable neutral counterparts.

Most of the studies reported in this thesis use "chemistry by computer" as an indispensable tool to interpret and rationalize the experimental findings. This is especially true for the work on proton-transport catalysis described in Chapters 3-5, which uses computational tools which have only become available during the past five years.

1.3 Tandem mass spectrometry and computational chemistry in the study of radical cations

This Section gives a brief introduction to the tools used in this study of the chemistry of organic ions in the gas-phase. Most of the ion chemistry experiments use so called MS/MS techniques, which are based upon Mass Spectrometry of Mass Selected ions. These mass selected ions are then characterized by their spontaneous or collision-induced dissociations. The corresponding spectra are called MI (metastable ion) spectra where it concerns the spontaneous dissociations and CID (collision-induced dissociation) spectra for the induced dissociations. Such experiments on ions in the mass range 50-300 Daltons, are conveniently performed on a reverse geometry magnetic deflection instrument, such as that shown in Figure 1.1. Characterization of ions by their bond dissociation energies and other thermodynamic properties involves appearance energy (AE) measurements [8], preferably on dedicated custom-built instrumentation.

The use of these techniques has been reviewed by Holmes in 1985 [9]. This review - 'assigning structures to ions in the gas phase' - covers the larger part of the experimental methods which are still in use to date. At the time of the review, two promising tandem mass spectrometry based techniques were being developed to characterize the structure of *neutral* species. Collision-Induced Dissociative Ionization (CIDI) experiments make it possible to identify the structure of neutrals generated from metastable ions. More importantly, neutralization-reionization mass spectrometry (NRMS) has extended the scope of the field to the study of highly reactive neutrals that cannot be isolated and characterized in condensed phases, where interaction with neighbouring molecules would cause them to immediately lose

their structure identity. One important offshoot of the further development of the NR techniques are MS/MS/MS experiments in which the isomeric purity of a given mass selected ion can be probed. This technique, which is commonly called NR/CID of survivor ions is briefly discussed in the Section 1.3.3.

Also, at the time that the review was written, the need for thermodynamic data on ions and neutrals tended to be more and more satisfied by a theoretical approach to gas-phase ion chemistry. As a consequence, results from *ab initio* molecular orbital theory calculations were gaining in importance. An excellent review of the interplay of theoretical and experimental methods in the determination of enthalpies for ions and neutrals is found in ref [8]. The steadily increasing ability of computers to perform complex and laborious calculations at extremely high speeds makes it now possible to obtain reliable thermochemical values using a variety of model chemistries. These methods may now be incorporated in the whole of investigation of gas-phase ion structures.

Section 1.3.1 gives an introduction to metastable ion and appearance energy measurements. The next section discusses collision induced dissociation of cations. These two sections cover "classical" experiments in gas-phase ion chemistry. The more recent development of neutral beam experiments is discussed in the third section. In the fourth section, the calculation of thermodynamic data is discussed. A full treatment of the subjects of these four paragraphs requires one or more books; therefore appropriate literature references are given in each paragraph. These four sections cover the methodology for the ion structure research in this thesis.

1.3.1 Metastable ions and appearance energies

The ions which are responsible for the signals in an electron ionization mass spectrum all result either directly from ionization (molecular ions) or, indirectly, from dissociation following ionization (fragment ions). The removal of an electron from a molecule occurs in approximately 10^{-16} seconds [4] which is two to three orders of magnitude faster than a molecular vibration (10^{-13} to 10^{-14} seconds). Consequently, ionization occurs at a fixed

internuclear distance, a so-called *vertical* ionization, and is governed by the Franck-Condon principle. If in fact the energy imparted by the electron is greater than the ionization energy (IE) of the molecule, the excess energy is deposited into the newly formed molecular ion as internal energy resulting in transitions to various excited vibrational, rotational and possibly electronic states. This may eventually give rise to bond cleavages and to chemical reactions within the resultant ion. In this context, it should be noted that in a typical EI experiment with electrons of energy, E_{el} , in the range 50-100 eV, a distribution of molecular ions is generated whose excess or internal energy varies from a fraction of an eV to $[E_{el} - IE]$. Typical time-scales for processes occurring in an EI type tandem mass spectrometer are listed in Table 1.1.

Table 1.1. Time-scale of events following the EI ionization of a molecule in a magnetic deflection type instrument.

Event	Total time elapsed (μs) (time of event)
Ionization	10^{-10}
Vibration (chemistry begins)	10^{-7} - 10^{-9}
Rotation	10^{-2}
Ions leave source	1
Ions pass field-free region 1	3
Ions reach collision cell 4 in field-free region 2	13
Collisional excitation	10^{-8} - 10^{-10}
Time for ions to traverse a collision cell	10^{-1}
Ions reach detector 1	23

ZAB-R mass spectrometer, for *m/z* 100 ions, accelerated by 8 kV

It follows from the above table, that the (maximum) residence time of any ion generated in the ion source is ~ 1 μs and that it takes another 20 μs before the ion reaches the detector. Thus, the dissociations of the incipient molecular ions that take place in the ion source have a minimum rate constant of 10^6 s^{-1}. The maximum rate constant depends on the type of reaction and varies from 10^{14} s^{-1} for direct bond cleavage reactions to 10^{10} s^{-1} for certain rearrangement processes. Molecular ions dissociating with $10^6 < k < 10^{14}$ s^{-1} do so in the source and these ions

are called unstable ions. On the other hand, molecular ions whose internal energy content is so low that dissociation cannot take place with a rate constant > 10^5 s^{-1} will reach the detector before they have time to fragment and they will be detected as intact ions. However, there will also be a fraction of molecular ions in the distribution with an internal energy that permits dissociation with a rate constant in the range $10^5 < k < 10^6$ s^{-1} . Such ions may dissociate after having left the source but before reaching the detector and they are commonly called *metastable* ions. Thus, the internal energy gain accompanying an ionization is the driving force behind the fragmentation of the resultant ion and allows the distinction of unstable, metastable and stable ions.

Under these conditions, the fragmentation reactions which follow the ionization are well described by statistical methods such as the Quasi-Equilibrium Theory (QET) and the Rice, Rampsperger, Kassel and Marcus (RRKM) Theory. In principle, fragmentation reactions of ions can then be characterized by reaction rate constants, whose magnitude depends on the ion internal energy [10] and the mechanism of the reaction. However, for the processes which take place in the ion source such a description is complicated by the above-noted wide spread in the internal energies of the ions and by the competition of many processes whose mechanisms are often difficult to establish.

Another approach to probe dissociation pathways is by studying the chemistry of low-energy ions in a metastable ion kinetic energy (MIKE or MI) experiment. The associated internal energy domain of the metastable ions is quite narrow and thus the experimental information obtainable from a MI study is better suited for interaction with computational chemistry where it concerns the analysis of the potential energy surface.

In experimental observations, metastable ions can be distinguished by their apparent masses and their kinetic energies. Metastable ion (MI) mass spectra are obtained by a selective transmission of stable and metastable precursor ions $m_1^{\bullet+}$ through the magnetic sector. Upon dissociation of metastable ions $m_1^{\bullet+}$ into $m_2^{\bullet+}$ + m_3, its kinetic energy will be distributed among the products. In this distribution, the law of conservation of momentum is obeyed and the kinetic energy of products is thus determined to be a mass weighted fraction of the kinetic energy of the precursor ion, $(m_2/m_1)V_{acc}$, where V_{acc} is the accelerating voltage. Thus the mass

of the product ion can be determined from its kinetic energy, as measured by the electric sector, and this enables the ESA to function as a 'mass' analyzer for unimolecularly generated products arising from a mass selected ion. The initial ion beam, the main beam, contains a mixture of stable and metastable ions and typically the overall intensity of the peaks in the MI spectrum amount to c. 1% of the main beam intensity.

A general observation in MI mass spectra is the broadening of the fragment ion peak with respect to the main beam [4]. This broadening results from a conversion of (part of) the internal energy of $m_1^{\bullet+}$ into kinetic energy of the products of reaction ($m_2^{\bullet+}$ and m_3). The minimum energy required for the dissociation of a solitary cation $m_1^{\bullet+}$ into $m_2^{\bullet+} + m_3$ - often an endothermic process - corresponds with the enthalpy difference between the precursor ion and the products: $E_{min} = \Delta H_f^\circ(m_2^{\bullet+}) + \Delta H_f^\circ(m_3) - \Delta H_f^\circ(m_1^{\bullet+})$.

However, many reactions, in particular rearrangement processes, have a barrier which is higher by the reverse activation energy, ε_{rev}, see Figure 1.2. In this Figure ε_o represents the minimum internal energy required to observe the dissociation of $m_1^{\bullet+}$ at the thermochemical threshold. Observing a given dissociation reaction requires a minimum rate constant, $k \approx 10^6$ s^{-1}, for ions dissociating in the source. The amount of internal energy required to raise the rate constant to the appropriate value for observation is called the excess energy, ε_{excess}. Within the range of excess energies a narrow band represents ions which fragment with a rate constant $\sim 1.5 \times 10^5 < k < \sim 10^6\ s^{-1}$. This range of reaction rate constants corresponds to ion lifetimes of metastable ions and is therefore called the metastable ion window.

In going from the barrier towards the products a certain amount of energy becomes available. The available energy consists of the 'reverse activation energy', ε_{rev}, and the excess energy, ε_{excess}. Thus it is seen that after passage of the barrier at least the reverse activation energy and at most the excess energy must be transferred to the products, $m_2^{\bullet+} + m_3$. The energy which is transferred to the products results in internal energy and kinetic energy of the products; its partitioning is strongly dependent upon the shape of the potential energy surface for the reaction [11]. A release of kinetic energy is measurable : it is observed in the broadening of the metastable ion peak. Typical metastable ion peak shapes which arise from kinetic energy releases have been discussed by several authors [4, 11].

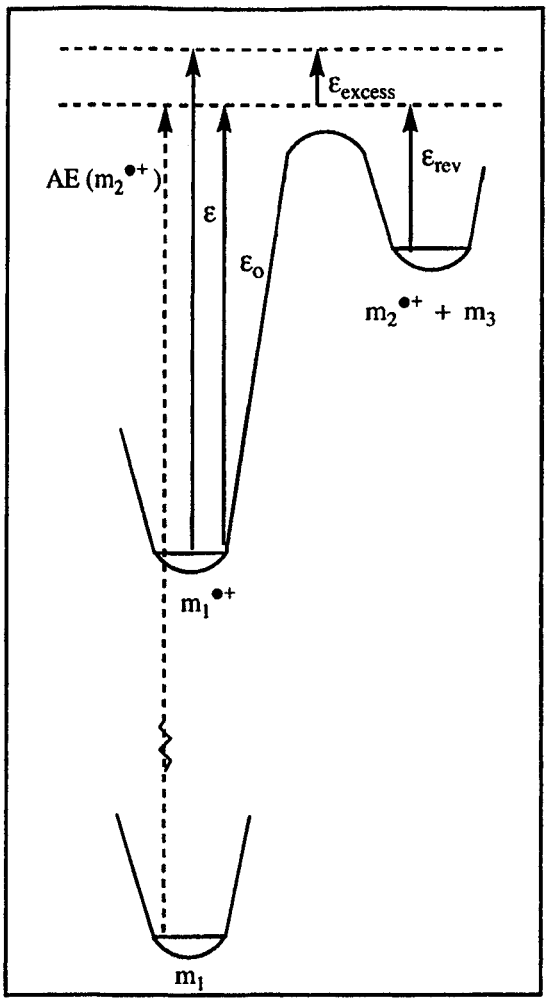

Figure 1.2 .Reaction co-ordinate diagram of an endothermic reaction.

The kinetic energy release T can be derived from the width of the metastable ion peak at height h by : $T_h = m_1^2 V_{acc}(\Delta E_h)^2 / 16 m_2 m_3 E^2$, where V_{acc} is the accelerating voltage, E is the electric sector voltage at which stable ions are transmitted, and ΔE_h is the width in energy units of the metastable peak at height h. It has become a custom to report only the kinetic energy release at half height of the metastable peak, $T_{0.5}$. Strictly this value is characteristic for purely Gaussian peak shapes and other peak shapes can only be characterized by different criteria. However, kinetic energy releases can also be characterized by the width at half height with peaks which are, within certain limitations, nearly Gaussian.

In summary, MI mass spectra provide information about the low energy, spontaneous fragmentation of ions. The kinetic energy releases and metastable ion peak shapes are specifically related to the fragmentation processes. The experimentally accessible information from MI mass spectra serves to characterize ion structures.

Appearance Energies

From the above Figure follows another experimentally accessible quantity : the minimum required internal energy for a given fragmentation equals ε_o. This ε_o can be approached by a (metastable ion) Appearance Energy measurement. In such a measurement the (metastable) product ion signal is monitored as a function of the ionizing electron energy; the AE is then determined as the energy at which $m_2^{\bullet +}$ just appears. The (metastable) AE of $m_2^{\bullet +}$ in the above reaction is given by :

$$AE\ (m_2^{\bullet +}) = \Delta H_f^\circ(m_2^{\bullet +}) + \Delta H_f^\circ\ (m_3) - \Delta H_f^\circ\ (m_1) + \varepsilon_{rev} + \varepsilon_{excess}$$

If the reverse activation energy, ε_{rev}, and the excess energy, ε_{excess}, are negligibly small, the metastable ion AE, as determined from a metastable ion study is equal to the 'normal' ion AE, as determined from source generated fragment ions. If this is the case, the AE provides information about the heat of formation of the product ion (and neutral) and this may serve to characterize the product ion structure.

The above only holds if no reverse energy barrier is involved and if the heat of formation of $m_1^{\bullet +}$ lies below the heat of formation of the products. The presence of an energy barrier results in too high a value for the AE, which then yields valuable information about the barrier. The AE is inherently measured to lie above or at the ionization energy, IE , of the precursor molecule m_1, because ionized m_1 must be formed before it can fragment to give $m_2^{\bullet +}$. The presence of an energy barrier for the reverse reaction, or the limiting IE of a precursor molecule both lead to a value of the AE that lies above the true value, i.e. the value corresponding to the formation of the reaction products in their ground states.

A further problem in the interpretation of an AE measurement is the operation of a kinetic shift. If the reaction rate - and thus the peak intensity - rises only slowly with excess energy, it is possible that a relatively large excess energy is necessary to ensure that

dissociation occurs within the limiting time scale of the experiment. This makes it difficult to assess the point where the signal vanishes, thus frequently resulting in too high a value of the AE. The problem can only satisfactorily be solved by the determination of the relationship between the reaction rate constant and the internal energy in a Photo Electron Photo Ion Coincidence (PEPICO) experiment or in a Time Resolved Experiment [12]. Such experiments require dedicated instrumentation, that is, an energy-selected electron ionization source or alternatively a photoionization mass spectrometer, as was used in Chapter 6 to obtain AE values for the formation of the methoxycarbonyl ion, $CH_3O\text{-}C{=}O^+$.

Another possible source of error comes from the occurrence of a hidden rearrangement. In many cases, the structure of the ion and the accompanying neutral fragment are not in doubt. However, a significant number of molecular ions undergo unpredicted rearrangements before they fragment. If there is any doubt as to the structure of the dissociation products, then appropriate experiments should be performed. An example that illustrates this problem is ionized methyl acetate, $CH_3C(=O)OCH_3^{\bullet+}$, whose dissociation into $CH_3\text{-}C{=}O^+$ and $[C, H_3, O]^{\bullet}$ seems to be trivial. The structure of the ion is as expected but, astonishingly, the isomeric hydroxymethyl radical $^{\bullet}CH_2OH$ is generated instead of the expected $CH_3O^{\bullet}$ species, at least for the low energy ions. In this case, profound rearrangements have preceded dissociation.

To conclude, carefully measured and evaluated AE values provide valuable benchmarks in the potential energy surface of an ion fragmentation reaction. If they are combined with the information from MI mass spectra of both $m_1^{\bullet+}$ and $m_2^{\bullet+}$ a first framework in ion structure determination is generally obtained. This first step alone, however, rarely suffices for a complete ion structure determination. In ion fragmentation mechanistic studies, labelling a molecule, and hence the ions generated therefrom, in strategic places with isotopes (D, ^{13}C, ^{18}O), can also provide information about the structure of the ion by means of the fragmentation characteristics of the labelled ion. These experiments can for example show which atoms do or do not actively participate in a certain fragmentation and so provide useful and sometimes crucial information about reaction mechanisms. In addition to the spontaneous dissociation just described, fragmentation can be induced, and this technique described below is known as Collision-Induced Dissociation (CID) mass spectrometry.

1.3.2 Collision Induced Processes

An important development in the structure analysis of gas-phase organic ions is the controlled introduction of an inert gas into one of the field free regions, as pioneered by Jennings and McLafferty [13]. The introduction of a gas into the analyzer tube, while conducting a MI experiment, leads to intense signals.

The internal energy gain following collision gives rise to fragmentation (Collision-Induced Dissociation (CID) mass spectrometry) or to the loss of one, or even more electrons from a cation, thus producing multiply charged ions (Charge Stripping (CS) mass spectrometry). Under these conditions (high translational energy collisions) the collision complexes formed are inherently unstable and chemical transformations do not occur in these complexes even if the collision gas is a (reactive) organic molecule. At low translational energy collisions, conventional ion-molecule type reactions can compete effectively with CID. In this case, the reactivity of the ion under investigation is probed by interactions with selected neutral molecules which may lead to structure specific associative ion-molecule reactions [14]. These low-energy collisions require a dedicated instrument, such as that available at the University of Mons. This instrument has been used in the study of Chapter 7 for the differentiation between the hydrogen shift isomers of the hydroxypyridines.

This paragraph briefly discusses CID and CS mass spectrometry, with a focus on the experimental conditions. A more thorough discussion of CID mass spectrometry is found in reviews by several authors [15].

Collision-Induced Dissociation

In a collision-induced dissociation experiment *stable* ions, of low internal energy, collide with gas molecules while they are at high velocity. The collision is a vertical process and involves energies in the eV range, like in electron impact; therefore CID mass spectra of molecular ions often resemble EI mass spectra. The sudden gain in ion internal energy opens dissociation pathways not accessible to the metastable ions. In a CID experiment the ions become highly energized resulting in fast dissociation, in the order of 10^{-8} s (compared to the

10^{-6} to 10^{-4} s time frame of metastable ions). At these short times, direct bond cleavages often prevail over rearrangement. Moreover, in a CID experiment stable ions are sampled, i.e. ions which lack the internal energy required for fragmentation. Hence, ideally CID mass spectra give a picture of structure characteristic direct bond cleavage reactions of ions of low internal energies and of well defined structures (relative to MI mass spectra).

The quality of the information obtained from CID mass spectra is largely determined by the experimental conditions, which were studied by several research groups with attention ranging from the fundamental physics of the collision process to the conditions for application in chemical analysis (Problems which cannot be solved by a change of the experimental conditions arise if isomeric ions yield indistinguishable CID mass spectra; here, other techniques may be of help). The appearance of a CID spectrum depends on the collision gas pressure, ion velocity, contributions from metastable ions and to a lesser extent the nature of the collision gas used and the internal energy content of the ions sampled.

Helium is the most widely used collision gas for CID mass spectrometry, because it has a high target collision efficiency, that is, competing processes such as neutralization and scattering are kept to a minimum. Oxygen, argon and nitrogen are other commonly used target gases. Recent studies [16] have demonstrated that oxygen can sometimes induce a unique reaction channel. This remarkable behaviour is attributed to the availability of the triplet state of O_2 which can populate excited states of the ions by spin-forbidden transitions.

The *pressure* of the collision gas is also an important consideration because it is related to the appearance of single or multiple collisions and because the collision gas also causes scattering of the ions. Although scattering has a minimum influence at low gas pressures, it can never be reduced to zero. Multiple collisions of ions lead to multiple fragmentation ; moreover the products formed after a first collision may themselves collide and fragment under these conditions. Multiple fragmentation obscures the signals which stem from the originally (mass) selected ion. Single collision conditions are most likely to lead to single fragmentations. Therefore single collision conditions yield the more specific CID mass spectra. Since the collision pressure can only be estimated using a remote ionization gauge located outside the collision cell, the gas concentration is defined in terms of the reduction of the intensity of the

main beam of ions. A main beam transmission which is reduced by 30 - 40 % in going form MI to CID is generally a good compromise between signal intensity, single collision conditions and minimum scattering.

Metastable ion contributions to a CID spectrum result from metastable ion fragmentations which are hardly influenced by the introduction of a collision gas. The intensity of the metastable ion signal is sometimes of the order of the intensity of the CID signals, as is observed for the loss of CO from ionized 2-hydroxypyridine (Chapter 7), and this may obscure a "true" CID mass spectrum. The interference of fragmentation of metastably generated product ions by collision excitation is usually negligible. Metastable ion interferences can be distinguished from true CID signals by floating the collision gas cell at a potential which may vary form a hundred to several thousands of volts. Upon floating the collision chamber voltage, the kinetic energy of ions which fragment inside the collision gas cell becomes different from the kinetic energy of ions which fragment outside the gas cell. The floating of the gas cell is also applied in the search for signals of collisional origin in MI mass spectra (as caused by residual gas inside the cell). In tabulated CID mass spectra peaks which suffer from metastable interference are often either omitted, or the intensity of these peaks is corrected for the MI contribution.

The *ion velocity* determines the internal energy gain of the ions upon collision. The 'structure' of an ion cannot be seen separate from its internal energy. Wherever possible, CID spectra of ions, generated in the ion source (wide range of internal energies) should be compared to CID spectra of low internal energy ions (for example, the CID spectrum collected in the 3ffr of metastable ions generated in the second-field free region). This allows detection of possible isomerization at higher internal energies.

Charge Stripping

Charge stripping mass spectra are often observed simultaneously with CID mass spectra. Only a very small fraction of the ions becomes multiply ionized, thus producing a charge stripping mass spectrum with very small (< 1 %) overall intensity as compared to the overall intensity of the CID mass spectrum. The width of Charge Stripping peaks is typically narrow relative to that of the CID peaks, because kinetic energy is not released in the charge stripping process. Charge Stripping which yields doubly charged ions, can easily be recognized in a CID mass spectrum because the signals typically appear at about half the kinetic energy of the precursor ion.

In cases where Charge Stripping signals are not overlapped by CID signals they may often provide specific information, either by their intensity ratio or by the accurate determination of the kinetic energy from the peak position [17]. The latter type of experiment gives the opportunity to determine the second IE of the cation, because the kinetic energy of the doubly charged ion is shifted with respect to the calculated kinetic energy (i.e. half the acceleration voltage of the precursor ion), by an amount proportional to the second IE. In contrast to CID mass spectra, CS mass spectra are very sensitive to the type of collision gas used and less sensitive to collision gas pressure. The use of diatomic gases like oxygen or nitrogen rather than helium increases the yield of the doubly charged ions but it also affects the relative intensities of the charge stripping signals. Until now CS mass spectrometry has proven to be useful in obtaining a distinction in isomeric ion structures which yield similar MI and CID mass spectra.

1.3.3 Mass spectrometry of fast neutrals

Mass spectrometric experiments with fast neutral beams were already described in the mid sixties [18]. However, it was not until twenty years later that this subject attracted the interest of ion chemists, not only as an auxiliary technique in ion structure determination, but also for the generation of unusually reactive but thermodynamically stable molecules, which, because of intermolecular reactions, cannot be studied in solution or even in the solid state.

Here the two experimental methods in the mass spectrometry of fast organic neutrals, Neutralization-Reionization Mass Spectrometry (NRMS) of ions and Collision-Induced Dissociative Ionization (CIDI) of metastably generated neutrals, will be outlined for a reverse geometry magnetic sector instrument.

NRMS of organic ions

The standard procedure in an NR experiment is to first generate the ion in the mass spectrometer and to establish its ion structure and its isomeric purity. Next the NR experiment is performed. A neutralization-reionization (NR) experiment consists of the steps outlined in Figure 1.3 and Scheme 1.1 below.

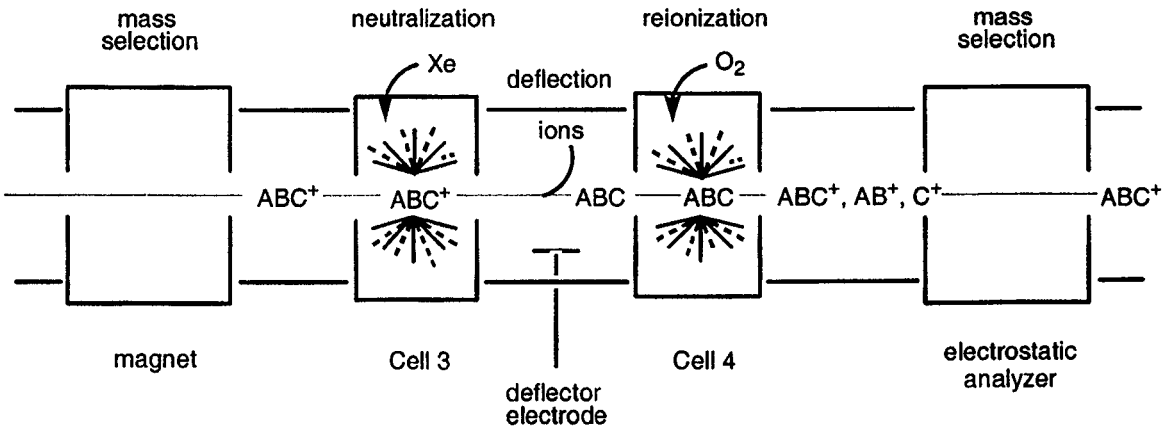

Figure 1.3. Schematic representation of a neutralization-reionization experiment.

In the first step of a NR experiment, the ions ABC^+ are mass selected and transmitted into the second field-free region. Within this field, ions ABC^+ enter the first collision gas chamber, Cell 3 in Figure 1.3, where electron-capture from a target gas G_1 results in the reduction to the neutral species ABC (Scheme 1.1, Eq. 1a) in a vertical Franck-Condon transition. All ions ABC^+ which have not been neutralized and also (the relatively minor faction of) their ionic dissociation products (Scheme 1.1, Eq. 2a and 2b) are removed from the beam using a charged deflector electrode. This allows only the neutral molecules ABC and their uncharged dissociation products AB and C, to enter the second collision gas chamber, Cell 4.

Subsequently, these fast moving neutrals are reionized by collision with a target gas G_2 in the second collision gas chamber (Scheme 1.1, eq. 3a and 3b). This oxidation step is performed in such a way that not only molecular ions ABC^+, but also charged fragments are generated. The spectrum of the latter can conveniently be recorded and it serves to characterize the structure of ABC^+. Upon its generation in Cell 3, it takes about a microsecond for a given neutral to reach the reionization cell, Cell 4. Thus, the presence of a signal ABC^+ in a NR mass spectrum signifies that the neutral has remained intact for > 1μs. However, the mere presence of a recovery (*survivor*) signal does not prove that the neutral counterpart of ABC^+ is a stable entity. As shown by process 1c, it is conceivable that all or part of the incipient neutral species ABC isomerize to a more stable isomer, BAC, prior to isomerization. Thus, a detailed analysis of the NR and CID mass spectra of isomeric ions is required, particularly in those systems where there is computational or experimental evidence for facile isomerization reactions of the neutral species. When the NR mass spectrum of a given ion is closely similar to its CID mass spectrum, the conclusion is often warranted that no isomerization has taken place, but only if it has been established (computationally) that there are high barriers towards isomerization.

Neutralization Chamber - Cell 3							
$G_1 + ABC^+$	→	$G_1^+ +$		ABC			1a
$G_1 + ABC^+$	→	$G_1^+ +$		ABC^*	→	$AB^\bullet + C^\bullet$	1b
					→	BAC^*	1c
$G_1 + ABC^+$	→	$G_1 +$		ABC^{+*}	→	$AB^+ + C^\bullet$	2a
						$AB^\bullet + C^+$	
				ABC^+	→	$AB^+ + C^\bullet$	2b
						$AB^\bullet + C^+$	
Reionization Chamber - Cell 4							
$G_2 + ABC$	→	$G_2 +$	$e^- +$	ABC^+	→	$AB^+ + C^\bullet$	3a
						$AB^\bullet + C^+$	
$G_2 + AB^\bullet, C^\bullet$	→	$G_2 +$	$e^- +$	AB^+, C^+			3b

Scheme 1.1

It follows from the processes outlined in Scheme 1.1 that the peaks in a NR spectrum originate from the following processes : (i) reionized neutrals ABC and their fragment ions on the basis of which a structure assignment is made, (ii) reionized neutrals AB$^{\bullet}$ and C$^{\bullet}$ (Scheme 1.1, Eq. 1b) produced by dissociation of neutrals ABC having too large an internal energy for survival of the neutralization, (iii) reionized neutrals AB$^{\bullet}$ and C$^{\bullet}$ (Scheme 1.1, Eq. 2a) produced by collision-induced dissociation of ABC^{+} rather than by charge transfer, and (iv) reionized neutrals AB$^{\bullet}$ and C$^{\bullet}$ (Scheme 1.1, Eq. 2b) produced by the spontaneous unimolecular dissociation of ABC^{+}.

Since the neutrals from (ii), (iii) and (iv) obscure the interpretation of the NR spectrum of a given species ABC^{+}, in an ideal NR experiment, reaction 1a would be the dominant process, i.e. the neutral ABC is generated in a *high* yield and *low* internal energy content and a *minimum* yield of neutrals generated from collision-induced dissociation. Contributions from reaction 2b can readily be identified by putting a small voltage (> 100 V) on the first cell, because most of these neutrals are generated outside the cell. However, the contributions resulting from the other two interference processes are often more difficult to verify.

The nature of the target gas (i.e. its ionization energy and its collision cross section) has an influence on the processes outlined in Scheme 1.1 and as such is one of the most important parameters in a NRMS experiment. For the neutralization reaction $ABC^{+} + G_1 + Q_N \rightarrow ABC^{+} + G_1^{+}$ a satisfactory yield of neutrals is generally obtained if the energy defect Q_N lies in the range of 0 - 4 eV. Q_N is defined as $IE(G_1) - RE(ABC^{+})$, where IE is the ionization energy of the target gas and RE is the recombination energy for the electron capture by AB^{+} ($RE[AB^{+}] \approx IE[AB]$, unless large geometry differences exist between the ground state of ion and neutral). If Q_N is nearly zero then near resonant charge exchange conditions obtain ; if Q_N is negative, the process is exothermic, whereas for positive Q_N the reaction is endothermic and the energy deficit (a few eV) is supplied by the translational energy (8 - 10 keV) of the fast beam of ABC^{+} ions.

Initially, the neutralization gases employed for NR of organic ions were mostly Xe and Hg. Nowadays, vapours from polyatomic organics with lower ionization energies such as cyclopropane, trimethylamine, N,N-dimethylaniline (NDMA) and dimethyldisulfide are

commonly employed as reducing agents. These gases have appropriate Q_N values for the neutralization of most organic ions (whose RE values are in the range of 7 to 10 eV) and they produce an acceptably small degree of interference from neutrals generated by collision-induced dissociation of the ions ABC^+ (Scheme 1.1, Eq. 2a). For reionization oxygen is preferred over helium because it combines a high efficiency with a low degree of dissociation.

Summarizing, it can be stated that a neutralization-reionization experiment (eg. using NDMA as the reducing agent and O_2 for subsequent reionization) of an organic neutral may be expected to yield a sizeable fraction of reionized non dissociating neutrals and structure characteristic dissociation products, unless either the neutral resides in a shallow potential well and/or has a geometry which is considerably different from that of the ion, as is exemplified by the relative stabilities of $H\text{-}N{\equiv}C\text{-}S\text{-}S^{\bullet+}$ versus its ring closed counterpart $H\text{-}N\text{-}CS_2^{\bullet+}$, in Chapter 9. The incipient neutrals $H\text{-}N{\equiv}C\text{-}S\text{-}S$ are only marginally stable towards ring-closure into $H\text{-}N\text{-}CS_2$ which is more stable by 17 kcal/mol. Consequently, most of the stable neutrals generated reach the potential well of $H\text{-}N\text{-}CS_2$ during their μs lifetime.

The interpretation of NR mass spectra relies heavily upon knowledge from thermochemistry and *ab initio* MO calculations on the height of dissociation and isomerization barriers in both the original ion and its neutralized counterpart. In addition, it is important to realize that NR efficiencies of 'survivor' ions of neighbouring mass or even among isomeric and isobaric ions can easily differ two orders of magnitude. It is therefore important to carefully consider the purity of the primary ion flux to be neutralized in terms of undesired species of the same *m/z* ratio. Such a contribution played a role in the interpretation of the NR spectrum of $CH_3O\text{-}B\text{-}H^{\bullet}$ reported in Chapter 8.

When the identity of the reionized species in a NR experiment and/or the purity of the ions being neutralized is in doubt, the ability to perform MS/MS/MS experiments, especially CID of the NR survivor ion, may prove invaluable. In this type of experiment, the 'survivor' ions are transmitted into the third field-free region where they travel through another collision gas chamber and are collisionally activated. The resulting CID spectrum may be compared directly with the CID spectrum of the source generated ions obtained under similar experimental conditions, providing information about the stability and isomerization behaviour

of the neutral. If the spectra are closely similar, this implies that the initial ion flux is pure and that structural integrity is maintained in the NR process. This is because isomeric (or isobaric) species will not normally have identical neutralization and reionization efficiencies.

CIDI spectra of neutral species generated in the dissociation of low-energy ions

Until the mid eighties, the question of the structure of the neutral species m_3 generated in the unimolecular dissociation of ions $m_1^{\bullet+}$, $m_1^{\bullet+} \rightarrow m_2^{\bullet+} + m_3$, had received relatively little attention. The most important reason perhaps was that, whereas a whole armoury of techniques was available to investigate the structure of the ions $m_1^{\bullet+}$ and $m_2^{\bullet+}$ the structure of the neutral m_3 could only be determined indirectly. The introduction of a variant of the NRMS technique, the Collision-Induced Dissociative Ionization, CIDI of neutral molecules [18b] removed this obstacle and made it possible to quickly identify the structure of the neutral.

A CIDI experiment is performed with the instrumental setup for NRMS of Figure 1.3, but without using collision gas chamber 3. A small fraction of the beam of fast moving ions $m_1^{\bullet+}$ under investigation will dissociate unimolecularly during the flight to Cell 4. Upon arrival at the charged deflector electrode all ions, i.e. $m_1^{\bullet+}$ and the ionic dissociation products $m_2^{\bullet+}$, are deflected away so that the only species entering the second collision gas chamber are the fast moving neutrals m_3.

This technique has for example, shown that HNC rather than HCN is lost from metastable aniline molecular ions and that ionized methyl acetate loses $^{\bullet}CH_2OH$ radicals rather than $^{\bullet}OCH_3$ as the lowest-energy fragmentation route [19]. Use of this technique played a key-role in Chapter 6, where it was determined that low energy dimethyl oxalate ions, CH_3O-C(=O)-C(=O)-$OCH_3^{\bullet+}$, dissociate into $CH_3^{\bullet}$ +CO_2 without the intermediacy of CH_3O-C=O$^{\bullet}$, to generate CH_3O-C=O$^+$.

1.3.4 Calculation of thermodynamic properties

Mechanistic understanding of chemical reactions also requires knowledge of their fundamental thermochemical properties such as enthalpies, entropies and heat capacities. A relatively simple and elegant method of summarizing the chemistry of a given system is the construction of the potential energy surface over which the ions decompose. The construction of the potential energy surface for an ionic system provides insight into those chemical transformations which are energetically permitted. Therefore the availability of accurate thermochemical data is essential for understanding issues of their reactivity. Such information is often obtained or estimated from accumulated tables of experimental results [20] or from data which is spread throughout the literature.

Besides this, the thermodynamic properties, such as the heat of formation of an ion or of a neutral molecule may be obtained basically from three calculational approaches : empirical, semi-empirical and *ab initio* calculations. The empirical calculation of the heat of formation of cations and neutrals is discussed first. Next, *ab initio* calculations on cations are discussed. Semi-empirical methods are not used in this thesis and will not form part of the discussion.

Empirical Calculations

The empirical methods of calculation of a heat of formation are based upon direct ways of extrapolation from experimentally determined heats of formation of similar, e.g. homologous compounds. The extrapolation methods which are most commonly used are isodesmic substitution (for ions and neutral molecules), 'Benson Additivity' schemes (for neutral molecules) and energy correlation schemes (for ions). These methods are briefly explained below.

Isodesmic substitution uses a thought experiment in which a functional group in a molecule (or ion) of known ΔH_f° is substituted to give the desired molecule of unknown ΔH_f°. An analogous substitution is then considered for two comparable molecules, both of known ΔH_f°. The increment of ΔH_f° for the substitution in the case of the unknown results from the

latter parallel case. Isodesmic substitution can straightforwardly be applied to neutral molecules but not to ions; for ions it should also be considered if substitution takes place at a formal charge bearing site or not [21], because this greatly influences the additivity. The unknown ΔH_f° can often be approached by different isodesmic substitutions. If these different isodesmic substitutions all yield about the same value, i.e. they lie within c. 4 kcal/mol, one can be quite confident about the ΔH_f° thus obtained.

The *Benson Additivity* scheme consists of an addition of increments for each non-hydrogen atom in a molecule. These increments are specified in a table, as a function of the bonding to neighbouring atoms or groups. The increments themselves are directly derived from experimental results. Some increments may therefore not be available, whereas others are not up to date. The values which result from such an additivity scheme may be accurate within less than 4 kcal/mol [22]

'Benson Additivity' schemes cannot be applied to cations, because there is no simple empirical and linear relationship between the functional groups and the heat of formation of an ion. Other correlation schemes are available but these are restricted to a few classes of ions. Holmes et al. have proposed a non-linear equation and a fit to experimental results, to obtain a correlation scheme for the estimation of ΔH_f° of a variety of odd electron ions [21]. Benoit and Harrison used a correlation of the proton affinity (PA) with the ionization energy to estimate the PA of certain oxygen containing molecules, which can subsequently be used in the estimation of ΔH_f° for some even electron ions[23]. Larson and McMahon experimentally derived an equation for ΔH_f° of a proton-bound cation, O•••H$^+$•••O and O•••H$^+$•••C, as a function of the proton affinity of the neutral dimer molecules [24a]. A similar equation was derived by Meot-Ner for the estimation of O•••H$^+$•••N bridged cations [24b]. The equation of Larson and McMahon also appears to hold fairly well for a limited set of hydrogen-bridged radical cations. ΔH_f° of cations can empirically be determined by several methods; the choice of method will depend on the ion's structure, because no general scheme is available.

Computational Methods

Nowadays, quantum chemistry offers new means of problem solving to mass spectrometrists. The sudden increase of the practical value of *ab initio* calculations, as compared to about 10-20 years ago, is largely due to the developments in computer technology and to the availability of computational program packages, like the Gaussian series of programs and GAMESS. Combined mass spectrometric and theoretical research has already led to remarkable results [25]. The diluted gas-phase in a mass spectrometer generally guarantees a minimal interaction between the ions and the environment. These experimental circumstances are best suited for a comparison with quantum chemical calculations on ions. Hence, theoretical chemistry and mass spectrometry are only at the start of a fruitful cooperation.

Next a brief discussion of the most widely applied methods of *ab initio* calculations in ion chemistry, in particular those used in Chapter 3-10, will be given. For a thorough discussion of the methods of theoretical chemistry in relation to ion chemistry the reader is referred to the literature [26]. To facilitate the readability of the following section, a brief summary of the terminology used in the calculations is first presented.

One of the first steps in a calculation is the *optimization* of the structure, that is finding a stationary point, a minimum, on the potential energy surface (PES). This occurs by the calculation of the force constants between atoms, using the direction of these forces to change the relationship of the atoms and minimizing these forces to a specified limit, to yield an equilibrium geometry. The next step is to verify the stability of the resulting structure. This involves a more accurate calculation of the force constants and is called a *frequency* calculation. This calculation generates the vibrational frequencies and these are used to differentiate between minima (all frequencies real) and transition states. A transition state (TS) is characterized by one imaginary vibrational frequency, that is an energy maximum in one direction (the reaction co-ordinate) whereas in all other directions it is a minimum. This transition state structure can be characterized further by performing another computation, which follows the reaction coordinate of the imaginary frequency and thereby connects the transition state to the minima. Typically, the method used to perform the geometry

optimization and the frequency calculation does not yield relative energies of chemical accuracy and a higher level theoretical method, a *single-point* calculation, is employed.

The two essential ingredients in these calculations are the basis set and the level of theory used in the calculation. The choice of basis set and electron correlation treatment determines the quality of a given ab initio molecular orbital calculation. In most cases, increasing the size of the basis set or improving the treatment of electron correlation improves the result [27].

Basis sets that are normally used are at least double zeta plus polarization (DZP) quality. Such basis sets contain two functions for each formal atomic orbital (e.g. 1s, 3d, etc.) on each atom plus one set of functions (polarization functions) on each atom with one quantum number higher than required in the isolated atoms. There are two versions of the basis set type, that due to Dunning and Hay and that developed by Pople and coworkers [28, 29]. The DZP and the triple zeta plus polarization (TZP) basis sets are Dunning and Hay type basis sets, while the 6-31G(d) and 6-31G(d,p) basis sets are Pople type basis sets. The Pople basis sets can be expanded by the addition of more d polarization functions or the addition of higher angular momentum functions such as f-functions. More recently larger basis sets that are suited for electron correlation have been developed. They are correlated consistent basis sets (cc-PVTZ and cc-PVQZ). The PVQZ basis set employs g polarization functions.

Electron correlation can be incorporated into a calculation in several ways. One of the more common ways is using many body perturbation theory. Pople and co-workers have developed levels of correlation within the Moller-Plesset (MP) formulation [30]. They are MP2, which is second order, MP3, third order, and MP4, fourth order. The MP4 calculation can be performed with single, double and quadruple excitations (SDQ) or with the inclusion of triple excitations (SDTQ). The inclusion of triple excitations can be quite important for the prediction of energetics, but they tend to be computationally expensive. The other form of electron correlation is coupled cluster theory. This theory is related to many body perturbation theory [31]. It is commonly formulated with the inclusion of single and double excitation (CCSD), single, double and triple excitations (CCSD(T)), or through quadruple excitations (CCSDTQ). Quadratic configuration (QCISD) is an approximation to CCSD methods which usually gives similar results [32].

In recent years, *density functional theory* (DFT), has become an increasingly popular complementary method in computational chemistry. DFT methods compute electron correlation via general functionals of the electron density. Several functionals have been defined, local and gradient-corrected, and these are generally distinguished by the way they treat the exchange and correlation components. The most commonly employed functional is the Becke-style hybrid, B3LYP, which is a combination of Hartree-Fock and the DFT gradient-corrected correlation function LYP.

It has become clear that DFT methods have many advantages; they scale well with system size, implicitly include electron correlation effects and their accuracy is comparable to correlated ab initio methods, such as MP2, which do not scale as well. DFT methods can therefore be applied to larger molecular systems than traditional ab initio methods. Nevertheless, the DFT methodology should not be oversold. It does have problems. One of the main difficulties is that there is currently no clear approach to systematically improve the exchange-correlation energy functionals, and this may lead to a poor description of certain reactions.

Throughout the studies described in Chapters 3-10, two commonly used computational chemistry methods are employed. These are the *Gaussian-2* (G2) and *CBS-QB3* collective methods. These two methods give results of demonstrated high accuracy (± 2 kcal/mol) and are easy to use and implement as many computer programs are readily available. G2 theory [33] and the complete basis set (CBS) methods [34] were developed by the Curtiss and Montgomery groups, respectively, with the aim to calculate accurate enthalpies of formation. G2 assumes certain additivity approximations to yield final energies effectively at the QCISD(T)/6-311+G(3df,2p) level of theory and an empirical correction is applied to account for systematic errors. The CBS methods involve an extrapolation of the MP2 energy to the complete basis set limit. The effect of high order electron correlation is determined by performing calculations with smaller basis sets and empirical corrections are applied to account for zero point energy, spin contamination in UHF wavefunctions and other correlation effects. CCSD(T) is the highest correlated wavefunction used.

Several groups [35] have evaluated the applicability of these methods for determining the heats of formation of selected molecules and radicals. All studies agree that, in general, the accuracy of the two models does not differ appreciably, and that it is the computational speed and the size of the system that determines the choice. What one obtains from the more expensive calculations is a demonstrated high level of accuracy (for example the ± 2 kcal/mol for G2) that may be relied on in studies of unknown systems. The method of choice is the most accurate one that is practical to use for the specific application. Feller and Peterson have compiled theoretical predictions of thermochemical quantities into a database to assist in the choice of basis set and method to achieve the desired accuracy for a particular application [36]

In summary, *ab initio* and density functional theory calculations are exceptionally valuable for probing mass spectrometric problems in that they provide information about (parts of) an ion's potential energy surface (PES), especially the saddle-points, transition states and minima. These characteristics can be used to predict if an ion is experimentally observable, because they give an impression of the possibility of rearrangement. Only a limited amount of information about the PES of a given system comes from the experiment, notably from AE data. The experimentally derived values are used as a reference for the calculated potential energy surface. For example, an experimental heat of formation is related to a minimum on the calculated surface. The energy/structure gaps which remain are then ideally filled in by further calculations. A resultant diagram of energy versus structure serves to get insight into the energetics of the process and into the possibility of the involvement of rearranged ion structures in a fragmentation reaction. The use of theoretical calculations in constructing PESs and in the interpretation of mass spectral data is a major component of the work described in Chapters 3-10.

1.4 Radical cations of unconventional structure and their role in proton-transport catalysis

Experimental and theoretical studies during the last two decades have firmly established the existence in the gas phase of simple organic ions with unusual structures, whose neutral counterparts are unknown or extremely reactive. One of the earliest examples investigated in great detail both theoretically (using *ab initio* calculations) and experimentally (using tandem mass spectrometry) was the methyleneoxonium radical cation, $CH_2OH_2^{\bullet+}$. This species has quite a short C-O distance and, perhaps surprisingly, lies lower in energy than its isomer of conventional structure, the methanol radical cation, $CH_3OH^{\bullet+}$. In contrast, the neutral ylide CH_2OH_2, resembles a weakly bonded complex of methylene with water. The discovery of this ion has greatly contributed to our understanding of the chemistry of ions in the gas phase. This species, in contrast to its conventional isomer, has the charge and radical site at formally separated atoms and as such it is referred to as a *distonic* ion, a term introduced by the Radom group [37], stemming from the Greek *diestos* and Latin *distans* meaning separate. If the radical and charge sites are on adjacent atoms such as in $^{\bullet}CH_2OH_2^{+}$, the distonic ion can be viewed as an ionized ylid, and as such it is also referred to as *ylid* ion. Since their inception in the 1980's, many distonic ions have been characterized as stable species in the gas phase and used to rationalize many otherwise unintelligible reactions. The reason for this detour in the dissociation route is usually the lower activation energy for dissociation into thermodynamically stable products.

Distonic ions can also serve as precursors for the genesis of novel species, including the hydrogen shift isomers of N-heterocycles, e.g. the α-, β- and γ-distonic ions of pyridine depicted in Scheme 1.2, where α, β and γ indicate the number of atoms separating the charge and radical.

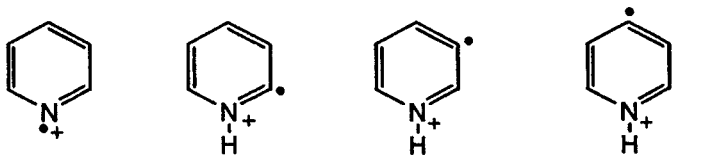

α-distonic ion (ylide ion) β-distonic ion γ-distonic ion

Scheme 1.2

In the mass spectrometer, the molecular ions of 2-picolinic acid and methyl-2-carboxypyiridne-3-carboxylate rearrange to distonic ions by way of a hydrogen shift and these intermediate distonic ions undergo further reactions to yield the desired products the α- and β-distonic ions of pyridine. (A suitable precursor for the generation of the γ-distonic ion by dissociative ionization cannot be evisaged. Instead these ions can be generated from the collisional decomposition of protonated 4-chloropyridine.) Characterization of these isomeric product ions, however, presented a rather challenging topic in mass spectrometry as the MI and CID mass spectra of the various species differ only in subtle details. It was not until the 1990's, following the recognition of NR and NR/CID as powerful tools in mass analysis, that these isomers could be well distinguished. In Chapter 7, a number of such H-shift isomers involved in the $C_5H_5NO^{\bullet+}$ system of ions and neutrals are probed using this methodology.

As shown in Scheme 1.3, even the relatively small system of $C_2H_6O^{\bullet+}$ radical cations comprises a number of such unconventional ions which have all been identified.

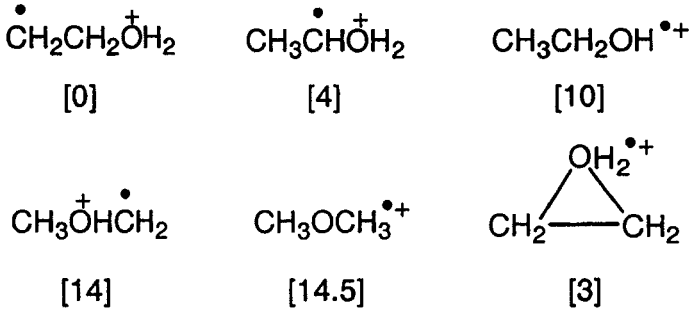

Scheme 1.3. $C_2H_6O^{\bullet+}$ structural isomers with calculated relative energies in [kcal/mol].

The most stable of the distonic and conventional isomers in Scheme 1.3 is the ethyleneoxonium ion, $CH_2CH_2OH_2^{\bullet+}$. Unlike many other distonic ions it readily adopts the structure of an ion-dipole complex, $CH_2{=}CH_2^{\bullet+}$ / H_2O, when its internal energy is raised to the dissociation threshold. This species can best be viewed as a positively charged ethene rod to which the water molecule is attached by its dipole, but which can move more or less freely along and about the positive rod.

Ion-dipole or ion-neutral complexes as they are sometimes called, consist of an ion and a neutral stabilized by electrostatic interactions, having a stabilization energy (SE) of 10-25 kcal/mol (the maximum SE is achieved when the dipole moment vector points away from the charge). This stabilization energy often gives rise to low barriers in all directions for rotation of the ion with respect to its neutral partner and also means that the ion can undergo internal rearrangements independent of the rest of the complex. This latter feature is especially important in understanding reactions that would otherwise be considered implausible for an intact ion.

Two distinct but related phenomena may be interpreted by means of ion-dipole interactions : the ionic component may react individually by isomerization to a more stable structure, or the ionic and neutral species may react with each other, for example by proton transfer, as depicted in the equations below.

$$I_1N^{\bullet+} \rightarrow I_1^{\bullet+}\bullet\bullet\bullet N \rightarrow I_2^{\bullet+}\bullet\bullet\bullet N \rightarrow I_2^{\bullet+} + N$$

$$\rightarrow [I_1 - H]^{\bullet}\bullet\bullet\bullet HN^{+} \rightarrow [I_1 - H]^{\bullet} + HN^{+}$$

Although the earliest suggestion of a complex-mediated dissociation dates back to 1956, it was not until the early 1980's that it became evident that their involvement in the unimolecular dissociations of both even- and odd-electron ions is a widespread phenomenon.

The formation of $CH_3CHCH_2CH_3^+$ rather than $CH_3CH_2CH_2CH_2^+$ by loss of $CH_3^{\bullet}$ from ionized n-pentane, $CH_3CH_2CH_2CH_2CH_3^{\bullet+}$, is illustrative of isomerization of the cation within an intermediate ion-dipole complex prior to dissociation. A stretching of the C2-C3 bond in the initial conventional isomer generates an ion-dipole complex of the form [$CH_3CH_2CH_2^+$ / $^{\bullet}CH_2CH_3$]. Within this complex, a $CH_3CH_2^{\bullet}$ mediated 1,2-H shift generates [$CH_3CHCH_3^+$ / $^{\bullet}CH_2CH_3$] which then goes on to generate $CH_3CH(CH_3)CH_2CH_3^{\bullet+}$ which serves as the immediate precursor for the loss of $CH_3^{\bullet}$. A characteristic property of the intermediate ion-neutral complexes is that they facilitate the formation of low-energy products.

The ion in an ion-neutral complex occupies a position between that of the solitary ion in the gas phase and its solvated counterpart in solution. Studies of ion-molecule complexes make it possible to establish the influence of a single "solvent" molecule on the rearrangement of the ion and this may provide a better understanding of the chemistry of ions in solution.

Direct experimental evidence that a given dissociation involves ion-dipole complexes as intermediates is often not available. However, when the final intermediate in a (complex) rearrangement reaction is an ion-dipole complex, the reaction is often associated with a very small kinetic energy release, that is a very narrow signal is observed in the MI spectrum of the ion. A case in point is the loss of H_2O from the distonic ion $CH_2CH_2OH_2^{\bullet+}$ where the final intermediate is the ion-dipole complex $CH_2{=}CH_2^{\bullet+}$ / H_2O. This reaction is associated with a kinetic energy release, $T_{0.5}$, of only ~ 0.2 meV whereas typical values for direct bond cleavage reactions from ions of conventional structure lie in the range 10-30 meV.

A more recently discovered class of ions closely related to ion-dipole species is that of the hydrogen-bridged radical cations (HBRC). These ion-molecule complexes form a challenging and fruitful area of research in the field of gas-phase ion chemistry. The identification of a H-bridged radical cation as a stable product ion is sometimes difficult : the ion may have isomers with closely similar reactivity and dissociation characteristics.

Formally HBRCs can be represented as proton-bound molecule-radical pairs $[M{\bullet\bullet\bullet}H^{+}{\bullet\bullet\bullet}R^{\bullet}]$, but they are better viewed as H-bridged ion-neutral complexes of the type $[MH^{+}{\bullet\bullet\bullet}R^{\bullet}]$ or $[M{\bullet\bullet\bullet}HR^{\bullet+}]$, with the bridging H closer to the partner of higher PA, where most of the stabilization energy is provided by ion-dipole attractions. The hydrogen bridge furnishes additional stabilization energy by c. 5 kcal/mol, but its main function is to direct the course of isomerization by allowing a facile proton transfer.

HBRCs are usually generated by elimination of a stable molecule from a molecular ion. An example reported in this thesis (Chapter 6) is the loss of CO from ionized dimethyloxalate, $CH_3O\text{-}C(=O)\text{-}C(=O)\text{-}OCH_3^{\bullet+}$. The experiments rule out a simple extrusion reaction yielding $CH_3O\text{-}C(=O)\text{-}OCH_3^{\bullet+}$, ionized methylcarbonate, but they are compatible with the formation of $CH_2{=}O{\bullet\bullet\bullet}H{\bullet\bullet\bullet}O{=}C\text{-}OCH_3^{\bullet+}$, an HBRC comprised of formaldehyde and an ionized carbene. Although the HBRC could be differentiated from its covalently bounded isomer, through its structure characteristic CID spectrum, the NR mass spectrum provided definitive evidence of its structure. As expected, and in contrast to ionized methylcarbonate, the H-bridged isomer does not survive neutralization.

The above H-bridged radical cation has also been invoked to explain the dissociation chemistry of ionized methyl glycolate, $HOCH_2$-C(=O)-$OCH_3^{\bullet+}$ [38]. The main dissociation route of the low-energy methyl glycolate ions is the loss of H-C=O$^{\bullet}$ which occurs via a double hydrogen transfer. The HBRC CH_2=O•••H•••O=C-$OCH_3^{\bullet+}$, generated as an intermediate, promotes the formaldehyde catalyzed conversion of HO-C-$OCH_3^{\bullet+}$ into H-C(=O)-$OCH_3^{\bullet+}$, a process which, unassisted by the molecule has a prohibitively high barrier. Once the formaldehyde molecule has performed its task, it becomes ionized so that it can donate a proton and be lost as H-C=O$^{\bullet}$. The catalytic step in the above rearrangement is an example of a process termed proton-transport catalysis by Böhme [39].

Such a catalysis is not only a key step in the dissociative rearrangement of oxygen-containing radical cations, as with ionized methyl glycolate, but it also occurs under certain conditions in bimolecular reactions. It was mentioned above that distonic radical cations are often more stable than their conventional counterparts and that they may be separated from those isomers by large barriers; see Figure 1.4 for the 1,2-H shift separating the conventional ion $CH_3OH^{\bullet+}$ from its distonic isomer $CH_2OH_2^{\bullet+}$.

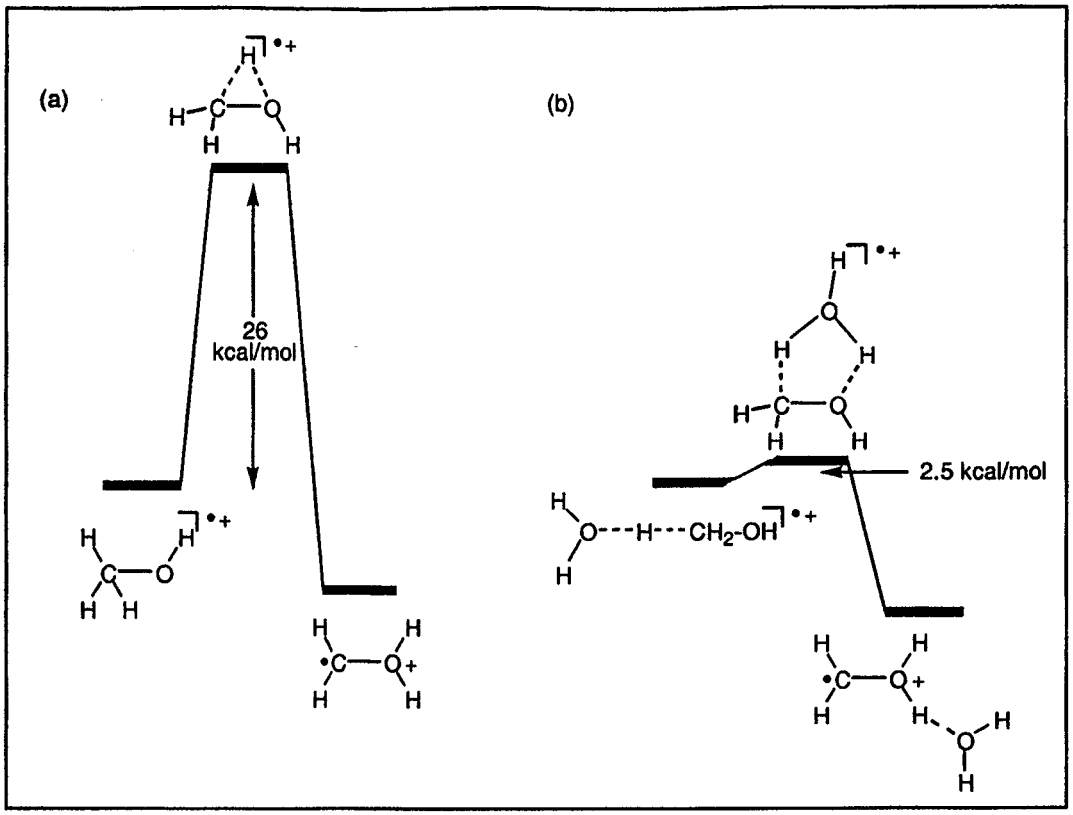

Figure 1.4. Energy diagram for (a) the unassisted 1,2-H shift isomerization $CH_3OH^{\bullet+}$ to $CH_2OH_2^{\bullet+}$ and (b) the rearrangement $CH_3OH^{\bullet+}$ to $CH_2OH_2^{\bullet+}$, catalyzed by water.

However, experiments and quantum chemical calculations show that interaction with a molecule of the correct basicity, such as water, greatly lowers the barrier, as depicted by item (b) in Figure 1.4. Thus the isomerization $CH_3OH^{\bullet+} \rightarrow CH_2OH_2^{\bullet+}$, which does not occur for the solitary ions, is greatly accelerated by the addition of water. That is the barrier, which for the unassisted reaction is 26 kcal/mol, is reduced to a mere 2.5 kcal/mol for the water catalyzed rearrangement. From detailed *ab initio* calculations [40], it follows that O•H•O and C•H•O hydrogen-bridged radical cations play a prominent role in this transformation. In more general terms the "catalysis" has been proposed [41] to take place when the proton affinity of the base B, lies between the proton affinity of [X-Y]$^{\bullet}$ at X and Y, according to :

$$[H\text{-}X\text{-}Y]^{\bullet+} + B \rightarrow [B\bullet\bullet\bullet H^{+}\bullet\bullet\bullet(X\text{-}Y)^{\bullet}] \rightarrow [B\bullet\bullet\bullet H^{+}\bullet\bullet\bullet(Y\text{-}X)^{\bullet}] \rightarrow B + [H\text{-}Y\text{-}X]^{\bullet+}$$

The isomerization of ionized methanol into the methylene oxonium ion is an example of a catalyzed 1,2-H transfer. An experimentally more challenging case is the molecule assisted isomerization of pyridine into its α-ylide isomer, reported in Chapter 4.

This type of catalysis is not restricted to a 1,2-H shift : as shown in Chapters 2 and 3, the enolization of ionized acetone and acetamide, whose unassisted isomerization requires a 1,3-H shift can also be realized in ion-molecule reactions, using benzonitrile as the base. However, as discussed in Chapter 3, the mechanisms associated with these two catalyzed enolization reactions are fundamentally different.

In summary, ion-dipole complexes and the related hydrogen-bridged radical cations open a wide field of challenging chemistry. These species play an important role in the chemistry of ions in the gas phase and this is mainly due to their flexibility and relatively large stability. Within such complexes, the components may rotate and undergo rearrangement or react together, new complexes being generated therefrom whose eventual decomposition may deliver products which show evidence for the rearrangement of atoms from remote positions of the original structure. Thus there is an increased number of degrees of freedom leading to a correspondingly longer lifetime for the intermediate, and hence higher probability that rearrangement processes occur.

References

[1] (a) H.E. Duckworth, *Mass Spectroscopy*, Cambridge University Press, London, **1958**; (b) S.H. Bauera, *J. Am. Soc. Mass Spectrom.*, **2001**, *12*, 975.

[2] R.W. Kiser, *Introduction to mass spectrometry and its applications*, Prentice Hall International Inc., London, **1965**.

[3] (a) A.G. Harrison, *Chemical Ionization Mass Spectrometry*, 2nd ed. CRC Press, Florida, **1992**; (b) J. Chapman, *Practical Organic Mass Spectrometry: A Guide for Chemical and Biochemical Analysis*, Wiley, New York, **1993**.

[4] R.G. Cooks, J.H. Beynon, R.M. Caprioli, G.R. Lester, *Metastable Ions*, Elsevier, Amsterdam, **1973**.

[5] B. Stevens, *Collisional Activation in Gases*, Pergamon Press, Oxford, **1967**.

[6] L. Radom, *Org. Mass Spectrom.* **1991**, *26*, 227.

[7] A.L. Burlingame, T.A. Baillie, P.J. Derrick, *Anal. Chem.* **1986**, *58*, 165R.

[8] J.C. Traeger in *Energetics of Organic Free Radicals*, J.A.M. Simoes, A. Greenberg, J.F. Liebman, Eds, Blackie Academic and Professional, London, **1996**.

[9] J.L. Holmes, *Org. Mass Spectrom.*, **1985**, *20*, 169.

[10] (a) T. Baer, J.A. Booze, *Advances in Classical Trajectory Methods* Vol. 2, W.L. Hase Ed., JAI Press Inc., Hampton Hill, **1994**; (b) T. Baer, W.L. Hase, *Unimolecular Reaction Dynamics, Theory and Experiments*, Oxford University Press, Oxford, **1996**; (c) L. Drahos, K. Vékey, *J. Mass Spectrom.* **2001**, *36*, 237, a modelling program for mass spectrometric fragmentations, *Mass Kinetics*, is available at http://www.chemres.hu/ms/masskinetics.

[11] (a) J.L. Holmes, J.K. Terlouw, *Org. Mass Spectrom.*, **1980**, *15*, 383; (b) J. Laskin, C. Lifshitz, *J. Mass Spectrom.*, **2001**, *36*, 459.

[12] K.M. Ervin, *Chem. Rev.*, **2001**, *101*, 391.

[13] (a) K.R. Jennings, *Int. J. Mass Spectrom. Ion Physics*, **1968**, *1*, 227; (b) W.F. Haddon, F.W. McLafferty, *J. Am. Chem. Soc.*, **1968**, *90*, 4745.

[14] P. Gerbaux, M. Barbieux-Flammang, J.K. Terlouw, R. Flammang, *Int. J. Mass Spectrom.* **2001**, *206*, 91.

[15] R.G. Cooks, *J. Mass Spectrom.* **1996**, *30*, 1216.

[16] (a) P. Gerbaux, V. Sciamanna, R. Flammang, M.-T. Nguyen, *J. Mass Spectrom.* **2001**, *36*, 97; (b) C. Aubry, J.L. Holmes, *J. Phys. Chem. A* **1998**, *102*, 6441; (c) G.A. McGibbon, P.C. Burgers, J.K. Terlouw, *Int. J. Mass Spectrom. Ion Processes* **1994**, *136*, 191.

[17] For a leading reference, see W. Koch, F. Mauin, D. Stahl, H. Schwarz, *Chimica*, **1985**, *39*, 276.

[18] For selected reviews see (a) C. Wesdemiotis, F.W. McLafferty, *Chem. Rev.*, **1987**, *87*, 485; (b) J.K. Terlouw, H. Schwarz, *Angew. Chem. Int. Ed. Engl.* **1987**, *26*, 805; (c) N. Goldberg, H. Schwarz, *Acc. Chem. Res.* **1994**, *27*, 34.

[19] P.C. Burgers, J.K. Terlouw in *A Specialist Periodical Report : Mass Spectrometry, Vol. 10*, Royal Society of Chemistry, Cambridge, **1989**.

[20] (a) S.G. Lias, J.E. Bartmess, J.F. Liebman, J.L. Holmes, R.O. Levin, W.G. Mallard, J. Phys. Chem. Ref. Data **17** (1988) Supplement 1; (b) S.G. Lias, E.P.L. Hunter, J. Phys. Chem. Ref. Data **27** (1998) No 3; (c) the NIST webbok at http://webbook.nist.gov.

[21] J.L. Holmes, F.P. Lossing, *Can. J. Chem.*, **1982**, *60*, 2365; see also the introduction of ref. 14a.

[22] N. Cohen, S.W. Benson, *Chem. Rev.*, **1993**, *93*, 2419.

[23] F.M. Benoit, A.G. Harrison, *J. Am. Chem. Soc.*, **1977**, *99*, 3980.

[24] (a) J.W. Larson, T.B. McMahon, *J. Am. Chem. Soc.*, **1982**, *104*, 6255; (b) M. Meot-Ner, *J. Am.Chem. Soc.*, **1984**, *106*, 1257.

[25] For leading references see : (a) H. Friedrichs, G.A. McGibbon, H. Schwarz, *Int. J. Mass Spectrom. Ion Processes*, **1996**, *1524*, 217; (b) F. Tureček, C.J. Cramer, *J. Am. Chem. Soc.* **1995**, *117*, 12243; (c) S. Hammerum, *Int. J. Mass Spectrom. Ion Processes* **1997**, *165/166*, 63; (d) P.E. Andersen, S. Hammerum, *Eur. Mass Spectrom.* **1995**, *1*, 499; (e) M. George, C.A. Kingsmill, D. Suh, J.K. Terlouw, J.L. Holmes, *J. Am. Chem. Soc.* **1994**, *116*, 7807; (f) P.M. Mayer, M.N. Glukhovstev, J.W. Gauld, L. Radom, *J. Am. Chem. Soc.* **1997**, *119*, 12889.

[26] *Computational Thermochemistry*, Ed. K.K. Irikura and D. Frurip, ACS Symposium Series No. 677, Washington, DC, **1998.**

[27] J.B. Foresman, A. Frisch, *Exploring Chemistry with Electronic Structure Methods*, 2nd Ed., Gaussian Inc., Pittsburgh, **1995-1996.**

[28] T.H. Dunning, P.J. Hay, *Methods of Electronic Structure Theory*, H.F. Schaefer (ed). Plenum Press, New York, **1977**, pp. 1-27.

[29] (a) M.S. Gordon, *Chem. Phys. Lett.* **1980**, *76*, 163; (b) M.M. Francl, W.J. Pietro, W.J. Hehre, J.S. Binkley, M.S. gordon, D.J. DFrees, J.A. Pople, *J. Chem. Phys.* **1982**, *77*, 3654.

[30] W.J. Hehre, L. Radom, P.v.R. Schleyer, J.A. Pople, *Ab Initio Molecular Orbital Theory*, Wiley, New York, **1986.**

[31] (a) R.J. Bartlett, *Ann. Rev. Phys. Chem.* **1981**, *32*, 59; (b) N. Oliphant, L. Adamowicz, *J. Chem. Phys.* **1991**, *95*, 6645.

[32] J.A. Pople, M. Head-Gordon, K. Raghavachari, *J. Chem. Phys.* **1987**, *87*, 5968.

[33] K. Raghavachari and L.A. Curtiss, in *Modern Electronic Structure Theory*, Ed. D.R. Yarkony, World Scientific, Singapore, **1995.**

[34] J.W. Ochterski, G.A. Petersson and J.A. Montgomery, *J. Chem. Phys.* **1996**, *104*, 2598.

[35] G.A. Petersson, D.K. Malick, W.G. Wilson, J.W. Ochterski, J.A. Montgomery, Jr. and M.J. Frisch, *J. Chem. Phys.* **1998**, *109*, 10570; (b) L.A. Curtiss, K. Raghavachari, P.C. Redfern and B.B. Stefanov, *J. Chem. Phys.* **1998**, *108*, 692; (c) J.A. Montgomery, Jr, M.J. Frisch, J.W. Ochterski, G.A. Petersson, K. Raghavachari and V.G. Zakrzewski, *J. Chem. Phys.* **1998**, *109*, 6505; (d) H.L. Schmider and A.D. Becke, *J. Chem. Phys.* **1998**, *109*, 8188; (e) P.M. Mayer, C.J. Parkinson, D.M. Smith and L. Radom, *J. Chem. Phys.*, **1998**, *108*, 604; (f) J.M.L. Martin, *Chem. Phys. Lett.* **1996**, *259*, 669; (g) M.W. Wong and L. Radom, *J. Phys. Chem. A.* **1998**, *102*, 2237.

[36] D. Feller and K.A. Petersson, *J. Chem. Phys.* **1998**, *108*, 154.

[37] L. Radom, W.J. Bouma, R.H. Nobes, B.F. Yates, *Pure and Appl. Chem.* **1984**, *56*, 1831.

[38] L.M. Fell, P.J.A. Ruttink, P.C. Burgers, M.A. Trikoupis, J.K. Terlouw, *Int. J. Mass Spectrom.* **2000**, *195/196*, 85.

[39] D.K. Böhme, *Int. J. Mass Spectrom. Ion Processes,* **1992**, *115*, 95.

[40] (a) J.W. Gauld, H.-E. Audier, J. Fossey, L. Radom, *J. Am. Chem. Soc.* **1996**, *118*, 6299; (b) J.W. Gauld, L. Radom, *J. Am. Chem. Soc.* **1997**, *119*, 9831; (c) A.J. Chalk, L. Radom, *J. Am. Chem. Soc.* **1997**, *119*, 7573; (d) A.J. Chalk, L. Radom, *J. Am. Chem. Soc.* **1999**, *121*, 1574.

[41] H.-E. Audier, D. Leblanc, P. Mourgues, T.B. McMahon, S. Hammerum *J. Chem. Soc. Chem. Commun.* **1994**, 2329.

Chapter 2

Enolization of Gaseous Acetone Radical Cations : Catalysis by a Single Base Molecule

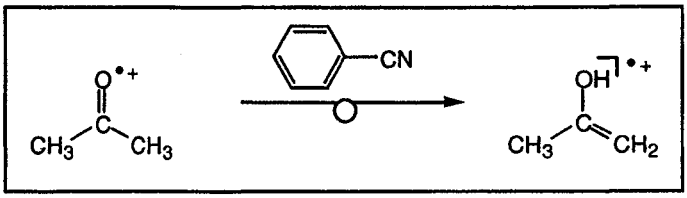

Under conditions of chemical ionization, the acetone radical cation rearranges to its more stable enol isomer by an ion-molecule reaction with a suitable reagent, such as benzonitrile. The initially formed [acetone$^{\bullet+}$•••benzonitrile] adduct isomerizes, by way of proton-transport catalysis, to a stable complex of benzonitrile with the enol ion which may dissociate.

The work described here has been published previously in an article under the same title: M.A. Trikoupis, J.K. Terlouw and P.C. Burgers, J. Am. Chem. Soc. 1998, 120, 12131-12132.

It is well known that simple neutral enols are thermodynamically less stable than their keto isomers [1]. For example, experiments in the gas-phase show that the enol of acetone is 14 ± 2 kcal/mol [2] less stable than acetone itself, in agreement with *ab initio* calculations [3]. In solution, ketonization can be catalyzed by either acid or base and thus, enols are usually present in very low concentrations.

Upon one-electron oxidation a reversal of stability takes effect [4]; that is, for radical cations it is usually the enol form which is the more stable isomer. For example, experiments show that the gaseous acetone radical cation is 14 kcal/mol [5] *less* stable than its enol isomer, paralleling observations from theory [3a,6]. For the solitary ions a large barrier (37 kcal/mol [7]) for the 1,3-hydrogen shift prevents enolization, and thus once formed acetone radical cations retain their structure, even when activated [8]. The energy diagram for the keto-enol acetone radical cation tautomerization is given in Figure 2.1. Because of the relatively weak C-C bond in ionized acetone (19 kcal/mol [9], compared to 87 kcal/mol [9] for the neutral), even high energy acetone ions do not isomerize; rather they dissociate to CH_3-C=O$^+$ + $CH_3^{\bullet}$.

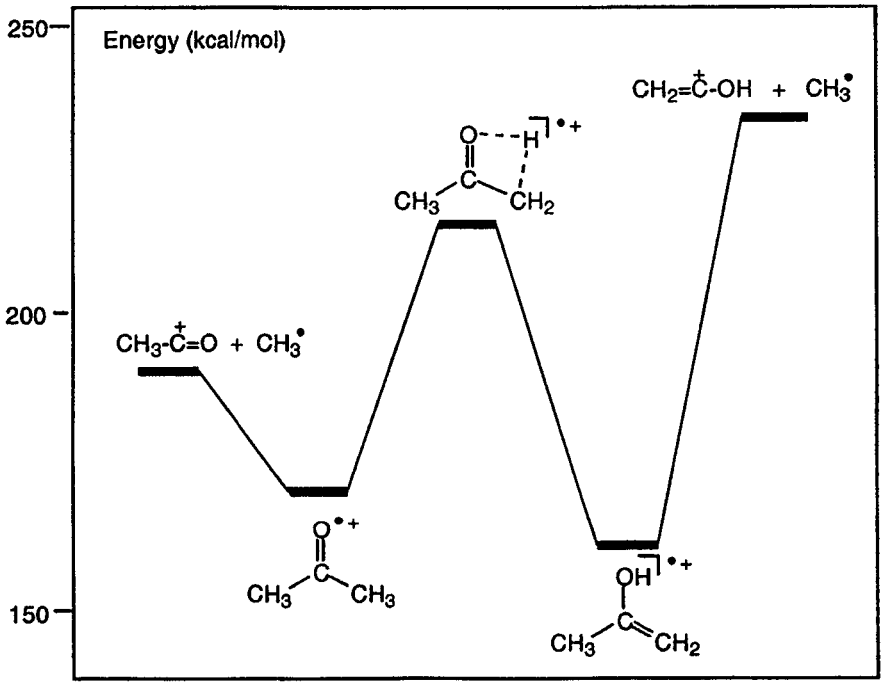

Figure 2.1. Energy diagram for the acetone keto and enol radical cations. Experimental data taken from references 5,7 and 9.

Recently, some elegant experimental [10] and theoretical studies [11] have reported a mechanism by which a gaseous conventional radical cation $[H\text{-}X\text{-}Y]^{\bullet+}$ (e.g., X = CH_2, Y = OH) may rearrange to a more stable distonic isomer $[X\text{-}Y\text{-}H]^{\bullet+}$ via a two-step proton-transfer through interaction with an appropriate base B, according to

$$[H\text{-}X\text{-}Y]^{\bullet+} + B \rightarrow B{\bullet\bullet\bullet}H^{+}{\bullet\bullet\bullet}[X\text{-}Y]^{\bullet} \rightarrow B{\bullet\bullet\bullet}H^{+}{\bullet\bullet\bullet}[Y\text{-}X]^{\bullet} \rightarrow B + \{X\text{-}Y\text{-}H]^{\bullet+} \quad (1)$$

This process has been termed "proton-transport catalysis" [10a]. It appears that it not only occurs under certain conditions in bimolecular reactions (see below), but that it also is a key step in the dissociation of a variety of oxygen-containing radical cations [12]. Gauld and Radom have evaluated conditions for efficient proton-transport catalysis [11b]. From thermochemical considerations they conclude that efficient catalysis will take place, see Eq. 1, when the proton affinity (PA) of the base B lies between the PA of [X-Y] at X and at Y. If the PA [B] is significantly lower than the PA [X-Y] at X, the first step in Eq. 1 will not take place. If on the other hand, PA [B] is significantly larger than PA [X-Y] at X, then the intermediate complex $B{\bullet\bullet\bullet}H^{+}{\bullet\bullet\bullet}[X\text{-}Y]^{\bullet}$ will dissociate to $[X\text{-}Y]^{\bullet}$ and HB^{+} via a unidirectional proton-transfer. In effect, if PA [B] is intermediate, the barrier becomes negative relative to the separated reactants and products and the base successfully catalyzes the isomerization [11b]. In this chapter evidence is presented that such a proton-transport catalysis can also accommodate keto-to-enol ionic tautomerizations. Applying the above arguments to the model keto compound ionized acetone, efficient enolization can take place when a base is chosen such that its PA lies between the PA of the radical $^{\bullet}CH_2C(=O)CH_3$ at C and at O. From ΔH_f [$^{\bullet}CH_2C(=O)CH_3$] = -12 ± 1.5 kcal/mol [13] and the heats of formation of ionized acetone (172 kcal/mol [9]), its enol (158 kcal/mol [9]), and H^{+} (366 kcal/mol [9]), PA [B] should lie between 182 kcal/mol and 196 kcal/mol. Interestingly then, acetone itself, having PA = 197 kcal/mol [14], would be a suitable candidate.

Acetone was introduced into the chemical ionization source of the McMaster VG ZAB-R mass spectrometer [14] to a maximum indicated pressure of 5 x 10^{-5} Torr. Unfortunately, under these conditions the acetone radical cations readily and preferentially undergo proton-transfer to acetone (self-protonation) to produce $CH_3C^{+}(OH)CH_3$ (ΔH_f = 117 kcal/mol [9]) and $^{\bullet}CH_2C(=O)CH_3$ (ratio *m/z* 58 : *m/z* 59 = 0.28), a reaction which is

exothermic by 15 kcal/mol (ΔH_f [acetone] = -52 kcal/mol [9]). In addition, an intense signal was found for the proton-bound dimer, but only a small signal was observed for the dimer radical cation (ratio *m/z* 116 : *m/z* 117 = 0.07) which would serve as a precursor for the enol of acetone, see Eq. 1. Nevertheless, the collision-induced dissociation (CI) [14] mass spectrum of the remaining *m/z* 58 ions revealed that some, but not complete, enolization had taken effect.

We decided to search for a better base, i.e., one that does not undergo self-protonation and which has the right PA. In addition, the ionization energy (IE) of the base should not be much lower than that for acetone, otherwise ionized acetone will be neutralized by charge exchange. It appeared that benzonitrile might be a more successful candidate, that is, it has the right PA (196 kcal/mol [9]), self-protonation of benzonitrile (9.62 eV [9]) is not much lower than that of acetone (9.71 eV [9]). (Note also that protonation of acetone by ionized benzonitrile is endothermic (by 6 kcal/mol)). Indeed, when C_6H_5CN is introduced into the chemical ionization source (via a quartz probe at room temperature) to a maximum indicated pressure of 1 x 10^{-4} Torr, the ratio *m/z* 104 : *m/z* 103 was 0.23, showing that only 15 % self-protonation takes effect. Other peaks observed in the mass spectrum correspond to dissociation products of ionized benzonitrile itself (*m/z* 39, *m/z* 63 and *m/z* 76), to adducts of these ionic products and benzonitrile (*m/z* 142, *m/z* 166 and *m/z* 179), and to the proton bound dimer (*m/z* 207); also, a relatively intense peak is observed for the dimer radical cation at *m/z* 206. Peaks in the region 54-61 were absent. Next, a small amount of acetone was injected into the ion source, and a significant peak at *m/z* 58 appeared together with a small peak at *m/z* 59 (*m/z* 58 : *m/z* 59 = 3). Other peaks appear at *m/z* 146 (a complex of C_6H_5CN and CH_3-C=O$^+$), at *m/z* 162 (the proton-bound dimer of benzonitrile and acetone), and at *m/z* 204 (a complex of C_6H_5CN, acetone and CH_3-C=O$^+$). Most importantly, and in sharp contrast to the chemical ionization experiments using acetone only, a relatively intense peak for the ["acetone"•••C_6H_5CN]$^{\bullet+}$ dimer radical cation was now clearly present at *m/z* 161. The CID mass spectrum of the *m/z* 58 ions generated in the ion source is shown as item c in Figure 2.2.

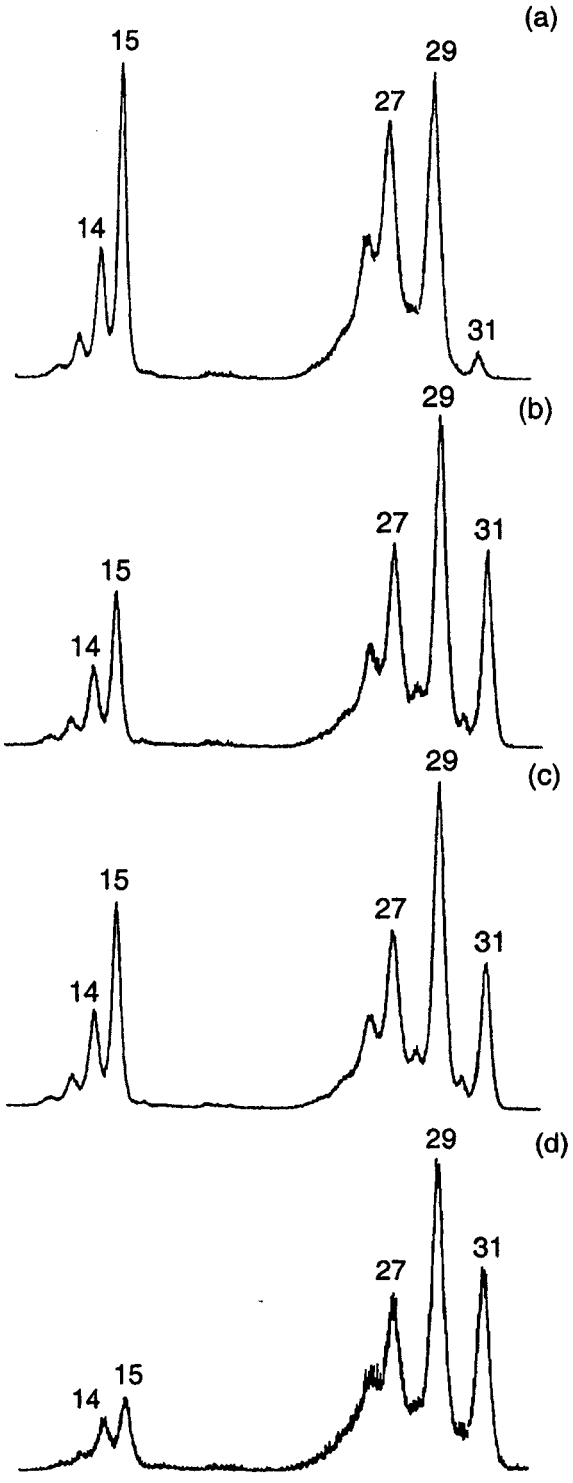

Figure 2.2. Collision-Induced Dissociation mass spectra of (a) acetone, reference; (b) enol of acetone, reference; (c) *m/z* 58 in the benzonitrile chemical ionization mass spectrum of acetone; (d) the collisionally formed *m/z* 58 from the ["acetone"$^{\bullet+}$ ••• benzonitrile] adduct.

The CID mass spectra of the acetone keto and enol ions are well known [8]; our (partial) reference spectra are shown in Figure 2.2a and 2.2b respectively, and they are characteristically different, especially in the region *m/z* 24 - *m/z* 31 [8]. These spectra leave no doubt that the original acetone keto ion has been converted, and virtually completely so, to its enol counterpart.

The CID mass spectra of the ["acetone"•••C_6H_5CN]$^{•+}$ complex at *m/z* 161 contains two intense peaks of almost equal intensity at *m/z* 58 and *m/z* 104 (protonated benzonitrile). The CID mass spectrum of these *m/z* 58 ions, as recorded in an MS/MS/MS experiment [16] and shown in Figure 2.2d, reveal that they have the enol structure [17]. This experiment clearly shows that the initially formed [acetone$^{•+}$•••C_6H_5CN] adduct has rapidly converted into a [enol acetone$^{•+}$•••C_6H_5CN] complex, probably the hydrogen-bridged [18] structure [CH_2=C(CH_3)-O•••H•••NC-C_6H_5]$^{•+}$. *This constitutes definitive evidence that benzonitrile catalyzes the enolization.*

Finally we note that if the PA of the base is significantly out of range, enolization does not take effect, as predicted by Gauld and Radom [11b]. For example, for the acetaldehyde$^{•+}$/vinyl alcohol$^{•+}$ tautomerization, the PA of the base should lie between 170 and 185 kcal/mol [19] (or 174 and 189 kcal/mol [20]); as predicted, interaction of ionized acetaldehyde with benzonitrile (PA = 196 kcal/mol) leads to protonated benzonitrile only, and the small amount of remaining *m/z* 44 ions have retained the acetaldehyde structure.

References

[1] Z. Rappoport, *The Chemistry of Enols*, Wiley, New York **1990**.

[2] J.L. Holmes, F.P. Lossing, *J. Am. Chem. Soc.* **1982**, *104*, 2648.

[3] (a) F. Tureček, C.J. Cramer, *J. Am. Chem. Soc.* **1995**, *117*, 12243 ; (b) D. Lee, C.K. Kim, B.S. Lee, I. Lee, B.C. Lee, *J. Comput. Chem.* **1997**, *18*, 56.

[4] G. Frenking, N. Heinrich, J. Schmidt, H. Schwarz, *Z. Naturforsch.* **1982**, *37b*, 1597.

[5] J.L. Holmes, F.P. Lossing, *J. Am. Chem. Soc.* **1980**, *102*, 1591.

[6] W.J. Bouma, J.K. MacLeod, L. Radom, *J. Am. Chem. Soc.* **1980**, *102*, 2246.

[7] (a) D.H. Williams, *Acc. Chem. Res.* **1977**, *10*, 280; (b) P.C. Burgers, J.L. Holmes, *Org. Mass Spectrom.* **1982**, *17*, 123.

[8] C.C. van de Sande, F.W. McLafferty, *J. Am. Chem. Soc.* **1975**, *97*, 4617.

[9] S. Lias, J.E. Bartmess, J.F. Liebman, J.L. Holmes, R.D. Levin, W.G. Mallard, *J. Phys. Chem. Ref. Data* **1988**, *17*, Supplement 1.

[10] (a) D.K. Bohme, *Int. J. Mass Spectrom. Ion Processes* **1992**, *115*, 95 ; (b) P. Mourgues, H.E. Audier, D. Leblanc, S. Hammerum, *Org. Mass Spectrom.* **1993**, *28*, 1098; (c) H.E. Audier, D. Leblanc, P. Mourgues, T.B. McMahon, S. Hammerum, *J. Chem. Soc. Chem. Commun.* **1994**, 2329; (d) H.E. Audier, J. Fossey, P. Mourgues, T.B. McMahon, S. Hammerum, *J. Chem. Phys.* **1996**, *100*, 18380.

[11] (a) J.W. Gauld, H.E. Audier, J. Fossey, L. Radom, *J. Am. Chem. Soc.* **1996**, *118*, 6299; (b) J.W. Gauld, L. Radom, *J. Am. Chem. Soc.* **1987**, *119*, 9831.

[12] P.J.A. Ruttink, P.C. Burgers, L.M. Fell, J.K. Terlouw, *J. Phys. Chem. A* **1998**, *102*, 2976 and references therein.

[13] J.L. Holmes, F.P. Lossing, J.K. Terlouw, *J. Am. Chem. Soc.* **1986**, *108*, 1086.

[14] H.F. van Garderen, P.J.A. Ruttink, P.C. Burgers, G. McGibbon, J.K. Terlouw, *Int. J. Mass Spectrom. Ion Processes* **1992**, *121*, 159.

[15] From $\Delta H_f [C_6H_5CN]^{\bullet+} = 274$ kcal/mol [9], $\Delta H_f [C_6H_5CN] = 52$ kcal/mol [9], $\Delta H_f [C_6H_5CNH^+] = 222$ kcal/mol [9], and $\Delta H_f [C_6H_4CN]^{\bullet} = 111$ kcal/mol; the latter value was obtained using the benzene C-H bond dissociation energy of 111 kcal/mol [9] and $\Delta H_f [H]^{\bullet} = 52$ kcal/mol [9].

[16] G.A. McGibbon, P.C. Burgers, J.K. Terlouw, *Int. J. Mass Spectrom. Ion Processes* **1994**, *191*, 191.

[17] The smaller intensity of the peaks at *m/z* 12-15 is due to the lower collisional energy.

[18] (a) P.C. Burgers, J.K. Terlouw in *Specialist Periodical Reports : Mass Spectrometry*, M.E. Rose Ed., The Royal Society of Chemistry, London **1989**, Vol. 10, Chapter 2; (b) J.S. Splitter in *Applications of Mass Spectrometry to Organic Stereochemistry*, J.S. Splitter, F. Tureček Eds., VCH, Weinheim **1994**, Chapter 3.

[19] From $\Delta H_f [CH_3C(H)=O]^{\bullet+} = 196$ kcal/mol [9], $\Delta H_f [CH_2=C(H)OH]^{\bullet+} = 181$ kcal/mol [9] and $\Delta H_f [^{\bullet}CH_2\text{-}C(H)=O] = 0.2$ kcal/mol [13].

[20] Using $\Delta H_f [^{\bullet}CH_2\text{-}C(H)=O] = 4.0$ kcal/mol from P.M. Mayer, M.N. Glukhovtsev, J.W. Gauld, L. Radom, *J. Am. Chem. Soc.* **1997**, *119*, 12889.

NOTE TO USERS

Page(s) missing in number only; text follows. Page(s) were scanned as received.

48, 76, 98, 168, 196

Page(s) not included in the original manuscript and are not available from the author or university. The manuscript was scanned as received.

This reproduction is the best copy available.

Chapter 3

The Benzonitrile Assisted Enolization of the Acetone and Acetamide Radical Cations : Proton-Transport Catalysis versus an Intermolecular $H^{+/\bullet}$ Transfer Mechanism

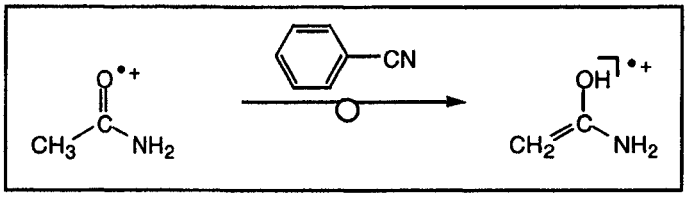

The acetamide radical cation, $CH_3C(=O)NH_2^{\bullet+}$, can be induced to rearrange into its more stable enol isomer, $CH_2=C(OH)NH_2^{\bullet+}$, by an ion-molecule interaction with benzonitrile, $C_6H_5C\equiv N$, under conditions of chemical ionization. (This enolization does not occur unassisted because of a prohibitively high energy barrier : 26 kcal/mol, from a CBS-QB3 calculation.) The initially formed $[C_6H_5C\equiv N\bullet\bullet\bullet acetamide]^{\bullet+}$ adduct ion isomerizes to a stable hydrogen bridged radical cation $[C_6H_5C\equiv N\bullet\bullet\bullet H\text{-}O\text{-}C(NH_2)=CH_2]^{\bullet+}$ en route to its dissociation into the enol ion. Multiple collision and deuterium labeling experiments on the acetamide/benzonitrile and the previously reported acetone/benzonitrile systems, indicate that the acetone ion enolizes via a base-catalyzed 1,3-proton shift ("proton-transport catalysis") but that a different mechanism must be operative in the acetamide system. *Ab initio* and density functional theory calculations at the PMP3//RHF/D95** and PMP3//B3LYP/D95** level of theory support a mechanism which can be described as a consecutive $H^+/H^\bullet$ transfer between the partners of the $[C_6H_5C\equiv N^{\bullet+}\bullet\bullet\bullet acetamide]$ encounter complex. The calculations provide a rationale for the observed isotope effects and lead to a tentative explanation for the differences in interaction of the title ions with benzonitrile.

The work described here has been published previously in an article under the same title: M.A. Trikoupis, P.C. Burgers, P.J.A. Ruttink, J.K. Terlouw, Int. J. Mass Spectrom. (Nico Nibbering Issue), 2001, 210/211, 489-501.

Introduction

For years biochemists and chemists have been studying proton exchange in amides, peptides and proteins in solution [1]. This has also been the topic of several gas-phase studies [2] aimed at evaluating the number of sites that may be involved in proton transfer within a gaseous species and at differentiating isomers. Recently, a number of elegant experimental and theoretical studies [3] have reported mechanisms by which a gaseous conventional radical cation $[H\text{-}X\text{-}Y]^{\bullet+}$ isomerizes into its more stable distonic isomer $[X\text{-}Y\text{-}H]^{\bullet+}$ via interaction with a single solvent molecule B. One prominent example concerns X = CH_2 and Y = OH, that is the α-distonic ion $[CH_2OH_2]^{\bullet+}$. This ion is c. 7 kcal/mol more stable than its isomer of conventional structure, $[CH_3OH]^{\bullet+}$, but the two isomers do not interconvert because the 1,2-H shift involved imposes a barrier of 26 kcal/mol. However a molecule of water (B) catalyzes this shift and promotes a smooth transformation of $[CH_3OH]^{\bullet+}$ into $[CH_2OH_2]^{\bullet+}$ [3b]. From detailed *ab initio* calculations [3c-f] it follows that O•H•O and C•H•O hydrogen-bridged radical cations play a prominent role in this transformation. In more general terms the "catalysis" has been proposed [3d] to take place when the proton affinity (PA) of the base B, lies between the PA of [X-Y] at X and Y, according to :

$$B + [H\text{-}X\text{-}Y]^{\bullet+} \rightarrow B\bullet\bullet\bullet H^{+}\bullet\bullet\bullet[X\text{-}Y]^{\bullet} \rightarrow B\bullet\bullet\bullet H^{+}\bullet\bullet\bullet[Y\text{-}X]^{\bullet} \rightarrow B + [H\text{-}X\text{-}Y]^{\bullet+} \qquad (1)$$

A similar mechanism has been proposed for the transport of methyl cations [4]. In a recent computational study, Radom et al [3f], using the G2** and G2(ZPE=MP2) methods investigated the catalysis of proton and methyl cation transport reactions. For proton-transport catalysis it was shown that when PA[B] is intermediate, the barrier becomes negative relative to the separated reactants and products and the base successfully catalyzes the isomerization. If the PA of B is lower than the PA of $[X\text{-}Y]^{\bullet}$ at X, then formation of the first complex cannot take place. However, if the PA of B is higher than the PA of $[X\text{-}Y]^{\bullet}$ at Y, the complex initially formed dissociates into BH^{+} and $[X\text{-}Y]^{\bullet}$. The same holds true for methyl cation transfers but it is noted that the dipole moment of the base plays a significant role in the catalysis; the intermediate complexes formed are stabilized by strong electrostatic interactions when the base has a significant dipole moment.

This catalysis not only works for 1,2-H transfers [3], it also operates on 1,3-H transfers [5]. One example is the enolization of acetone radical cations [5b] which readily occurs when benzonitrile is used as the base. Further, in a recent FT-ICR study, Audier and co-workers [5c] demonstrated that acetone catalyzes the enolization of the acetophenone radical cation, $[C_6H_5C(=O)CH_3]^{\bullet+}$. This is an intriguing system where the catalyzed transfer follows a different route from the unimolecular isomerization : a 1,3-H transfer occurs rather than two 1,4-H shifts. In this context, it is of interest to note that some 20 years ago, Nibbering and co-workers [6] elegantly demonstrated that the loss of $CH_3^{\bullet}$ from o-hydroxybutyrophenone is preceded by an **intra**molecular "proton-transport catalysis" reaction involving the ortho OH-group as the catalyst for the observed enol to keto isomerization.

Inspired by these findings we set out to examine the "single solvent molecule assisted" isomerization of ionized acetamide $[CH_3C(=O)NH_2]^{\bullet+}$ into its more stable enol form $[CH_2=C(OH)NH_2]^{\bullet+}$. We chose this system because preliminary considerations led us to believe that the acetamide ion would behave in much the same way as the acetone radical cation [5b]. That is, with benzonitrile the acetamide ion should also easily enolize via proton-transport catalysis. However, it quickly became clear, see below, that enolization of the acetamide ion proceeds via an entirely different mechanism.

Results and Discussion

The unimolecular chemistry of the acetamide ion and its enol and iminol counterparts

The acetamide radical cation $CH_3C(=O)NH_2^{\bullet+}$, $\mathbf{1}^{\bullet+}$, has two stable hydrogen shift isomers, the enol ion $CH_2=C(OH)NH_2^{\bullet+}$, $\mathbf{1a}^{\bullet+}$ and the iminol ion $CH_3C(OH)=NH^{\bullet+}$, $\mathbf{1b}^{\bullet+}$. For ions $\mathbf{1}^{\bullet+}$ and $\mathbf{1a}^{\bullet+}$, Schwarz et al. [2b], in an early *ab initio* study, found the enol ion to be more stable than its keto counterpart, by 16 kcal/mol. At this level of theory, MP3/6-31G(d,p)//HF/3-21G+ZPVE, we found the iminol ion $\mathbf{1b}^{\bullet+}$ to lie higher in energy than both its enol and its keto counterpart, by 28 and 12 kcal/mol respectively. These values agree remarkably well with those obtained from the more sophisticated G2 and CBS-QB3 procedures, see Table 3.1.

Table 3.1. CBS-QB3 and G2 derived enthalpies (298 K, kcal/mol) for ions and neutrals associated with the isomerization and dissociation of the acetamide radical cation.

Species		CBS-QB3	G2	Exp. [12a]
$CH_3C(=O)NH_2^{\bullet+}$	**1**$^{\bullet+}$	168.5	169	165
$CH_2=C(OH)NH_2^{\bullet+}$	**1a**$^{\bullet+}$	152	153	--
$CH_3C(OH)=NH^{\bullet+}$	**1b**$^{\bullet+}$	180	180	--
TS (**1**$^{\bullet+}$ → **1a**$^{\bullet+}$)		194	--	--
TS (**1**$^{\bullet+}$ → **1b**$^{\bullet+}$)		210.5	--	--
TS (**1a**$^{\bullet+}$ → **1b**$^{\bullet+}$)		213.5	--	--
$CH_2NH_3^{\bullet+} + CO$		176.5	176.5	175
$CH_3C{=}O^+ + NH_2^{\bullet}$		203	203	203.5
$NH_2C{=}O^+ + CH_3^{\bullet}$ [b]		199.5	200	196
$CH_3C(OH)NH_2^+$		105	102.5	103
$^{\bullet}CH_2C(=O)NH_2$		-10	-10.5	--
$CH_3C(=O)NH^{\bullet}$ [a]		3	--	--
$CH_3C(=O)NH_2$	**1**	-56.5	-58	-57
$CH_2=C(OH)NH_2$	**1a**	-31.5	-32	--
$CH_3C(OH)=NH$	**1b**	-42.5	-42.5	--

[a] This calculation suffered from a spin contamination ($<s^2>=0.89$).
[b] using ΔH_f [$NH_2C{=}O^+$] = 161 kcal/mol, see ref. 12c.

From Table 3.1, it follows that the tautomeric ions are separated by high energy barriers. This is in line with the detailed experimental observations of Schwarz et al. [2b] who showed that the keto and enol ions **1**$^{\bullet+}$ and **1a**$^{\bullet+}$ have characteristically different metastable ion (MI) and collision-induced dissociation (CID) spectra. In brief, the MI spectrum of **1**$^{\bullet+}$ is dominated by a rearrangement ion at *m/z* 31, $CH_2NH_3^{\bullet+}$, whereas the enol ion **1a**$^{\bullet+}$ largely dissociates into *m/z* 44, $NH_2C{=}O^+$. A characteristic feature of the CID spectrum of **1a**$^{\bullet+}$, compare Figure 3.1a and 3.1c, is the prominent *m/z* 42 $CH_2{=}C{=}O^{\bullet+}$ ion, generated by loss of NH_3.

So far, no experimental observations have been reported on the iminol ion, $CH_3C(OH)=NH^{\bullet+}$, **1b**$^{\bullet+}$. Considering that ionized formamide's iminol counterpart, ionized formimidic acid, can cleanly be generated from N-formylhydrazone [2a], we decided to examine the N-acetyl-acetichydrazone **I**, as a precursor to **1b**$^{\bullet+}$. Indeed, the 70 eV EI mass spectrum of **I** shows a prominent peak at *m/z* 59 which could correspond to iminol ions generated via a McLafferty type rearrangement :

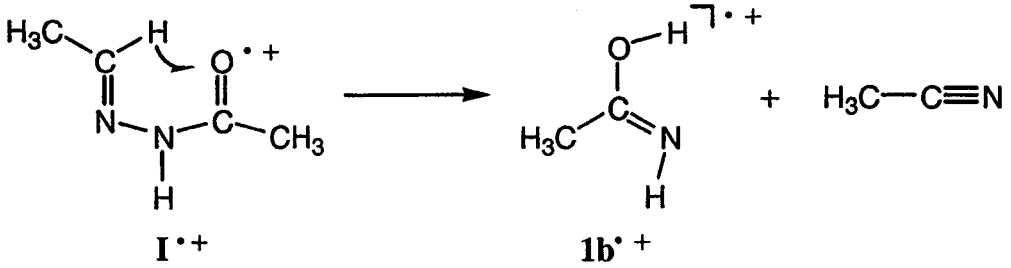

I$^{\bullet+}$ **1b**$^{\bullet+}$

EI ionization of N-hydroxymethylacetamide, **II**, also yields *m/z* 59 ions, which again could be ions **1b**$^{\bullet+}$ generated by loss of $CH_2=O$ in a McLafferty type rearrangement:

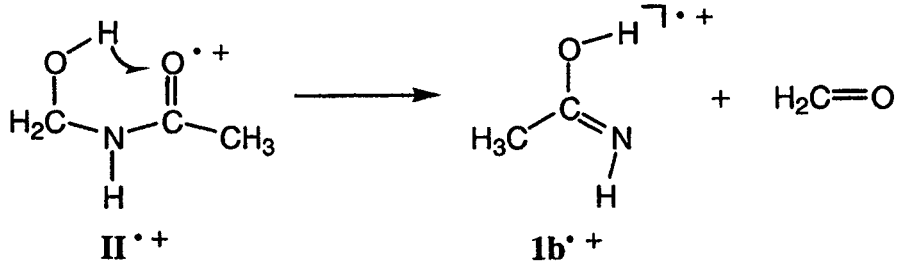

II$^{\bullet+}$ **1b**$^{\bullet+}$

The CID spectra of the *m/z* 59 ions from the above precursor molecules were obtained and found to be identical within experimental error, see Figure 3.1b for a representative spectrum. However, this spectrum is also very close to that of the keto ion **1**$^{\bullet+}$, compare Figures 3.1a and 3.1b. This raises the question whether it is the keto ion which is generated in the above dissociations. One rationalization would be that en route to the losses of $CH_3C\equiv N$ and $CH_2=O$, these neutral species lower the high barrier for the exothermic ketonization, see Table 3.1, of the incipient iminol ions by an intramolecular proton-transport catalysis process [13].

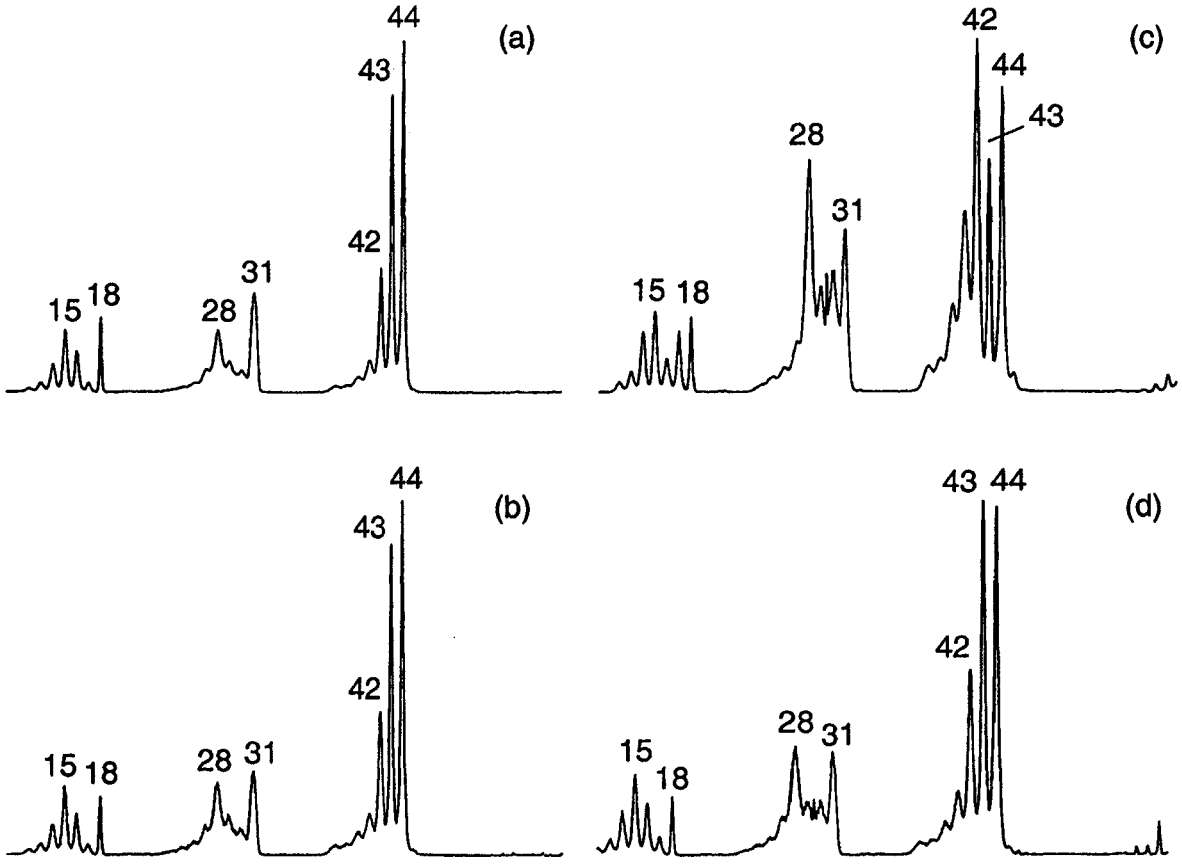

Figure 3.1. 8 keV Collision-Induced Dissociation (CID) mass spectra of : (a) acetamide; (b) iminol of acetamide; (c) enol of acetamide; (d) *m/z* 59 ions generated in the benzonitrile chemical ionization mass spectrum of acetamide.

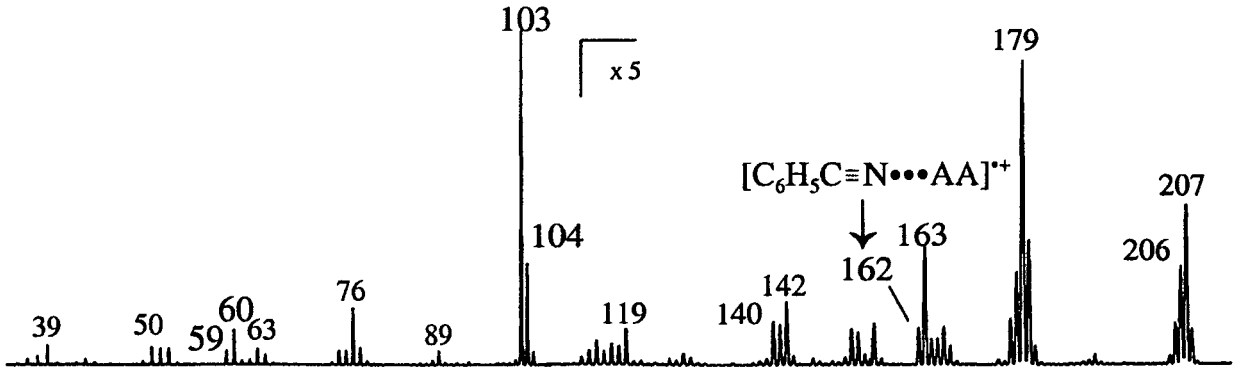

Figure 3.2. Chemical Ionization (CI) mass spectrum of the benzonitrile/acetamide system.

However, this is probably not the case since the closely similar MI spectra of the *m/z* 59 ions from the two precursor molecules are uniquely different from those of the keto and the enol isomers. These spectra are dominated by *m/z* 43 ($CH_3C{=}O^+$) and *m/z* 44 ($NH_2C{=}O^+$) ions of equal abundance. This is readily understandable considering the calculated energy level of TS (**1b**$^{\bullet+}$ → **1**$^{\bullet+}$) vis à vis those of the dissociation products $CH_3C{=}O^+ + {}^{\bullet}NH_2$ and $NH_2C{=}O^+ + {}^{\bullet}CH_3$, see Table 3.1. The similarity between the CID spectra is therefore probably due to post-collisional isomerization of the iminol ion into energy-rich keto ions.

Thus, while enolization of the keto ions can easily be monitored by CID experiments, their iminolization cannot be detected. However, it is not expected that iminolization occurs in our chemical ionization type experiments, because the reaction is endothermic and associated with a high barrier, see Table 3.1.

The benzonitrile assisted enolization of ionized acetamide, experimental observations

As argued in the previous section, the unassisted enolization of the acetamide ion **1**$^{\bullet+}$ does not occur. However, the proton-transport catalysis criterion represented by Eqn (1) predicts that efficient enolization of ions **1**$^{\bullet+}$ should take place in an ion-molecule encounter complex with a neutral base whose PA lies between the PA of ${}^{\bullet}CH_2C(=O)NH_2$ at C and at O.

From the ΔH_f values for $[{}^{\bullet}CH_2C(=O)NH_2]$ = - 10 kcal/mol (Table 3.1), $[CH_3C(=O)NH_2^{\bullet+}]$ = 165 kcal/mol [12a], $[CH_2{=}C(OH)NH_2^{\bullet+}]$ = 152 kcal/mol (Table 3.1) and $[H^+]$ = 366 kcal/mol [12a], the PA values for protonation of ${}^{\bullet}CH_2C(=O)NH_2$ at C and at O are estimated to be 191 and 204 kcal/mol respectively.

Benzonitrile, a suitable base for the enolization of the acetone ion [5b], also appeared to be a candidate for the enolization of ionized acetamide : it has a PA, 196 kcal/mol [12b], that lies in the above mentioned range and it does not readily self-protonate (a process that is estimated to be endothermic by 7 kcal/mol) [14]. Further, benzonitrile and acetamide have similar ionization energies (IE), 9.62 and 9.65 eV [12a], and substantial dipole moments, 4.2 and 3.8 Debye respectively [15]. As a result, in our type of chemical ionization experiment, see below, the ion-molecule encounter complexes between benzonitrile and acetamide (AA),

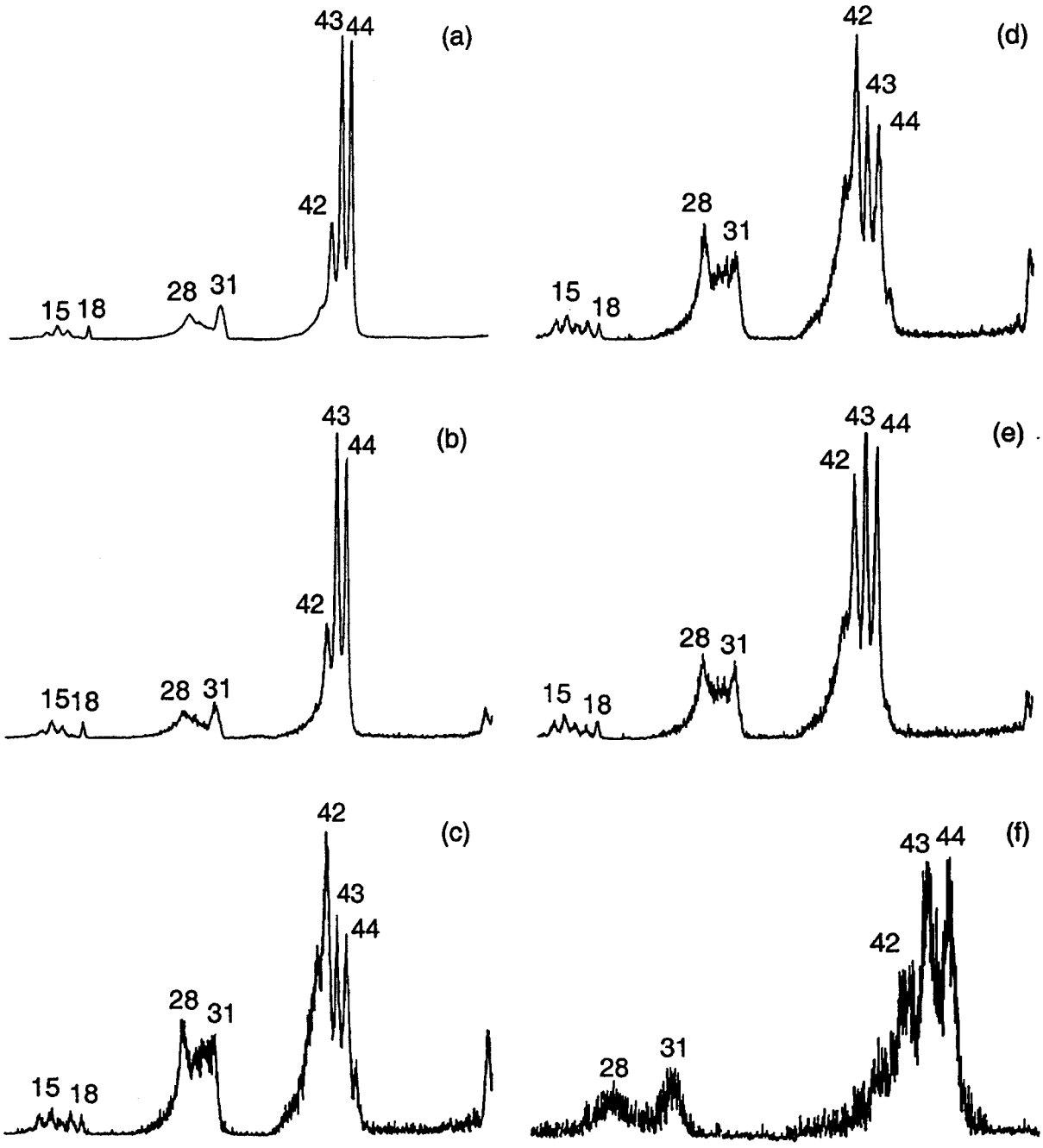

Figure 3.3. 4 keV Collision-Induced Dissociation mass spectra (CID) of : (a) acetamide ; (b) iminol of acetamide; (c) enol of acetamide ; (d) the metastably generated *m/z* 59 ions from the $[C_6H_5CN\bullet\bullet\bullet\text{"acetamide"}]^{+}$ complex; (e) the collisionally formed *m/z* 59 ions from the $[C_6H_5CN\bullet\bullet\bullet\text{"acetamide"}]^{+}$ complex ; (f) the *m/z* 59 ions generated from NR of the *m/z* 162 ions.

are likely to be of two types, *viz.* $[C_6H_5C{\equiv}N{\bullet\bullet\bullet}AA^{\bullet+}]$ and $[C_6H_5C{\equiv}N^{\bullet+}{\bullet\bullet\bullet}AA]$ which may interconvert via charge transfer (CT).

Benzonitrile, when introduced into the chemical ionization (CI) source to an indicated pressure of 6 x 10^{-5} Torr, shows little self-protonation : *m/z* 103 ($M^{\bullet+}$) : *m/z* 104 ($M+H^+$) = 4. Other peaks observed in the spectrum include dissociation products of $M^{\bullet+}$ at *m/z* 76, 63 and 39, adducts of these ions and benzonitrile at *m/z* 179, 166 and 142 and a prominent proton bound dimer ion at *m/z* 207. In addition, a relatively intense peak is observed for the dimer radical cation at *m/z* 206. Peaks in the region *m/z* 54-61 were absent.

Next, a small amount of acetamide (AA) was introduced into the ion source and in the resulting spectrum, see Figure 3.2, a relatively intense peak appeared at *m/z* 59 $[AA]^{\bullet+}$ in addition to a more intense *m/z* 60 $[AA+H]^+$; the latter is not unexpected since the self-protonation of acetamide and also that by benzonitrile are exothermic processes, by 15 and 3 kcal/mol respectively [16]. Other peaks appeared at *m/z* 119, the proton bound dimer $[AA{\bullet\bullet\bullet}H{\bullet\bullet\bullet}AA]^+$, *m/z* 140, and *m/z* 163, the proton bound dimer $[C_6H_5C{\equiv}N{\bullet\bullet\bullet}H{\bullet\bullet\bullet}AA]^+$. Most importantly, a peak at *m/z* 162 corresponding to the $[C_6H_5C{\equiv}N{\bullet\bullet\bullet}\text{"acetamide"}]^{\bullet+}$ ion also features in the spectrum.

The MI spectrum of the *m/z* 162 $[C_6H_5C{\equiv}N{\bullet\bullet\bullet}\text{"acetamide"}]^{\bullet+}$ complex displays intense peaks at *m/z* 59 and 60 ($CH_3C(OH)NH_2^+$) and a minor signal at *m/z* 103, $[C_6H_5CN]^{\bullet+}$, see Figure 3.4a. The CID mass spectrum of these *m/z* 59 ions obtained from an MS/MS/MS experiment [17], see Figure 3.3d, reveals that they have the enol structure **1a**$^{\bullet+}$. This experiment leaves no doubt that the original acetamide keto ion has been converted to its enol counterpart, compare Figure 3.3d and 3.3c.

The CI mass spectrum of Figure 3.2 also displays a weak signal at *m/z* 118. From its MI and CID spectra it follows that these ions represent the acetamide dimer radical cation $[AA]_2^{\bullet+}$, in admixture with a benzonitrile derived adduct ion. Characteristic of the $[AA]_2^{\bullet+}$ component are prominent peaks at *m/z* 59 and 60 in the MI spectrum. Acetamide itself has a PA of 206 kcal/mol [12b] and it could therefore promote the enolization of the ionic component of the $[AA]_2^{\bullet+}$ complex. This is indeed the case : the *m/z* 59 ions generated from

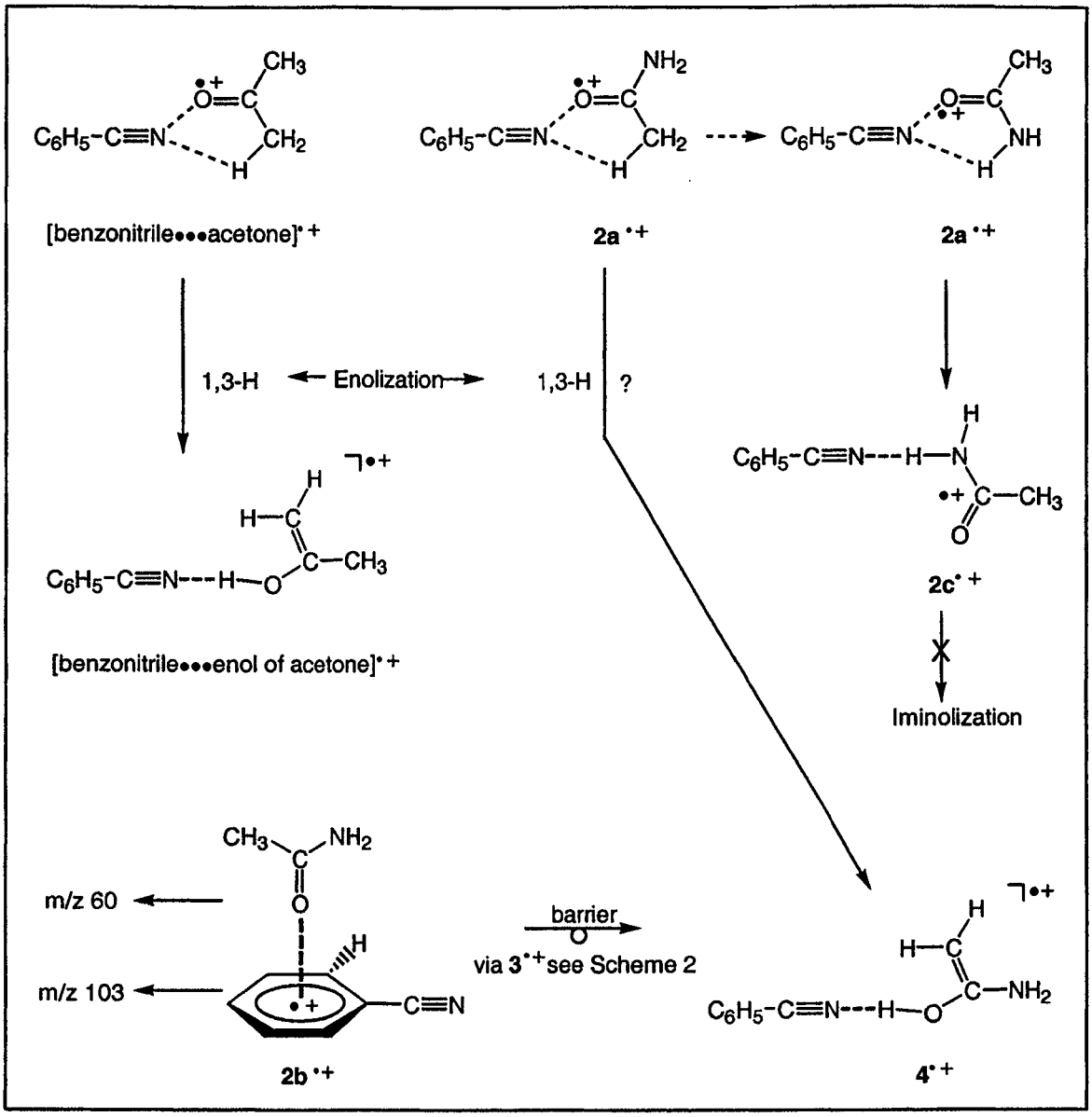
[benzonitrile•••acetone]•+
2a •+
2a •+
1,3-H
Enolization
1,3-H ?
[benzonitrile•••enol of acetone]•+
2c• +
Iminolization
m/z 60
m/z 103
barrier
via 3•+ see Scheme 2
2b •+
4• +

Scheme 3.1

the metastable *m/z* 118 ions transmitted into the 3ffr yield a CID mass spectrum which is clearly that of the enol ion **1a**$^{\bullet+}$.These matters will be discussed in a forthcoming paper.

In a previous study [5b] on the benzonitrile catalyzed enolization of the acetone ion, we had concluded that prior to its spontaneous or collision-induced dissociation, the initially formed [$C_6H_5C{\equiv}N{\bullet\bullet\bullet}$acetone]$^{\bullet+}$ complex completely rearranges, via proton-transport catalysis, to the very stable hydrogen-bridged radical cation (HBRC), [$C_6H_5C{\equiv}N{\bullet\bullet\bullet}$enol of acetone]$^{\bullet+}$. If the benzonitrile/ acetamide system behaves in the same way, then, see Scheme 3.1, the initially formed [$C_6H_5C{\equiv}N{\bullet\bullet\bullet}$acetamide$^{\bullet+}$] complex ion **2a**$^{\bullet+}$ will have completely rearranged to [$C_6H_5C{\equiv}N{\bullet\bullet\bullet}$enol of acetamide]$^{\bullet+}$, **4**$^{\bullet+}$, in the microsecond time-frame. Upon collisional activation, the complex ion will then uniquely yield *m/z* 59 ions having the enol ion structure **1a**$^{\bullet+}$ as this is the energetically most favourable dissociation reaction of the HBRC **4**$^{\bullet+}$.

The actual experiment, however, points to a different scenario : in Figure 3.3e is given the CID mass spectrum of the collisionally activated *m/z* 59 ions recorded in an MS/MS/MS experiment and it is clear that a mixture of enol and keto ions is produced, compare Figures 3.3e, 3.3a and 3.3c. Thus, a significant fraction of the complex ions **2**$^{\bullet+}$ has not rearranged into **4**$^{\bullet+}$, even on the μs time-frame. In line with this, the *m/z* 59 ions present in the ion source have largely retained their keto identity, see Figure 3.1d.

To further probe the structure of the *m/z* 162 ion, its Neutralization-Reionization (NR) spectrum [18] was obtained. As expected for an ion-dipole complex, it was observed that a survivor signal is clearly absent and instead the spectrum displayed narrow peaks at *m/z* 59 and 103, indicative of the collisional ionization of the neutral(ized) components of the complex. The CID spectrum of the *m/z* 59 ions in the NR spectrum was obtained and, compare Figures 3.3f and 3.3a, these ions clearly represent the keto form, which further attests to the presence of unrearranged precursor ions **2**$^{\bullet+}$. By contrast, similar NR experiments on the [$C_6H_5C{\equiv}N{\bullet\bullet\bullet}$"acetone"]$^{\bullet+}$ complex [19] show that the neutral *m/z* 58 species consist solely of the enol form of acetone.

The internal energy of the precursor ions sampled by the different techniques falls in the order MI > CID > NR [20] and this is precisely what we observe : compare Figures 3.3d,

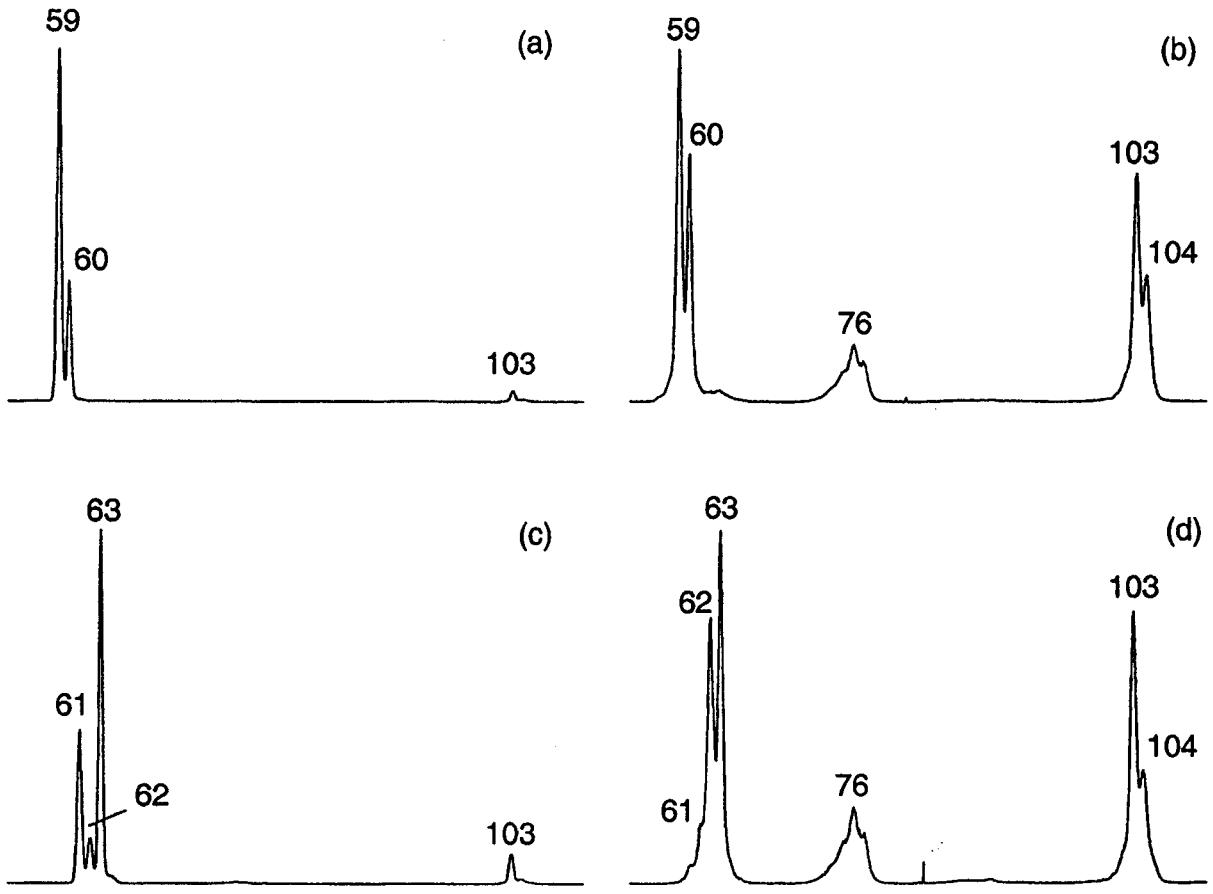

Figure 3.4. Metastable Ion (MI) mass spectra of : (a) the $[C_6H_5CN\bullet\bullet\bullet\text{"acetamide"}]^{\bullet+}$ complex; (c) the $[C_6H_5CN\bullet\bullet\bullet\text{"acetamide-}d_3\text{"}]^{\bullet+}$ complex ; and their respective CID mass spectra (b) and (d).

3.3e and 3.3f. These results show that there is a significant barrier for the proton-transport catalysis putatively operative in the $[C_6H_5C{\equiv}N{\bullet\bullet\bullet}acetamide]^{\bullet+}$ complex, whereas no such barrier exists for the $[C_6H_5C{\equiv}N{\bullet\bullet\bullet}acetone]^{\bullet+}$ complex. In fact, the labelling experiments presented below indicate that proton-transport catalysis does not operate for the acetamide system and that an entirely different mechanism comes into play. In this context we further note, see Scheme 3.1, that acetamide's enolization is not necessarily associated with the route $\mathbf{2a}^{\bullet+} \rightarrow \mathbf{4}^{\bullet+}$. The pathway $\mathbf{2b}^{\bullet+} \rightarrow \mathbf{4}^{\bullet+}$ which starts from adduct ions in which the benzonitrile carries the charge may well be a more viable alternative, not least because $\mathbf{2a}^{\bullet+}$ type ions could collapse into the undoubtedly more stable HBRC $\mathbf{2c}^{\bullet+}$. This ion may serve as the precursor for a benzonitrile assisted iminolization but, as pointed out above, this process is not feasible on energetic grounds.

Analysis of the MI spectrum of the *m/z* 162 complex ion presented in Figure 3.4a further underlines that the initially generated complex ions do not easily rearrange into the enolized complex ion $\mathbf{4}^{\bullet+}$. Formation of *m/z* 60 $[AA+H]^+$ ions from $\mathbf{2a}^{\bullet+}$ has a minimum energy requirement [21] which is slightly higher than that for the generation of $C_6H_5C{\equiv}NH^+$ (*m/z* 104) + $^{\bullet}CH_2C(=O)NH_2$, yet the latter reaction is not observed in the MI spectrum. Moreover, the even more energy demanding [21] dissociation into $C_6H_5C{\equiv}N^{\bullet+} + CH_3C(=O)NH_2$ is observed. These observations suggest that a sizeable fraction of the *m/z* 162 complex ions has retained the acetamide keto structure $\mathbf{2}^{\bullet+}$ and that, unlike the acetone case [5b], the benzonitrile assisted enolization of acetamide is still associated with a high energy barrier.

The D-labelled ions $[C_6H_5C{\equiv}N{\bullet\bullet\bullet}CD_3C(=O)NH_2]^{\bullet+}$ and $[C_6D_5C{\equiv}N{\bullet\bullet\bullet}CH_3C(=O)NH_2]^{\bullet+}$

To unravel the mechanism by which the enol ions are formed from the $[C_6H_5C{\equiv}N{\bullet\bullet\bullet}AA]^{\bullet+}$ ion, chemical ionization experiments using $CD_3C(=O)NH_2$ and $C_6H_5C{\equiv}N$ as well as $CH_3C(=O)NH_2$ and $C_6D_5C{\equiv}N$ were performed.

If an initially formed stable complex $\mathbf{2a/c}^{\bullet+}$ would rearrange to the HBRC $\mathbf{4}^{\bullet+}$ via proton-transport catalysis, then in the D-labelled isotopomer $[C_6H_5C{\equiv}N{\bullet\bullet\bullet}CD_3C(=O)NH_2]^{\bullet+}$ the complexed ion $CD_3C(=O)NH_2^{\bullet+}$, *m/z* 62, should rearrange to $CD_2{=}C(OD)NH_2^{\bullet+}$. An intense peak at *m/z* 62 is then expected in the MI spectrum of the complex which is presented in Figure

3.4c. From a comparison with the unlabelled result, see Figure 3.4a, it follows that this is not the case.

As mentioned earlier, the IE's of $C_6H_5C{\equiv}N$ and $CH_3C(=O)NH_2$ are virtually the same, so that a complex **2a/c**$^{\bullet+}$ may interconvert with **2b**$^{\bullet+}$ via charge transfer [22] or else ions **2b**$^{\bullet+}$ may be generated directly. We propose that $C_6H_5C{\equiv}N^{\bullet+}$ in the latter complex donates a **proton** to its partner to produce $CH_3C(OH)NH_2^+$, *m/z* 60. As expected, this signal shifts to *m/z* 63 for the labelled ion. However, the peak at *m/z* 59 shifts to *m/z* 61 with the *m/z* 62 peak being much weaker. The CID mass spectrum of the metastably generated *m/z* 61 ions is shown in Figure 3.5a. This spectrum is dominated by loss of NH_3 and this reveals that the *m/z* 61 ions have the enol structure $CD_2{=}C(OH)NH_2^{\bullet+}$. Thus the transformation : $[C_6H_5C{\equiv}N + CD_3C(=O)NH_2]^{\bullet+} \rightarrow [C_6H_4DC{\equiv}N + CD_2{=}C(OH)NH_2]^{\bullet+}$ is established and this leads to the tentative proposal presented in Scheme 3.2.

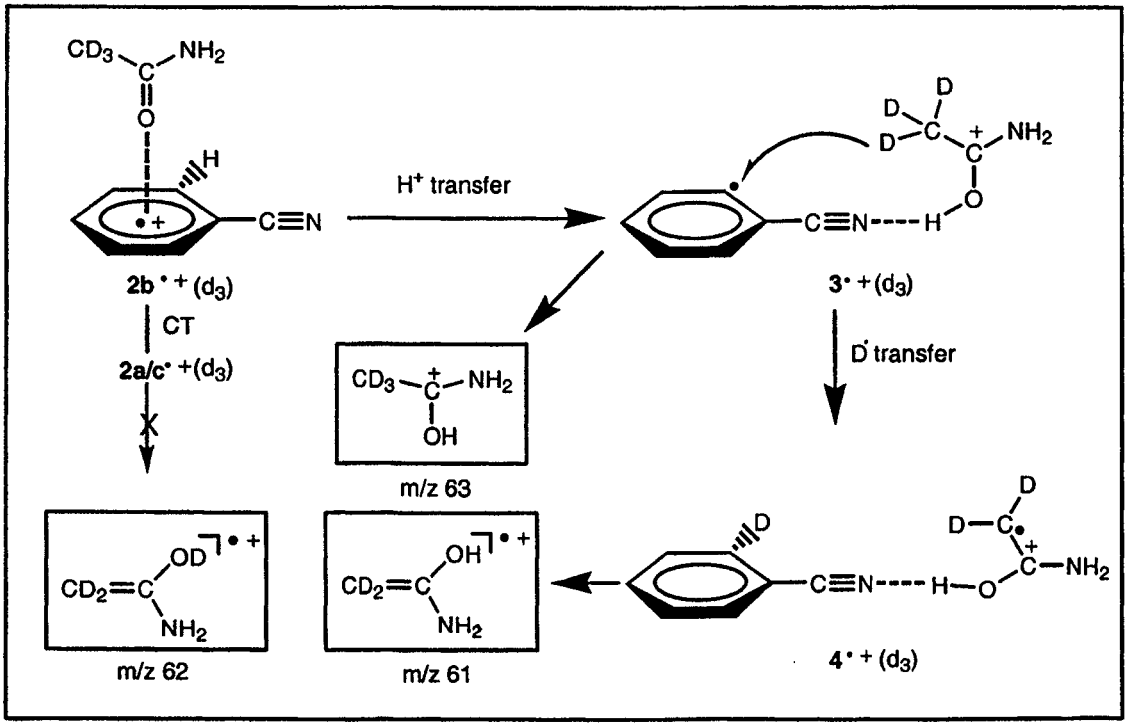

Scheme 3.2

The CID mass spectrum of the metastably generated *m/z* 62 ions is given in Figure 3.5b; it can be seen that losses of $NH_2^{\bullet}$ and $CD_3^{\bullet}$ are important processes and thus *m/z* 62 has the **keto** structure $CD_3C(=O)NH_2^{\bullet+}$. This ion, we propose, originates from dissociation of the unrearranged complex ion $\mathbf{2a}^{\bullet+}$ (d_3) in Scheme 3.2. The results from Figure 3.4c further reveal that an isotope effect (of magnitude 7) operates against the formation of *m/z* 61. From this we derive that the keto structure contributes only 3% to the unlabelled ions which is entirely compatible with the CID mass spectrum of the metastably generated unlabelled ions, see above.

Thus, in the isomerization of the complex ion $\mathbf{2b}^{\bullet+}$ (d_3) a D-transfer to the benzonitrile partner takes place, step $\mathbf{3}^{\bullet+} \rightarrow \mathbf{4}^{\bullet+}$ suggested in Scheme 3.2, and the above isotope effect indicates that this step may be rate-determining.

Next, the complex $[C_6D_5C{\equiv}N{\bullet\bullet\bullet}CH_3C(=O)NH_2^{\bullet+}]$ was studied and its MI spectrum contains signals at *m/z* 59, 60, 61 and 108 with an intensity ratio of 45 : 100 : 55 : 25. CID experiments showed that *m/z* 59 represents the keto ion $CH_3C(=O)NH_2^{\bullet+}$, whereas *m/z* 60 is the enol ion $CH_2{=}C(OD)NH_2^{\bullet+}$. The signals at *m/z* 59 and *m/z* 108 will not suffer from an isotope effect and thus the reduced intensity of *m/z* 60 and 61 compared to *m/z* 59 and *m/z* 60 in the unlabelled spectrum, see Figure 3.4a, must be due to an isotope effect associated with the formation of $CH_2{=}C(OD)NH_2^{\bullet+}$ (*m/z* 60) and $CH_3C(OD)NH_2^{+}$ (*m/z* 61). Thus in Scheme 3.2, two isotope effects are operative, one for the abstraction of a hydrogen at the carbon atom from acetamide and one for the abstraction of a carbon hydrogen from benzonitrile. The order in which these processes occur remains 'tentative', but they are both associated with relatively high energy barriers of comparable magnitude.

Further support for the proposed mechanism comes from the CID mass spectra presented in Figures 3.4b and 3.4d. In the CID spectrum of the unlabelled complex, Figure 3.4b, additional peaks are present compared to its MI spectrum, notably *m/z* 104, protonated benzonitrile, $C_6H_5C{\equiv}NH^{+}$. Surprisingly, for the CD_3 labelled species, see Figure 3.4d, this signal does **not** shift to *m/z* 105, but remains at *m/z* 104 and thus upon collisional activation, $CD_3C(=O)NH_2^{\bullet+}$ donates an H, not a D, to benzonitrile, i.e.

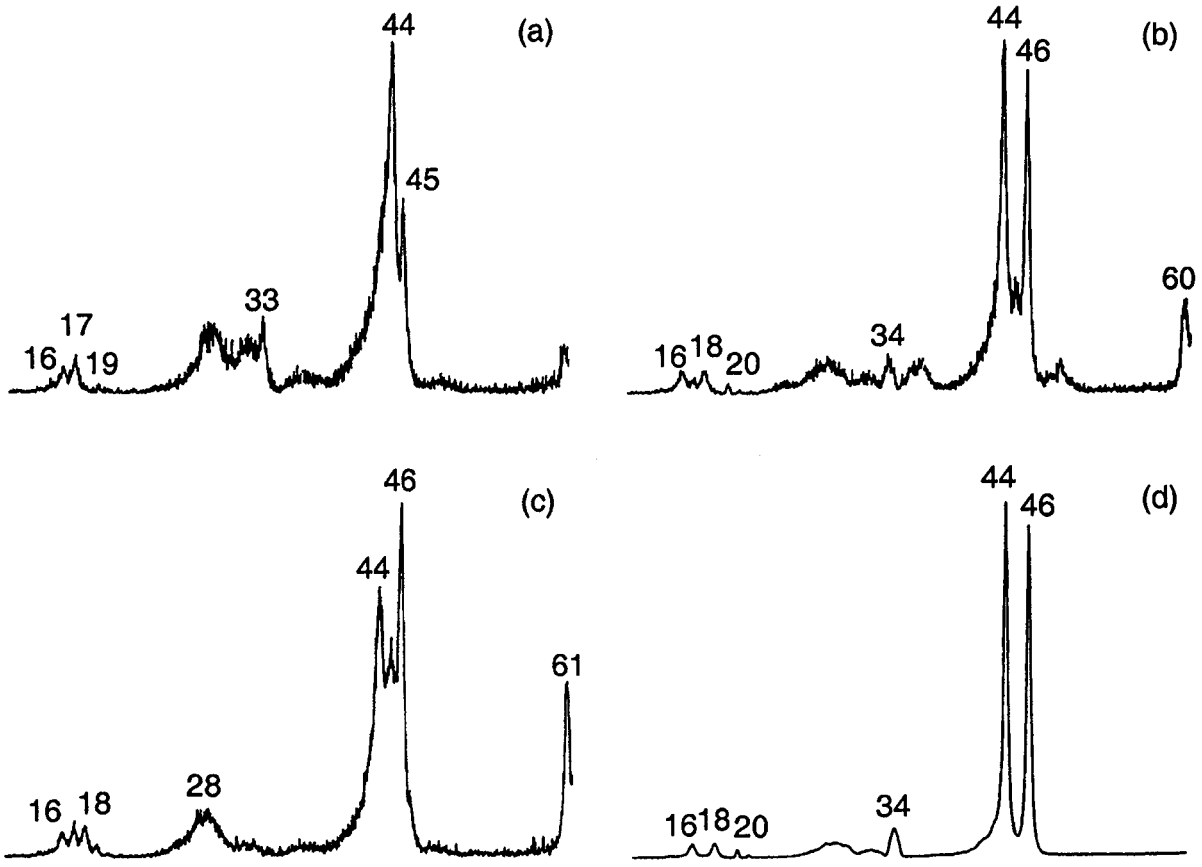

Figure 3.5. Collision-Induced Dissociation (CID) mass spectra of the metastably generated: (a) *m/z* 61, (b) *m/z* 62, (c) *m/z* 63 ions from the $[C_6H_5CN\bullet\bullet\bullet\text{“acetamide-}d_3\text{”}]^{\bullet+}$ complex; (d) *m/z* 62 ions in the benzonitrile chemical ionization mass spectrum of acetamide-d_3, having 4 keV translational energy.

$$[C_6H_5C{\equiv}N\bullet\bullet\bullet\ CD_3C(=O)NH_2^{\bullet+}]\ \mathbf{2a}^{\bullet+}(d_3) \not\longrightarrow C_6H_5C{\equiv}ND^+ + {}^{\bullet}CD_2{=}C(OH)NH_2$$

$$\text{but } [C_6H_5C{\equiv}N\bullet\bullet\bullet\ H_2NC(=O)CD_3^{\bullet+}]\ \mathbf{2c}^{\bullet+}(d_3) \longrightarrow C_6H_5C{\equiv}NH^+ + {}^{\bullet}HNC(=O)CD_3$$

Thus ionized acetamide does **not** donate a carbon proton to the benzonitrile moiety, not even upon collisional activation. This despite the fact that a D^+ transfer is less endothermic than a H^+ transfer, by 13 kcal/mol, see Table 3.1. In contrast, in the $[C_6H_5C{\equiv}N\bullet\bullet\bullet$acetone$^{\bullet+}]$ complex a carbon proton is readily transferred to the benzonitrile moiety [5b].

These observations may well indicate that the encounter complex $\mathbf{2a}^{\bullet+}$ readily adopts the structure of the HBRC $\mathbf{2c}^{\bullet+}$ depicted in Scheme 3.1, as suggested above.

Theoretical Calculations

As mentioned in the previous section, in the initially formed complex $[C_6H_5C{\equiv}N\bullet\bullet\bullet AA]^{\bullet+}$, the charge will be on the benzonitrile moiety, see ion $\mathbf{2b}^{\bullet+}$ in Scheme 3.1. Charge transfer may furnish the complex $\mathbf{2a}^{\bullet+}$. Exploratory calculations indicated that if ionized acetamide and neutral benzonitrile meet to form such a complex, proton transfer from the carbon atom of ionized acetamide to benzonitrile would be associated with a large barrier but due to computational difficulties, the exact level of the transition state could not be assessed. Instead, we noted that ions of the type $\mathbf{2a}^{\bullet+}$ readily collapsed into the stable HBRC $\mathbf{2c}^{\bullet+}$, see Scheme 3.1.

However, when the charge is on the benzonitrile moiety, proton transfer in ion $\mathbf{2b}^{\bullet+}$ can yield the complex $[C_6H_4C{\equiv}N^{\bullet}\bullet\bullet\bullet CH_3C(OH)NH_2^+]$, $\mathbf{3}^{\bullet+}$, where acetamide becomes protonated. If this complex lies in a sufficiently deep well a hydrogen **atom** transfer from the carbon atom of $CH_3C(OH)NH_2^+$ to $C_6H_4C{\equiv}N^{\bullet}$ might be possible leading to the HBRC $\mathbf{4}^{\bullet+}$ which then dissociates to $CH_2{=}C(OH)NH_2^{\bullet+}$ as observed. The labelling experiments discussed above, indicate that the transition states $\mathbf{2b}^{\bullet+} \rightarrow \mathbf{3}^{\bullet+}$ and $\mathbf{3}^{\bullet+} \rightarrow \mathbf{4}^{\bullet+}$ should be relatively high and of comparable magnitude.

The calculations were started with RHF/DZP geometry optimizations of the various ions, transition states and dissociation products depicted in Scheme 3.4, see also Scheme

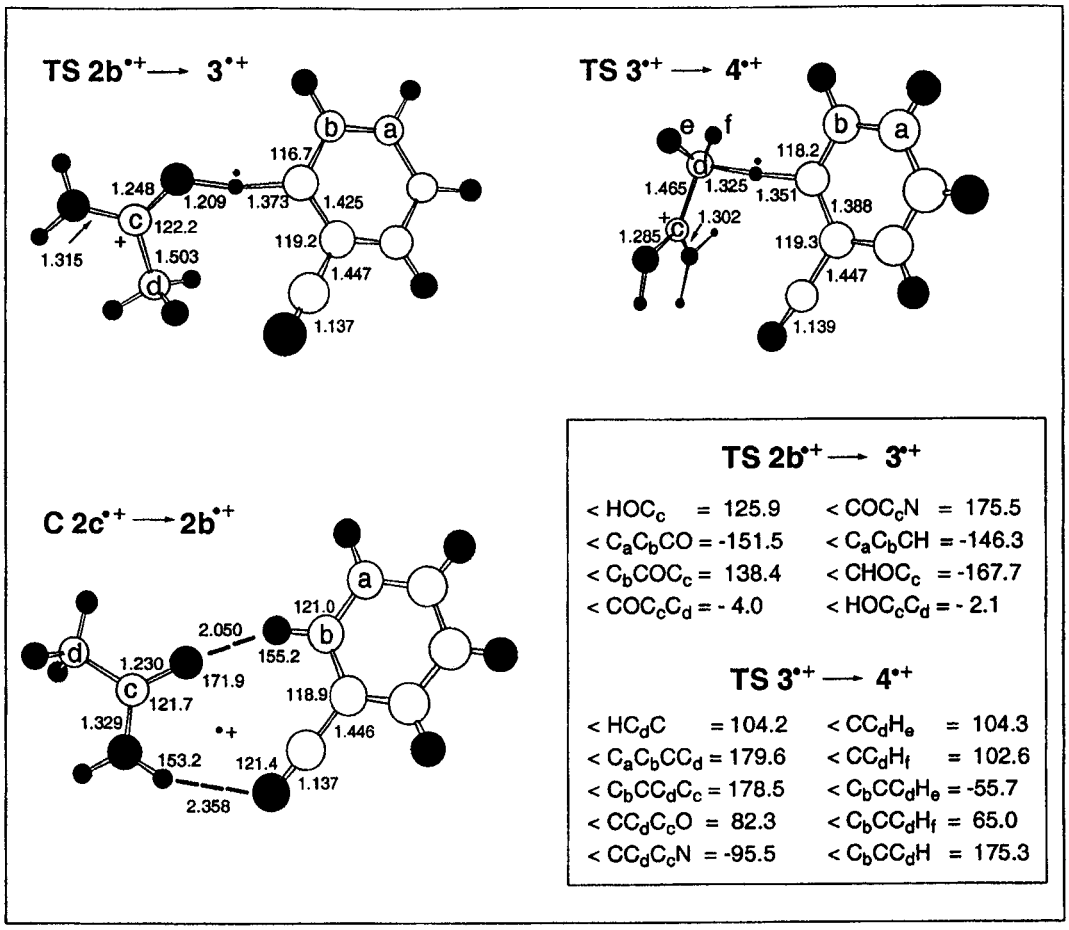

Scheme 3.3. Structures of the crossing C $\mathbf{2c}^{\bullet+} \rightarrow \mathbf{2b}^{\bullet+}$ and the transition states TS $\mathbf{2b}^{\bullet+} \rightarrow \mathbf{3}^{\bullet+}$ and TS $\mathbf{3}^{\bullet+} \rightarrow \mathbf{4}^{\bullet+}$

3.1/3.2. Detailed geometries are only presented for the transition states, see Scheme 3.3 : for all other species they are available upon request from the authors. All stationary points were checked for the correct number of imaginary frequencies. The transition from ion **2c**$^{\bullet+}$ to ion **2b**$^{\bullet+}$ appears to be a crossing : the charge is either located on the benzene ring or on the acetamide moiety. This holds for all levels of calculation used (RHF, UHF and MP4). The Minimum Energy Crossing Point was determined using Morokuma's method [23] and single point calculations were performed with both choices of charge localization. The resulting energies are slightly different due to different electronic correlation effects for the two representations of the ground state in the crossing geometry.

Single point UMP2/D95** calculations for the geometries found, showed that several ions suffer from a large spin contamination. This is especially true if the radical character is localized on the benzene ring, e.g. the $C_6H_4C{\equiv}N^{\bullet}$ radical has $\langle s^2 \rangle = 1.47$. In this model TS **2b**$^{\bullet+}$ → **3**$^{\bullet+}$ and TS **3**$^{\bullet+}$ → **4**$^{\bullet+}$ (also highly spin contaminated) turn out to lie 10 and 16 kcal/mol respectively above our anchor point, $C_6H_5C{\equiv}N + CH_3C(=O)NH_2^{\bullet+}$. This clearly is incompatible with the experimental observations. Therefore the UMP2 method was deemed unsuitable to obtain better geometries and the RHF geometries were used in all other *ab initio* calculations. To check whether this defect persists in the next higher orders of perturbation theory, UMP4SDTQ calculations were performed for the two transition states. Unfortunately, this does not significantly improve the results, TS **3**$^{\bullet+}$ → **4**$^{\bullet+}$ still lies 11 kcal/mol above the anchor point. Better results are, however, obtained if the spin-projected energies are used. The UMP2 calculation also yields PMP2-O energies, where only the next higher spin component (the quartet in our case) is projected out. This yields a dramatic lowering of the relative energy of TS **3**$^{\bullet+}$ → **4**$^{\bullet+}$: it now lies 10 kcal/mol **below** the anchor point. Further improvements may be expected by going to higher orders. This yields the results given in Table 3.2.

The results in Table3.2 show that projecting out the quartet component has a large effect, but it still does not remove the spin contamination sufficiently. Although the annihilation of the higher components is still not complete in the PMPn calculations, a detailed inspection of the output shows that the results have converged to within 0.5 kcal/mol,

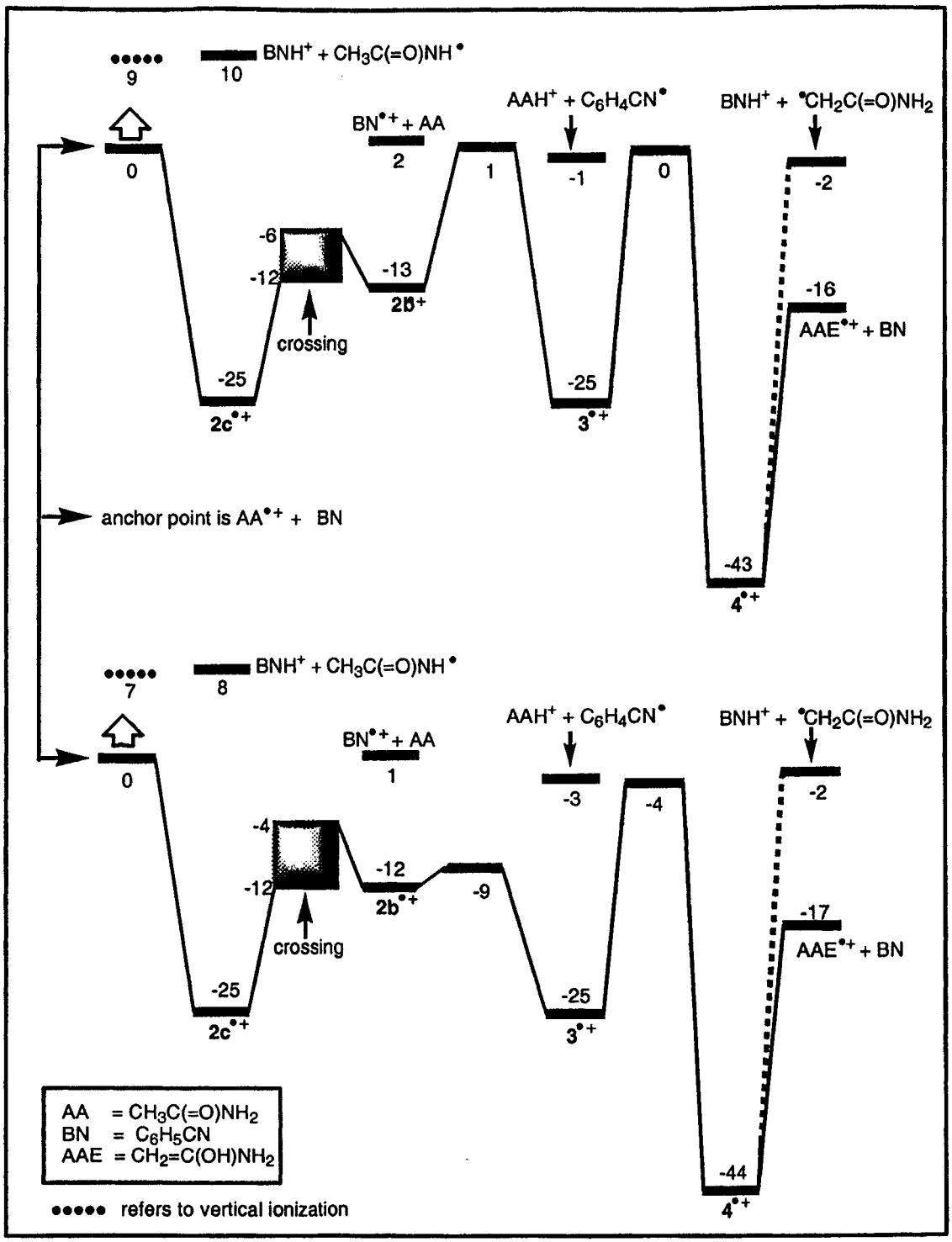

Scheme 3.4. Computationally derived energy diagram for the benzonitrile assisted isomerization of the acetamide radical cation $CH_3C(=O)NH_2^{\bullet+}$. Top part : RHF based calculations ; Bottom part : B3LYP based calculations, see text. Relative energies are given in kcal/mol.

which is quite satisfactory considering the other inaccuracies still present. To obtain PMP4 results full MP4 calculations have to be performed, i.e. calculations including the triple excitations. Such calculations appear to be very time consuming for a system of this size and complexity (the triples take ca 95 % of the CPU time). We therefore decided to restrict ourselves in our computational analysis of the present system to the MP4SDQ level of theory needed to obtain the PMP3 energies.

Table 3.2. Energies of TS **2b**$^{\bullet+}$ → **3**$^{\bullet+}$ and TS **3**$^{\bullet+}$ → **4**$^{\bullet+}$ (in kcal/mol) relative to the anchor point, $CH_3C(=O)NH_2$ $^{\bullet+}$ + $C_6H_5C{\equiv}N$, for various theoretical models.

Model	TS **2b**$^{\bullet+}$ → **3**$^{\bullet+}$	TS **3**$^{\bullet+}$ → **4**$^{\bullet+}$
RHF	18	23
UMP2	10	16
UMP3	9	14
UMP4SDQ	4	9
UMP4SDTQ	6	11
PMP2-O [a]	-3	-10
PMP2 [b]	-1	-2
PMP3 [b]	1	0
PMP4 [b]	-3	-4

[a] Only the quartet (s = 3/2) component is projected out.
[b] The components with s = 3/2, 5/2, 7/2 and 9/2 are projected out.

The above results were obtained using RHF optimized geometries. Since the RHF energies appear not to be very useful, we thought it worthwhile to try the DFT method for optimizing geometries. For this purpose the B3LYP parameterization was used. The B3LYP results do not suffer from the spin contamination problem : the largest $<s^2>$ value is 0.77 (for $C_6H_4C{\equiv}N^{\bullet}$). The crossing situation for the **2c**$^{\bullet+}$ → **2b**$^{\bullet+}$ transition persists even in the B3LYP calculation which tends to delocalize the charge. The resulting geometries were again used for MP4SDQ single point calculations. The energies obtained from these PMP3//RHF/D95** and PMP3//B3LYP/D95** calculations are presented in Table 3.3.

Table 3.3 *Ab initio* energies for the acetamide/benzonitrile system. Electronic energies are in Hartrees and ZPEs in kcal/mol. Data in parentheses are without ZPE contribution.

	RHF	ZPE (*0.9)	E(rel)	PMP3//RHF	E(rel)	B3LYP	E(rel)	PMP3//B3LYP	E(rel)	exp [a] 298 K	$<s^2>$ [b]
1	-208.03103	44.4		-208.66487	1.9	-209.26397		-208.66611			0
1 + $BN^{\bullet+}$	-530.19655	103.1	14.9	-531.87367		-533.451	-3	-531.87827	1.1	0	
$BN^{\bullet+}$	-322.16552	58.7		-323.2088		-324.18703		-323.21216			0.966
$\mathbf{1}^{\bullet+}$ [c]	-207.71594		-10.7	-208.31201	-9.2	-208.90784	-6	-208.31542	-7.3		0.763
$\mathbf{1}^{\bullet+}$	-207.73302	44.8		-208.32666		-208.91733		-208.32709			0.76
$\mathbf{1}^{\bullet+}$ + BN	-530.22279	104.7	0	-531.87949	0	-533.44888	0	-531.88281	0	0	
BN	-322.48977	59.9		-323.55283		-324.53155		-323.55572			0
BN + $\mathbf{1a}^{\bullet+}$	-530.23853	104.6	-10	-531.90519	-16.2	-533.47556	-16.8	-531.90984	-17.1		
$\mathbf{1a}^{\bullet+}$	-207.74876	44.7		-208.35236		-208.94401		-208.35412			0.77
AA•(C) [d]	-207.38317	35.9		-207.9854		-209.57922		-207.98819			0.766
AA•(C) + BNH^{+}	-530.19777	102.5	13.5	-531.86076		-533.43825	4.6	-531.86607	8.4		
BNH^{+}	-322.8146	66.6		-323.87557		-323.85903		-323.87788			0
BNH^{+} + AA•(N)	-530.21283	102.8	4.4	-531.87913	-1.7	-533.4568	-6.9	-531.88325	-1.6		
AA•(N) [d]	-207.39823	36.2		-208.00356		-208.59777		-208.00537			0.783
AAH^{+}	-208.38371	53.1		-209.01571		-209.61089		-209.01571			0
AAH^{+} + BN•	-530.2165	105.4	4.6	-531.87681	-1.1	-533.45092	-0.7	-531.8778	-2.5	-3 [e]	
BN•	-321.83279	52.3		-322.8611		-323.84003		-322.8609			1.472
$\mathbf{2c}^{\bullet+}$	-530.26111	105.8	-22.9	-531.92151	-25.3	-533.4914	-25.6	-531.92475	-25.2		0.735
C $\mathbf{2c}^{\bullet+}$ - $\mathbf{2b}^{\bullet+}$	-530.22381		-0.6	-531.88841	(-5.6)	-533.47175	(-14.4)	-531.88905	(-3.9)		0.762
C $\mathbf{2c}^{\bullet+}$ - $\mathbf{2b}^{\bullet+}$	-530.22381		-0.6	-531.89827	(-11.8)	-533.47175	-14.4	-531.90549	(-12.3)		0.978
$\mathbf{2b}^{\bullet+}$	-530.22657	104.3	-2.8	-531.90192	-13	-533.49236	-26.7	-531.90352	-12.4		0.992
TS $\mathbf{2b}^{\bullet+}$ → $\mathbf{3}^{\bullet+}$	-530.18971	101.9	18	-531.87367	0.8	-533.46366	-12.1	-531.8725	-9.3		1.169
$\mathbf{3}^{\bullet+}$	-530.25672	106.3	-19.7	-531.92132	-24.6	-533.50086	-31	-531.92589	-25.3		1.408
TS $\mathbf{3}^{\bullet+}$ → $\mathbf{4}^{\bullet+}$	-530.18382	102.9	22.7	-531.87685	-0.2	-533.45682	-6.9	-531.87892	-4.3		1.434
$\mathbf{4}^{\bullet+}$	-530.28025	105.7	-35.1	-531.94987	-43.3	-533.52441	-46.5	-531.95352	-43.5		0.764

[a] See reference 12.

[b] In the large basis UHF calculation.

[c] Vertical ionization : calculated using the geometry of neutral acetamide. The relative energies are calculated from the electronic energies of this ion + neutral benzonitrile.

[d] AA•(C) → $^{\bullet}CH_2C(=O)NH_2$, AA•(N) → $CH_3C(=O)NH^{\bullet}$

[e] $\Delta H_f(BN^{\bullet}) = 111$ kcal/mol from ref. 5b.

The B3LYP energies appear to deviate significantly from the *ab initio* results, particularly for the transition states, whose relative energies are 13 and 17 kcal/mol below the *ab initio* results. Also, for **2b**$^{\bullet+}$ the B3LYP method yields E(rel) = -27 kcal/mol, whereas the PMP3//RHF calculation yields E(rel) = -13 kcal/mol. It is also noteworthy that one of the two possible B3LYP charge distributions in the crossing geometry is delocalized over both moieties, even though they are far apart.

Although some of the B3LYP geometries also differ considerably from their RHF counterparts, the final (PMP3) relative energies, see Table 3.3 and the energy level diagrams of Scheme 3.4, are rather close. However, there is one notable exception and this concerns, see Scheme 3.4, TS **2c**$^{\bullet+}$ → **2b**$^{\bullet+}$ which is comparable in energy with **TS 3**$^{\bullet+}$ → **4**$^{\bullet+}$ in the calculation based on RHF geometries but lower in the B3LYP based model. We note, see below, that the RHF geometries yield results which are in good agreement with the experimental observations and surmise that the B3LYP calculation underestimates the height of this TS. We further note that both computational approaches satisfactorily reproduce the position of the various dissociation levels : e.g. the energy difference between AA$^{\bullet+}$ (**1**$^{\bullet+}$) and AAE$^{\bullet+}$ (**1a**$^{\bullet+}$) in Scheme 3.4, 16-17 kcal/mol, agrees quite well with the CBS-QB3 and G2 derived values, 16 kcal/mol, presented in Table 3.1. Moreover, the marginal energy difference between BN$^{\bullet+}$ + AA and the anchor point AA$^{\bullet+}$ + BN is in keeping with the experimental observation that the IE's of AA and BN are virtually the same.

Using Scheme 3.4 as a guide, we propose that the reaction starts with either complex **2c**$^{\bullet+}$ or **2b**$^{\bullet+}$. Complex **2c**$^{\bullet+}$ is an HBRC whose stabilization energy (SE) can be estimated from the empirical relationship SE = 23.2 - 0.25ΔPA (kcal/mol) [24], where ΔPA is the difference in proton affinity between benzonitrile (196 kcal/mol) and the radical $CH_3C(=O)NH^{\bullet}$ (206 kcal/mol, Table 3.1). We then obtain SE = 21 kcal/mol, compared to 25 kcal/mol derived computationally, see Scheme 3.4.

Charge transfer may lead to complex **2b**$^{\bullet+}$ where the acetamide neutral lies perpendicular to the plane of the benzonitrile ion. Proton transfer from the benzonitrile to acetamide is only possible if the benzonitrile and acetamide components lie in the same plane, TS **2b**$^{\bullet+}$ → **3**$^{\bullet+}$ in Scheme 3.3. The resulting complex **3**$^{\bullet+}$ can be viewed as protonated acetamide

interacting with the $C_6H_4C{\equiv}N^{\bullet}$ radical. This radical can then rotate until a TS is reached, TS $\mathbf{3}^{\bullet+} \rightarrow \mathbf{4}^{\bullet+}$, where a H *atom* lies midway between the benzonitrile and the enol of acetamide moiety, see Scheme 3.3. This yields the very stable HBRC $\mathbf{4}^{\bullet+}$ which represents the ionized enol of acetamide interacting with the benzonitrile dipole. This ion then dissociates to $CH_2{=}C(OH)NH_2^{\bullet+}$, as observed.

The computationally derived scenario for the interactions and dissociations of the $[C_6H_5C{\equiv}N{\bullet\bullet\bullet}AA]^{\bullet+}$ system in Scheme 3.4, supports the tentative mechanistic proposal of Scheme 3.3 and the associated experimental observations. First, complex $\mathbf{2c}^{\bullet+}$ accounts for the formation of the acetamide ion, $\mathbf{1}^{\bullet+}$, in the metastable time-frame and it also, upon activation, generates $C_6H_5C{\equiv}NH^{+} + CH_3C(=O)NH^{\bullet}$, as observed. Complex $\mathbf{2b}^{\bullet+}$ can generate $C_6H_5C{\equiv}N^{\bullet+}$ metastably, while ion $\mathbf{3}^{\bullet+}$ may serve as the precursor for $CH_3C(OH)NH_2^{+}$. In the RHF based calculation, the transition $\mathbf{2b}^{\bullet+} \rightarrow \mathbf{3}^{\bullet+}$ lies sufficiently high to account for the observed isotope effect in the complex ion $[C_6D_5C{\equiv}N{\bullet\bullet\bullet}CH_3C(=O)NH_2]^{\bullet+}$. Finally, complex $\mathbf{4}^{\bullet+}$ yields the enol of acetamide ion, $\mathbf{1a}^{\bullet+}$, and its formation from $\mathbf{3}^{\bullet+}$ is associated with a barrier of such a magnitude that it could account for the observed isotope effect in the dissociation of the complex ion $[C_6H_5C{\equiv}N{\bullet\bullet\bullet}CD_3C(=O)NH_2]^{\bullet+}$. The stabilization energy of the HBRC $\mathbf{4}^{\bullet+}$ may be estimated from the empirical relationship SE = 30.0 - 0.26 PA(kcal/mol) [24] : SE = 28 kcal/mol which compares well with the computationally derived value of 27 kcal/mol.

Conclusions

The acetamide radical cation $CH_3C(=O)NH_2^{\bullet+}$, $\mathbf{1}^{\bullet+}$, is separated from its more stable enol isomer $CH_2{=}C(OH)NH_2^{\bullet+}$, $\mathbf{1a}^{\bullet+}$, by a large barrier (26 kcal/mol) which prevents its unimolecular enolization. However, this barrier can be lowered sufficiently by interaction with an appropriate neutral molecule, such as benzonitrile, for the enolization to occur. Under conditions of chemical ionization the $[C_6H_5C{\equiv}N{\bullet\bullet\bullet}\text{“acetamide”}]^{\bullet+}$ dimer radical cation is readily formed which rearranges to a $[C_6H_5C{\equiv}N{\bullet\bullet\bullet}\text{“enol of acetamide”}]$ complex. Analysis of the behaviour of labelled ions, and comparative experiments with $[C_6H_5C{\equiv}N{\bullet\bullet\bullet}\text{acetone}]^{\bullet+}$ adduct ions, demonstrate that this isomerization does not occur by way of proton-transport catalysis, but rather by an intermolecular $H^{+}/H^{\bullet}$ transfer mechanism. In the initial

[$C_6H_5C{\equiv}N$ $^{\bullet+}$•••"acetamide"] complex, benzonitrile, acting as an acid and not a base, transfers a proton to the carbonyl oxygen. In the next transformation a hydrogen atom is donated back to the $C_6H_5C{\equiv}N$ moiety, leading to the hydrogen-bridged radical cation [$C_6H_5C{\equiv}N$•••H-O-$C(NH_2){=}CH_2$]$^{\bullet+}$, **4**$^{\bullet+}$, which can dissociate into the enol ion **1a**$^{\bullet+}$ and benzonitrile. Theory and experiment agree that both H-transfers are associated with fairly high energy barriers.

In support of our mechanistic proposal, we note that if a "base" is used whose ionization energy is considerably higher than that of the acetamide, that enolization does not take effect. For example, acrylonitrile has an IE of 10.9 eV [11a], a PA of 190 kcal/mol [11b] and a dipole moment of 3.9 Debye [14] but its interaction with acetamide leads to complexes in which the acetamide moiety retains its keto structure.

Finally, we note that the reason why the proton-transport catalysis in the [$C_6H_5C{\equiv}N$•••acetone]$^{\bullet+}$ encounter complex does not feature in the [$C_6H_5C{\equiv}N$•••acetamide]$^{\bullet+}$ ion may find its explanation in the following two differences between the systems. First, as pointed out in the preceding sections the initial encounter complex **2a**$^{\bullet+}$ in Scheme 3.1, may easily collapse into the more stable but unreactive HBRC **2c**$^{\bullet+}$, an option not open to the [$C_6H_5C{\equiv}N$•••acetone $^{\bullet+}$] ion. Secondly, and perhaps more importantly, in the case of the acetamide system, the transformation **2a**$^{\bullet+}$ → **4**$^{\bullet+}$ may be associated with a large barrier. Thus, when in **2a**$^{\bullet+}$ a proton is shifted from the ionized acetamide carbon to the benzonitrile nitrogen, the dipole vector of the incipient $^{\bullet}CH_2$-$C(=O)NH_2$ radical may point in the wrong direction leading to ion-dipole repulsion.

References

[1] C.L. Perrin, *Acc. Chem. Res.* **1989**, *22*, 268.

[2] (a) G.A. McGibbon, P.C. Burgers, J.K. Terlouw, *Int. J. Mass Spectrom. Ion Processes* **1994**, *136*, 191 and references cited therein; (b) T. Drewello, N. Heinrich, W.P.M. Maas, N.M.M. Nibbering, T. Weiske, H. Schwarz, *J. Am. Chem. Soc.* **1987**, *109*, 4810.

[3] (a) P. Mourgues, H.-E. Audier, D. Leblanc, S. Hammerum, *Org. Mass Spectrom.* **1993**, *28*, 1098; (b) H.-E. Audier, D. Leblanc, P. Mourgues, T.B. McMahon, S. Hammerum, *J. Chem. Soc. Commun.* **1994**, 2329; (c) J.W. Gauld, H.-E. Audier, J. Fossey, L. Radom, *J. Am. Chem. Soc.* **1996**, *118*, 6299; (d) J.W. Gauld, L. Radom, *J. Am. Chem. Soc.* **1997**, *119*, 9831; (e) A.J. Chalk, L. Radom, *J. Am. Chem. Soc.* **1997**, *119*, 7573; (f) A.J. Chalk, L. Radom, *J. Am. Chem. Soc.* **1999**, *121*, 1574; (g) M.A. Trikoupis, D.J. Lavorato, J.K. Terlouw, P.J.A. Ruttink, P.C. Burgers, *Eur. Mass Spectrom.* **1999**, *5*, 431 (h) For an early review see : D.K. Bohme, *Int. J. Mass Spectrom. Ion Processes* **1992**, *115*, 95.

[4] V. Baranov, S. Petrie, D.K. Bohme, *J. Am. Chem. Soc.* **1996**, *118*, 4500, see also : A. Cunje, C.F. Rodriquez, D.K. Bohme, A.C. Hopkinson, *J. Phys. Chem. A* **1998**, *102*, 478.

[5] (a) G. Van der Rest, P. Mourgues, J. Tortajada, H.-E. Audier, *Int. J. Mass Spectrom.* **1998**, *179/180*, 293, and references cited therein; (b) M.A. Trikoupis, P.C. Burgers, J.K. Terlouw, *J. Am. Chem. Soc.* **1998**, *120*, 12131; (c) J. Chamot-Rooke, G. Van der Rest, P. Mourgues, H.-E. Audier, *Int. J. Mass Spectrom.* **2000**, *195/196*, 385; (d) A. Nixdorf, H.-F. Grützmacher, *J. Am. Chem. Soc.* **1997**, *119*, 6544.

[6] T.A. Molenaar-Langeveld, N.M.M. Nibbering, R.P. Morgan, J.H. Beynon, *Org. Mass Spectrom.* **1978**, *13*, 172.

[7] E.C. Taylor, H.W. Altland, R.H. Danforth, G. McGillivray, *J. Am. Chem. Soc.* **1970**, *92*, 3520.

[8] Gaussian 98, Revision A.7, M.J. Frisch, G.W. Trucks, H.B. Schlegel, G.E. Scuseria, M.A. Robb, J.R. Cheeseman, V.G. Zarzewski, J.A. Montgomery Jr., R.E. Stratmann, J.C. Burant, S. Dapprich, J.M. Millam, A.D. Daniels, K.N. Kudin, M.C. Strain, O. Farkas, J. Tomasi, V. Barone, M. Cossi, R. Cammi, B. Mennucci, C. Pomelli, C. Adamo. S. Clifford, J. Ochterski, G.A. Petersson, P.Y. Ayala, Q. Cui, K. Morokuma, D.K. Malick, A.D. Rabuck, K. Raghavachari, J.B. Foresman, J. Cioslowski, J.V. Ortiz, A.G. Baboul, B.B. Stefanov, G. Liu, A. Liashenko, P. Piskorz, I. Komaromi, R. Gomperts, R.L. Martin, D.J. Fox, T. Keith, M.A. Al-Laham, C.Y. Peng, A. Nanayakkara, C. Gonzalez, M. Challacombe, P.M.W. Gill, B. Johnson, W. Chen, M.W. Wong, J.L. Andres, C. Gonzalez, M. Head-Gordon, E.S. Replogle, J.A. Pople, Gaussian Inc., Pittsburgh PA, **1998**.

[9] (a) M. Dupuis, D. Spangler, J. Wendolowski, NRCC Software Catalogue 1 Program No. QG01, GAMESS (**1980**); (b) M. Guest, J. Kendrick, GAMESS User Manual, An Introductory Guide, CCP/86/1, Daresbury Laboratories (**1986**).

[10] (a) J.A. Montgomery Jr., M.J. Frisch, J.W. Ochterski, G.A. Petersson, *J. Chem. Phys.* **2000**, *112*, 6532 ; (b) J.A. Montgomery Jr., M.J. Frisch, J.W. Ochterski, G.A. Petersson, *J. Chem. Phys.* **1999**, *110*, 2822.

[11] L.A. Curtiss, K. Raghavachari, G.W. Trucks, J.A. Pople, *J. Chem. Phys.* **1991**, *94*, 7221.

[12] (a) S.G. Lias, J.E. Bartmess, J.F. Liebman, J.L. Holmes, R.O. Levin, W.G. Mallard, *J. Phys. Chem. Ref. Data* **1988**, *17*, Supplement 1; (b) S.G. Lias, E.P.L. Hunter, *J. Phys. Chem. Ref. Data* **1998**, *27*, No 3; (c) C.E.C.A. Hop, P.J.A. Ruttink, G. Schaftenaar, J.K. Terlouw, *Chem. Phys. Lett.* **1989**, *156*, 251.

[13] For a brief review see : J.K. Terlouw, *Proton-Transport Catalysis in Hydrogen-Bridged Radical Cations and Ion-Dipole Complexes* in The 8th ISMAS Symposium on Mass Spectrometry Volume 1, Hyderabad, India, **1999**, 421.

[14] From $\Delta H_f[C_6H_5CN]^{\bullet+}$ = 274 kcal/mol [12a], $\Delta H_f[C_6H_5CN]$ = 52 kcal/mol [12a], $\Delta H_f[C_6H_5CNH]^+$ = 222 kcal/mol [12a] and $\Delta H_f[C_6H_4CN]^\bullet$ = 111 kcal/mol; the latter value was obtained using the benzene C-H bond dissociation energy of 111 kcal/mol [12a] and $\Delta H_f[H]^\bullet$ = 52 kcal/mol [12a].

[15] R.C. Weast (Ed), The CRC Handbook of Chemistry and Physics, CRC Press Inc., Ohio **1974**, E-64.

[16] Using $\Delta H_f[CH_3C(=O)NH_2]^{\bullet+}$ = 165 kcal/mol [12a], $\Delta H_f[CH_3C(=O)NH_2]$ = -57 kcal/mol [11a], $\Delta H_f[CH_3C(OH)NH_2]^+$ = 103 kcal/mol [12a] and the values given in ref. 14.

[17] G.A. McGibbon, P.C. Burgers, J.K. Terlouw, *Int. J. Mass Spectrom. Ion Processes* **1994**, *191*, 191.

[18] For a recent review see : N. Goldberg and H. Schwarz, *Acc. Chem. Res.* **1994**, *27*, 34.

[19] M.A. Trikoupis, P.C. Burgers, P.J.A. Ruttink, J.K. Terlouw, unpublished results.

[20] P.C. Burgers, G.A. McGibbon, J.K. Terlouw, *Eur. Mass. Spectrom.* **1995**, *1*, 261.

[21] From $\Sigma\,\Delta H_f\,[CH_3C(OH)NH_2^+ + C_6H_4CN^\bullet]$ = 214 kcal/mol ([12a],[14]) and $\Sigma\,\Delta H_f\,[C_6H_5CNH^+ + {}^\bullet CH_2C(=O)NH_2]$ = 212 kcal/mol ([12a], Table 3.1).

[22] P.J.A. Ruttink, P.C. Burgers, *Org. Mass Spectrom.* **1993**, *20*, 1087.

[23] H.B. Schlegel, *J. Phys. Chem.* **1988**, *28*, 371.

[24] M. Meot-Ner (Mautner), *J. Am. Chem. Soc.* **1984**, *106*, 1257.

NOTE TO USERS

Page(s) missing in number only; text follows. Page(s) were scanned as received.

48, 76, 98, 168, 196

Page(s) not included in the original manuscript and are not available from the author or university. The manuscript was scanned as received.

This reproduction is the best copy available.

Chapter 4

Lowering large 1,2-H shift barriers by proton-transport catalysis : the challenging case of the pyridine radical cation

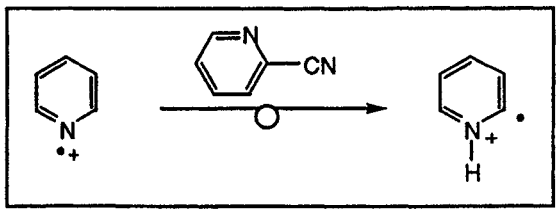

Under conditions of chemical ionization, the pyridine radical cation rearranges to its more stable α-ylide isomer by an ion-molecule reaction with a suitable reagent, such as 2-cyanopyridine. The initially formed [pyridine$^{\bullet+}$•••2-cyanopyridine] adduct isomerizes by way of proton transport catalysis to a stable complex of 2-cyanopyridine with the α-ylide ion which may dissociate. Multiple collision experiments on deuterium labelled pyridines, indicate that a further isomerization may occur : about half of the (metastable) complex ions undergo a cyano transfer leading to a very stable distonic ion. A subsequent 1,4-hydrogen shift may lead to the di-2-pyridyl ketimine ion which could account for the observed survivor signal in the Neutralization-Reionization mass spectrum of the complex. *Ab initio* calculations at the RHF/6-31G(d) level of theory fully support these findings and provide a rationale for the observed cyano transfer reaction.

The work described here has been published previously in an article under the same title: M.A. Trikoupis, D.J. Lavorato, P.C. Burgers, P.J.A. Ruttink and J.K. Terlouw, Eur. Mass Spectrom. 1999, 5, 431-439.

Introduction

In 1993, in a commemorative article Allan Maccoll wrote : "Sir Christopher Ingold... developed the framework for interpreting organic reactions and studying mechanisms that is still used today" [1]. Allan has clearly taken his master's lead when he entered the field of organic mass spectrometry. One example from his early work in the field concerns ion structures. Nowadays, we readily invoke five-membered rings in the interpretation of electron ionization mass spectra, but it was Allan Maccoll who, in 1967, first proposed these as attractive stable species [2]. He also was one of the first to realize the importance of ion dipole-complexes [3], in particular that such complexes permit hydrogen transfer between the incipient products [4]. In fact, these early studies helped to pave the way for the discovery of a process which is now known as proton-transport catalysis [5]. Such a proton transport reaction has been demonstrated in several small systems e.g. the carbon monoxide assisted isomerization of ionized H-C≡N into its more stable H-N≡C tautomer.

This tautomerization has a barrier of 27 kcal/mol and does not occur spontaneously. However, in the presence of CO the barrier becomes vanishingly small [5]. More recently, a number of elegant experimental and theoretical studies [6] have reported mechanisms by which a gaseous conventional radical cation $[H\text{-}X\text{-}Y]^{\bullet+}$ isomerizes into its more stable distonic isomer $[X\text{-}Y\text{-}H]^{\bullet+}$ via interaction with a single solvent molecule B. One prominent example concerns X = CH_2 and Y = OH, that is the α-distonic $[CH_2OH_2]^{\bullet+}$ ion, the methylene oxonium ion. This ion is c. 7 kcal/mol more stable than its isomer of conventional structure $[CH_3OH]^{\bullet+}$ but the two isomers do not interconvert because the 1,2-H shift involved imposes a barrier of 26 kcal/mol. However, a molecule of water (B) catalyzes this shift and promotes a smooth transformation of $[CH_3OH]^{\bullet+}$ into $[CH_2OH_2]^{\bullet+}$ [6b,g]. From detailed *ab initio* calculations [6c-f] it follows that O•H•O and C•H•O hydrogen-bridged radical cations play a prominent role in this transformation. Such a catalysis not only occurs under certain conditions in bimolecular reactions, it also is a key step in the dissociative rearrangement of oxygen-containing radical cations via a double H transfer such as the loss of $HCO^{\bullet}$ from ionized ethylene glycol [7].

As an appropriate background to this contribution we first present a brief description of the concept of proton transport catalysis vis-à-vis that of a hydrogen atom shift [8], using Figure 4.1 as a guide. Consider the $[H\text{-}X\text{-}Y]^{\bullet+}$ ion in the rarefied gas phase as well as its hydrogen shifted isomer $[X\text{-}Y\text{-}H]^{\bullet+}$; for X = CH_2 and Y = OH this represents the $CH_3OH^{\bullet+}$ / $CH_2OH_2^{\bullet+}$ system linked by a 1,2-H shift [6] while for X = CH_2 and Y = CH_3CO we are dealing with the $CH_3C(=O)CH_3^{\bullet+}$ / $CH_2=C(OH)CH_3^{\bullet+}$ system linked by a 1,3-H shift [9]. If the barrier for the hydrogen atom shift is sufficiently high, that is, higher than the lowest dissociation level, isomerization will not take place. In this case the isomers can readily be differentiated by their Metastable Ion (MI) or Collision-Induced Dissociation (CID) mass spectra [10a] or alternatively specific ion-molecule reactions [10b,c]. Next, consider the situation when a molecule B approaches the $[H\text{-}X\text{-}Y]^{\bullet+}$ ion. At a distance of a few Angstroms between the components, hydrogen bridging takes place in the encounter complex and the resulting $B\bullet\bullet\bullet[H\text{-}X\text{-}Y]^{\bullet+}$ ion is stabilized by ion-dipole (or ion-induced dipole) attractions. What can happen next depends on the Proton Affinity (PA) of B. If the PA of B is sufficiently low, B cannot accept the proton from $[H\text{-}X\text{-}Y]^{\bullet+}$. The hydrogen, still bonded with B, can move over from X to Y and if the Transition State (TS) enjoys the same stabilization as the reactants and products, the situation in Figure 4.1b will ensue. This situation occurs if B is a non-polar molecule such as a noble gas atom [6b-d, 8]. This scenario could be described as a catalysis, but the isomerization remains a hydrogen atom shift. In this context it is also possible that B binds to a proton from a different site of the substrate, and if the PA of B is sufficiently large, it may even accept such a proton. In this "spectator" mechanism [6f] the molecule B is not directly involved in the isomerization process.

Next, consider the case that B can accept the proton from $[H\text{-}X\text{-}Y]^{\bullet+}$ to produce complex ions - not "complexions" [1] - of the type $B\text{-}H^+\bullet\bullet\bullet[X\text{-}Y]^{\bullet}$. This will happen when PA(B) is larger than PA$[X\text{-}Y]^{\bullet}$ at X. Now, if the PA$[X\text{-}Y]^{\bullet}$ at Y is larger than PA(B) then the proton may be donated back to $[X\text{-}Y]^{\bullet}$ at site Y:

$$[H\text{-}X\text{-}Y]^{\bullet+} + B \rightarrow B\bullet\bullet\bullet H^+\bullet\bullet\bullet[X\text{-}Y]^{\bullet} \rightarrow B\bullet\bullet\bullet H^+\bullet\bullet\bullet[Y\text{-}X]^{\bullet} \rightarrow B + [X\text{-}Y\text{-}H]^{\bullet+} \qquad (1)$$

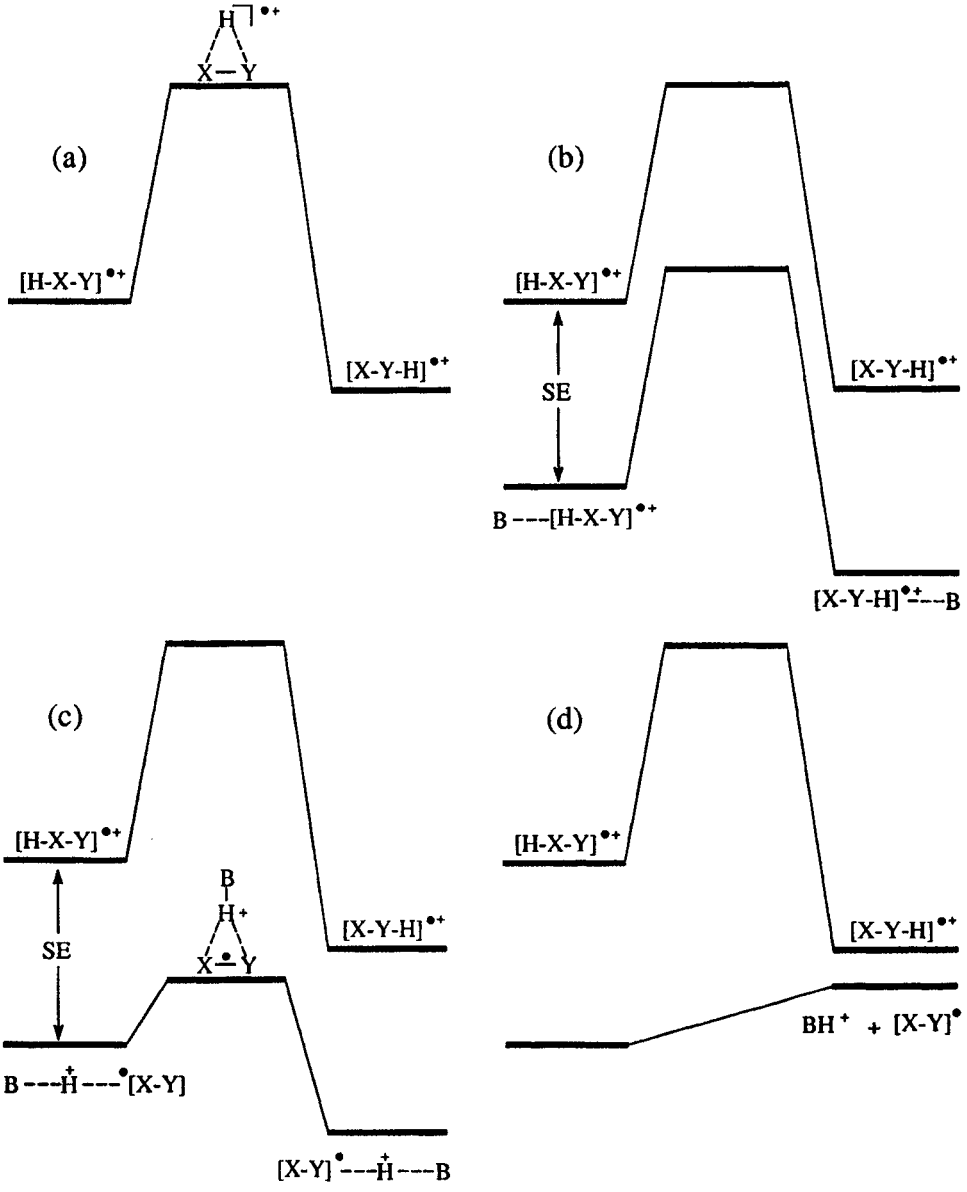

Figure 4.1. Schematic potential energy profile of (a) solitary $[H\text{-}X\text{-}Y]^{\bullet+}$ and its 1,2-hydrogen shifted isomer $[X\text{-}Y\text{-}H]^{\bullet+}$; (b) ions $[H\text{-}X\text{-}Y]^{\bullet+}$ interacting with a molecule B; (c) proton transport catalysis; (d) dissociation of the intermediate $B\bullet\bullet\bullet H^{+}\bullet\bullet\bullet[X\text{-}Y]^{\bullet}$.

Since the isomerization now proceeds via proton transfers as opposed to hydrogen atom shifts, a significant reduction of the barrier may be achieved, see Figure 4.1c; compared to the reactants and products, the barrier may even become negative [6d-f]. This process has been termed proton-transport catalysis [5].

What conditions should apply for efficient proton-transport catalysis? A most important criterion has already been outlined above and may be termed the Radom transport criterion [6d]. It states that efficient catalysis will take effect when the PA of the base B lies between the PA of $[X\text{-}Y]^{\bullet}$ at X and at Y. If PA(B) is significantly lower than PA$[X\text{-}Y]^{\bullet}$ at X, the first step in eq 1 will not take place. If, on the other hand, PA(B) is significantly larger than PA$[X\text{-}Y]^{\bullet}$ at Y, then the intermediate complex $B{\bullet\bullet\bullet}H^{+}{\bullet\bullet\bullet}[X\text{-}Y]^{\bullet}$ will dissociate to $[X\text{-}Y]^{\bullet}$ and BH^{+} via a unidirectional proton transfer, as depicted in Figure 4.1d.

From an experimentalist's point of view, other properties of the base must also be considered [9]. First, the Ionization Energy (IE) of the base should not be much lower than that of the substrate, otherwise the incipient ion $[H\text{-}X\text{-}Y]^{\bullet+}$ will be neutralized by charge exchange. In addition, the base should not undergo self-protonation, because BH^{+} thus formed may protonate the substrate. In addition, BH^{+} may react further to produce the proton bound dimer $B{\bullet\bullet\bullet}H^{+}{\bullet\bullet\bullet}B$ as well as the proton bound base-substrate dimer. When these side reactions are suppressed, the system has no choice but to produce the dimer radical cation $B{\bullet\bullet\bullet}H^{+}{\bullet\bullet\bullet}[X\text{-}Y]^{\bullet}$. This species can then be isolated and its unimolecular dissociation chemistry may provide definitive evidence for the isomerization of the substrate by the molecule B [9].

In this paper we describe the successful application of the above criteria to a particularly challenging case, the transformation of the pyridine radical cation, $\mathbf{1}^{\bullet+}$, to its slightly more stable α-ylide isomer, $\mathbf{1a}^{\bullet+}$ [11] :

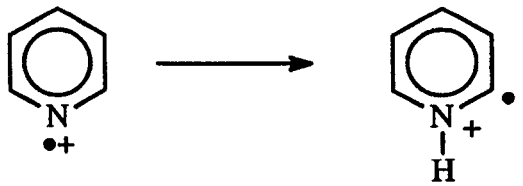

$\mathbf{1}^{\bullet+}$ $\mathbf{1a}^{\bullet+}$

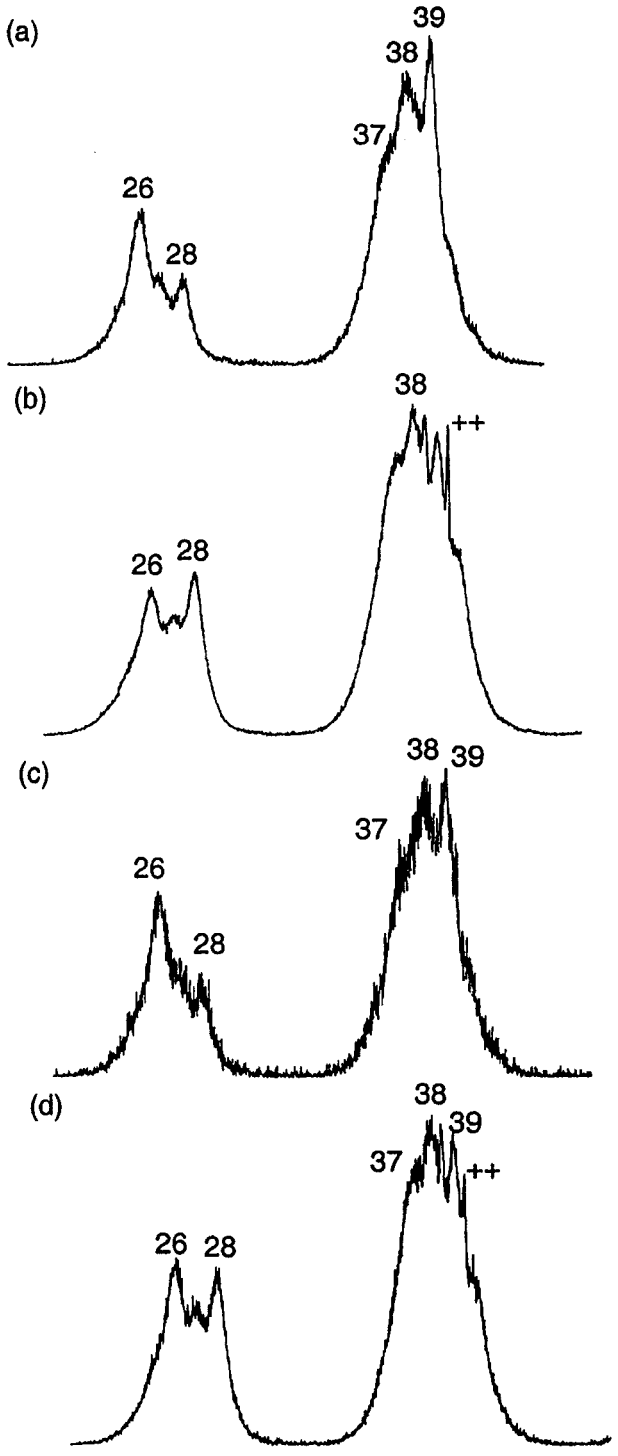

Figure 4.2. Collision-induced dissociation mass spectra (3ffr, O_2) of : (a) ionized pyridine, $1^{\bullet+}$, reference spectrum 4 keV ions ; (b) α-ylide ion of pyridine, $\mathbf{1a}^{\bullet+}$, reference spectrum 4 keV ions; (c) the collisionally formed *m/z* 79 ions from 10 keV ["pyridine"$^{\bullet+}$•••benzonitrile] adduct ions ; (d) the collisionally formed *m/z* 79 ions from 10 keV ["pyridine"$^{\bullet+}$•••2-CP] complex ions. (For sensitivity reasons spectra (c) and (d) were obtained with all slits open, i.e. at a lower energy resolution.)

This isomerization is of particular interest, because the barrier for the 1,2-H shift separating the isolated ions has been calculated to be as high as ~ 60 kcal/mol [11b]. It will be shown that, in the presence of a suitable base, this barrier reduces to a mere 9 kcal/mol.

Results and Discussion

Computational and experimental studies [11] have shown that the pyridine radical cation has three stable hydrogen-shift isomers, the α-ylide ion **1a**$^{\bullet+}$ discussed above, and the β- and γ-distonic ions **1b**$^{\bullet+}$ and **1c**$^{\bullet+}$ depicted in Scheme 4.1, which presents the structures we are dealing with in this study. These hydrogen shift isomers are all slightly more stable than the parent **1**$^{\bullet+}$. Their facile (inter)conversion via 1,2-hydrogen shifts is prevented by large barriers which do however lie below the common reaction of lowest energy requirement, loss of HCN. Nevertheless, all four isomeric ions can be uniquely characterized on the basis of their high energy CID mass spectra [11b] or alternatively, associative ion-molecule reactions [10c]. We further note that, whereas the high 1,2-H shift barrier for the isomerization **1**$^{\bullet+}$ → **1a**$^{\bullet+}$ might be reduced by proton-transport catalysis, no such process is available for the isomerizations **1a**$^{\bullet+}$ → **1b**$^{\bullet+}$ and **1b**$^{\bullet+}$ → **1c**$^{\bullet+}$.

As argued before [11], a distinction of ionized pyridine, **1**$^{\bullet+}$ from its isomer **1a**$^{\bullet+}$ is readily available on the basis of the *m/z* 28 : *m/z* 26 intensity ratio in their CID mass spectra. Figure 4.2a and 4.2b represent the structure-diagnostic portions of the CID mass spectra of **1**$^{\bullet+}$ and **1a**$^{\bullet+}$, respectively. As reported earlier, isomer **1a**$^{\bullet+}$ is characterized by a *m/z* 28 : *m/z* 26 peak intensity ratio of 0.86 ± 0.03 (for ions having 6 keV translational energy and using O_2 as collision gas), whereas fewer $HCNH^+$ ions at *m/z* 28 are generated from **1**$^{\bullet+}$ (intensity ratio 0.41 ± 0.03). Note that the CID spectra also show intensity ratio differences in the *m/z* 37 - 39 region and that the ylide ion **1a**$^{\bullet+}$ features a pronounced doubly charged ion of *m/z* 39.5 that is virtually absent in the CID mass spectrum of ionized pyridine **1**$^{\bullet+}$. In the deuterium labelled isotopomers the doubly charged ion is of less diagnostic value because it may coincide with regular CID peaks.

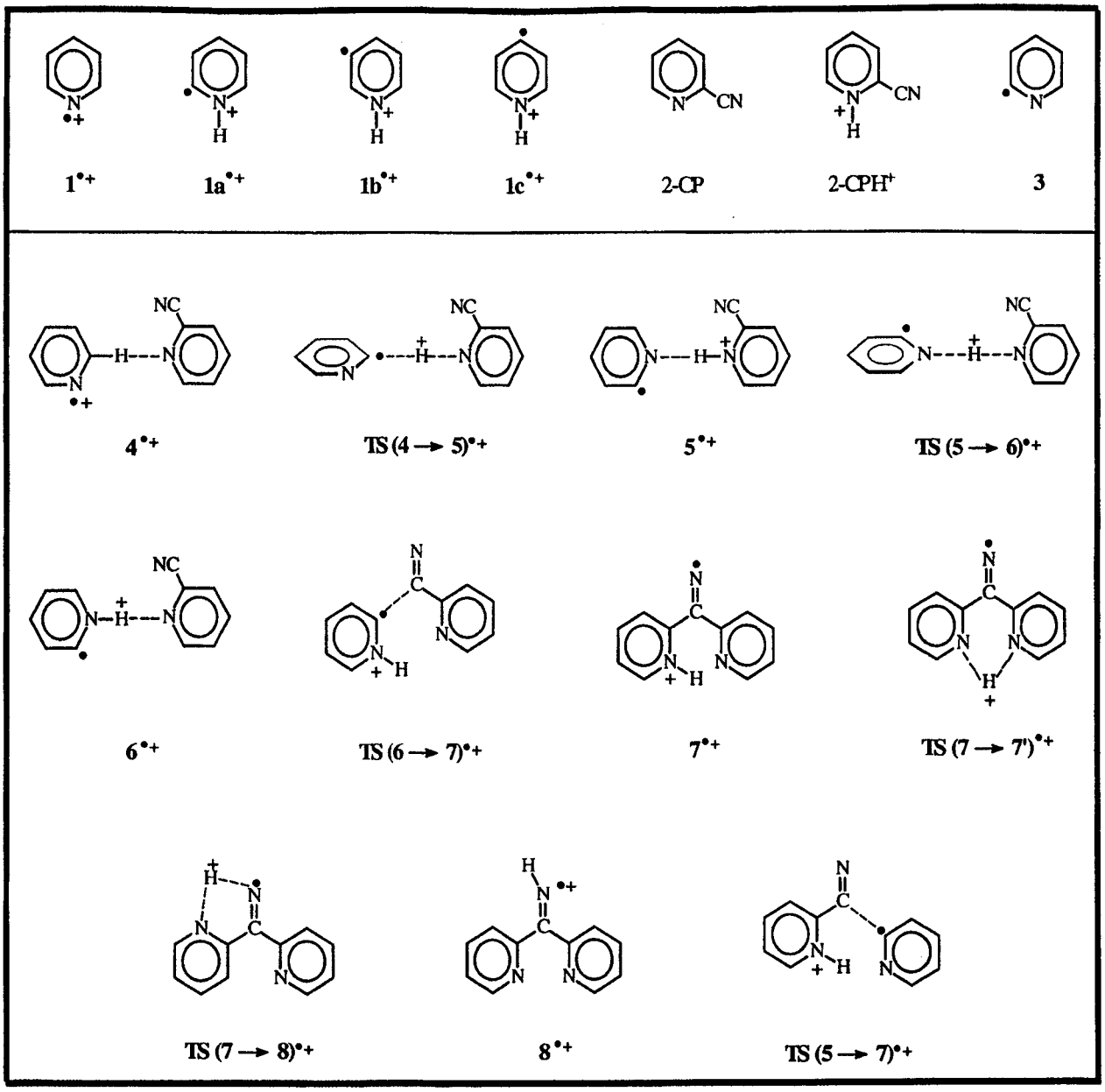

Scheme 4.1

The search for a suitable base

First we deal with the Radom PA criterion. From shock wave experiments and RRKM calculations [12] the C-H bond strength (most probably that of the α-hydrogen) in neutral pyridine has been determined, 105 kcal/mol. From the known ΔH_f of pyridine [13], that of the ortho-pyridyl radical, **3**, is then calculated as 86.3 kcal/mol. From ΔH_f ($\mathbf{1}^{\bullet+}$) = 247 kcal/mol, we calculate PA(**3**) at C$^{\bullet}$ as 205 kcal/mol. Since ΔH_f ($\mathbf{1a}^{\bullet+}$) = 237 kcal/mol [11], the PA (**3**) at N becomes 215 kcal/mol. Thus we need a base having a PA in the range of 205-215 kcal/mol. In a previous study [9] of the base induced isomerization of the acetone radical cation, benzonitrile appeared a suitable base. The advantage of using aromatic bases is that self-protonation is usually endothermic. However, the PA of benzonitrile (196 kcal/mol) is too low to catalyze the isomerization of pyridine ions. When benzonitrile was used, the CI mass spectrum did show a sizeable signal at *m/z* 182 corresponding with a [pyridine$^{\bullet+}$•••benzonitrile] adduct. The MI and CID mass spectra of this dimer radical cation are dominated by *m/z* 79 ions, but MS/MS/MS [14] experiments, see Figure 4.2c, clearly show that the pyridine moiety has retained its structure. Thus although ionized pyridine and benzonitrile do form a complex, isomerization does not take place, as predicted. In contrast, the related compound 2-cyanopyridine (2-CP), has a PA (208 kcal/mol [13b]) that does satisfy the proton affinity criterion and so it may be able to catalyze the isomerization. Moreover, 2-CP has an ionization energy, 10.1 eV, that is slightly higher than that of the pyridine substrate, 9.2 eV [13a].

Proton-transport catalysis

When only 2-CP was introduced into the ion source at an indicated pressure of 4 x 10^{-5} Torr, the most intense peak observed in the spectrum was at *m/z* 105, indicating that self protonation of the base does occur. Nevertheless, the intensity of the *m/z* 104 molecular ion remained about half that of *m/z* 105, and thus B$^{\bullet+}$ ions for charge exchange and complexation with the substrate are available. As expected, the protonated species reacted further to produce

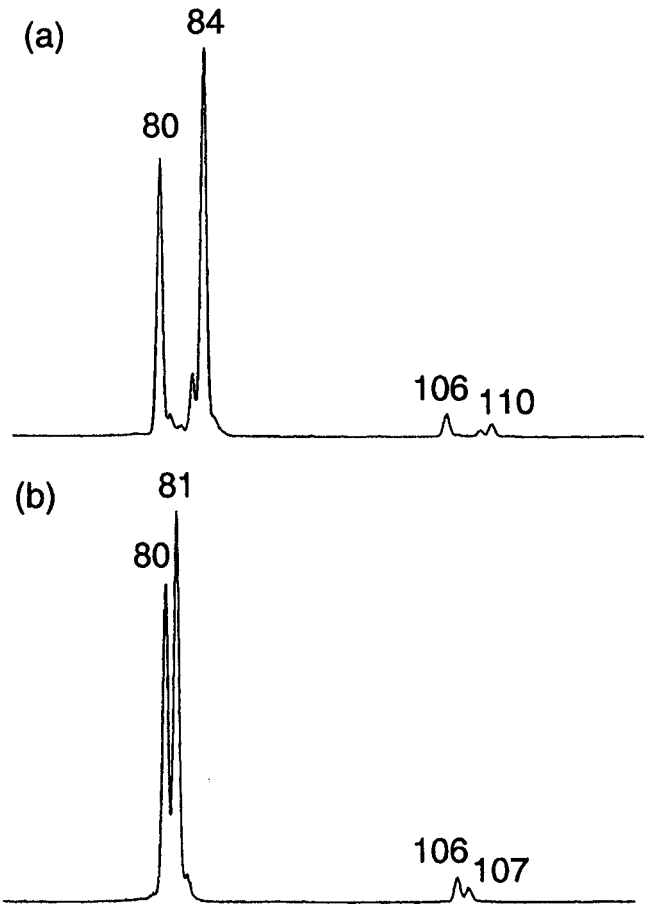

Figure 4.3. Metastable ion mass spectra of : (a) the ["pyridine-d_5"$^{\bullet+}$•••2-CP] complex ions at *m/z* 188; (b) the ["pyridine-d_2"$^{\bullet+}$•••2-CP] complex ions at *m/z* 185.

the proton bound dimer at *m/z* 209. When a small amount of pyridine was then injected into the ion source, peaks of equal abundance appeared at *m/z* 79 and *m/z* 80 (protonated pyridine) with an intensity of c. 10% of the *m/z* 105 ion. Also present was a signal in the 5-10 % intensity range at *m/z* 184 representing the proton bound dimer of pyridine and 2-CP. More importantly, this peak was flanked by a *m/z* 183 peak of similar abundance, representing the desired ["pyridine"•••2-CP]$^{\bullet+}$ complex. The MI mass spectrum of this complex is dominated by *m/z* 79 ions. Upon collisional activation, the weak MI peak at *m/z* 105, protonated

2-cyanopyridine, 2-CPH$^+$, becomes more intense. The CID mass spectra of the metastably and the collisionally generated *m/z* 79 ions from the complex were very similar and a representative spectrum is shown in Figure 4.2d. Comparison with the reference spectra in Figures 4.2a and 4.2b reveals that the *m/z* 79 ions have the ylide structure **1a**$^{\bullet+}$. Thus, the initially formed [pyridine$^{\bullet+}$•••2-CP] ion-dipole complex has converted into a [α-ylide$^{\bullet+}$•••2-CP] complex. Our *ab initio* calculations, see below, indicate that these ions represent the hydrogen bridged species **5**$^{\bullet+}$ and **6**$^{\bullet+}$. These experiments clearly show that 2-cyanopyridine catalyses the isomerization.

It is in principle possible that the base accepts a proton from the substrate and then donates back a different proton to the conjugate base as is the case for the benzonitrile assisted isomerization of ionized acetamide [15]. To determine whether this process takes place, we examined the behaviour of pyridine-d_5 in admixture with 2-cyanopyridine. The [substrate$^{\bullet+}$•••base] adduct now appears at *m/z* 188. The MI spectrum of this peak is given in Figure 4.3a. As expected from a "back-and-forth" [16] mechanism, the most intense peak is at *m/z* 84; MS/MS/MS experiments, see Figure 4.4a and 4.4b, indicate that they have the ylide structure. The signal at *m/z* 83 indicates that the base may donate back a different proton but this clearly is only a minor process.

More surprising is that the spectrum of Figure 4.3a also displays an intense signal at *m/z* 80. Its CID mass spectrum is presented in Figure 4.4c, together with that of the closely similar reference spectrum of **1a**$^{\bullet+}$(N-D), see Figure 4.4d. The latter ion was independently generated by dissociative ionization of methyl-d_3 picolinate, as depicted in Scheme 4.2.

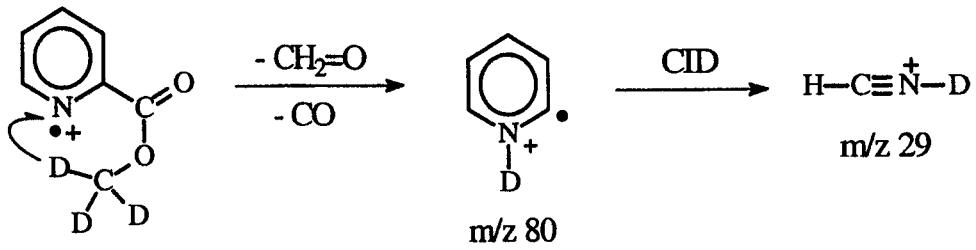

Scheme 4.2

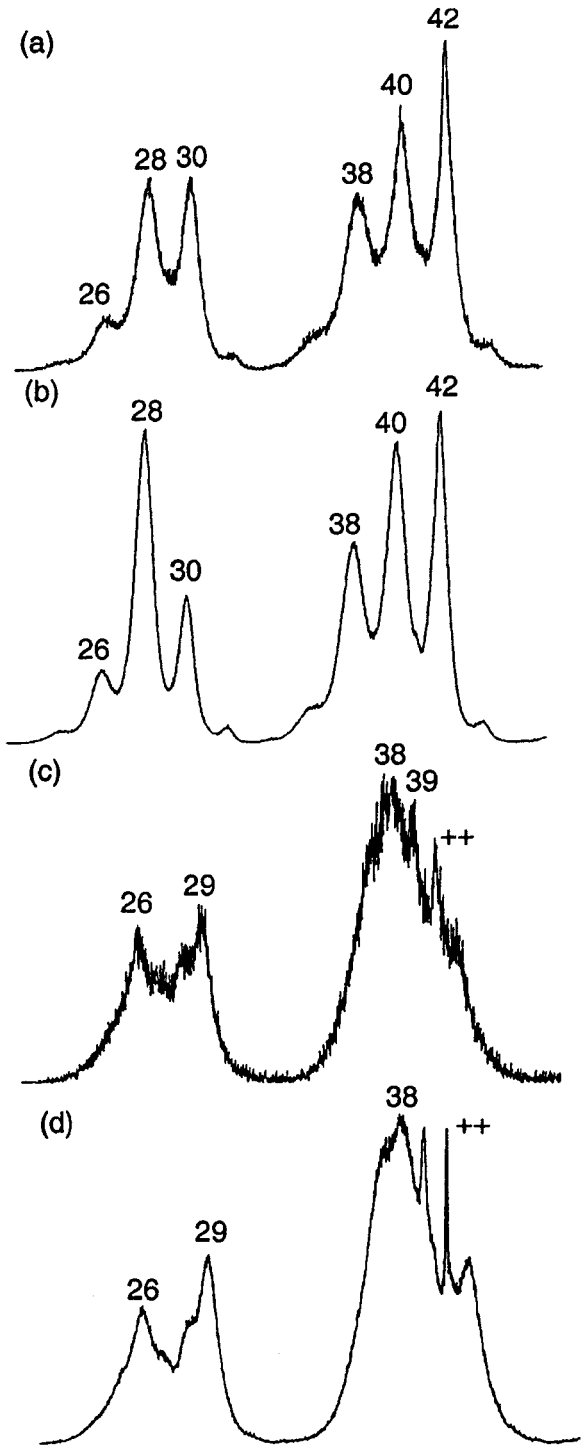

Figure 4.4. Collision-induced dissociation mass spectra (3ffr, O_2) of : (a) collisionally formed *m/z* 84 ions from the 10 keV ["pyridine-d_5"$^{\bullet+}$•••2-CP] adduct ions ; (b) ionized pyridine-d_5, reference spectrum 5 keV ions ; (c) collisionally formed *m/z* 80 ions from the 10 keV ["pyridine-d_2"$^{\bullet+}$•••2-CP] adduct ions ; (d) (N-D) labelled α-ylide ions $\mathbf{1a}^{\bullet+}$, reference spectrum 4 keV ions. (For sensitivity reasons spectrum (c) was obtained at a lower energy resolution than spectrum (d).)

These observations leave little doubt that the *m/z* 80 ion generated from the ["pyridine-d_5"•••base]$^{\bullet+}$ complex is the N-D labelled α-ylide ion **1a**$^{\bullet+}$. Similar experiments were performed using pyridine-2,6-d_2. The MI mass spectrum of the ["pyridine-d_2"•••2-CP]$^{\bullet+}$adduct ion, see Figure 4.3b, again shows two peaks representing the pyridine moiety, now at *m/z* 80 and 81. We further note that the signal for 2-CPH$^+$ is also split, in approximately the same ratio. These results are best explained in terms of a cyano group transfer taking place in complex **6**$^{\bullet+}$, as depicted in Scheme 4.3:

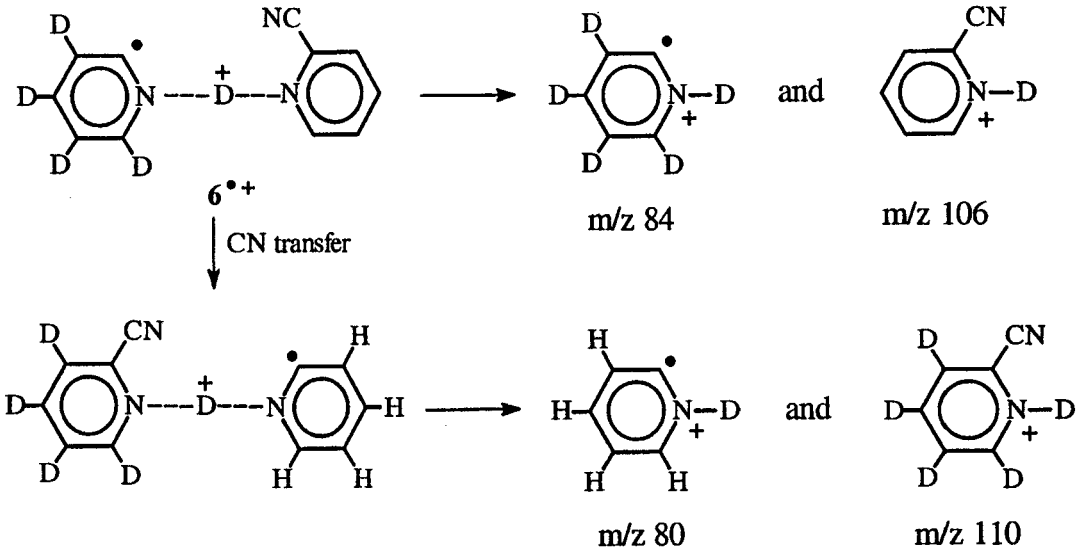

Scheme 4.3

In the following we present the results of our *ab initio* calculations on the 2-CP assisted isomerization of the pyridine radical cation and the intriguing cyano transfer reaction mentioned above. The central question is: by how much is the isomerization barrier reduced and is the CN transfer an energetically favourable process ?

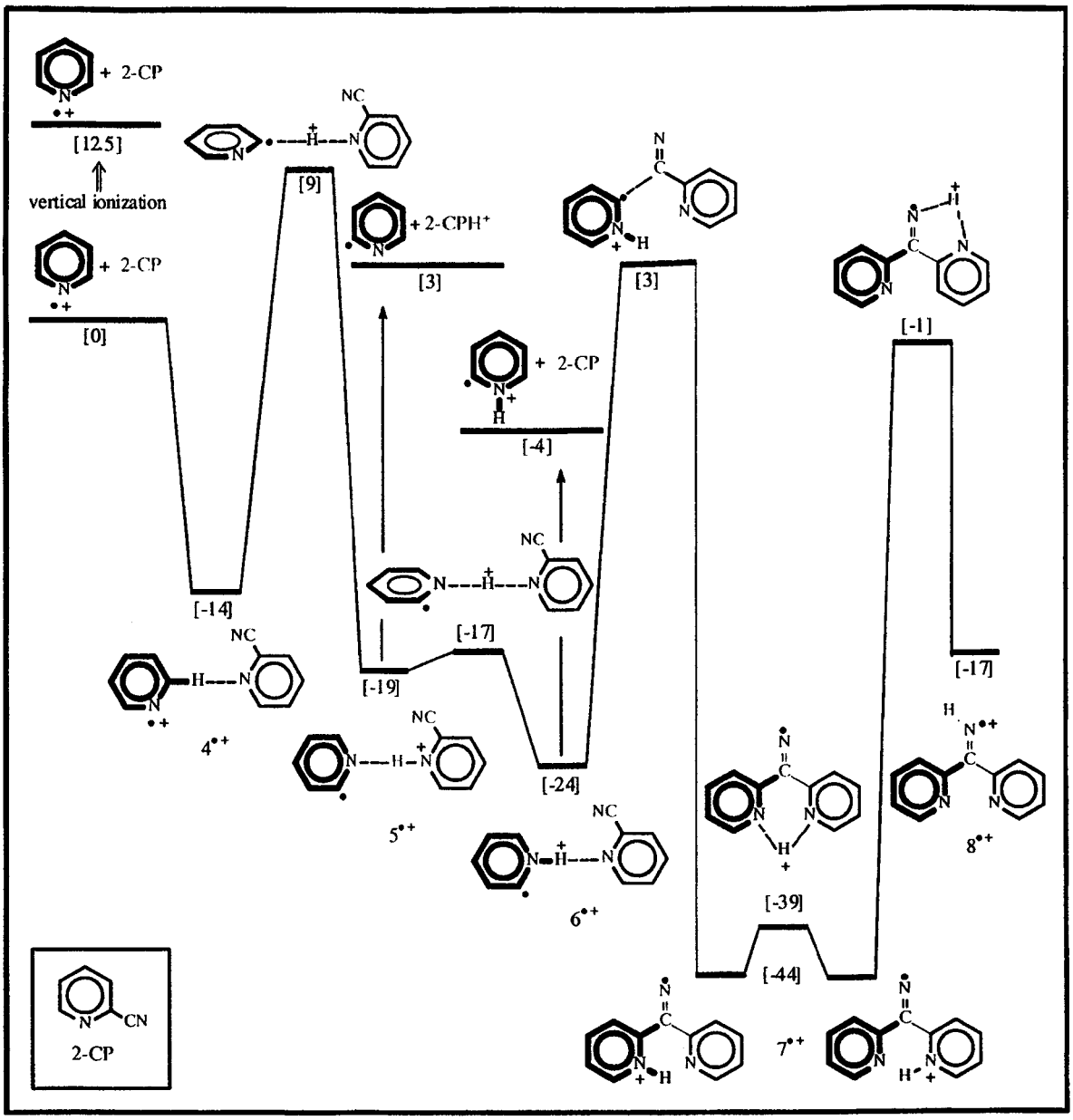

Figure 4.5. Energy diagram derived from *ab initio* calculations for the 2-CP assisted isomerization of ionized pyridine, $1^{\bullet+}$ into its 1,2-H shift isomer $\mathbf{1a}^{\bullet+}$ and the subsequent cyano transfer reaction; numbers in square brackets refer to relative energies in kcal/mol.

Theoretical calculations

Standard RHF geometry searches using the standard 6-31G(d) basis set were performed to identify the stationary points on the potential energy surface (PES), using the GAMESS-UK program system [17]. The ZPVE was calculated with the same method and basis set and corrected for electronic correlation effects by scaling [18a] the results with a factor of 0.9 [19]. All stationary points were identified either as minima or as saddle points with only one imaginary frequency. All connections between the transition states and the minima were checked by performing geometry optimizations starting from geometries near to, but on either side of, the transition state geometries. Scheme 4.1 lists the various minima and transition state structures located - the actual optimized geometries are not presented but are available upon request - while Table 4.1 presents their relative energies. For comparison, single point calculations on selected minima at the B3LYP/cc-pVTZ//B3LYP/6-31G(d) level of theory [18b] are also presented. Considering the size of the system, the agreement between theory and experiment is quite satisfactory.

Figure 4.5, the energy diagram derived from the computational results, serves as a guide for the following discussion. First, the barrier for the unassisted reaction $\mathbf{1}^{\bullet+} \rightarrow \mathbf{1a}^{\bullet+}$ was calculated at 71 kcal/mol, compared to a previously calculated value of 61 kcal/mol [11]. When a pyridine radical cation approaches a neutral 2-CP molecule a significant ion-dipole interaction may occur (μ (2-CP) = 5.8 Debye [20]) paving the way for the formation of the C•H•N bonded hydrogen-bridged radical cation $\mathbf{4}^{\bullet+}$ at -14 kcal/mol. As depicted in Figure 4.5, this species is planar. Next, the bridging proton may move over from the ionized pyridine moiety to the cyanopyridine partner and in doing so the pyridyl ring rotates 90° until eventually a transition state is reached, **TS (4→5)**$^{\bullet+}$ (+9 kcal/mol). (Note that the proton moves to the ring N of 2-CP and not to the cyano N: the PA of the latter site is calculated to be 17 kcal/mol lower than the PA at the ring N.) Next the proton moves further and as it moves, the pyridyl ring rotates back and at the same time it rotates 30° along the axis perpendicular to the pyridyl plane to generate the N•H•N bonded species $\mathbf{5}^{\bullet+}$ (- 19 kcal/mol). This species may

Table 4.1. Electronic energies (hartrees), scaled zero-point vibrational energies (ZPVEs, kcal/mol) and relative energies, E_{rel} (kcal/mol) of the species involved in the 2-cyanopyridine (2-CP) assisted isomerization of the pyridine radical cation.

Species	Energy (-584.)	ZPVE	E_{rel} (calc)		E_{rel} (exp)
1$^{\bullet+}$ + 2-CP	.82705 [a]	106.5	0	[0] [b]	0 [c]
4$^{\bullet+}$	.85042	107.2	-14	[-15]	
TS (4 → 5)$^{\bullet+}$	.80936	104.4	9		
5$^{\bullet+}$	.85940	108.2	-19	[-16.5]	
TS (5 → 6)$^{\bullet+}$	.85200	105.3	-17		
6$^{\bullet+}$	.86783	108.4	-24	[-22.5]	-26 [d]
TS (6 → 7)$^{\bullet+}$	.82310	107.5	3.5		
7$^{\bullet+}$	.90333	110.1	-44	[-46]	
TS (7 → 7')$^{\bullet+}$	.88959	107.1	-39		
TS (7 → 8)$^{\bullet+}$	.82849	106.4	-1		
8$^{\bullet+}$	.85644	108.2	-17		
TS (5 → 7)$^{\bullet+}$	.81725	107.7	7		
2-CPH^{+} + **3**	.82348 [e]	107.5	3		-3
1a$^{\bullet+}$ + 2-CP	.83523	107.5	-4		-10 [f]
TS (1 → 1a)$^{\bullet+}$ + 2-CP	.70864	103.2	71 [g]		

[a] Individual energies are -246.40038 and -338.42667 hartrees.
[b] Values in square brackets represent the results of selected B3LYP/cc-pVTZ//B3LYP/6-31G(d) calculations, see text.
[c] Using the data (± 1 kcal/mol) given in ref. 13a.
[d] Estimated from the empirical relationship in ref. 20.
[e] Individual energies are -338.77532 and -246.40817 hartrees.
[f] From ref. 11, the uncertainty is ± 5 kcal/mol.
[g] Relative to ionized pyridine, **1**$^{\bullet+}$; the value in ref. 11b is 61 kcal/mol.

dissociate directly to produce protonated 2-cyanopyridine (+3 kcal/mol). In the transformation $\mathbf{4}^{\bullet+} \rightarrow \mathbf{5}^{\bullet+}$ the proton moves from carbon to nitrogen and the fairly high barrier for this migration, 23 kcal/mol, indicates that intermolecular proton transfers can have a significant energy requirement. In ion $\mathbf{5}^{\bullet+}$, the proton may be donated back to the pyridyl moiety leading to $\mathbf{6}^{\bullet+}$ which may then dissociate to produce the α-ylide $\mathbf{1a}^{\bullet+}$. The transformation $\mathbf{4}^{\bullet+} \rightarrow \mathbf{6}^{\bullet+}$ constitutes an example of proton-transport catalysis. Although the barrier for the transformation $\mathbf{1}^{\bullet+} \rightarrow \mathbf{1a}^{\bullet+}$ has been considerably lowered by proton-transport catalysis, it has not become negative as is the case for the water catalyzed isomerization of $CH_3OH^{\bullet+}$ into $CH_2OH_2^{\bullet+}$ [6d].

The question may arise whether the starting ion $\mathbf{1}^{\bullet+}$ will have sufficient energy to surmount the barrier represented by **TS (4→5)**$^{\bullet+}$ (+9 kcal/mol). The starting energy level labelled [0] in Figure 4.5 corresponds to the adiabatic ionization energy (IE) of pyridine. From the photoelectron spectrum [13c], it follows that the vertical IE is c. 0.5 eV higher. Indeed, the calculated electronic energy of a pyridine radical cation having the geometry of the neutral, is ~ 12.5 kcal/mol higher than that of the ground state ion, see Figure 4.5. Thus pyridine ions generated by vertical ionization can surmount the highest transition state en route to the isomerization, **TS (4→6)**$^{\bullet+}$. The stabilization energy of the N•H•N type hydrogen-bridged radical cation $\mathbf{6}^{\bullet+}$ may be assessed from the empirical relationship SE (kcal/mol) = 23.2 - 0.25ΔPA [21], where ΔPA is the difference in proton affinity between 2-CP (208 kcal/mol) and the ortho-pyridyl radical at N (215 kcal/mol, see above). We then obtain SE = 21 kcal/mol, in good agreement with the computationally derived number, 20 kcal/mol, see Figure 4.5.

When the incipient α-ylide ion in complex $\mathbf{6}^{\bullet+}$ rotates by 180° along the N•H•N axis - according to our calculations which are not further discussed here, this is a more or less free rotation - and then by 30° along the axis perpendicular to the plane, a transition state is reached, **TS (6→7)**$^{\bullet+}$, which has the radical site in close proximity to the CN group. Complete proton transfer from N to N is then accompanied by covalent C-C bond formation leading to a surprisingly stable distonic ion, $\mathbf{7}^{\bullet+}$, at -44 kcal/mol. A proton shift via the low lying **TS (7→7')**$^{\bullet+}$ leads to a degenerate isomerization, making the two rings indistinguishable. This

mechanism, we propose, rationalizes the formation of the two different labelled products in the experiments with pyridine-d_5 and pyridine-d_2, see Figure 4.3. Alternatively, and for reasons of clarity this is not shown in Figure 4.5, species $\mathbf{5}^{\bullet+}$ may rearrange directly to $\mathbf{7}^{\bullet+}$, via **TS (5→7)**$^{\bullet+}$ depicted in Scheme 4.1. This step closely resembles that of $\mathbf{6}^{\bullet+} \rightarrow \mathbf{7}^{\bullet+}$ but lies slightly higher in energy, at + 7 kcal/mol vis-à-vis +3.5 kcal/mol for the transformation $\mathbf{6}^{\bullet+} \rightarrow \mathbf{7}^{\bullet+}$, see Table 4.1.

So far, we have only encountered hydrogen-bridged radical cations and distonic ions on the potential energy surface. It is unlikely that their neutral counterparts are sufficiently stable to generate a significant survivor ion signal in Neutralization-Reionization (NR) experiments [22] at kilovolt translational energies. Nevertheless, the NR mass spectrum of the ["pyridine-d_5"•••2-CP]$^{\bullet+}$adduct ion at *m/z* 188 not only showed expected dissociation products, like *m/z* 104 (100%, ionized 2-CP) and *m/z* 108 (75%, ionized 2-CP-d_4), but also a survivor signal of 25% relative intensity. This points to the presence of a neutral species of conventional structure. According to our calculations the distonic ion $\mathbf{7}^{\bullet+}$ could undergo a 1,4-hydrogen shift to the radical site to produce, via **TS (7→8)**$^{\bullet+}$, ionized di-2-pyridyl ketimine, $\mathbf{8}^{\bullet+}$. The ketimine ion is expected to produce a stable neutral molecule upon neutralization and this may account for the observed survivor signal.

Conclusion

The pyridine radical cation $\mathbf{1}^{\bullet+}$ is separated from its more stable α-ylide isomer $\mathbf{1a}^{\bullet+}$ by a large barrier (71 kcal/mol) and thus $\mathbf{1}^{\bullet+}$ and $\mathbf{1a}^{\bullet+}$ do not interconvert. However, when $\mathbf{1}^{\bullet+}$ encounters a suitable base, the barrier can be significantly reduced - to 9 kcal/mol using 2-CP - by proton transport catalysis. In general, successful catalysis is achieved when the base B satisfies the following criteria : (i) the PA of the base should lie between the PA of conjugate base $[X\text{-}Y]^{\bullet}$ at X and at Y, see eq (1) ; (ii) the IE of the base should not be much lower than that of the substrate and (iii) the base should not readily undergo self protonation. Under these conditions, the dimer radical cation $B{\bullet\bullet\bullet}H^{+}{\bullet\bullet\bullet}[X\text{-}Y]^{\bullet}$ may be formed. This species can be isolated and its unimolecular chemistry may provide evidence for the isomerization of the

substrate. For ions $\mathbf{1}^{\bullet+}$, the base 2-cyanopyridine (2-CP) fulfills the above criteria ; under chemical ionization conditions [pyridine$^{\bullet+}$•••2-CP] complex ions are formed which rearrange to a [α-ylide of pyridine•••2-CP]$^{\bullet+}$ complex. In the metastable time-frame about half of these complex ions further isomerize via a cyano transfer.

Ab initio calculations on this system yield a valuable picture of the transformations occurring during the proton transport catalysis. Moreover, they provide a rationale for the observed cyano transfer reaction in terms of a degenerate *and facile* N to N hydrogen transfer in the intermediate distonic ion, $\mathbf{7}^{\bullet+}$ which is surprisingly low in energy.

References

[1] A. Maccoll, *Chem. Brit.* **1993**, 880.

[2] M.A. Baldwin, A.G. Loudon, A. Maccoll and D. Smith, *Chem. Commun.* **1967**, 350.

[3] T. H. Morton, *Tetrahedron* **1982**, *38*, 3195.

[4] R.D. Bowen and A. Maccoll, *J. Chem. Soc. Perkin Trans. II* **1984**, 1005.

[5] D.K. Bohme, *Int. J. Mass Spectrom. Ion Processes* **1992**, *115*, 95 and references cited therein.

[6] (a) P. Mourges, H.-E. Audier, D. Leblanc and S. Hammerum, *Org. Mass Spectrom.* **1993**, *28*, 1098 ; (b) H.-E. Audier, D. Leblanc, P. Mourgues, T.B. McMahon and S. Hammerum, *J. Chem. Soc. Chem. Commun.* **1994**, 2329 ; (c) J.W. Gauld, H.-E. Audier, J. Fossey and L. Radom, *J. Am. Chem. Soc.* **1996**, *118*, 6299 ; (d) J.W. Gauld and L. Radom, *J. Am. Chem. Soc.* **1997**, *119*, 9831 ; (e) A.J. Chalk and L. Radom, *J. Am. Chem. Soc.* **1997**, *119*, 7573 ; (f) A.J. Chalk and L. Radom, *J. Am. Chem. Soc.* **1999**, *121*, 1574 ; (g) Y.-P. Tu and J.L. Holmes, *J. Am. Chem. Soc.* **2000**, *122*, 3695.

[7] (a) P.J.A. Ruttink and P.C. Burgers, *Org. Mass Spectrom.* **1993**, *28*, 1087 ; (b) P.C. Burgers, L.M. Fell, A. Milliet, M. Rempp, P.J.A. Ruttink and J.K. Terlouw, *Int. J. Mass Spectrom. Ion Processes* **1997**, *167/168*, 291 ; (c) P.J.A. Ruttink, P.C. Burgers, L.M. Fell and J.K. Terlouw, *J. Phys. Chem. A.* **1998**, *102*, 2977.

[8] T.D. Fridgen and J. M. Parnis, *Int. J. Mass Spectrom.* **1999**, *190/191*, 181.

[9] M.A. Trikoupis, J.K. Terlouw and P.C. Burgers, *J. Am. Chem. Soc.* **1998**, *120*, 12131.

[10] (a) P.C. Burgers and J. K. Terlouw in *Encyclopedia of Spectroscopy and Spectrometry*, J.C. Lindon, G.E. Tranter and J.L. Holmes (eds.), Academic Press, Vol. 1, 1999, 990-1000 ; (b) K.M. Stirk, L.K.M. Kiminkinen and K.I. Kenttamaa, *Chem. Rev.* **1992**, *92*, 1649 ; (c) P. Gerbaux, M. Barbieux-Flammang, Y. Van Haverbeke and R. Flammang, *Rapid Commun. Mass Spectrom.* **1999**, *13*, 1707.

[11] (a) D. Lavorato, J.K. Terlouw, T.K. Dargel W. Koch, G.A. McGibbon and H. Schwarz, *J. Am. Chem. Soc.* **1996**, *118*, 11898 ; (b) D.J. Lavorato, J.K. Terlouw, G.A. McGibbon, T. K. Dargel, W. Koch and H. Schwarz, *Int. J. Mass Spectrom.* **1998**, *179/180*, 7.

[12] J.H. Kiefer, Q. Zhang, R.D. Kern, J. Yao and B. Jursic, *J. Phys. Chem A* **1997**, *101*, 7061.

[13] (a) S.G. Lias, J.E. Bartmess, J.F. Liebman, J.L. Holmes, R.D. Levin and W.G. Mallard, *J. Phys. Chem. Ref. Data, Suppl. 1* **1998**, *17* ; (b) E.P.L. Hunter and S.G. Lias, *J. Phys. Chem. Ref. Data* **1998**, *27*, 413 ; (c) K. Kimura, S. Katsumata, Y. Achiba, T. Yamazaki amd S. Iwata, *Handbook of HeI Photoelectron Spectra of Fundamental Organic Molecules* Halsted Press, New York **1981**.

[14] G.A. McGibbon, P.C. Burgers and J.K. Terlouw, *Int. J. Mass Spectrom. Ion Processes* **1994**, *136*, 191.

[15] M.A. Trikoupis, J.K. Terlouw, P.C. Burgers and P.J.A. Ruttink, *Int. J. Mass Spectrom.* **2001**, *210/211*, 489.

[16] E.E. Ferguson, *Chem. Phys. Lett.* **1989**, *156*, 319.

[17] (a) M. Dupuis, D. Spangler and J. Wendolowski, NRCC Software Catalogue 1, Program No QG01, GAMESS (**1980**) ; (b) M. Guest and J. Kendrick, GAMESS User Manual, an Introductory Guide, CCP/86/1. Daresbury Laboratories (**1986**).

[18] (a) J.A. Pople, H.B. Schlegel, R. Krishnan, D.J. deFrees, J.S. Binkley, M. Frisch, R.A. Whiteside, R.F. Hout Jr and W.J. Hehre, *Int. J. Quantum Chem.* **1981**, *15*, 269 ; (b) J.B. Foresman and A. Frisch, *Exploring Chemistry with Electronic Structure Methods*, 2nd Ed. Gaussian Inc., Pittsburgh, PA (**1996**).

[19] The pyridine radical cation calculation at +12.5 kcal/mol in Figure 4.5 was performed at the optimized geometry of the neutral pyridine molecule and therefore no ZPVE is available in this case.

[20] R.G. Ford, *J. Mol. Spectros.* **1975**, *58*, 178.

[21] M. Meot-Ner (Mautner), *J. Am. Chem. Soc.* **1984**, *106*, 1257.

[22] For a recent review see : N. Goldberg and H. Schwarz, *Acc. Chem. Res.* **1994**, *27*, 34.

[23] M. Tsuda and Y. Kawazoe, *Chem. Pharm. Bull.* **1968**, *16*, 702.

NOTE TO USERS

Page(s) missing in number only; text follows. Page(s) were scanned as received.

48, 76, 98, 168, 196

Page(s) not included in the original manuscript and are not available from the author or university. The manuscript was scanned as received.

This reproduction is the best copy available.

Chapter 5

Self-catalysis in the gas-phase: enolization of the acetone radical cation

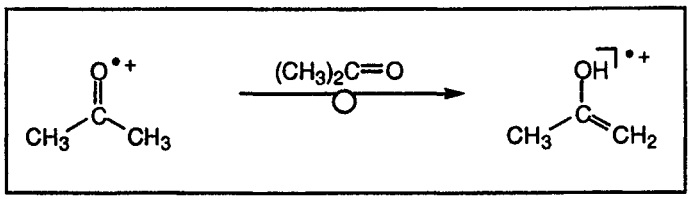

Because of a prohibitively large barrier, the solitary acetone radical cation, $CH_3C(=O)CH_3^{\bullet+}$ ($\mathbf{1}^{\bullet+}$) does not rearrange, neither spontaneously nor by activation, to its more stable enol isomer, $CH_2=C(OH)CH_3^{\bullet+}$ ($\mathbf{1a}^{\bullet+}$). However, this isomerization occurs smoothly by an ion-molecule interaction with neutral acetone itself. The dimer radical cation, [$\mathbf{1}^{\bullet+}$•••**1**], generated under conditions of chemical ionization dissociates to *m/z* 58 and collision-induced dissociation experiments show that these ions have the enol structure $\mathbf{1a}^{\bullet+}$. Labelling experiments indicate that the reaction can be viewed as a simple 1,3-hydrogen shift within the acetone radical cation of the complex. *Ab initio* calculations at the CBS-Q / DZP level of theory indicate that this isomerization is best described as a proton-transport catalysis rather than as a spectator model. Our calculations show that the incipient radical formed during the proton abstraction is not $CH_3C(=O)CH_2^{\bullet}$, but rather the less stable configuration $CH_3C(-O^{\bullet})=CH_2$ stabilized by $CH_3C(OH)CH_3^{+}$. This behaviour can be rationalized by arguments based on ion-dipole interactions. The incipient radical $CH_3C(-O^{\bullet})=CH_2$ is transformed to its more stable configuration $CH_3C(=O)CH_2^{\bullet}$ via surface crossing. However, this process does not occur via the usual "minimum to minimum crossing" but rather by the novel process of "transition state to minimum crossing". The abstracted proton is then donated back to the oxygen atom of $CH_3C(=O)CH_2^{\bullet}$ to yield the hydrogen-bridged radical cation [$\mathbf{1a}^{\bullet+}$•••**1**]. The observed tautomerization of the acetone radical cation by acetone itself can be viewed as "self-catalysis".

The work described here has been published previously in an article under the same title: M.A. Trikoupis, P.C. Burgers, P.J.A. Ruttink and J.K. Terlouw, Int. J. Mass Spectrom. (P. Longevialle issue), in press.

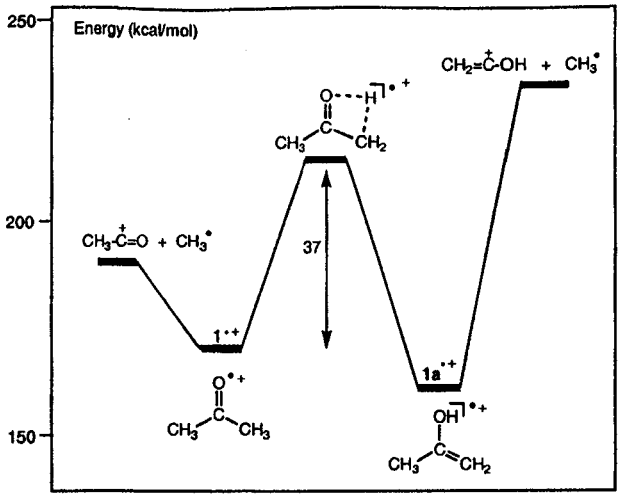

Figure 5.1. Energy diagram for the isomerization and dissociation of acetone keto and enol radical cations.

Table 5.1. Electronic energies (hartrees), scaled zero-point vibrational energies (ZPVEs, kcal/mol) and relative energies, E_{rel} (kcal/mol), of the species involved in the acetone assisted enolization of the acetone radical cation.

Species		RHF/DZP	ZPVE	CBS-Q/DZP	E_{rel}
$CH_3C(=O)CH_3$	1	-192.00868	56.2	-192.82080	
$CH_3C(=O)CH_3^{\bullet+}$	$\mathbf{1}^{\bullet+}$	-191.69909	55.5	-192.46038	0
$CH_2=C(OH)CH_3^{\bullet+}$	$\mathbf{1a}^{\bullet+}$	-191.71279	56.4	-192.47648	-10.1
$CH_3C(=O)CH_2^{\bullet}$	$[1 - H]^{\bullet}$	-191.37823	47.2	-192.16828	
$CH_3C(-O^{\bullet})=CH_2$	$[1 - H]_{\alpha}^{\bullet}$	-191.35477	47.7	-192.15709	
$CH_3C(OH)CH_3^{+}$	$[1 + H]^{+}$	-192.33943	64.9	-193.12670	
TS ($\mathbf{1}^{\bullet+} \rightarrow \mathbf{1a}^{\bullet+}$)		-191.60130	52.4	-192.40404	35.3
$\mathbf{1} + \mathbf{1}^{\bullet+}$		-383.70777	117.7	-385.28118	0
$\mathbf{1} + \mathbf{1a}^{\bullet+}$		-383.72147	112.6	-385.29728	-10.1
Complex $\mathbf{2}^{\bullet+}$		-383.73128	112.6	-385.30689	-16.1
TS ($\mathbf{2}^{\bullet+} \rightarrow \mathbf{3a}^{\bullet+}$)		-383.70023	110.0	-385.29036	-5.8
Complex $\mathbf{3a}^{\bullet+}$		-383.71013	113.7	-385.29347	-7.7
TS ($\mathbf{3a}^{\bullet+} \rightarrow \mathbf{3}^{\bullet+}$)		-383.70693	113.4	-385.29742	-10.2
PGCP [a]		-383.70706	-	-385.46737	-16.3
Complex $\mathbf{3}^{\bullet+}$		-383.76335	112.9	-385.34341	-39.1
TS ($\mathbf{3}^{\bullet+} \rightarrow \mathbf{4}^{\bullet+}$)		-383.76164	110.2	-385.35012	-42.6
Complex $\mathbf{4}^{\bullet+}$		-383.76529	113.2	-385.34469	-39.9
$[1 - H]_{\alpha}^{\bullet} + [1 + H]^{+}$		-385.69420	112.6	-385.28379	-1.6
$[1 + H]^{\bullet} + [1 + H]^{+}$		-383.71766	112.1	-385.29498	-8.7
TS Spectator Mechanism		-383.64105	109.6	-385.25647	15.5

[a] no ZPVE included, the CBS-Q/DZP total energy for $\mathbf{1} + \mathbf{1}^{\bullet+}$ = -385.44137 H.

Introduction

The mass spectrometer has long been recognized as the instrument of choice to study isomerization and dissociation reactions of solitary ions. In the words of Professor Longevialle: "... le spectromètre de masse .. joue le double rôle de réacteur (ionisation des molécules, fragmentation, etc...) et d'analyseur des produits de la réaction." [1]. Over the past 40 years, numerous studies have appeared dealing with the unimolecular chemistry of isolated ions, in particular radical cations, and as a result of these investigations we think that today we have a reasonable understanding of the properties of such species. If there is one thing that chemists have learned from these studies it is that one-electron oxidation can drastically change the chemistry of the system. For example, simple neutral enols are thermodynamically less stable than their keto isomers, but the opposite is true for the corresponding radical cations. A case in point is acetone. Experiments show that the gaseous acetone radical cation is 14 kcal/mol [2] *less* stable than its enol isomer, paralleling observations from theory [3]. However, a large barrier of 37 kcal/mol for the 1,3-hydrogen shift [4] prevents enolization, and thus once formed, the acetone radical cation retains its structure. The energy diagram for the keto-enol acetone radical cation tautomerization is given in Fig. 5.1 and note that even energized acetone ions will not isomerize; rather they will dissociate by loss of $CH_3^{\bullet}$.

Recently, experimental [5] and theoretical [6] studies have reported a mechanism by which a gaseous conventional radical cation can rearrange to a more stable isomer via a two-step proton-transfer through interaction with an appropriate base B according to Eq (1).

$$B + [H\text{-}X\text{-}Y]^{\bullet+} \rightarrow B\bullet\bullet\bullet H^{+}\bullet\bullet\bullet[X\text{-}Y]^{\bullet} \rightarrow B\bullet\bullet\bullet H^{+}\bullet\bullet\bullet[Y\text{-}X]^{\bullet} \rightarrow B + [H\text{-}Y\text{-}X]^{\bullet+} \quad (1)$$

This process has been termed "proton-transport catalysis"[5a]. The process not only occurs under certain conditions of bimolecular reactions (see below), but it also plays a key role in the dissociation of a variety of oxygen-containing radical cations [7]. The first studies of proton-transport catalysis of radical cations [5b-5d] focused on isomers separated by a 1,2-H shift, such as $CH_3OH^{\bullet+}$ which by interaction with a suitable base can rearrange into its more stable ylid isomer, $CH_2OH_2^{\bullet+}$, X = CH_2 and Y = OH in Eq (1). More recent experiments and *ab initio* calculations [5e, 5i] show that 1,3-H shifts can also be catalyzed by interaction with a suitable base molecule although the associated mechanism is not always that of a true proton-

transport catalysis [5i]. For example, the acetone radical cation rearranges smoothly to its enol via interaction with benzonitrile [5e], X = CH_2 and Y = $C(=O)CH_3$ in Eq (1) via proton-transfer catalysis.

Gauld and Radom [6b] have evaluated conditions for efficient proton-transport catalysis. First, and as indicated in Eq (1), the base should be able to abstract a proton from the radical cation. Secondly, the incipient protonated base should be able to donate back this same proton, but at a different site. That is to say, efficient catalysis will take place only when the proton affinity (PA) of the base lies between the PA of [X-Y] at X and at Y. Using this criterion, we concluded that benzonitrile should be a suitable candidate for a base and indeed, subsequent experiments showed that benzonitrile can catalyze the enolization of the acetone radical cation [5e].

However, during an evaluation of criteria for successful catalysis of 1,3-H shifts in a variety of radical cations, we noted an interesting, and possibly general, phenomenon. Taking acetone as an example, we observed that the PA of the incipient radical $[CH_2C(O)CH_3]^{\bullet}$ at oxygen is virtually identical to the PA of acetone itself, *viz* 196 kcal/mol. This simple observation indicates that acetone itself would be a suitable candidate to catalyze the 1,3-H shift in its partner radical cation. By contrast, 1,2-H shifts may not be catalyzed by the neutral molecule itself. For example, the PA of CH_3OH (180 kcal/mol [8]) is much larger than the PA of $CH_2OH^{\bullet}$ at O (166 kcal/mol [8]) and so in this case proton abstraction of $CH_3OH^{\bullet+}$ by CH_3OH will be unidirectional leading to $CH_3OH_2^+$ only.

There is another mechanism by which 1,2-H and 1,3-H shifts may be induced to occur by the encounter with a neutral base molecule. If the barrier for the unassisted reaction is not too large, then an ion-dipole interaction of the radical cation with the "base" may produce sufficient stabilization in itself to lower the unassisted barrier to below the separated starting components, thus promoting rearrangement. This is called the "spectator" mechanism and we do not know of any experimental method to differentiate between this mechanism and a "true" proton-transport catalysis. (For a description of the spectator model vs. proton-transport catalysis, see ref. 5f). However, a decision between the mechanisms can be made on the basis of *ab initio* calculations, *vide infra.*

In this report we present our results on the catalysis of the enolization of the acetone radical cation by acetone itself. Our experiments show that acetone can indeed catalyze this isomerization and our ab initio calculations show that the associated mechanism is a "true" proton-transport catalysis as opposed to a spectator process. We consider such a reaction whereby an acetone molecule catalyses enolization of its partner radical cation an example of "self-catalysis" as defined by Clennan et al. [9]. Thus, the starting species, neutral acetone is oxidized to its radical cation which then undergoes a further reaction catalyzed by the starting material. By contrast, in an autocatalytic process it is a reaction product which acts as catalyst.

Results and Discussion

The acetone molecule assisted isomerization of the acetone radical cation $\mathbf{1}^{\bullet+}$*, experimental observations*

The major dissociation observed in the Metastable Ion (MI) mass spectrum of the acetone dimer radical cation [$\mathbf{1}^{\bullet+}\bullet\bullet\bullet\mathbf{1}$], involves the formation of the monomer "acetone" cation. A smaller peak (c. 30%) is found at *m/z* 59 corresponding to $CH_3C^+(OH)CH_3$, $[1 + H]^+$, the result of a unidirectional proton transfer, i.e. a proton transfer immediately followed by dissociation. Dissociations, characteristic of the acetone monomer radical cation, *viz.* the losses of $CH_3^\bullet$ and CH_4 [13] are absent for the dimer radical cation. The energy requirement for formation of *m/z* 59 from the dimer radical cation is 105 kcal/mol (from ΔH_f $[\mathbf{1} + H]^+$ = 117 kcal/mol [8] and ΔH_f [$^\bullet CH_2C(=O)CH_3$] = -12 kcal/mol [5e]. If *m/z* 58 corresponds to ionized acetone, then the calculated threshold energy is 120 kcal/mol (from ΔH_f [$\mathbf{1}^{\bullet+}$] = 172 kcal/mol [8] and ΔH_f [**1**] = -52 kcal/mol [8]. However, if *m/z* 58 has the enol structure $\mathbf{1a}^{\bullet+}$, the energy requirement becomes 106 kcal/mol (from ΔH_f [$\mathbf{1a}^{\bullet+}$] = 158 kcal/mol [8]. However, it cannot be concluded from these data that the *m/z* 58 product ion has the enol structure, because formation of *m/z* 59, even though this reaction is a simple proton transfer, may be associated with a forward barrier [5i]. Therefore, it was decided to probe the structure of the *m/z* 58 ions by collision-induced dissociation (CID) experiments. In Figs 5.2a and 5.2b are given the reference CID mass spectra of the keto and enol forms respectively and these spectra are characteristically different in the

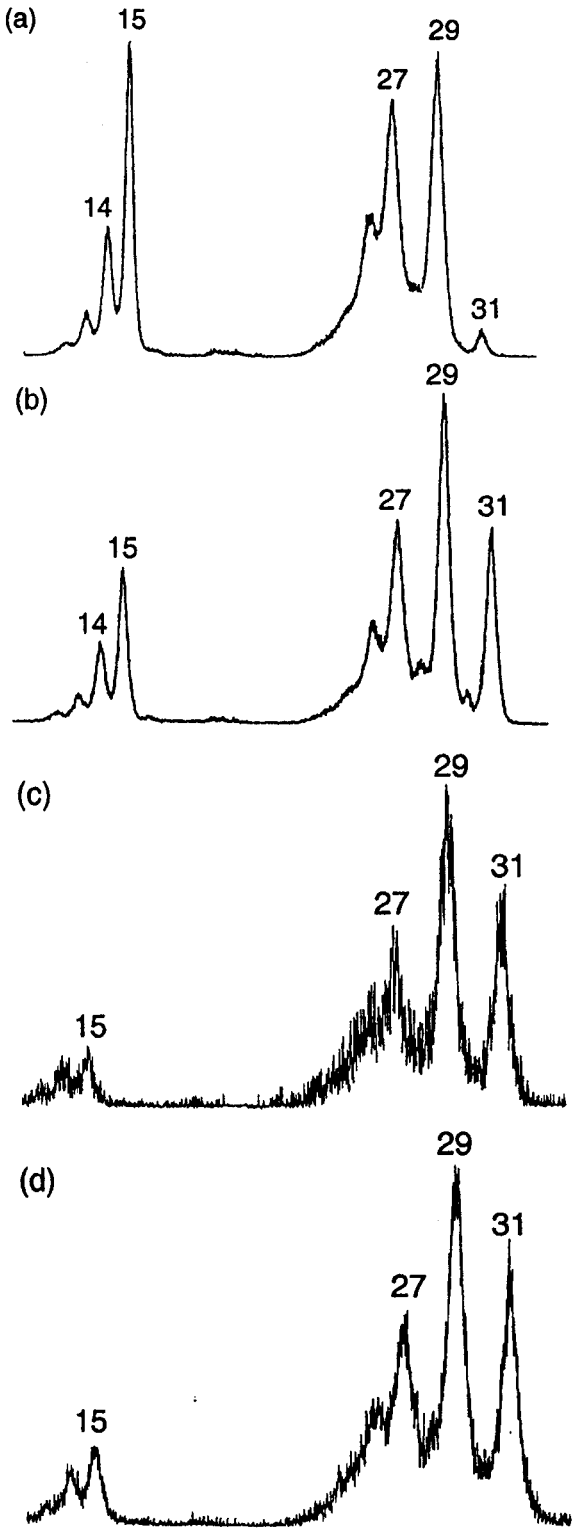

Figure 5.2. 8 keV Collision-Induced Dissociation (CID) mass spectra of : (a) acetone; (b) enol of acetone; (c) the metastably generated *m/z* 58 ions from the $[CH_3C(=O)CH_3]_2^{\bullet+}$ complex ; (d) the collisionally formed *m/z* 58 ions from the $[CH_3C(=O)CH_3]_2^{\bullet+}$ complex.

m/z 24 - 31 region. In Fig. 5.2c is given the CID mass spectrum of the *m/z* 58 ions generated from the metastable dimer radical cation and this spectrum leaves no doubt that the metastably dissociating dimer radical cations produce the enol ions **1a**$^{\bullet+}$. The question now arises : do the non-decomposing ions also isomerize into an [enol acetone$^{\bullet+}$•••acetone] complex ? This is an important question, because an answer, either way, would provide an indication as to the height of the barrier.

In our previous study [5e] on the benzonitrile (BN) catalyzed enolization of the acetone ion **1**$^{\bullet+}$, we had concluded that for the non-decomposing ions, the initially formed [**1**$^{\bullet+}$•••BN] complex completely rearranges, via proton transport catalysis, to the complex cation [**1a**$^{\bullet+}$•••BN], the very stable hydrogen-bridged radical cation $[CH_2{=}C(CH_3){-}O{\bullet\bullet\bullet}H{\bullet\bullet\bullet}N{\equiv}C{-}C_6H_5]^{\bullet+}$. If the acetone dimer radical cation behaves in the same way, then the initially formed [**1**$^{\bullet+}$•••**1**] complex will have completely rearranged in the microsecond time-frame to the adduct [**1a**$^{\bullet+}$•••**1**], the hydrogen-bridged radical cation $[CH_2{=}C(CH_3){-}O{\bullet\bullet\bullet}H{\bullet\bullet\bullet}O{=}C(CH_3)_2]^{\bullet+}$. Upon collisional activation, the complex will then yield *m/z* 58 ions having the enol of acetone structure as this is the energetically most favourable dissociation of the [**1a**$^{\bullet+}$•••**1**] complex. Experiments are in complete agreement with this hypothesis : the CID mass spectrum of the collisionaly generated *m/z* 58 ions recorded in an MS/MS/MS experiment, see Fig. 5.2d, shows that pure enol ions are produced. Thus, stable complex cations [**1**$^{\bullet+}$•••**1**] also completely rearrange to the adduct ion [**1a**$^{\bullet+}$•••**1**] on the microsecond time-scale. This experiment shows that the barrier for isomerization within the complex lies lower than the energy for the separated components, **1**$^{\bullet+}$ + **1**.

The mixed labelled dimer ion $[CD_3C(=O)CD_3{\bullet\bullet\bullet}CH_3C(=O)CH_3]^{\bullet+}$, where the charge may be on either moiety, was also investigated and its partial MI spectrum is given in Figure 5.3. It can be seen that the *m/z* 58 signal is split into *m/z* 58 and *m/z* 64 peaks, precisely as expected on the basis of proton-transport catalysis (or the spectator model). CID experiments on the metastable mixed labelled dimer ion showed that *m/z* 58 and *m/z* 64 correspond to pure enol ions as was the case for the unlabelled dimer ion. It can also be seen that *m/z* 60, $CH_3C(OD)CH_3^+$ which results from the competing process of complete D^+ abstraction is

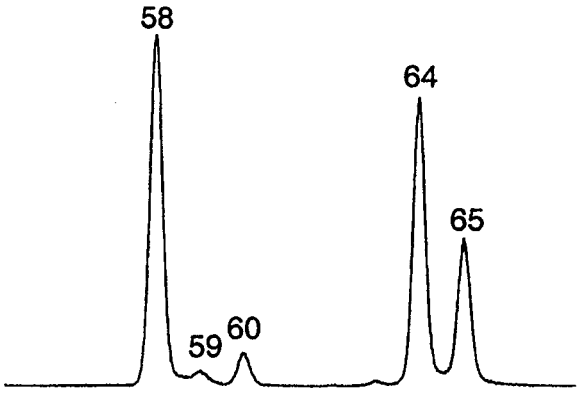

Figure 5.3. 8 keV Metastable Ion (MI) mass spectrum of the *m/z* 122 $[CH_3C(=O)CH_3 / CD_3C(=O)CD_3]^{\bullet+}$ complex ion.

significantly weaker than *m/z* 65 $CD_3C(OH)CD_3^+$ which results from H^+ abstraction. This shows that complete proton transfer from one partner to another is associated with a significant isotope effect; thus this simple proton transfer may well be associated with a significant barrier. It is of interest to note that the unidirectional proton transfer suffers from an appreciable isotope effect (as evidenced by the ratio *m/z* 60 : *m/z* 65), but that no such isotope effect appears to operate in the enolization process. However, if it is assumed that the second proton transfer, i.e. the donation back of the abstracted proton, suffers from a similar isotope effect, then both effects cancel out and an intensity ratio of 1 is expected for *m/z* 58 and *m/z* 64. Apart from the expected peaks at *m/z* 58, 60, 64 and 65, there are also minor signals at *m/z* 59 and 63. These minor products we propose arise by isomerization via a process which involves a sequential proton and a hydrogen (or deuterium *atom*) transfer within the $[\mathbf{1}^{\bullet+}\bullet\bullet\bullet\mathbf{1}]$ complex as is the case for the isomerization of ionized acetamide using benzonitrile as base [5i]. These minor processes were not further investigated.

Theoretical Calculations

An important energetic constraint to guide us in our *ab initio* calculations is provided by the MS/MS/MS experiment described above and that is that the barrier for the catalyzed isomerization should lie below the energy of the separated starting components, $\mathbf{1}^{\bullet+} + \mathbf{1}$. This

finding will become important when we need to decide between proton-transport catalysis and a spectator model. For ionized acetone, proton-transport catalysis involves the following sequence. The acetone radical cation $\mathbf{1}^{\bullet+}$ reacts with neutral acetone, **1**, to give the initial complex $[\mathbf{1}^{\bullet+}\bullet\bullet\bullet\mathbf{1}]$, ion $\mathbf{2}^{\bullet+}$ in Scheme 5.1. This complex then undergoes proton transfer to generate the complex $[\mathbf{1} - H]^{\bullet}\bullet\bullet\bullet[1 + H]^{+}$, $\mathbf{3}^{\bullet+}$, which then donates back the proton to generate the final complex $[\mathbf{1a}^{\bullet+}\bullet\bullet\bullet\mathbf{1}]$, $\mathbf{4}^{\bullet+}$, which then dissociates to the enol of acetone radical cation, $\mathbf{1a}^{\bullet+}$, and **1**. The competing process of unidirectional proton transfer leads to $CH_3C^{+}(OH)CH_3$ and $CH_3C(=O)CH_2^{\bullet}$, $[1 + H]^{+}$ and $[\mathbf{1} - H]^{\bullet}$.

The characterization of the potential energy surface (PES) was started by performing RHF / DZP calculations to locate the stationary points for the proton-transport catalysis model : i.e. the reaction sequence $\mathbf{2}^{\bullet+} \rightarrow$ TS $(\mathbf{2} \rightarrow \mathbf{3})^{\bullet+} \rightarrow \mathbf{3}^{\bullet+} \rightarrow$ TS $(\mathbf{3} \rightarrow \mathbf{4})^{\bullet+} \rightarrow \mathbf{4}^{\bullet+}$. According to these calculations the ions $\mathbf{3}^{\bullet+}$ and $\mathbf{4}^{\bullet+}$ are quite stable species. The transition $\mathbf{3}^{\bullet+} \rightarrow \mathbf{4}^{\bullet+}$ has a very low activation energy as may be expected for an $O\bullet\bullet\bullet H^{+}\bullet\bullet\bullet O$ proton transfer. Ion **2** has a stabilization energy of 16 kcal/mol. The structures encountered on the surface are shown in Scheme 5.1 and detailed structures are given in Scheme 5.2. It is of interest to note that from the structure TS $(\mathbf{2} \rightarrow \mathbf{3a})^{\bullet+}$ in Scheme 5.2, it may be inferred that the H-shift is indeed a proton shift and not an H atom shift. If it were an H atom shift then the dipole vector of the right-hand neutral species would point to the wrong direction. The calculated energies are shown in Table 5.1 and the energy diagrams derived therefrom are given in Figure 5.4.

Since the first step should also correspond to a proton transfer, the transition was expected to feature a structure like $[CH_3C(=O)CH_2^{\bullet}\bullet\bullet\bullet H^{+}\bullet\bullet\bullet O=C(CH_3)_2]$. However, a TS of this form could not be found. This may be rationalized by the fact that a structure of the above form has no electrostatic stabilization after passing the transition state ; this is because the vector of the dipole moment of the radical moiety points in the wrong direction. However, another possibility for the transition $\mathbf{2}^{\bullet+} \rightarrow \mathbf{3}^{\bullet+}$ originates from the idea that the deprotonated acetone radical $[\mathbf{1} - H]^{\bullet}$ may have two electronic configurations, i.e. the normal, low energy form $CH_3C(=O)CH_2^{\bullet}$ and the alternative, higher energy form $CH_3C(O^{\bullet})=CH_2$, $[\mathbf{1} - H]_{\alpha}^{\bullet}$, which features a small C = CH_2 distance and a large C – O distance. This leads to a TS of the form

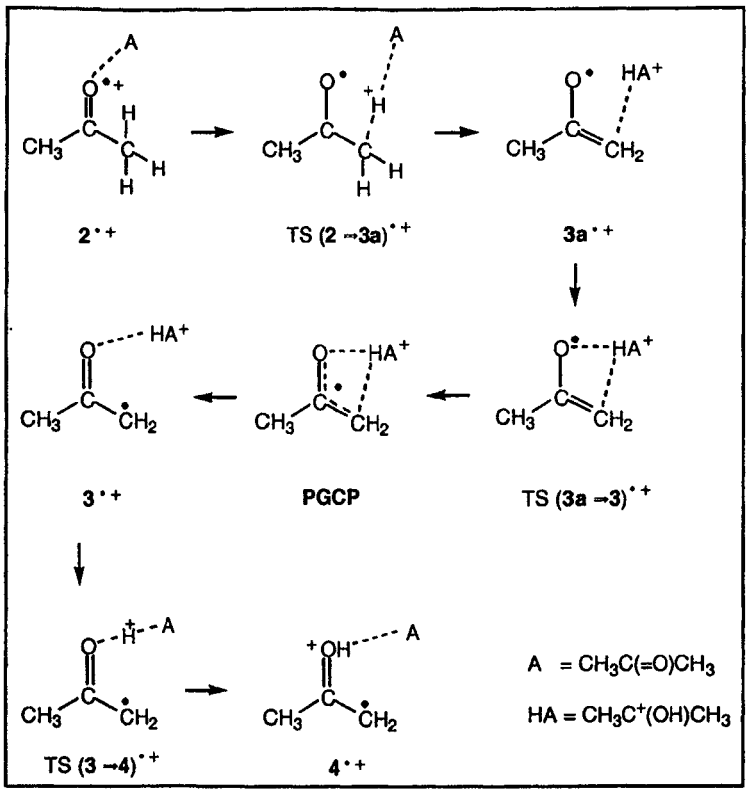

Scheme 5.1

$[CH_3C(O^{\bullet})=CH_2 \bullet\bullet\bullet H^+ \bullet\bullet\bullet O=C(CH_3)_2]$, TS ($2^{\bullet+} \rightarrow 3a^{\bullet+}$) in Schemes 5.1 and 5.2. This structure has some stabilization from the interaction of the positive charge on the protonated acetone with the C=C double bond of the alternative form of the radical, $[1 - H]_{\alpha}^{\bullet}$. A geometry optimization starting from this TS leads to ion $\mathbf{3a}^{\bullet+}$ with almost the same geometry (apart from the $H^+ - O$ distance) and an energy just below the TS ($2^{\bullet+} \rightarrow \mathbf{3a}^{\bullet+}$) energy. The next step would be to find a TS for the transition $CH_3C(-O^{\bullet})=CH_2 \rightarrow CH_3C(=O)CH_2^{\bullet}$ in the radical moiety of the complex. However, this TS could not be found. TS searches for the above transition for the isolated radical also proved unsuccessful. Instead, we find that the PESs for the two forms of the radical have an intersection, where the RHF wave functions of the two radical forms correspond to two different solutions of the RHF equations with the same energy. Calculations on the complex with protonated acetone show the same behaviour, although the energies are affected by the interaction with the charge on the protonated acetone : the alternative form of the radical is stabilized if the hydroxyl group of the protonated acetone points towards the p-electrons of the double bonded CH_2 group in the radical. The transition to the normal form of

the radical, as required in order to form ion $\mathbf{3}^{\bullet+}$, is stimulated by moving this hydroxyl group to the oxygen of the radical. The next logical step is then to find the Minimum Energy Crossing Point (MECP) for the intersection, i.e. the geometry corresponding to the minimum energy of the complex with the restriction that the search is confined to the intersection of the two PESs.

However, it turns out that there is a complication in this case, because these calculations lead to geometries which are not useful for defining the transition point for the reaction step at hand. This situation is clarified by Figure 5.5. In the usual case, represented by Figure 5.5a, optimizations starting from the MECP will lead to different minima, as is the case for a transition state. This follows from the fact that the gradients in the MECP have opposite directions. However, in the situation depicted in Fig 5.5b the lower energy points within the intersection have gradients pointing more or less in the *same* direction. As a consequence, optimizations starting from these points would eventually lead to the *same* minimum. The reason for this behaviour is the fact that the RHF solution corresponding to the upper PES will become unstable if the geometry is too far from the intersection. It will then collapse to the wave function corresponding to the lower PES. As seen in Fig 5.5b, a situation with gradients pointing to the same minimum is possible if one of the PESs has a transition state near the intersection. Although the reaction path cannot be defined in a unique way in this situation, useful information may be obtained by monitoring the gradients during the search for the MECP. A reasonable choice for the point where the intersection should be crossed is the point where one of the gradients lies in a plane parallel to the intersection. We will call this point the Parallel Gradient Crossing Point (PGCP), see Fig. 5.5b. In order to find the activation energy for the transition $\mathbf{3a}^{\bullet+} \rightarrow \mathbf{3}^{\bullet+}$, TS ($\mathbf{3a}^{\bullet+} \rightarrow \mathbf{3}^{\bullet+}$) in Scheme 5.1 and Scheme 5.2, it is then necessary to find the transition state indicated in Figure 5.5b, starting from the PGCP. This transition state turns out to have virtually the same energy as the PGCP.

As a result, the first step in our mechanism in fact corresponds to a two-step process. In the first step a proton is abstracted from the acetone radical cation without changing the radical site (on the O atom of the radical cation). In the second step the protonated acetone migrates to the O atom of the radical. After passing the TS ($\mathbf{3a}^{\bullet+} \rightarrow \mathbf{3}^{\bullet+}$), see Scheme 5.1 and

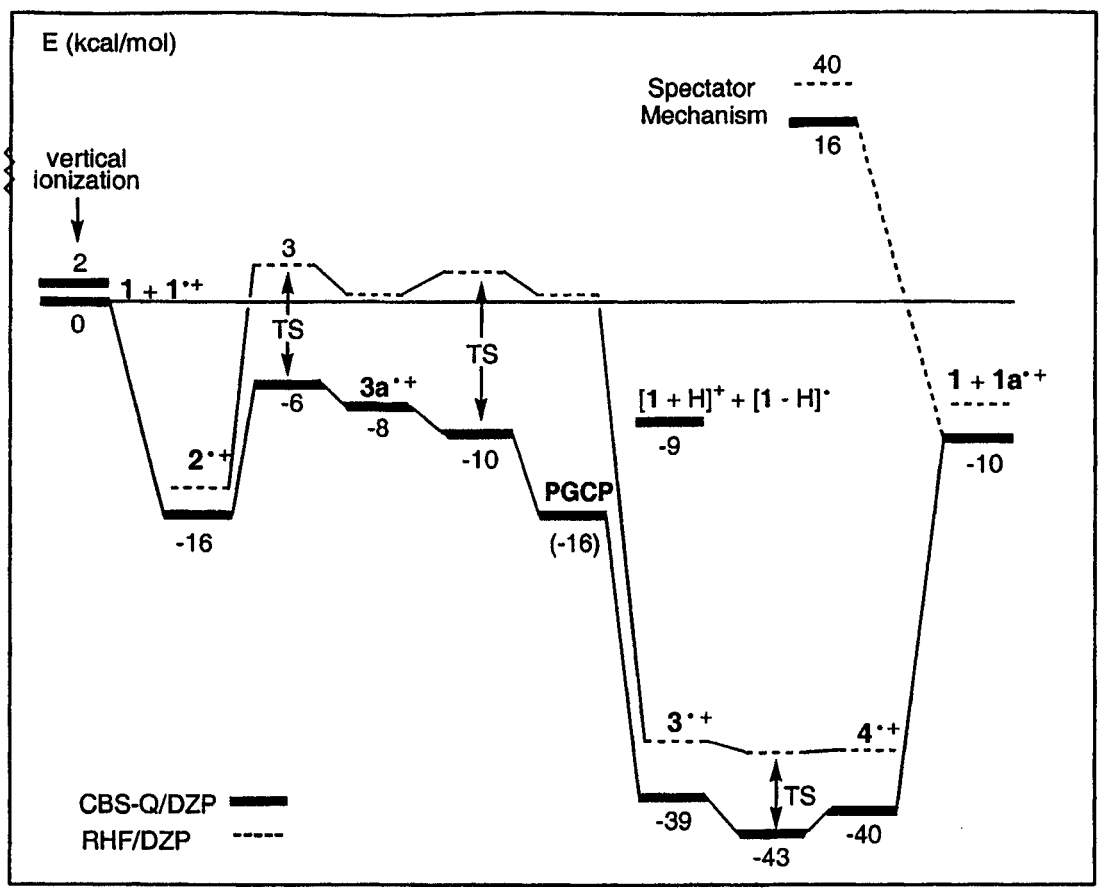

Figure 5.4. Computationally derived energy diagram for the self-catalyzed isomerization of the acetone radical cation $CH_3C(=O)CH_3^{\bullet+}$ ($\mathbf{1}^{\bullet+}$) based on calculations at the CBS-Q/DZP (solid lines) and RHF/DZP (dashed lines) levels of theory. Relative energies are given in kcal/mol.

Figure 5.5b, the complex starts to move in the direction of an O•H•O bridged structure of the form $[CH_3C(O^{\bullet})=CH_2 \bullet\bullet\bullet HO\text{-}C^{+}(CH_3)_2]$. However, as the protonated acetone approaches the O atom in the radical, the intersection is crossed and the wave function changes character, yielding $\mathbf{3}^{\bullet+}$.

Although this mechanism gives a complete description of the proton transfer catalysis for the enolization of the acetone radical cation, the RHF energies are too high for a satisfactory explanation of the experimental results. Therefore single point calculations were performed according to the CBS model, using geometries obtained using RHF / DZP instead of UHF / 6-31G(d'), as in the CBS-Q model. According to these calculations, the first step TS ($\mathbf{2}^{\bullet+} \rightarrow \mathbf{3a}^{\bullet+}$), abstraction of the proton from the acetone radical cation, is rate-determining with

all other transition states and the PGCP being lower in energy. This is in full agreement with experiment from which it was concluded that proton abstraction is rate-determining. We also find that the energy found for TS ($\mathbf{3}^{\bullet+} \rightarrow \mathbf{4}^{\bullet+}$), the O•••H$^+$•••O proton transfer concluding the enolization, is lower than the energies for the ions $\mathbf{3}^{\bullet+}$ and $\mathbf{4}^{\bullet+}$, indicating that the O•H•O bridge corresponds to a single minimum potential. The energy level of the highest transition state in Figure 5.5, TS ($\mathbf{2}^{\bullet+} \rightarrow \mathbf{3a}^{\bullet+}$), lies 6 kcal/mol below that of the reactants $\mathbf{1}^{\bullet+}$ + **1**. Theory, therefore, predicts that the proton-transport catalysis may occur at threshold, as is observed. Also included in Figure 5.4 are the results for calculations using a spectator model. The RHF and CBS-Q calculations both predict that the enolization barrier associated with this model greatly exceeds that associated with proton-transport catalysis and so the spectator mechanism is not expected to play a role in this system.

Conclusions

The acetone radical cation $CH_3C(=O)CH_3^{\bullet+}$ ($\mathbf{1}^{\bullet+}$)which, because of a large barrier, does not rearrange to its more stable enol form $CH_2=C(OH)CH_3^{\bullet+}$ ($\mathbf{1a}^{\bullet+}$) on its own, can be induced to tautomerize by the interaction of a neutral acetone molecule. Labelling experiments show that the associated mechanism can be viewed as a 1,3-H shift taking place within the acetone dimer radical cation. *Ab initio* calculations indicate that the process actually occurs via proton-transport catalysis. The neutral acetone partner first abstracts a proton from the acetone radical cation and then donates this proton back to the oxygen atom of the incipient $CH_3C(=O)CH_2^{\bullet}$ radical. This process occurs via a "transition state to minimum crossing" as opposed to a conventional "minimum to minimum crossing". Enolization via a spectator mechanism lies too high in energy to compete with proton-transport catalysis.

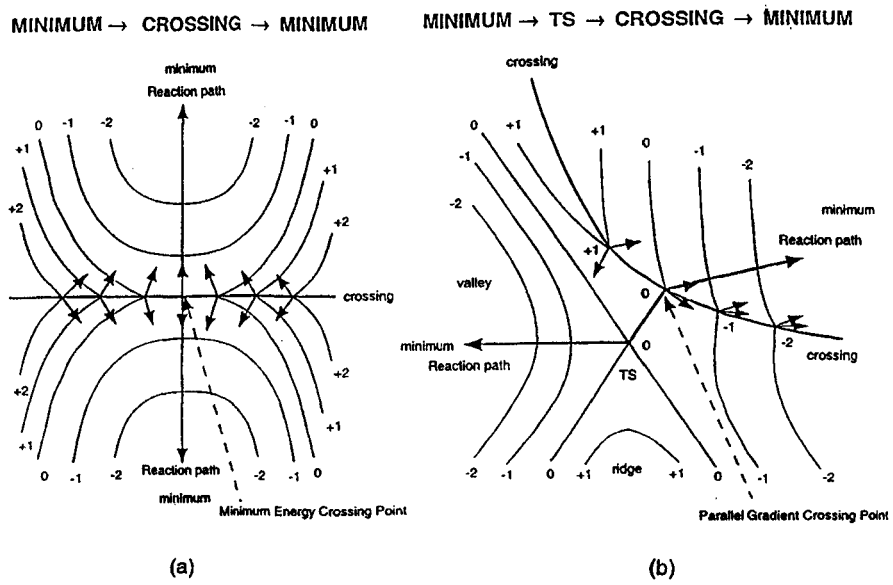

Figure 5.5. Schematic Potential Energy Surfaces with an intersection : (a) The Minimum Energy Crossing Point is the transition point for the reaction; (b) The Parallel Gradient Crossing Point is the transition point for the reaction.

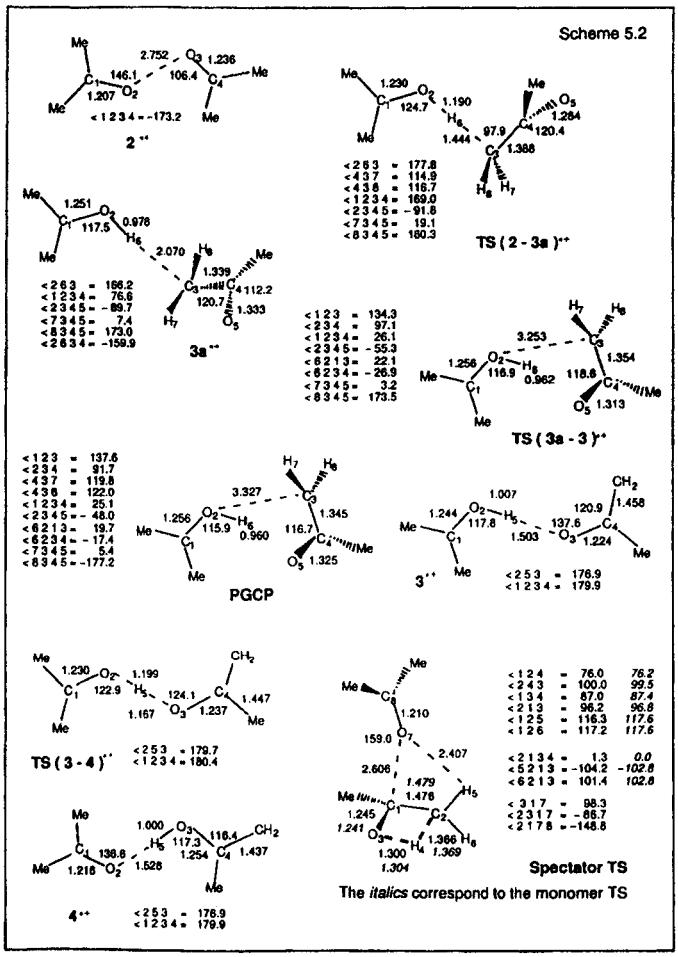

References

[1] P. Longevialle, *Principes de la Spectrométrie de Masse des Substances Organiques*, Masson, Paris,**1980.**

[2] J.L. Holmes, F.P. Lossing, *J. Am. Chem. Soc.* **1982**, *104*, 2648.

[3] (a) F. Tureček, C.J. Cramer, *J. Am. Chem. Soc.* **1995**, *117*, 12243; (b) D. Lee, C.K. Kim, B.S. Lee, B.C. Lee, *J. Comput. Chem.***1997**,*18*, 56.

[4] (a) D.H. Williams, *Acc. Chem. Res.* **1977**, *10*, 280; (b) P.C. Burgers, J.L. Holmes, *Org. Mass Spectrom.* **1982**, *17*, 123.

[5] (a) D.K. Bohme, *Int. J. Mass Spectrom. Ion Processes* **1992**, *115*, 95; (b) P. Mourgues, H.E. Audier, D. Leblanc, S. Hammerum, *Org. Mass Spectrom.* **1993**, *28*, 1098; (c) H.E. Audier, D. Leblanc, P. Mourgues, T.B. McMahon, S. Hammerum, *J. Chem. Soc. Chem. Commun.* **1994**, 2329; (d) H.E. Audier, J. Fossey, P. Mourgues, T.B. McMahon; S. Hammerum, *J. Chem. Phys.* **1996**, *100*, 18380; (e) M.A. Trikoupis, J.K. Terlouw, P.C. Burgers, *J.Am. Chem. Soc.* **1998**, *120*, 12131; (f) M.A. Trikoupis, D.J. Lavorato, J.K. Terlouw, P.J.A. Ruttink, P.C. Burgers, *Eur. Mass Spectrom.* **1999**, *5*, 431; (g) G. Van der Rest, P. Mourues, J. Tortajada, H.E. Audier, *Int. J. Mass Spectrom.* **1998**, *179/180*, 293; (h) J. Chamot-Rooke, G. Van der Rest, P. Mourgues, H.E. Audier, *Int. J. Mass Spectrom.* **2000**, *195/196*, 385 (i) M.A. Trikoupis, P.C. Burgers, P.J.A. Ruttink, J.K. Terlouw, *Int. J. Mass Spectrom.* **2001**, *210/211*, 489; (j) P. Mourgues, J. Chamot-Rooke, G. van der Rest, H. Nedev, H.-E. Audier, T.B. McMahon, *Int. J. Mass Spectrom.* **2001**, *210/211*, 429.

[6] (a) J.W. Gauld, H. Audier, J. Fossey, L. Radom, *J. Am. Chem. Soc.* **1996**, *118*, 6299; (b) J.W. Gauld, L. Radom, *J. Am. Chem. Soc.* **1997**, *119*, 9831; (c) A.J. Chalk, L. Radom, *J. Am. Chem. Soc.* **1999**, *121*, 1574.

[7] (a) P.J.A. Ruttink, P.C. Burgers, *Org. Mass Spectrom.* **1993**, 28, 1087; (b) P.C. Burgers, L.M. Fell, A. Milliet, M. Rempp, P.J.A. Ruttink, J.K. Terlouw, *Int. J. Mass Spectrom. Ion Processes* **1997**, *167/168*, 291; (c) P.J.A. Ruttink, P.C. Burgers. L.M. Fell, J.K. Terlouw, *J. Phys. Chem. A.* **1998**, *102*, 2977.

[8] (a) S.G. Lias, J.E. Bartmess, J.F. Liebman, J.L. Holmes, R.O. Levin, W.G. Mallard, *J. Phys. Chem. Ref. Data* **1988**, *17*, Supplement 1; (b) S.G. Lias, E.P.L. Hunter, *J. Phys. Chem. Ref. Data* **1998**, *27*, No3

[9] E.L. Clennan, P. Dobrowolski and A. Green, *J. Am. Chem. Soc.* **1995**, *117*, 9800.

[10] Gaussian 98, Revision A.7, M.J. Frisch, G.W. Trucks, H.B. Schlegel, G.E. Scuseria, M.A. Robb, J.R. Cheeseman, V.G. Zarzewski, J.A. Montgomery Jr., R.E. Stratmann, J.C. Burant, S. Dapprich, J.M. Millam, A.D. Daniels, K.N. Kudin, M.C. Strain, O. Farkas, J. Tomasi, V. Barone, M. Cossi, R. Cammi, B. Mennucci, C. Pomelli, C. Adamo. S. Clifford, J. Ochterski, G.A. Petersson, P.Y. Ayala, Q. Cui, K. Morokuma, D.K. Malick, A.D. Rabuck, K. Raghavachari, J.B. Foresman, J. Cioslowski, J.V. Ortiz, A.G. Baboul, B.B. Stefanov, G. Liu, A. Liashenko, P. Piskorz, I. Komaromi, R. Gomperts, R.L. Martin, D.J. Fox, T. Keith, M.A. Al-Laham, C.Y. Peng, A. Nanayakkara, C. Gonzalez, M. Challacombe, P.M.W. Gill, B. Johnson, W. Chen, M.W. Wong, J.L. Andres, C. Gonzalez, M. Head-Gordon, E.S. Replogle, J.A. Pople, Gaussian Inc., Pittsburgh PA, **1998.**

[11] (a) M. Dupuis, D. Spangler, J. Wendolowski, NRCC Software Catalogue 1 Program No. QG01, GAMESS (**1980**); (b) M. Guest, J. Kendrick, GAMESS User Manual, An Introductory Guide, CCP/86/1, Daresbury Laboratories (**1986**).

[12] (a) J.W.Ochterski, G.A.Petersson, and J.A.Montgomery, Jr., *J. Chem. Phys.* **1996**, *104*, 2598; (b) J.A.Montgomery, Jr., M.J.Frisch, J.W.Ochterski, G.A.Petersson, K.Raghavachari, and V.G.Zakrzewski, *J. Chem. Phys.* **1998**, *109*, 6505.

[13] N. Heinrich, H. Schwarz, *Int. J. Mass Spectrom Ion Processes* **1987**, *79*, 295.

Chapter 6

How Do Dimethyl Oxalate Ions CH_3O-C(=O)-C(=O)-$OCH_3^{\bullet+}$ Break in Half? Loss of $CH_3^{\bullet}$ + CO_2 versus CH_3O-C=O$^{\bullet}$

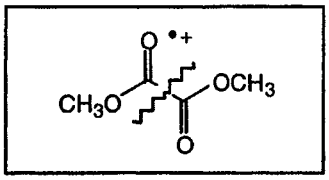

The interesting unimolecular dissociation chemistry of dimethyl oxalate (DMO) ions, $CH_3OC(=O)$-C(=O)$OCH_3^{\bullet+}$, has been studied by vacuum ultraviolet photoionization and tandem mass spectrometry based experiments. The measured appearance energy (AE) for the generation of CH_3O-C=O$^+$ (10.5 eV) is not compatible with a simple bond cleavage involving the cogeneration of the radical CH_3O-C=O$^{\bullet}$ whose calculated AE is 11 kcal/mol higher. However, because the CH_3O-C=O$^{\bullet}$ radical is thermodynamically less stable than its dissociation products $CH_3^{\bullet}$ and CO_2, by 19 kcal/mol, a two-step dissociation of ionized DMO into CH_3O-C=O$^+$ + $CH_3^{\bullet}$ + CO_2 is energetically feasible. Collision induced dissociative ionization experiments clearly show that low energy DMO ions dissociate into $CH_3^{\bullet}$ +CO_2 without the intermediacy of CH_3O-C=O$^{\bullet}$. Experiments using a charged collision chamber further indicate that CO_2 is released first, followed by loss of $CH_3^{\bullet}$ and not vice versa and a mechanism is proposed. The measured AE, which we assign to the two-step process, is 8 kcal/mol higher than the calculated value. This could be due to a competitive shift caused by a prominent low energy decarbonylation reaction yielding the hydrogen bridged radical cation CH_2=O•••H•••O=C-$OCH_3^{\bullet+}$. However, from metastable ion observations and AE measurements on deuterium labeled DMO ions, it follows that there is no competitive shift and that the elevated AE for the two-step process corresponds to the barrier for the first step, loss of CO_2. Finally, neutralization-reionization experiments on ionized DMO and CH_3O-C=O$^+$ provide evidence for the existence of CH_3O-C=O$^{\bullet}$ as a kinetically stable radical.

The work described here has been published previously in an article under the same title: M.A. Trikoupis, J.K. Terlouw, P.C. Burgers, M. Peres, C. Lifshitz, J. Am. Soc. Mass Spectrom. 1999, 10, 869-877.

Introduction

More than 10 years ago, the structure, dissociation characteristics, and enthalpy of formation (ΔH_f) of the methoxycarbonyl cation, $CH_3O\text{-}C{=}O^+$, and 11 of its isomers was investigated with the fruitful combination of tandem mass spectrometry and *ab initio* molecular orbital (MO) calculations [1]. The proposed ΔH_f [$CH_3O\text{-}C{=}O^+$] = 120 kcal/mol was based on the *ab initio* calculated energy difference (-21 kcal/mol) with the hydroxyoxiranyl isomer, $\overline{OCH_2C^+OH}$, whose ΔH_f (141 ± 1 kcal/mol) was obtained from an accurate appearance energy (AE) measurement using monochromatic electrons [1]. Shortly after that report, the methyl cation affinity (MCA) of CO_2 was reported [2] and the ΔH_f [$CH_3O\text{-}C{=}O^+$] value derived therefrom supported the above 120 kcal/mol. This value was in poor agreement with the reported results (Table 3 in ref. 1) of direct AE measurements on *m/z* 59, $CH_3O\text{-}C{=}O^+$ ions generated from a large set of precursor molecules. These experiments gave ΔH_f [$CH_3O\text{-}C{=}O^+$] = 130 ± 4 kcal/mol, but these higher values were reasonably attributed to a competitive shift. However, a very recent Gaussian-2 theoretical study, which also includes a reassessment of the experimental data from refs. 1 and 2, yields a recommended value ΔH_f [$CH_3O\text{-}C{=}O^+$] = 129 ± 2 kcal/mol [3].

One hitherto unpublished key experimental observation seems to be at odds with this recommended value. It concerns the behaviour of dimethyl oxalate (DMO), $CH_3OC(=O)\text{-}C(=O)\text{-}OCH_3$, whose 70 eV electron ionization mass spectrum [4] is dominated by peaks at *m/z* 59 ($CH_3O\text{-}C{=}O^+$, base peak) and *m/z* 45 (35 %). Beynon et al. [4], in a detailed metastable ion study, investigated the origins of the *m/z* 45 ($CH_3\text{-}O\text{-}CH_2^+$) ions and concluded that they result from a high energy rearrangement reaction initiated by a 1,5-H transfer, but no further low energy processes were reported. The *m/z* 59 ions clearly have the $CH_3O\text{-}C{=}O^+$ structure (from comparison with reference CID spectra) whereas collision induced dissociative ionization (CIDI) [5] experiments reported in ref 6 indicate that the neutral lost is $CH_3O\text{-}C{=}O^{\bullet}$. Thus ionized DMO seems to generate $CH_3O\text{-}C{=}O^+$ ions via a simple bond cleavage reaction and because it has a discrete molecular ion, it may reasonably be expected to serve as a suitable precursor molecule to establish a reliable heat of formation for the methoxycarbonyl cation. The AE (*m/z* 59) from DMO was measured by the late Dr. F.P. Lossing as 10.48 ±

0.05 eV (sharp onset) [7] in the context of the work reported in ref. 1, but combining this result with the experimental ΔH_f values of $CH_3O\text{-}C{=}O^+$ and DMO available at that time, viz., -40 ± 2 [8] and -169.5 ± 0.1 [9,10a] kcal/mol, respectively, yielded an incomprehensibly low apparent ΔH_f [$CH_3O\text{-}C{=}O^+$] = 112 kcal/mol !

However, in 1996 Liebman et al. [11] remeasured DMO's sublimation enthalpy and arrived at -162.9 ± 0.2 kcal/mol for its gaseous enthalpy of formation at 298 K. This new ΔH_f [DMO] value (which is not quoted in the compilation of [10b]) is in excellent agreement with the expected methyl substitution effect, +5.5 kcal/mol per methyl group [12], on the ΔH_f of the parent acid, ΔH_f [oxalic acid] = -173 kcal/mol [13], and a CBS-4 calculation performed in our laboratory which gave ΔH_f^{298} [DMO] = -163 kcal/mol [14]. Using this new value in conjunction with the above AE measurement yields an apparent ΔH_f [$CH_3O\text{-}C{=}O^+$] = 119 kcal/mol, supporting the original value proposed in [1], but being clearly at odds with the recommended value of 129 ± 2 kcal/mol [3].

In this context we note that if the neutral species lost in the dissociation would not be $CH_3O\text{-}C{=}O^\bullet$ but rather its (exothermic!) dissociation products $CH_3^\bullet + CO_2$ ($\Sigma\Delta H_f$ = -59 kcal/mol [10]), the apparent ΔH_f [$CH_3O\text{-}C{=}O^+$] would become 138 kcal/mol, considerably higher than the recommended value. Using ΔH_f [$CH_3O\text{-}C{=}O^+$] = 129 kcal/mol and assuming threshold generation of $CH_3^\bullet + CO_2$ as the accompanying neutral products in the dissociation of DMO, the AE is calculated as 10.1 eV, some 0.5 eV lower than the measured value, but this would only be reasonable if the reaction suffered from a considerable competitive shift due to a low energy rearrangement. We further note that apart from the evidence presented in [6] there is as yet only indirect evidence [8] for the existence of the $CH_3O\text{-}C{=}O^\bullet$ radical as a stable neutral, albeit that calculations at a fairly high level of theory (B3LYP/6-311G(d,p) + ZPE) [15] predict it to be kinetically stable with a barrier of 27 kcal/mol preventing its exothermic dissociation into $CH_3^\bullet + CO_2$.

To resolve the above noted dilemma, we report here on the results of a tandem mass spectrometry study of low energy DMO ions and their deuterium labeled isotopomers

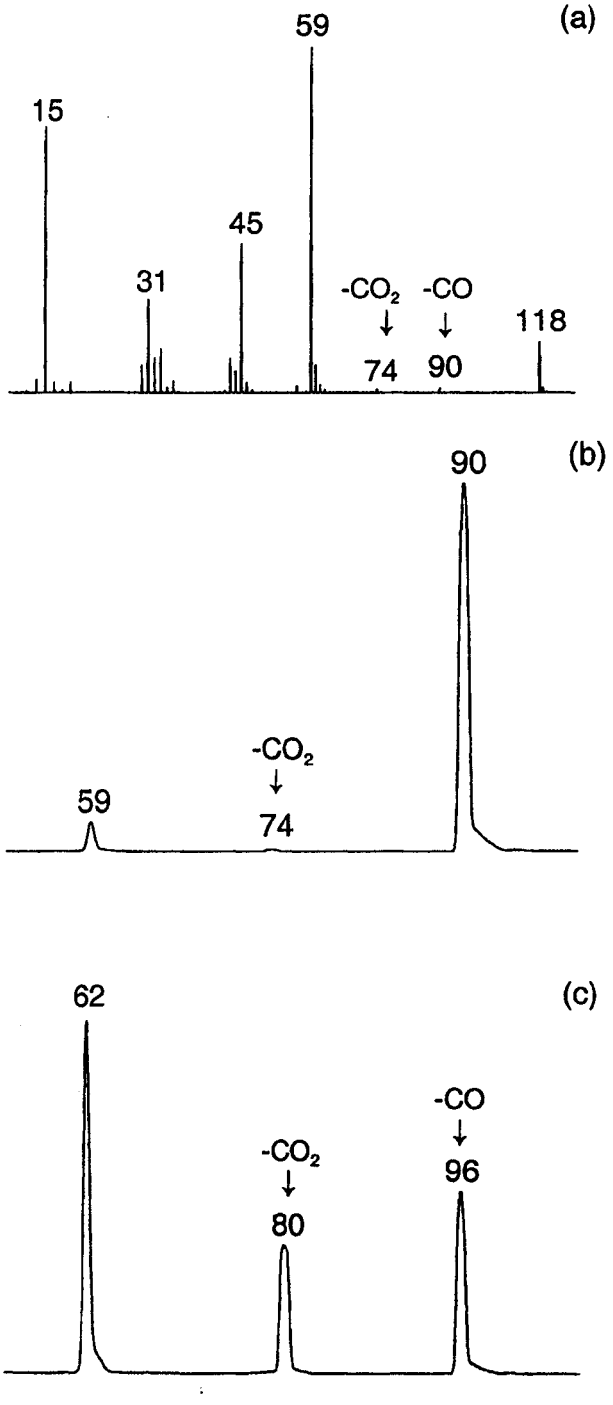

Figure 6.1. (a) The EI mass spectrum of DMO; (b) and (c) MI spectra of DMO and DMO-d_6 molecular ions, respectively. For dimethyl oxalate and its two labeled isotopomers (CH_3O/CD_3O and CD_3O/CD_3O), the sum of the intensities of all the metastable ions over the intensity of the main beams are 1.37, 1.23 and 0.40 (all x 10^{-3}), respectively.

$CD_3OC(=O)$-$C(=O)OCH_3$ and $CD_3OC(=O)$-$C(=O)OCD_3$ in conjunction with selected photoionization experiments. It will be shown that the CIDI spectrum of $DMO^{\bullet+}$, unlike that of ionized methyl pyruvate, $CH_3C(=O)$-$C(=O)OCH_3^{\bullet+}$, is not compatible with the formation of the CH_3O-$C{\equiv}O^+$ neutral in the dissociation of the low energy molecular ions but rather with the formation of $CO_2 + CH_3^{\bullet}$. The measured AE corresponds to this two-step process and does not suffer from a competitive shift; rather, the elevated AE corresponds to a barrier for the first step, loss of CO_2. A rationale will be given for the (incorrect) structure assignment of the CIDI spectrum of DMO presented in [6] and this will be followed by an analysis of the strikingly different CIDI and NR behaviour of the CH_3O-$C{\equiv}O^+$/CH_3O-$C{\equiv}O^+$ system.

Results and Discussion

The Dissociation Chemistry of Low Energy Dimethyl Oxalate Ions : Single or Two-Step Process ?

Although CH_3O-$C{\equiv}O^+$ is the base peak in the normal mass spectrum of DMO, $\mathbf{1}^{\bullet+}$ (see Figure 6.1a), it is but a minor signal in the metastable ion (MI) mass spectrum, which instead is dominated by loss of CO (see Figure 6.1b), obviously the result of rearrangement. Figure 6.1a,b represents textbook examples of the enormous differences that can be encountered between conventional and MI masss spectra [19]: while for the higher energy ions, i.e., those fragmenting with rate constants > 10^6 s^{-1}, the (putative) direct bond cleavage is the dominant process, the rearrangement reaction is the major process for the lower energy ions. Thus, the rearrangement reaction has a low activation energy and a low frequency factor, whereas the direct bond cleavage has a high activation energy and a high frequency factor and so the k versus E curves for the two processes will cross. In such cases the measured AE for the simple cleavage process may be too high because (and as exemplified by the MI mass spectrum; see Figure 6.1b) close to threshold this reaction cannot compete with the rearrangement process sufficiently to be observed. This is the so-called "competitive shift" [20] mentioned in the Introduction and such a shift could be the reason that the observed AE is some 0.4 eV larger than the calculated value. The MI spectrum (Figure 6.1b) also contains a weak signal for loss

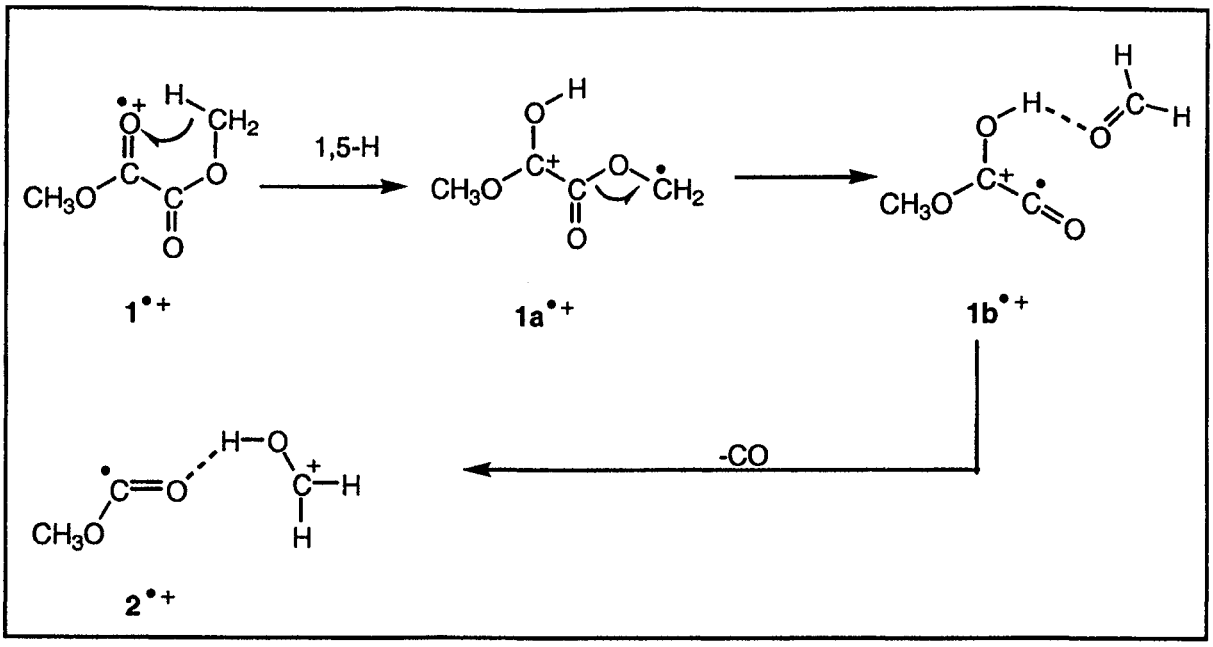

Scheme 6.1

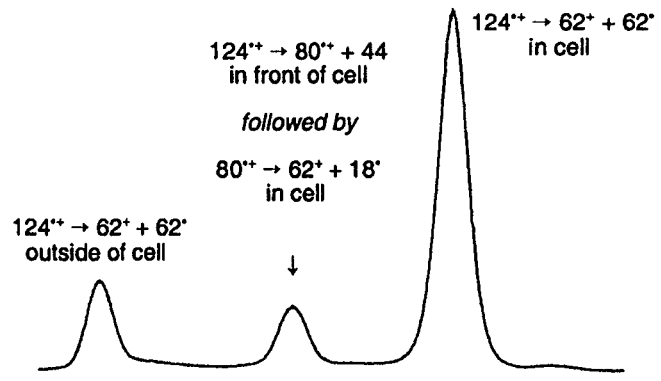

Figure 6.2. CID peaks for the generation of $CD_3O\text{-}C{=}O^+$ ions from 10 kV *m/z* 124 DMO-d_6 molecular ions with + 1000 V applied on the collision chamber.

of CO_2, which too must be the result of a rearrangement reaction. Although the corresponding peak at *m/z* 74 is weak, this reaction will prove to be of critical importance for our understanding of the unimolecular chemistry of $DMO^{\bullet+}$ ions. Interestingly, we observed that a large isotope effect operates among the low energy ions which operates against the loss of CO. In the MI mass spectrum of $CD_3OC(=O)\text{-}C(=O)OCD_3^{\bullet+}$ (DMO-d_6) (see Figure 6.1c), loss of CO is considerably suppressed and the loss of CO_2 (leading to *m/z* 80) and the formation of $CD_3O\text{-}C{\equiv}O^+$ (*m/z* 62) now become major processes. To trace the origin of this large effect, we need to establish the structure and mechanism of formation of the $[M\text{-}CO]^{\bullet+}$ ions.

In a previous study [6] we had proposed that prior to dissociation, ionized methyl glycolate, $HOCH_2C(=O)OCH_3^{\bullet+}$, rearranges to dimethyl carbonate, $CH_3OC(=O)OCH_3^{\bullet+}$ via the key intermediate hydrogen bridged radical cation $CH_2{=}O{\bullet\bullet\bullet}H{\bullet\bullet\bullet}O{=}COCH_3^{\bullet+}$, $\mathbf{2}^{\bullet+}$, formed by hydrogen bridging and concomitant C-C cleavage. Ions $\mathbf{2}^{\bullet+}$ could be independently generated, as a product ion, rather than a rearranged molecular ion, by the loss of the indicated **CO** from the ionized methylester of α-hydroxy pyruvic acid, $HOCH_2\mathbf{C}(=\mathbf{O})\text{-}C(=O)OCH_3^{\bullet+}$ [21], again by intramolecular hydrogen bridging and C-C cleavage, followed by loss of CO. The CID mass spectrum of $\mathbf{2}^{\bullet+}$ contains two intense signals of almost equal intensity at *m/z* 31, CH_2OH^+, and *m/z* 60, the ionized carbene $CH_3O\text{-}C\text{-}OH^{\bullet+}$, and considering the very similar proton affinities of $CH_2{=}O$ and $CH_3O\text{-}C{\equiv}O^{\bullet}$ (170 and 168 kcal/mol, respectively, [8,10]), this is precisely what is expected for the hydrogen bridged structure $CH_2{=}O{\bullet\bullet\bullet}H{\bullet\bullet\bullet}O{=}COCH_3^{\bullet+}$, $\mathbf{2}^{\bullet+}$. It was observed that the CID mass spectrum of the $[M\text{-}CO]^{\bullet+}$ ions generated from DMO ions was superimposable to that of $\mathbf{2}^{\bullet+}$ and so we conclude that $DMO^{\bullet+}$ also decarbonylates into $\mathbf{2}^{\bullet+}$. The mechanism proposed for this dissociation in Scheme 6.1 is similar to that proposed by Tajima et al. for the decarbonylation of ionized dimethyl malonate [22].

The reaction commences with a 1,5-hydrogen shift to produce the distonic on $\mathbf{1a}^{\bullet+}$. The formaldehyde dipole then moves along the electrostatic field of the incipient methoxy hydroxy ketene radical cation to produce the hydrogen bridged species $\mathbf{1b}^{\bullet+}$, which then releases CO to produce $\mathbf{2}^{\bullet+}$. The large isotope effect mentioned above can now be associated with the 1,5-H shift being rate determining and if this is so, this 1,5-H shift does not take place prior to the

loss of CO_2 and also not prior to formation of $CH_3O\text{-}C{=}O^+$ because these processes do not suffer from the isotope effect. With respect to loss of CO_2, CID and MI experiments showed that the product ions are ionized dimethoxy carbene, $CH_3O\text{-}C\text{-}OCH_3^{\bullet+}$ [23] and not any other isomer, such as ionized methyl acetate. We further note that metastable $CH_3O\text{-}C\text{-}OCH_3^{\bullet+}$ ions lose $CH_3^\bullet$ to produce $CH_3O\text{-}C{=}O^+$ and that this reaction is associated with a relatively large kinetic energy release, $T_{0.5}$ = 180 meV. This parallels earlier observations [24] that loss of $R_1^\bullet$ from ionized oxycarbenes $R_1OC\text{-}R_2^{\bullet+}$ proceeds via large (0.7-1.35 eV) reverse barriers. Thus, it is possible in principle that formation of $CH_3O\text{-}C{=}O^+$ from $DMO^{\bullet+}$ ions proceeds via consecutive [25a] losses of CO_2 and $CH_3^\bullet$, rather than by direct loss of $CH_3O\text{-}C{=}O^\bullet$. However, as mentioned above, loss of $CH_3^\bullet$ from $CH_3O\text{-}C\text{-}OCH_3^{\bullet+}$ proceeds via a large barrier and so at first sight a consecutive fragmentation would not appear energetically attractive. However, the radical $CH_3O\text{-}C{=}O^\bullet$ is one of those few neutral species whose direct dissociation products lie below the species itself : thus the separate products $CO_2 + CH_3^\bullet$ lie 19 kcal/mol *below* the intact structure $CH_3O\text{-}C{=}O^\bullet$ [8]. Now, if $DMO^{\bullet+}$ can first release CO_2 (which it does; see above) and then $CH_3^\bullet$ without the intermediacy of $CH_3O\text{-}C{=}O^\bullet$, then in principle a significant amount of energy could be saved, perhaps sufficient to overcome the barrier for loss o $CH_3^\bullet$ from the putative intermediate $CH_3O\text{-}C\text{-}OCH_3^{\bullet+}$. These matters will be addressed in the next section. That consecutive losses of $CO_2 + CH_3^\bullet$ do occur becomes evident from an experiment using a charged collision chamber [25b]. The CID mass spectrum of $CD_3OC(=O)\text{-}C(=O)OCD_3^{\bullet+}$ was recorded (accelerating voltage 10 kV) and +1000 V was applied to the collision chamber. The peaks for the losses of CO and CO_2 behaved as expected and were split into two components, one for reactions taking place outside the cell and one for processes occurring inside the cell. However, the signal for $CD_3O\text{-}C{=}O^+$ was split into three components; see Figure 6.2. The peaks at 5000 and 5500 V correspond to dissociations taking place outside and inside the cell, respectively, but the third peak at 5225 V corresponds to a consecutive process : *m/z* 124 → *m/z* 80 (+ CO_2) taking place in front of the cell and *m/z* 80 → *m/z* 62 (+ $CD_3^\bullet$) occurring in the chamber. This experiment shows that excited ions may indeed first lose CO_2 and then $CD_3^\bullet$. The absence of a signal at 5415 V shows that the reverse process, i.e., first loss of $CD_3^\bullet$ and then loss of CO_2, does not take place.

Assuming that at threshold the reaction is also a two-step process, there are two rationalizations for the high AE for *m/z* 59 from DMO: (i) the reaction suffers from a competitive shift and (ii) there is no competitive shift and one step has a reverse barrier and is rate determining.

Photoionization Measurements : Competitive Shift or Barrier ?

The IE of DMO and the AE of its most important dissociation products were measured using the technique of photoionization mass spectrometry [18]. The ion lifetime sampled prior to dissociation is 24 μs, well beyond the metastable time frame. The results are compiled in Table 6.1 (included is the AE measured using monochromatic electrons [7]) and some representative ionization efficiency curves are given in Figure 6.3. The adiabatic IE (9.95 eV) corresponds well with the onset of the first band in the photoelectron spectrum of DMO [26]. It can be seen from Table 6.1 that the processes observed in the metastable time frame (loss of CO from $DMO^{\bullet+}$, as well as formation of $CD_3O\text{-}C{=}O^+$ and loss of CO_2 from DMO-$d_6^{\bullet+}$) all have, within experimental error, the same AE. Thus, the AE for formation of $CD_3O\text{-}C{=}O^+$ may well be a true threshold value and not suffer from a competitive shift. From the PI data an energy diagram may be constructed; see Figure 6.4.

Table 6.1. Appearance energies, measured by photoionization, of dissociation products of dimethyl oxalate (DMO) and its deuterium labeled isotopomer DMO-d_6.

Product Ion	Neutral Lost	AE (eV)
$CH_3O\text{-}C{=}O^+$ from DMO	$CH_3O\text{-}C{=}O^{\bullet}$ or $CH_3^{\bullet} + CO_2$	10.40 ± 0.1 (10.48 ± 0.05)[a]
$CH_3O\text{-}C{=}O^+$ from DMO-d_6	$CD_3O\text{-}C{=}O^{\bullet}$ or $CD_3^{\bullet} + CO_2$	10.50 ± 0.05
$CD_2{=}O{\bullet\bullet\bullet}D{\bullet\bullet\bullet}O{=}C\text{-}OCD_3^{\bullet+}$	CO	10.40 ± 0.1
$CH_3O\text{-}C\text{-}OCH_3^{\bullet+}$ from DMO	CO_2	10.40 ± 0.05

[a] From [7].

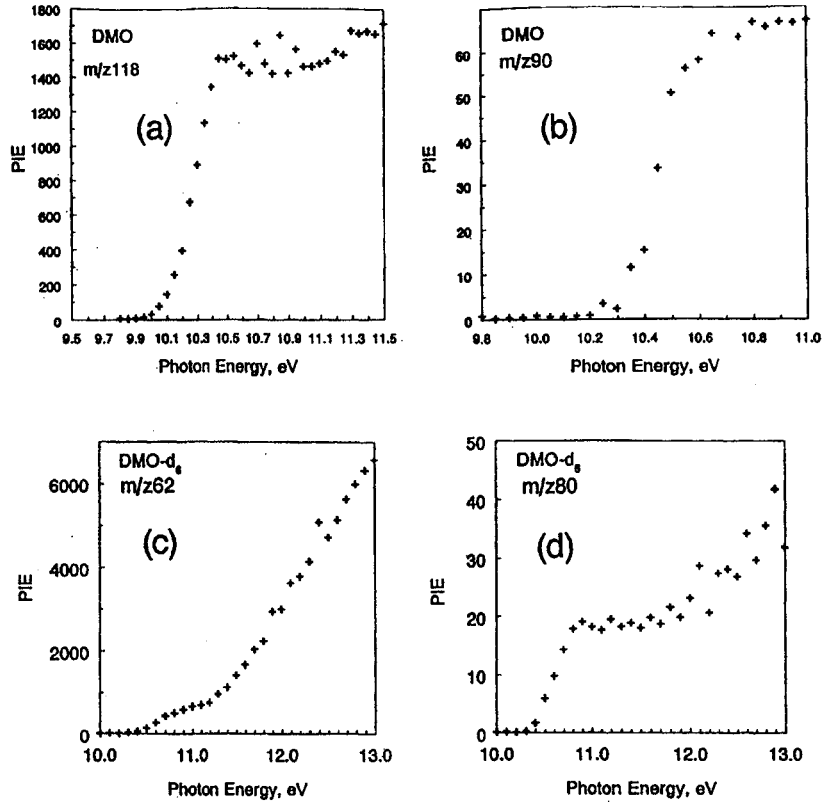

Figure 6.3. Photoionization efficiency curves for DMO and its isotopomer DMO-d_6 : (a) $DMO^{\bullet+}$; (b) $[DMO - CO]^{\bullet+}$; (c) $CD_3O\text{-}C{=}O^+$ from DMO-d_6 ; (d) $[DMO\text{-}d_6 - CO_2]^{\bullet+}$.

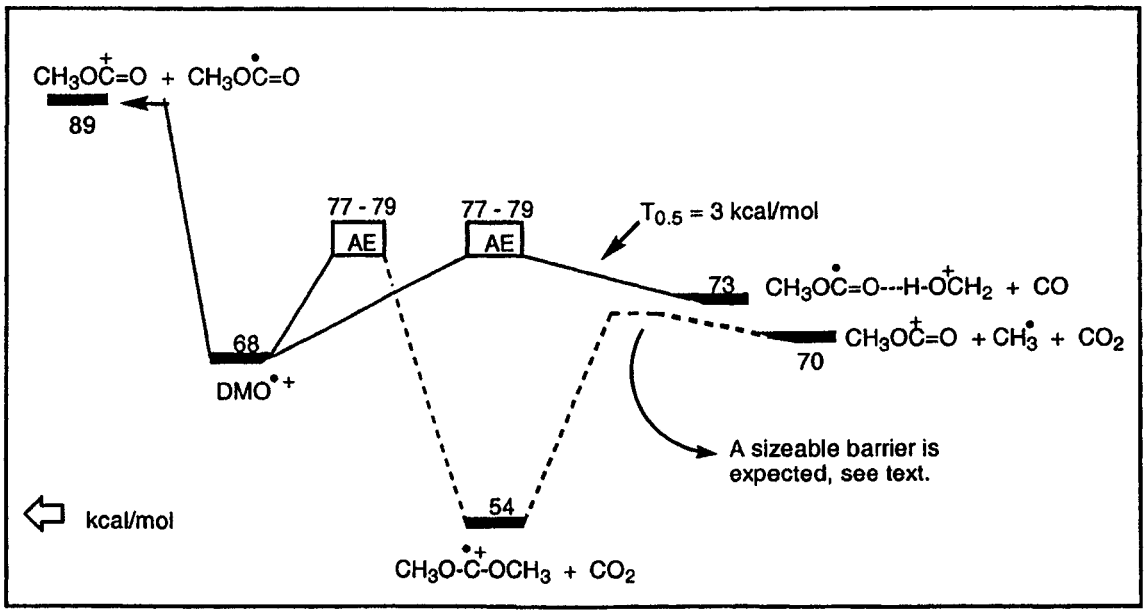

Figure 6.4. Energy diagram for the low energy dissociations of $DMO^{\bullet+}$. heats of formation from ref 10(a). $\Delta H_f[CH_2{=}O{\bullet\bullet\bullet}H{\bullet\bullet\bullet}O{=}C\text{-}OCH_3]^{\bullet+}$ (99 kcal/mol) from [27]; $\Delta H_f[CH_3O\text{-}C\text{-}OCH_3]^{\bullet+}$ (148 kcal/mol) from [23].

The energy requirement for the dissociations in the metastable time frame is only ~10 kcal/mol and this is too small to allow DMO molecular ions to be metastable, unless more stable forms can be accessed via rearrangement reactions [28]. One such stable species is the distonic ion **1a**$^{\bullet+}$ in Scheme 6.1 but this ion is only involved in the decarbonylation reaction which is greatly suppressed in the MI spectrum of the D_6 labeled isotopomer. Another is the distonic ion $^{\bullet}CH_2OC^{+}(OH)\text{-}C(=O)OCH_3$, but formation of this (unreactive) species involves a 1,4-H shift with an expected activation energy in the 10 kcal/mol range [6]. A more likely explanation is that upon ionization the initially generated DMO ions relax to a more stable long bonded species of the type $[CH_3O\text{-}(=O)C]^{+}$ — $^{\bullet}[C(=O)\text{-}OCH_3]$. Support for this proposal comes from computational studies on $HOCH_2\text{-}CH_2OH$, $HOCH(CH_3)\text{-}CH_2OH$, and $CH_3C(=O)\text{-}CH_2OH$ [29] which indicate that the initially generated molecular ions of conventional structure spontaneously rearrange to a considerably more stable species characterized by a long one electron C-C bond. In agreement with the proposal that significant geometry changes take place in DMO upon ionization is the observation that a survivor signal is absent in its NR spectrum (see below). Thus we propose that the long bonded ions **1c**$^{\bullet+}$ in Scheme 6.2 contribute to the "metastability" of the DMO ions and also that such ions play a key role in the mechanism for loss of CO_2. As proposed in Scheme 6.2, the long bonded ions **1c**$^{\bullet+}$ may promote migration of the $CH_3O\text{-}C{=}O^{\bullet}$ dipole within the electrostatic field of the $CH_3O\text{-}C{=}O^{+}$ ion to produce **1d**$^{\bullet+}$ which then undergoes a methyl cation [29,30] transfer to produce dimethoxycarbene product ions. The 10 kcal/mol barrier, we propose, is associated with the actual methyl cation transfer.

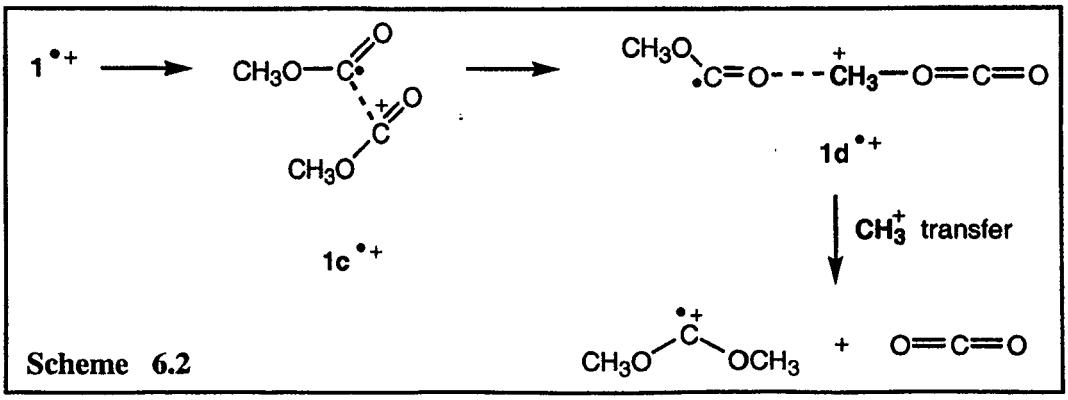

Scheme 6.2

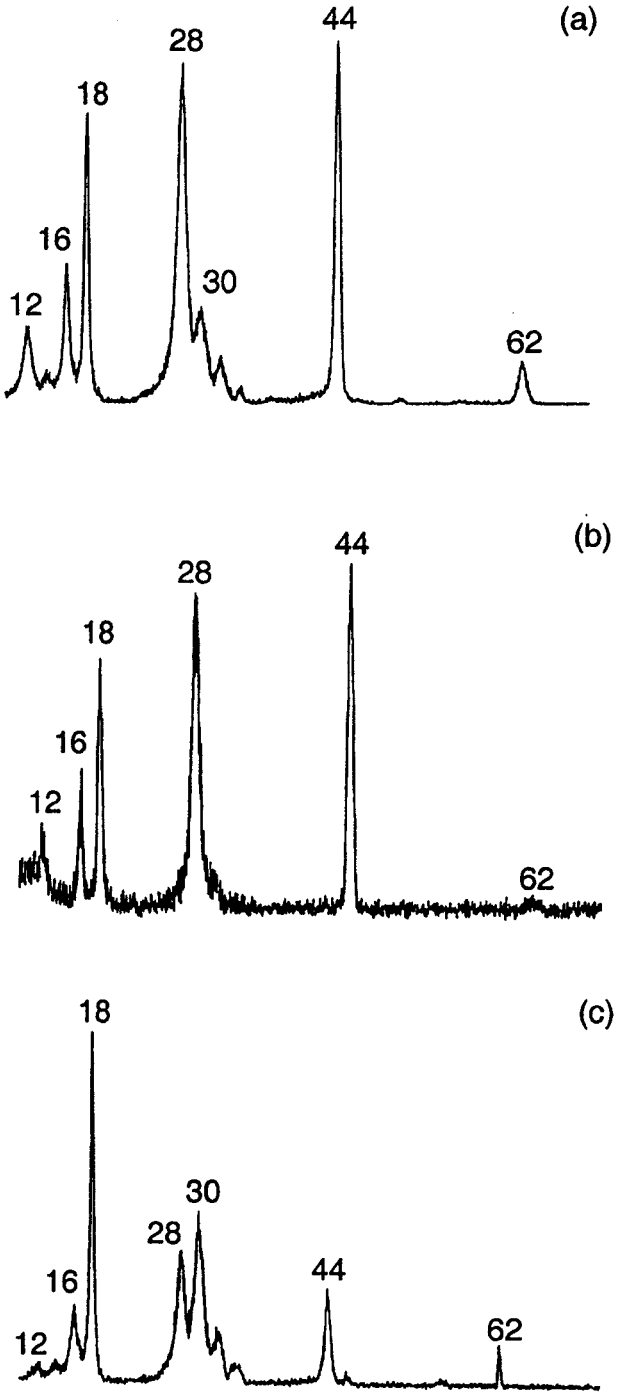

Figure 6.5. CIDI mass spectra of : (a) fully deuterated dimethyl oxalate (DMO-d_6), pressure 5 x 10^{-7} torr ; (b) DMO-d_6, pressure 8 x 10^{-8} torr ; (c methyl pyruvate (OCD_3), pressure 8 x 10^{-8} torr.

It is further shown in Figure 6.4 that the direct cleavage of DMO ions into $CH_3O\text{-}C{=}O^+$ + $CH_3O\text{-}C{=}O^{\bullet}$ lies too high in energy, but that the products formed by consecutive losses are energetically accessible. We therefore propose that formation of $CH_3O\text{-}C{=}O^+$ occurs first by loss of CO_2 to produce $CH_3O\text{-}C\text{-}OCH_3^{\bullet+}$ (itself a stable species) which then loses $CH_3^{\bullet}$. That the metastable ions do indeed form CO_2 and $CH_3^{\bullet}$ (as opposed to intact $CH_3O\text{-}C{=}O^{\bullet}$) follows from the experiments described in the following section.

CIDI Experiments

The CIDI mass spectrum of $CH_3O\text{-}C{=}O^{\bullet}$ produced from metastable $DMO^{\bullet+}$ ions has been discussed previously [6] in the context of rearrangement / dissociation reactions of ionized methyl glycolate. Because (see Figure 6.1b,c) DMO-d_6 yields more $CD_3O\text{-}C{=}O^+$ relative to other products, it was decided to use DMO-d_6 for our new CIDI experiments. The CIDI mass spectrum of DMO-$d_6^{\bullet+}$ is given in Figure 6.5a (this spectrum is better mass-resolved than that in ref. 6 because the precursor ion is fully deuterated). The signals at *m/z* 44, 28, 16, and 12 can be attributed to dissociative reionization of CO and CO_2. The peaks at *m/z* 62, 32, 30 and 14 could be due to reionized $CD_3O\text{-}C{=}O^{\bullet}$ (formed directly from the molecular ion) and its dissociation products. However, other processes may contribute to the CIDI mass spectrum. For example, gas may leak out of the cell to the region upstream of the deflector electrode, where it may dissociatively neutralize DMO-$d_6^{\bullet+}$ itself into $CD_3O\text{-}C{=}O^{\bullet}$ which is then reionized in the cell leading to a signal at *m/z* 62. When the pressure was reduced to 8 x 10^{-8} Torr, the spectrum in Figure 6.5b was obtained. This reduction in pressure has two effects: it reduces diffusion of the gas into the drift tube and it reduces second order processes, such as neutralization-reionization. Indeed, it can be seen that *m/z* 62 (and its dissociation products) has almost disappeared. This spectrum represents the CIDI mass spectra of $CD_3^{\bullet}$, CO, and CO_2. Thus, most DMO-d_6 molecular ions do indeed undergo consecutive losses of CO_2 and $CD_3^{\bullet}$. That $CD_3O\text{-}C{=}O^{\bullet}$ radicals are not formed does not mean that $CD_3O\text{-}C{=}O^{\bullet}$ is intrinsically unstable : as shown in Figure 6.5c (also recorded at a pressure of 8 x 10^{-8} Torr), they are clearly generated in the dissociation of ionized methyl pyruvate, $CD_3OC(=O)C(=O)CH_3^{\bullet+} \rightarrow CD_3O\text{-}C{=}O^{\bullet} + CH_3\text{-}C{=}O^+$ as evidenced by the peak at *m/z* 62.

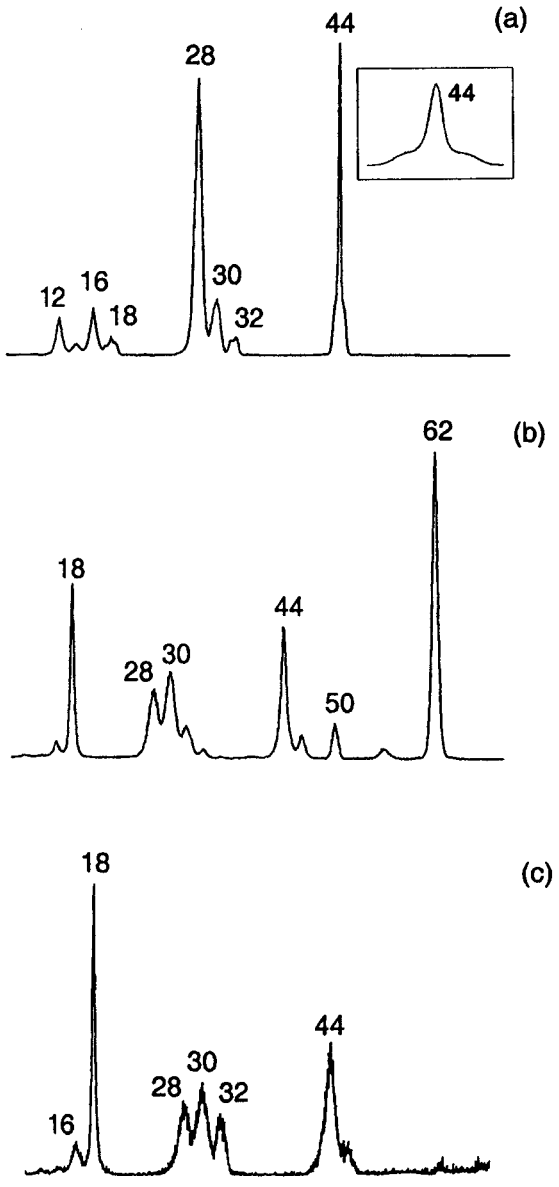

Figure 6.6. NR mass spectra of : (a) $CD_3O\text{-}C{=}O^+$; inset peak at *m/z* 44; (b) the molecular ion of fully deuterated dimethyl oxalate (DMO-$d_6^{\bullet+}$); (c) collision-induced dissociation mass spectrum of the *m/z* 62 $CD_3O\text{-}C{=}O^+$ ion in spectrum 6b.

Note also that, in contrast to *m/z* 62 in Figure 6.5a, the peak in Figure 6.5c is narrow, which is to be expected for an undissociated reionized species.

We now have solid evidence from AE measurements and CIDI experiments that metastable $DMO^{\bullet+}$ ions dissociate to $CH_3O\text{-}C{=}O^+$ and $CO_2 + CH_3^\bullet$, to the exclusion of intact $CH_3O\text{-}C{=}O^\bullet$. In addition, the CID experiments with a charged cell as described above show that first CO_2 is lost and then $CH_3^\bullet$ is released. The whole process takes place some 10 kcal/mol below the calculated threshold for $CH_3O\text{-}C{=}O^+ + CH_3O\text{-}C{=}O^\bullet$. As can be seen from Figure 6.3c, the ionization efficiency curve for the formation of *m/z* 62 from DMO-d_6 (as well as that for *m/z* 59 from DMO) at first rises slowly, and then after 11.2 eV it increases rapidly. This steeply rising curve may well correspond to the higher energy formation of $CH_3O\text{-}C{=}O^+$ and (intact) $CH_3O\text{-}C{=}O^\bullet$, a simple cleavage reaction. Thus at low internal energies the sequential losses follow the kinetics of a rearrangement process (such as loss of CO_2) which rapidly levels off, but at high internal energies direct dissociation takes over and the kinetics of a simple cleavage is followed.

Neutralization of $CD_3O\text{-}C{=}O^+$ and $DMO^{\bullet+}$; Formation of $CD_3O\text{-}C{=}O^\bullet$

According to the calculations of Mebel et al. [15] $CH_3O\text{-}C{=}O^\bullet$ is a kinetically stable species with a barrier of 27 kcal/mol preventing its exothermic dissociation into $CH_3^\bullet + CO_2$, but there is as yet only indirect evidence for its existence [8]. One way to produce novel neutral species is by neutralization of the corresponding cations [17]. In Figure 6.6a is given the neutralization-reionization (NR) mass spectrum of $CD_3O\text{-}C{=}O^+$; the spectrum is dominated by a peak for $CO^{\bullet+}$ and a composite peak for $CO_2^{\bullet+}$ (which is also shown in the inset), but a recovery signal at *m/z* 62 is completely absent. Parallel with neutralization part of the $CD_3O\text{-}C{=}O^+$ ions may undergo CID; it is known [1] that upon CID, $CD_3O\text{-}C{=}O^+$ abundantly forms $CD_3^+ + CO_2$ with a small kinetic energy release and these CO_2 molecules enter the cell and become collisionally ionized to produce a narrow peak at *m/z* 44. The presence of the broad component and the absence of a recovery signal, we propose, have a

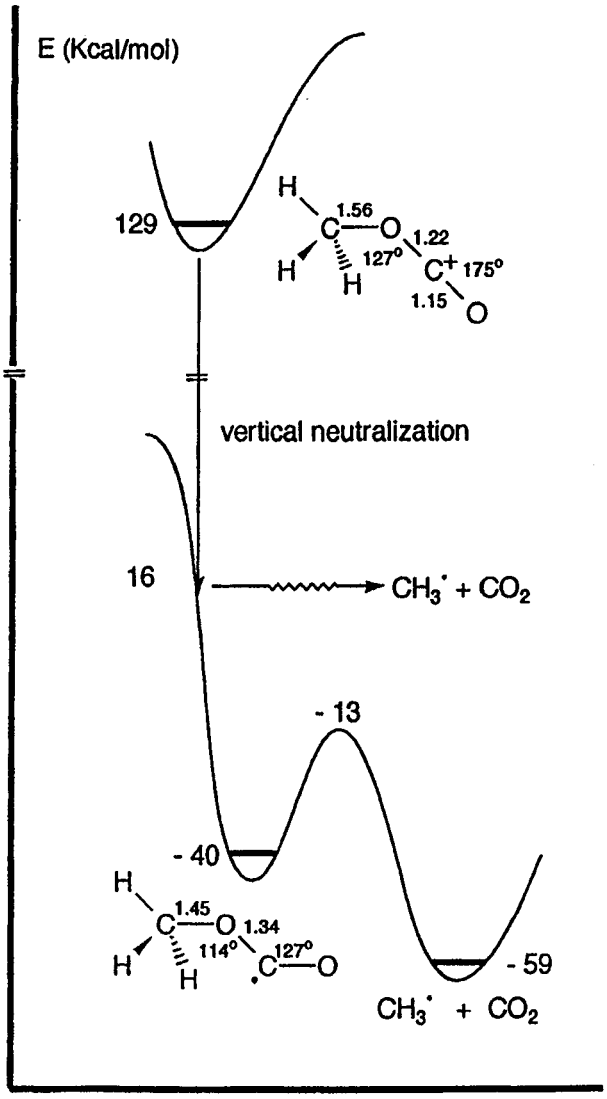

Figure 6.7 Energy diagram for the dissociative neutralization of the methoxycarbonyl cation $CH_3O\text{-}C{=}O^+$.

common origin. Electron transfer between kilovolt species is a fast, vertical process, so that the neutral is generated with the geometry of the ionic species; thus the neutrals may be formed with a distorted geometry having a high energy and they may in fact dissociate. In Figure 6.7 are given the geometries and energies of the $CH_3O\text{-}C{=}O^+$ cation and radical optimized at the 6-311G** level of theory with QCISD(T) single point calculations [3] and it is seen that the O-C-O moiety is almost linear in the cation, but bent in the radical. If the radical is frozen in

the ionic geometry and its energy is then calculated, it is found to lie as much as 55.6 kcal/mol above the ground state; see Figure 6.7. This is much higher than the barrier for the dissociation into $CH_3^{\bullet}$ + CO_2 (27 kcal/mol), so that the neutralized species will rapidly dissociate. This dissociation is exothermic by 75 kcal/mol and this leads to the large kinetic energy release, T, observed (from the "horns" of the peak we estimate T ~ 20 kcal/mol, so that about 20 % of the excess energy appears as translational energy which considering the number of degrees of freedom (10) appears reasonable [31]).

The NR mass spectrum of DMO-d_6 is given in Figure 6.6b, and in contrast to the CIDI mass spectrum (Figure 6.5a) *m/z* 62 is now the base peak. (This lends further support for our proposal that the "recovery" signal at *m/z* 62 in the CIDI mass spectrum of DMO-$d_6^{\bullet+}$ is indeed due to dissociative neutralization.) The CID mass spectrum of these *m/z* 62 ions, Figure 6.6c, demonstrates that they have retained the CD_3O-C=O^+ structure. These experiments clearly show that CD_3O-C=O^+ are kinetically stable species. The peak for $CO_2^{\bullet+}$ in the NR mass spectrum of DMO-d_6 still contains the broad component mentioned above. The NR mass spectrum can be rationalized on the basis of structure **1c**$^{\bullet+}$ in Scheme 6.2. This species can be viewed as an ion-dipole complex of linear CH_3O-C=O^+ and bent CH_3O-C=$O^{\bullet}$. As shown in Scheme 6.3, upon dissociative neutralization two types of CD_3O-C=$O^{\bullet}$ radicals are formed, one with a linear geometry which, as discussed above, dissociates to $CD_3^{\bullet}$ + CO_2 and one with a bent geometry which does not dissociate and is reionized as an intact species.

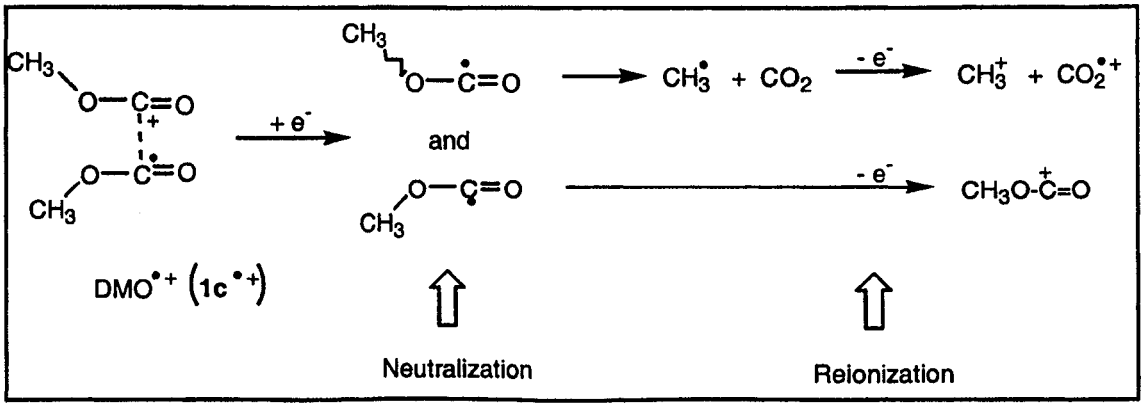

Scheme 6.3

Conclusions

From the experiments on DMO described above we conclude the following :

i. At threshold, DMO ions fragment step-wise by first losing CO_2 to generate the ionized carbene $CH_3O\text{-}C\text{-}OCH_3^{\bullet+}$ and this species then releases a $CH_3^{\bullet}$ group. There is no competitive shift. At higher energies direct dissociation to intact $CH_3O\text{-}C{=}O^{\bullet}$ takes place. Dissociation by the consecutive loss of CO_2 and $CH_3^{\bullet}$ is possible because $CH_3O\text{-}C{=}O^{\bullet}$ is thermodynamically *less stable*.

ii. The competitive loss of CO generates via a rate determining 1,5-H shift, the hydrogen-bridged radical cation $CH_2{=}O{\bullet\bullet\bullet}H{\bullet\bullet\bullet}O{=}COCH_3^{\bullet+}$, **2**$^{\bullet+}$.

iii. Neutralization of $CH_3O\text{-}C{=}O^{+}$ leads to excited $CH_3O\text{-}C{=}O^{\bullet}$ radicals which rapidly dissociate to $CH_3^{\bullet} + CO_2$. This occurs because neutralization is a vertical process and the radical is generated with a distorted high energy geometry.

iv. Neutralization of DMO ions too is completely dissociative, the major product being $CH_3O\text{-}C{=}O^{\bullet}$ radicals. Half of these radicals are formed in the ground state and these survive reionization. Thus, despite its thermodynamic instability, $CH_3O\text{-}C{=}O^{\bullet}$ is a kinetically stable species.

References

[1] M.C. Blanchette, J.L. Holmes, C.E.C.A. Hop, F.P. Lossing, R. Postma, P.J.A. Ruttink, J.K. Terlouw, *J. Am. Chem. Soc.* **1986**, *108*, 7589.

[2] T.B. McMahon, T. Heinis, G. Nicol, J.K. Hovey, P. Kebarle, *J. Am. Chem. Soc.* **1988**, *110*, 7591.

[3] P.J.A. Ruttink, P.C. Burgers, L.M. Fell, J.K. Terlouw, *J. Phys. Chem. A* **1999**, *103*, 1426.

[4] J.G. Liehr, E.A. Larka, J.H. Beynon, *Org. Mass Spectrom.* **1981**, *16*, 34.

[5] For a recent review see : G. Schalley, G. Hornung, D. Schröder, H. Schwarz, *Chem. Soc. Rev.* **1998**, *27*, 91.

[6] D. Suh, C.A. Kingsmill, P.J.A. Ruttink, P.C. Burgers, J.K. Terlouw, *Int. J. Mass Spectrom. Ion Processes* **1995**, *146/147*, 305.

[7] J.L. Holmes, Private Communication, **1998**: this AE measurement was performed by the late Dr. F.P. Lossing (item 890106) with the instrumentation described in [1].

[8] J.L. Holmes, F.P. Lossing, P.M. Mayer, *J. Am. Chem. Soc.* **1991**, *113*, 9723.

[9] M.E. Anthoney, A.S. Carson, P.G. Laye, M. Yürekli, *J. Chem. Thermodyn.* **1976**, *8*, 1009.

[10] (a) S. Lias, J.E. Bartmess, J.F. Liebman, J.L. Holmes, R.D. Levin, W.G. Mallard, *J. Phys. Chem. Ref. Data* **1988**, *17*, Suppl. 1. Note that the ΔH_f [DMO] value given in this compilation is not based on the quoted reference (ref 9). (b) H.Y. Afeefy, J.F. Liebman, S.E. Stein, "Neutral Thermochemical Data", in NIST Chemistry WebBook, NIST Standard Reference Database No. 69, W.G. Mallard, P.J. Linstrom, Eds, November **1998**, National Institute of Standards and Technology, Gaithersburg, MD 20899 (http://webbook.nist.gov/chemistry/).

[11] J.S. Chickos, R. Sabbah, S. Hosseini, J.F. Liebman, *Struct. Chem.* **1996**, *7*, 391.

[12] J.L. Holmes, F.P. Lossing, *J. Am. Chem. Soc.* **1980**, *102*, 1591.

[13] J.B. Pedley, R.D. Naylor, S.P. Kirby, Eds. *Thermochemical Data of Organic Compounds*, Chapman and Hall, London, **1986**.

[14] J.W. Ochterski, G.A. Petersson, J.A. Montgomery Jr., *J. Chem. Phys.* **1996**, *104*, 2598 and references cited therein.

[15] A.M. Mebel, E.W.G. Diau, M.C. Lin, K. Morokuma, *J. Am. Chem. Soc.* **1996**, *118*, 9759.

[16] H.F. van Garderen, P.J.A. Ruttink, P.C. Burgers, G.A. McGibbon, J.K. Terlouw, *Int. J. Mass Spectrom. Ion Processes* **1992**, *121*, 159.

[17] For a recent review see : C.A. Schalley, G. Hornung, D. Schröder, H. Schwarz, *Chem. Soc. Rev.* **1998**, *27*, 91.

[18] C. Lifshitz, *Int. J. Mass Spectrom. Ion Processes* **1991**, *106*, 159.

[19] K. Levsen, *Fundamental Aspects of Organic Mass Spectrometry*, Verlag Chemie Weinheim, **1978**.

[20] F.W. McLafferty, T. Wachs, C. Lifshitz, G. Innorta, P. Irving, *J. Am. Chem. Soc.* **1970**, *92*, 6867.

[21] L.M. Fell, P.C. Burgers, P.J.A. Ruttink, J.K. Terlouw, *Can. J. Chem.* **1998**, *76*, 335.

[22] S. Tobita, K. Ogino, S. Ino, S. Tajima, *Int. J. Mass Spectrom. Ion Processes* **1988**, *85*, 31.

[23] T. Wong, J. Warkentin, J.K. Terlouw, *Int. J. Mass Spectrom. Ion Processes* **1992**, *115*, 33.

[24] P.C. Burgers, J.L. Holmes, J.K. Terlouw, *Chem. Commun.* **1984**, 621.

[25] (a) C.J. Proctor, B. Kralj, A.G. Brenton, J.H. Beynon, *Org. Mass Spectrom.* **1980**, *15*, 619; (b) S. Howells, A.G. Brenton, J.H. Beynon, *Int. J. Mass Spectrom. Ion Phys.* **1980**, *32*, 379.

[26] S.P. McGlynn, J.L. Meeks, *J. Electron Spectrom. Relat. Phenom.* **1976**, *8*, 85.

[27] L.M. Fell, P.C. Burgers, P.J.A. Ruttink, J.K. Terlouw, unpublished.

[28] P.C. Burgers, J.K. Terlouw in *Specialist Periodical Reports: Mass Spectrometry*, M.E. Rose, Ed., The Royal Society of Chemistry, London, **1989**, Vol. 10, Chapter 2.

[29] (a) P.J.A. Ruttink, P.C. Burgers, L.M. Fell, J.K. Terlouw, *J. Phys. Chem. A* **1998**, *102*, 2976; (b) P.C. Burgers, L.M. Fell, A. Milliet, M. Rempp, P.J.A. Ruttink, J.K. Terlouw, *Int. J. Mass Spectrom. Ion Processes* **1997**, *167/168*, 291; (c) P.J.A. Ruttink, P.C. Burgers, J.K. Terlouw, *Can. J. Chem.* **1996**, *74*, 1078; (d) J. Chamot-Rooke, B. Amekraz, J. Tortajada, P. Mourges, H.E. Audier, *J. Mass Spectrom.* **1997**, *32*, 779.

[30] V. Baranov, S. Petrie, D.K. Bohme, *J. Am. Chem. Soc.* **1996**, *118*, 4500.

[31] P.C. Burgers, J.L. Holmes, *Rapid Commun. Mass Spectrom.* **1989**, *3*, 279.

Chapter 7

Hydrogen-shift isomers of ionic and neutral hydroxypyridines : a combined experimental and computational investigation

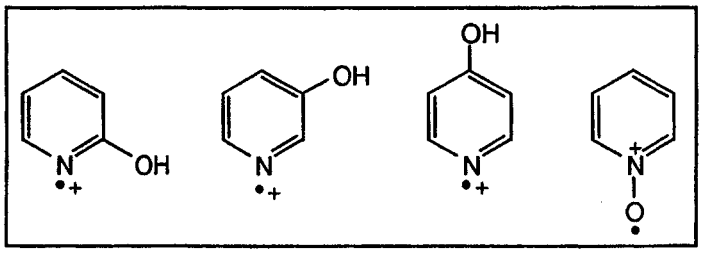

Apart from pyridine N-oxide (**1a**), the C_5H_5NO family of stable molecules comprises, 2-, 3- and 4-hydroxypyridine (**2a**, **3a** and **4a**) as well as their keto counterparts 2-, 3- and 4(1H)-pyridone (**2b**, **3b** and **4b**). This study focuses on the characterization of their radical cations and a number of stable H-shift isomers, which are α- or β-distonic ions. This was done by using a combination of mass spectrometric experiments and computational chemistry, at the B3LYP/CBSB7 level of theory. The ionic species were identified on the basis of both their collision-induced dissociation characteristics and specific associative ion-molecule reactions with dimethyl disulfide and *tert*-butyl isocyanide as substrates.

The distonic ions (**1b**$^{\bullet+}$, **2c**$^{\bullet+}$, **2d**$^{\bullet+}$ and **3c**$^{\bullet+}$) were obtained by dissociative electron impact ionization and subjected to neutralization-reionization mass spectrometry (NRMS). From collision-induced dissociation (CID) spectra of the intense survivor ions, it follows that the neutral counterparts of the α-distonic ions **2c**$^{\bullet+}$ and **3c**$^{\bullet+}$ are viable chemical species in the rarefied gas phase. The energy-rich ylide type neutrals **1b**, on the other hand, readily isomerize into pyridine N-oxide, **1a**, or else dissociate.

The neutral counterpart of the β-distonic ion **2d**$^{\bullet+}$ only has a marginal stability and part of these neutrals are proposed to isomerize into energy-rich 2-pyridone molecules **2b**. This is in agreement with the computational results. However, ionized 2-pyridone cannot readily be differentiated from its enol isomer 2-hydroxypyridine. In contrast, the keto isomers of ionized 3- and 4-hydroxypyridine display characteristically different CID spectra.

The work described here has been accepted for publication as an article under the same title: M.A. Trikoupis, P. Gerbaux, D.J. Lavorato, R. Flammang, J.K. Terlouw, Int. J. Mass Spectrom. (P. Longevialle Issue), in press.

Introduction

Proton transfer plays a key role in a wide range of chemical and biochemical processes. In particular, the proton transfer associated with keto-enol tautomerizations has long been of interest because such reactions may catalyze certain biochemical transformations [1]. In this context, the prototropic tautomerization of 2- and 4-hydroxypyridine has been much studied [2]. A key feature of this system is that the gaseous enthalpies of formation of the two tautomeric forms, the pyridinol structures **2a / 4a** vs the pyridone structures **2b / 4b** in Scheme 7.1, are closely similar. The 3-isomer on the other hand, exclusively exists as 3-hydroxypyridine, **3a**, because its keto counterpart, **3b**, is a betaine type molecule of much higher energy.

The chemical environment plays an important role in the tautomerism of 2- and 4-hydroxypyridine. For the 2-isomer, x-ray crystallography experiments revealed that 2-pyridone is the only tautomer present in the solid state [3]. It is also the preferred tautomer in aqueous solutions. This is readily understood in terms of solvation effects with the hydroxy form becoming the most important isomer in solvents of low polarity [4]. In the gas-phase, under conditions where an **inter**molecular proton transfer allows the tautomers to equilibrate, a variety of spectroscopic measurements (UV, IR and microwave spectroscopy), provide evidence that the hydroxy form dominates, representing roughly 75 % of the population [5]. In the condensed phase, the 4-isomer also largely exists in the pyridone form. However, as shown by photoelectron spectroscopy, in the gaseous state at least 95 % of the 4-isomer consists of the 4-hydroxypyridine tautomer [6].

This tautomerization has also received considerable attention from computational chemistry [7]. The hydroxy forms of the 2- and 4- isomers are calculated to be slightly more stable than their keto structure, by 1 and 3 kcal/mol respectively [7a,g]. For the 2-isomer, an experimental value of 1 kcal/mol has been reported [8]. Unlike the two 4-isomers, which can only equilibrate via an intermolecular proton transfer, the 2-isomers could interconvert via an intramolecular 1,3-H shift. However, computations at various levels of theory all predict that

the barrier associated with this shift is quite high, 38 kcal/mol at the CISD/DZP1 level of theory [7g].

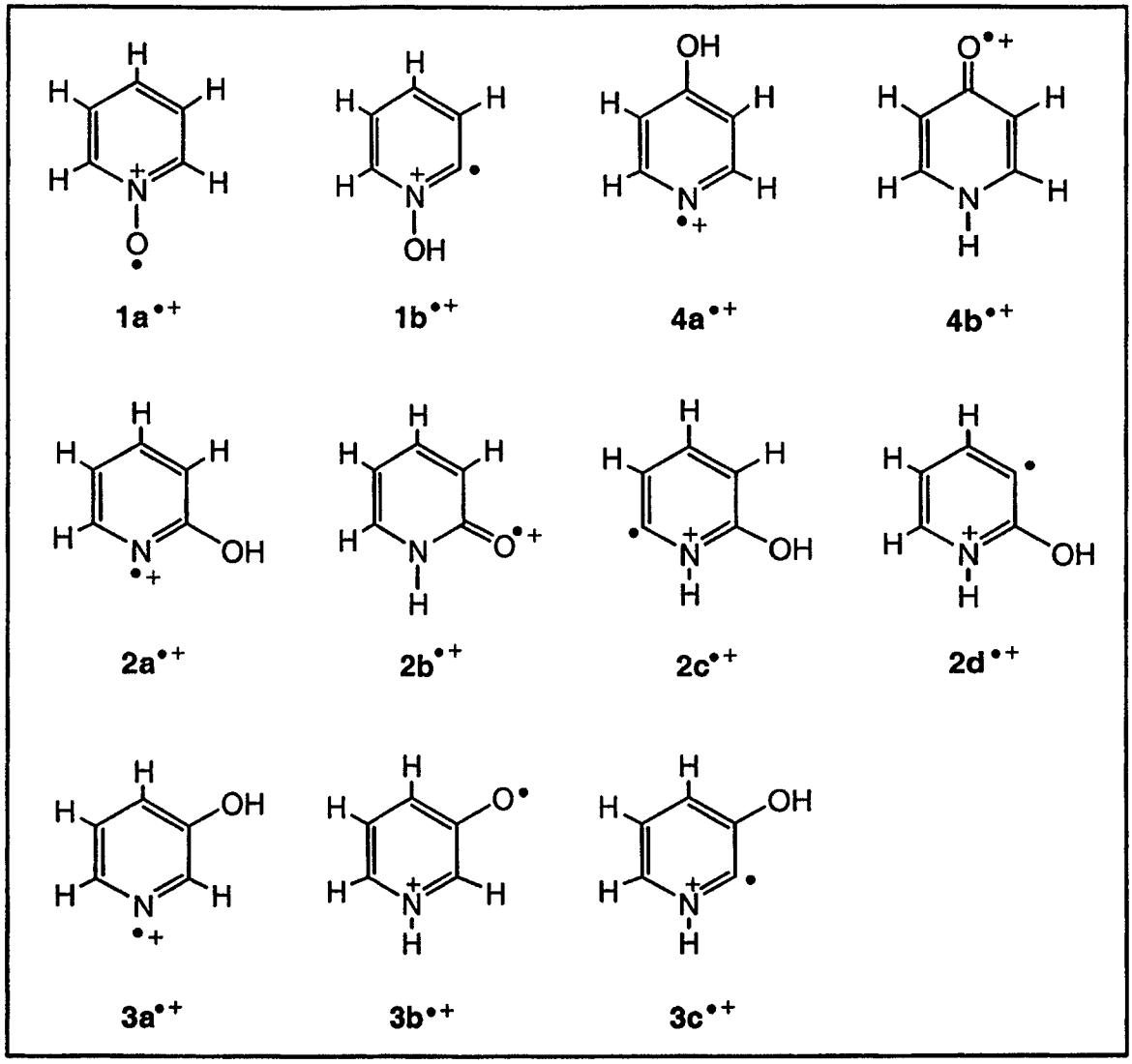

Scheme 7.1

The hydroxypyridines have also been extensively studied by mass spectrometry [9,10]. Early studies include analysis of deuterium isotope effects on the dissociation of the metastable molecular ions [10b] and ion-molecule reactions under conditions of chemical ionization [10c]. These studies indicate that, prior to ionization in the rarefied gas-phase, all three isomers exist in their pyridinol form and that the resulting hydroxypyridine radical cations are separated by a high 1,3-H shift barrier for the ketonization. In a subsequent

metastable ion study [11], it was concluded from an analysis of the metastable peak shape for loss of CO, that the ionized 2-isomer exists solely in its hydroxy form.

This result seems to be at odds with the spectroscopic evidence quoted above that, in the gas phase, the keto form comprises 25 % of the sample population. One explanation is that under the experimental conditions used in mass spectrometry, the sample vaporizes as the hydroxy form and does not equilibrate [6]. However, there is another possibility which will be discussed below.

Despite the interest in the tautomerization of ionized hydroxypyridines, little or no information is available on the behaviour of their distonic H-shift isomers. Such ionic species (and some of their neutral counterparts) are well characterized by theory and experiment for simple heterocycles, including pyridine, pyrazine, pyrimidine and pyridazine [12].

In the present study, we focus on the dissociation chemistry and reactivity of the 2-, 3- and 4-hydroxypyridine ions and their keto counterparts vis à vis a number of other potentially stable H-shift isomers, *viz.* the α- and β- distonic ions shown in Scheme 7.1. An additional α-distonic isomer pertinent to this study is the 1,3-H shift isomer of pyridine N-oxide.

The experimental approach uses a variety of tandem mass spectrometry based techniques: metastable ion (MI) and collision-induced dissociation (CID) characteristics, neutralization-reionization (NR) mass spectrometry [13] and associative ion-molecule reactions [14]. In addition, collision-induced dissociation experiments (denoted as NR/CID experiments [12d]) were performed on those isomeric ions that survived the neutralization-reionization process. Such experiments not only provide information about the structure and stability of the neutral counterparts of the ion, they also probe the isomeric purity of the ions [12d]. To assist in the interpretation of the experimental observations, density functional theory calculations are used to obtain relative energies for the radical cations and neutrals and barriers for selected H-shifts.

Results and Discussion

Computation of energies for the $C_5H_5NO^{\bullet+}$ isomers and their neutral counterparts

The potential energy surface comprising the $C_5H_5NO^{\bullet+}$ radical cations $\mathbf{1}^{\bullet+}$ - $\mathbf{4}^{\bullet+}$ of Scheme 7.1, as well as that of the corresponding neutrals and selected connecting transition structures of the 1,3-H shifts, was explored at a level of theory (B3LYP/CBSB7) that has proven adequate for related species [12e]. This level of theory is also used in the CBS-QB3 model chemistry [17]. The calculations were performed on a PC using the Gaussian 98W program [18]. Analytical frequency calculations confirmed the assignment of stable or transition structures based on the correct number of negative eigenvalues of the Hessian matrix, 0 or 1 respectively. The geometric parameters (which are not presented but are available upon request) and energies of the structures were obtained with the CBSB7 basis set using the standard hybrid density functional theory option (HF/DFT) designated B3LYP [19]. Relative energies were corrected for non-scaled zero point vibrational energy (ZPVE) contributions. All $\langle s^2 \rangle$ expectation values of the open shell systems were within 5 % of the expected value and show that the B3LYP wave functions do not suffer appreciably from spin contamination.

The energy data for the isomeric ions and their neutral counterparts are collected in Tables 7.1a and 7.1b, respectively. Among the H-shift isomers of ionized 2-hydroxypyridine, $\mathbf{2a}^{\bullet+}$, the keto isomer $\mathbf{2b}^{\bullet+}$ is the most stable species. It is calculated to lie 11.5 kcal/mol lower in energy than the pyridinol ion $\mathbf{2a}^{\bullet+}$, in satisfactory agreement with a recent ZEKE photoelectron spectroscopic measurement which found the difference in the two ionic species to be 0.5 eV in favour of $\mathbf{2b}^{\bullet+}$ [20]. The transition state for the 1,3-H shift connecting $\mathbf{2a}^{\bullet+}$ and $\mathbf{2b}^{\bullet+}$ was also calculated. The barrier for the interconversion is substantial, 28 kcal/mol relative to $\mathbf{2a}^{\bullet+}$, so that the keto ion may well be an observable species in the gas-phase [21]. This point will be further addressed in the next section. The distonic ions, $\mathbf{2c}^{\bullet+}$ and $\mathbf{2d}^{\bullet+}$, are both stable species but they lie higher in energy, by ca 10-15 kcal/mol, than the 2-hydroxypyridine ion. This contrasts with the pyridine system where ionized pyridine and its distonic H-shift isomers are comparable in stability. For the neutral counterparts of $\mathbf{2}^{\bullet+}$, our calculations predict the keto and enol forms to be of comparable stability, in agreement with experiment.

Table 7.1a. Calculated energies (B3LYP/CBSB7) for the $C_5H_5NO^{\bullet+}$ ions $\mathbf{1}^{\bullet+}$-$\mathbf{4}^{\bullet+}$ and selected isomerization barriers for 1,3-hydrogen migrations.

Species	Doublet (Hartree)	ZPVE (kcal/mol)	E_{rel}[a] (kcal/mol)
2a$^{\bullet+}$	-323.286262	57.5	0.0
2b$^{\bullet+}$	-323.304605	57.8	-11.2
2c$^{\bullet+}$	-323.263124	57.6	14.6
2d$^{\bullet+}$	-323.271971	58.2	9.7
3a$^{\bullet+}$	-323.270412	56.9	9.3
3b$^{\bullet+}$	-323.289970	57.7	-2.1
3c$^{\bullet+}$	-323.259365	58.0	17.4
4a$^{\bullet+}$	-323.265260	56.6	12.3
4b$^{\bullet+}$	-323.285058	58.3	1.6
1a$^{\bullet+}$	-323.232927	57.5	33.5
1b$^{\bullet+}$	-323.193687	56.8	57.4
TS 2a$^{\bullet+}$**→2b**$^{\bullet+}$	-323.237256	54.4	27.7
TS 1a$^{\bullet+}$**→1b**$^{\bullet+}$	-323.125811	53.3	96.3

[a] Relative energies are corrected for zero-point vibrational energy (ZPVE)

Table 7.1b. Calculated energies (B3LYP/CBSB7) for the C_5H_5NO neutrals **1-4** and selected isomerization barriers for 1,3-hydrogen migrations.

Species	Singlet (Hartree)	ZPVE (kcal/mol)	E_{rel}[a] (kcal/mol)
2a	-323.605640	58.0	0.0
2b	-323.607008	58.0	-0.9
2c	-323.524243	57.5	50.6
2d	-323.520109	57.6	53.3
3a	-323.589567	57.5	9.6
3b	-323.569299	57.8	22.6
3c	-323.533444	58.0	45.3
4a	-323.593277	57.7	7.5
4b	-323.590992	57.9	9.1
1a	-323.531436	57.5	46.1
1b	-323.477795	56.9	79.1
TS 2a→2b	-323.547497	54.8	33.3
TS 1a→1b	-323.449632	54.2	94.1
TS 2b→2d	-323.495113	54.8	66.2

[a] Relative energies are corrected for zero-point vibrational energy (ZPVE)

The α-ylide **2c** and the zwitterion **2d** are both calculated to be stable species but, not surprisingly, they lie considerably higher in energy, by ca 50 kcal/mol. Consequently their IEs, see Table 7.2, are considerably lower than those of their conventional isomers **2a/b**. This difference in IE provides an important criterion for isomer differentiation by ion-molecule reactions as discussed in a separate section below.

Table 7.2. Calculated (B3LYP/CBSB7) recombination (RE) and ionization (IE) energies (eV) of the C_5H_5NO isomers of Scheme 1.

Species	RE(vertical)	IE(adiabatic)		IE(vertical)	
1a	8.1	8.1	(8.4) [a]	8.2	
1b	7.2	7.7		8.2	
2a	8.5	8.7	(8.9)	8.9	(9.1) [b]
2b	8.1	8.2	(8.4)	8.4	(8.6)
2c	6.4	7.1		7.5	
2d	6.3	6.8		7.2	
3a	8.4	8.7	(9.1)	8.9	(9.1)
3b	7.5	7.6		7.7	
3c	7.0	7.5		8.0	
4a	8.4	8.9	(9.7)	9.5	(9.8)
4b	8.1	8.3		8.5	

[a] Experimental values quoted in ref. 21, with the exception of IE **2a/2b** which were taken from the ZEKE PES study of ref. 20.
[b] Experimental values form the PES study of ref. 6.

For the 3-isomers, neutral 3-hydroxypyridine, **3a**, is predicted to be considerably more stable than its highly polar pyridone tautomer **3b**, by 13 kcal/mol. Upon ionization there is a reversal of stabilities and the betaine-type ion $\mathbf{3b}^{\bullet+}$ is calculated to lie as much as 10 kcal/mol lower in energy than $\mathbf{3a}^{\bullet+}$. The distonic H-shift isomer, $\mathbf{3c}^{\bullet+}$, is of comparable stability, but its neutral counterpart, the α-ylide **3c**, lies 35 kcal/mol higher in energy than **3a**.

The 4-isomers behave analogously to the 2-isomers : their neutral forms are comparable in stability while the energy between the two ions is larger, 11 kcal/mol in favour of the keto ion $\mathbf{4b}^{\bullet+}$.

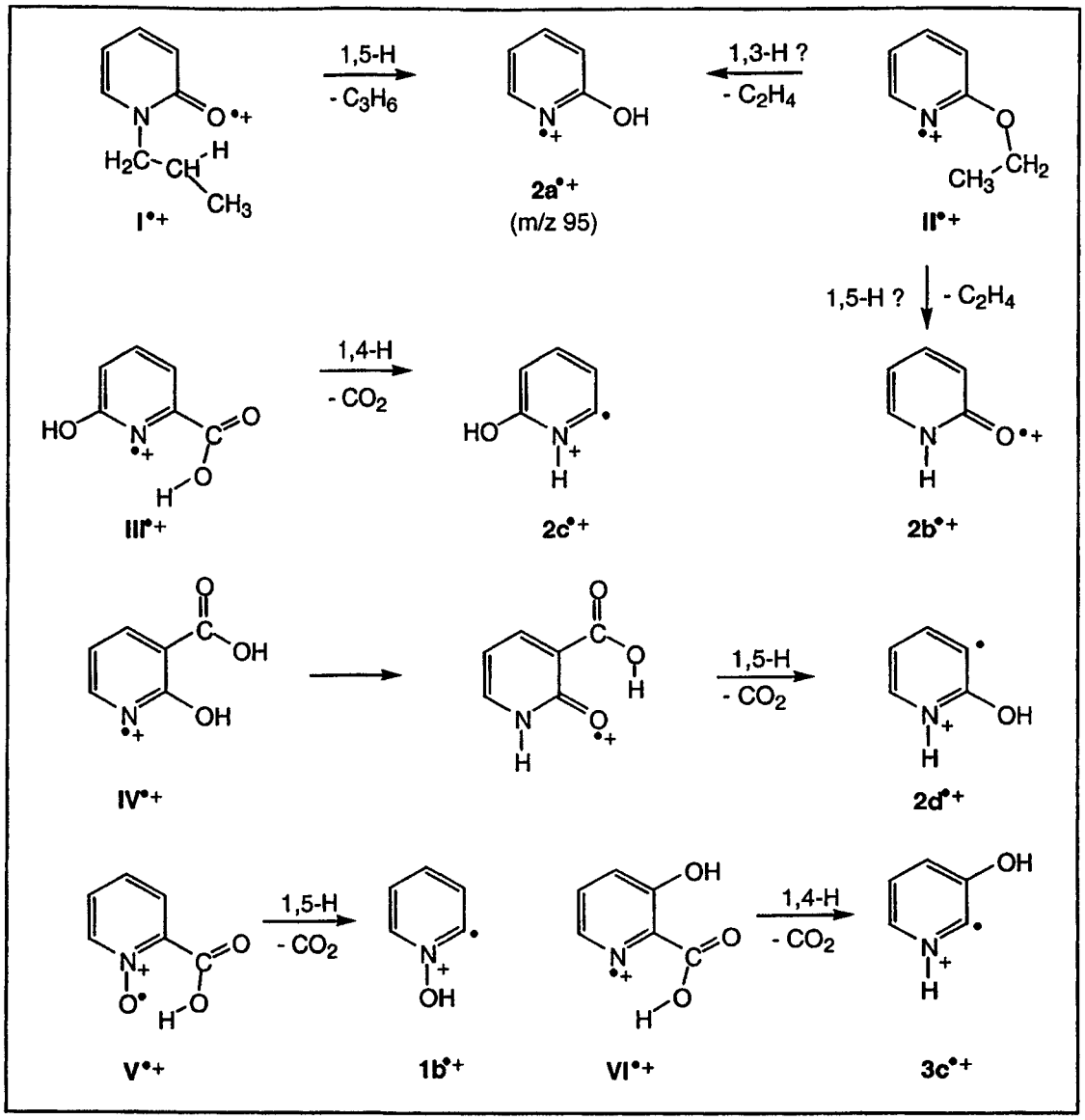

Scheme 7.2

The doublet states of **1a**$^{\bullet+}$ and **1b**$^{\bullet+}$ differ by 24 kcal/mol, and thus the pyridine N-oxide ion is considerably more stable than its α-ylide isomer. However, a facile isomerization via a 1,3-H shift is prohibited by a high barrier, TS (**1b**$^{\bullet+}$ → **1a**$^{\bullet+}$) is 39 kcal/mol, and thus the ylide ion **1b**$^{\bullet+}$ should be a viable species in the gas-phase. Upon neutralization, the energy difference between the two isomers remains approximately the same, 33 kcal/mol, but the connecting TS (**1b** → **1a**) is much lower, 15 kcal/mol. Such a relatively low barrier may not be sufficient to

prevent a (partial) isomerization into the more stable isomer when ions **1b**$^{\bullet+}$ are neutralized in a NRMS experiment. The neutralization step in such an experiment is a vertical process [13]. Therefore energy-rich neutrals are generated if the geometries of the ion and its corresponding ground state neutral differ considerably.

To gauge the importance of this effect, we have obtained the Franck-Condon recombination energies, RE_v, for the neutralization of the ions by vertical electron capture. This was done by calculating the difference in energy between the ion and the neutral using the optimized geometry of the ion. The RE_v value derived from this calculation is then compared with the adiabatic ionization/recombination energy. The results are tabulated in Table 7.2. From the difference between IE_a and RE_v, 11 kcal/mol (0.5 eV), it follows that the vertical neutralization of ions **1b**$^{\bullet+}$ is expected to yield energy-rich neutrals **1b**. Considering that the isomerization barrier **1b** → **1a** is fairly low, see above, neutralized ions **1b**$^{\bullet+}$ may well undergo a partial isomerization.

The same may hold for the distonic ion **2d**$^{\bullet+}$: from the results in Table 7.2 it follows that its neutral counterpart is generated with at least 0.5 eV excess energy while the barrier for isomerization into its keto isomer **2b** is fairly low, TS (**2d** → **2b**) is 13 kcal/mol.

Generation of the $C_5H_5NO^{\bullet+}$ radical cations

The pyridine N-oxide radical cation **1a**$^{\bullet+}$, and the three isomeric hydroxypyridine ions **2a**$^{\bullet+}$, **3a**$^{\bullet+}$ and **4a**$^{\bullet+}$ were generated by electron ionization (EI) of their neutral counterparts. Considering, see the introduction, that for 2-hydroxypyridine a substantial amount of the keto isomer may co-exist in the vapour phase, ions of putative structure **2a**$^{\bullet+}$ were also generated by the dissociative ionization of N-propyl 2-pyridone, **I**, as shown in Scheme 7.2. Since the keto ion **2b**$^{\bullet+}$ is predicted by theory to be considerably more stable than its enol counterpart, **2a**$^{\bullet+}$, we have also entertained the possibility that this ion may be generated by loss of C_2H_4 from ionized 2-ethoxypyridine, **II**$^{\bullet+}$. However, see Scheme 7.2, this precursor molecule could also yield ions **2a**$^{\bullet+}$ (via a β-H transfer to the ether oxygen atom) or

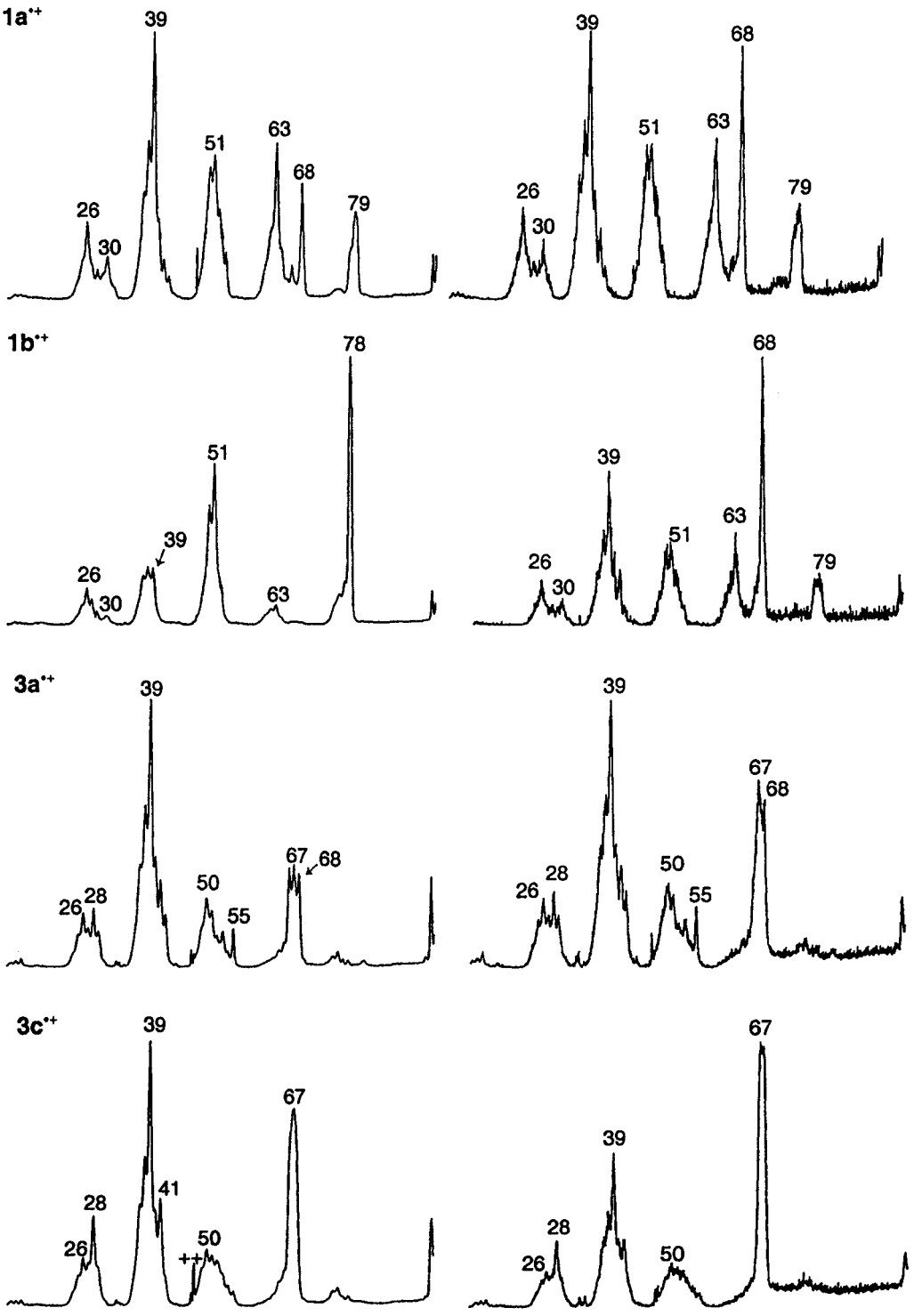

Figure 7.1a. 10 keV Collision-Induced Dissociation (CID) mass spectra of source generated ions (3ffr, left hand column) and survivor ions generated in the neutralization-reionization experiments depicted in Figure 7.2 (right hand column).

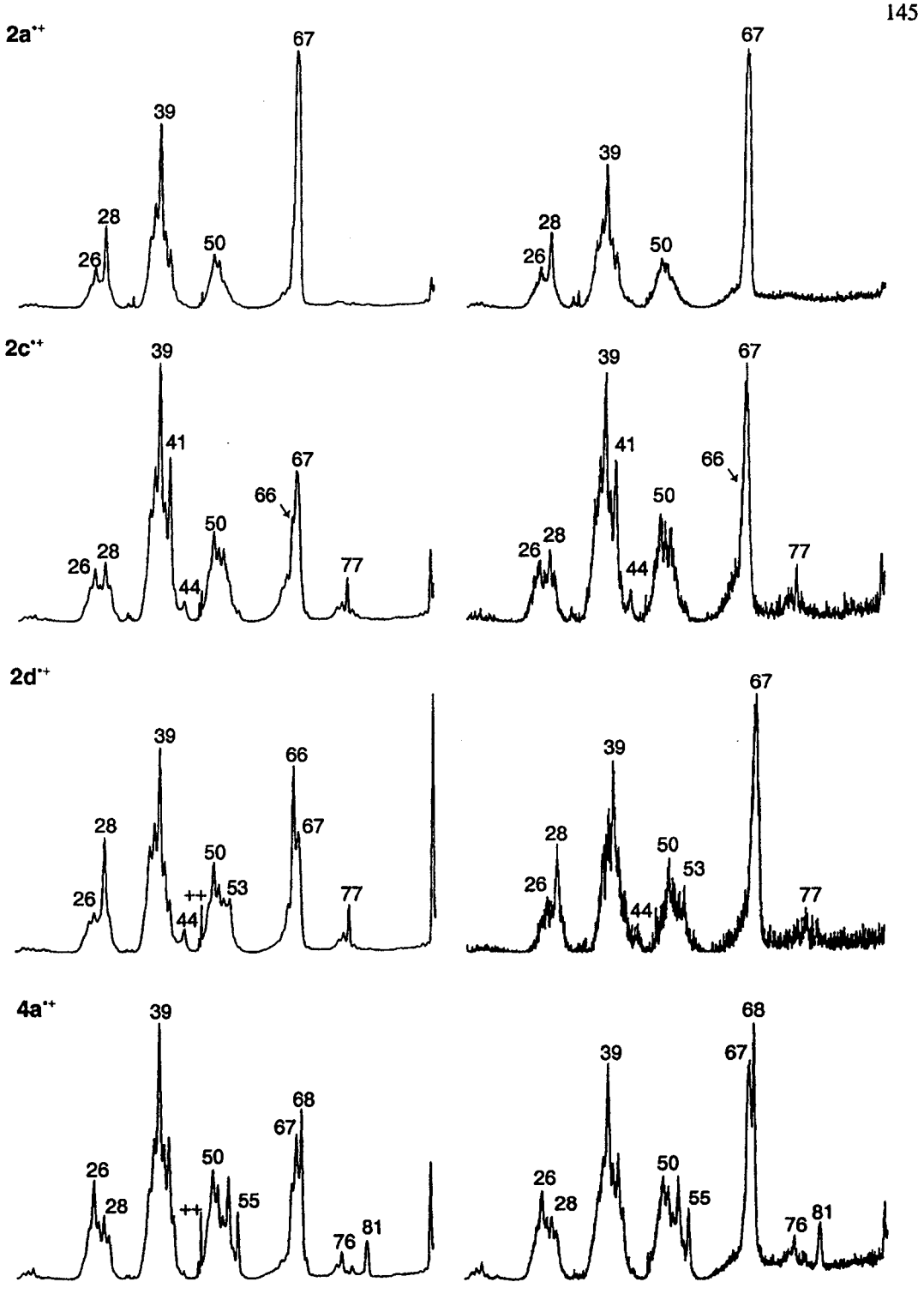

Figure 7.1b. 10 keV Collision-Induced Dissociation (CID) mass spectra of source generated ions (3ffr, left hand column) and survivor ions generated in the Neutralization-Reionization experiments depicted in Figure 7.2.

a mixture of **2a**$^{\bullet+}$ and **2b**$^{\bullet+}$. The keto counterparts of **3a**$^{\bullet+}$ and **4a**$^{\bullet+}$ are also predicted by theory to be lower in energy than their enol counterparts but suitable precursor molecules for their generation by dissociative ionization could not be envisaged. Guided by earlier work on the generation of various distonic ions derived from simple N-heterocycles [12], we envisaged that the distonic ions **1b**$^{\bullet+}$, **2c**$^{\bullet+}$, **2d**$^{\bullet+}$ and **3c**$^{\bullet+}$ should be obtainable by dissociative electron ionization via the pathways shown in Scheme 7.2.

Characterization of the C_5H_5NO radical cations and neutrals on the basis of their dissociation reactions

The collision-induced dissociation (CID) mass spectra of the various isomeric ions are presented in the left hand columns of Figures 7.1a/b. Figure 7.2 presents the corresponding neutralization-reionization (NR) mass spectra, whereas the right hand columns of Figures 7.1a/b display the CID spectra of the survivor ions in these NR spectra. In a recent CID study [23], it was shown that oxygen as a collision gas greatly enhances the structure diagnostic loss of O (peak at *m/z* 79) from the pyridine N-oxide radical cations **1a**$^{\bullet+}$. We have therefore obtained all three sets of spectra with O_2 as the target gas.

The dissociation characteristics of the radical cations of pyridine N-oxide and the three hydroxypyridine isomers

It is readily seen from Figure 7.1a/b, that the CID spectra of the isomers of conventional structure, *viz.* those of **1a**$^{\bullet+}$, **2a**$^{\bullet+}$, **3a**$^{\bullet+}$ and **4a**$^{\bullet+}$, are distinctly different. The same holds for their NR spectra which, see Figure 7.2, display prominent "recovery" or "survivor ion" signals at *m/z* 95. The CID spectra of these survivor ions, the NR/CID spectra of Figure 7.1a/b, right column, are closely similar to the CID spectra of the source generated ions. The only notable difference(s) lie in the enhanced intensity of the *m/z* 68 peak in the NR/CID spectrum of **1a**$^{\bullet+}$, *m/z* 67 in that of **2a**$^{\bullet+}$ and *m/z* 67/68 in those of **3a**$^{\bullet+}$ and **4a**$^{\bullet+}$. However, this merely reflects the somewhat higher internal energy content of ions generated by the NR sequence : such ions contain a larger fraction of metastable ions that dissociate via the reaction(s) of lowest energy requirement [12]. Indeed, metastable ions **1a**$^{\bullet+}$ predominantly lose

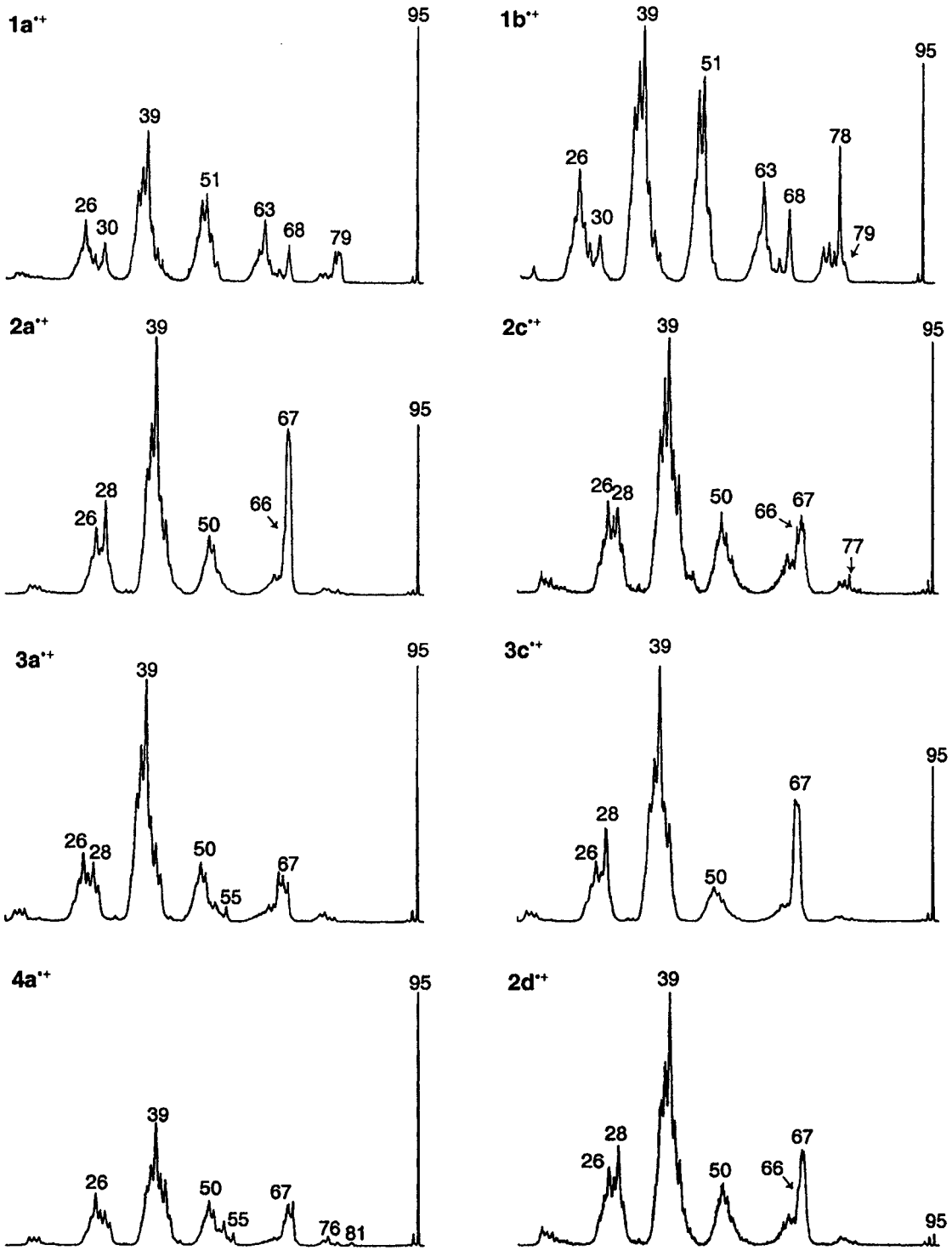

Figure7.2. 10 keV Neutralization-reionization (NR) mass spectra of source generated ions (2ffr).

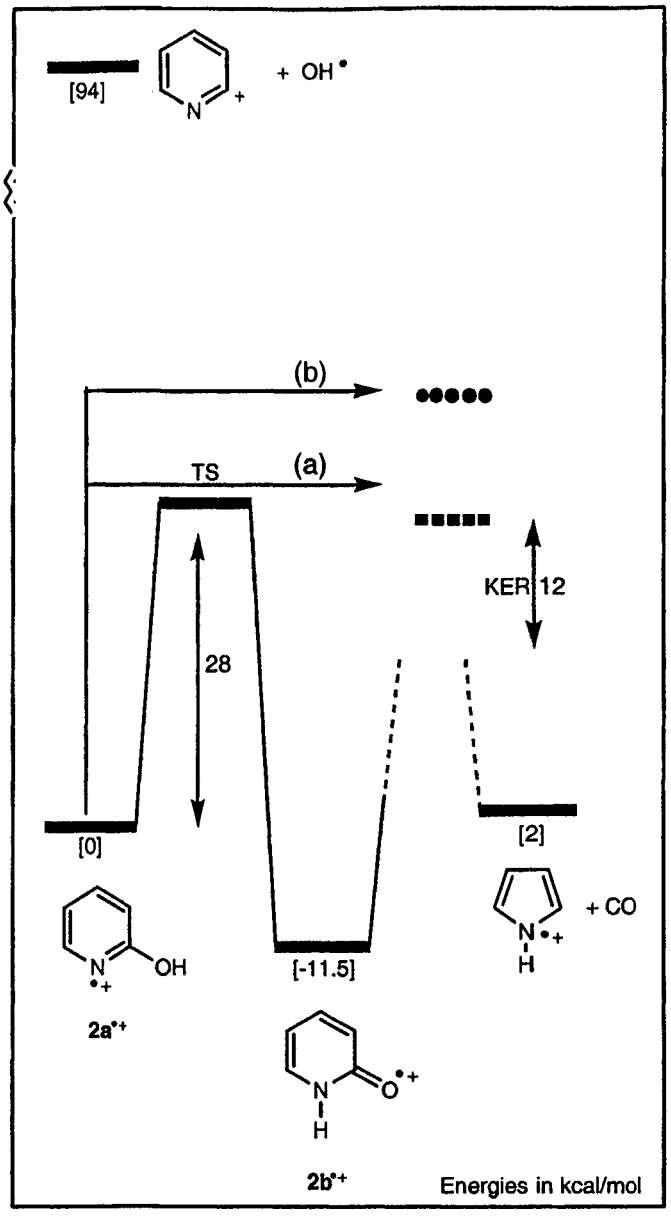

Scheme 7.3

HCN to yield *m/z* 68 $C_4H_4O^{\bullet+}$ ions, whereas the low energy ions **2a**$^{\bullet+}$, **3a**$^{\bullet+}$ and **4a**$^{\bullet+}$ readily decarbonylate to yield *m/z* 67 $C_4H_5N^{\bullet+}$ product ions. Metastable ions **3a**$^{\bullet+}$ and **4a**$^{\bullet+}$, but not **2a**$^{\bullet+}$, also undergo a competing loss of HCN to yield *m/z* 68 ions. This close similarity between the CID and NR/CID spectra for the intensity distributions of the product ions resulting from the high energy dissociation reactions, attests to the isomeric purity of the source generated ions.

In other words, stable ions $\mathbf{1a}^{\bullet+}$, $\mathbf{2a}^{\bullet+}$, $\mathbf{3a}^{\bullet+}$ and $\mathbf{4a}^{\bullet+}$ retain their structure integrity, and any isomerization that is observed in the CID spectrum results from post-collisional isomerization.

This conclusion is undoubtedly warranted for ions $\mathbf{1a}^{\bullet+}$ and also the hydroxypyridine isomers $\mathbf{3a}^{\bullet+}$ and $\mathbf{4a}^{\bullet+}$. The latter two isomers, either as metastable ions or else as stable ions energized by collisional activation, competitively lose HCN and CO. The decarbonylation reaction obviously requires a 1,3-H shift and is associated with a large kinetic energy release. The intermediate ions resulting from the 1,3-H shift are clearly high-energy species which upon ring-opening decarbonylate to yield 3-H pyrrole ions (from $\mathbf{4a}^{\bullet+}$) or a mixture of 2-H and 3-H pyrrole ions (from $\mathbf{3a}^{\bullet+}$), as evidenced by a CID study of the product ions [10e].

However, an entirely different situation obtains for the 2-hydroxypyridine isomer $\mathbf{2a}^{\bullet+}$. Here, decarbonylation is the only low energy reaction observed in the MI spectrum and unlike the situation with ions $\mathbf{3a}^{\bullet+}$ and $\mathbf{4a}^{\bullet+}$, the 1,3-H transfer that initiates the decarbonylation does not yield a high energy intermediate ion but rather the more stable keto ion $\mathbf{2b}^{\bullet+}$! Scheme 7.3 summarizes the information available on the decarbonylation of $\mathbf{2a}^{\bullet+}$: theory indicates that the reaction is associated with a ketonization barrier of 28 kcal/mol and the CID study of ref 10e leaves little doubt that the product ions have the 1-H pyrrole structure. The reaction is associated with a dished metastable peak [24] whose half height kinetic energy release, $T_{0.5}$, is 520 meV (12 kcal/mol). Baldwin and Langley [11] have argued that this large energy release and the fact that the metastable peak shape is non-composite, provides strong evidence that the stable ions generated by EI of 2-hydroxypyridine all have the structure $\mathbf{2a}^{\bullet+}$ and that ketonization only takes place en route to their dissociation, i.e. via pathway (a) in Scheme 7.3. Note that in this scenario the final step in the decarbonylation, $\mathbf{2b}^{\bullet+} \rightarrow$ 1-H pyrrole$^{\bullet+}$ + CO, can have a significant reverse activation energy. However, it should not exceed the level indicated by the bold squares (▪▪▪▪) in Scheme 7.3.

To further probe this point, we have compared the MI, CID and NR/CID spectra of ionized 2-hydroxypyridine with those of the $\mathbf{2a/b}^{\bullet+}$ type ions generated via the dissociative ionization routes depicted in Scheme 7.2. It appears that the resulting spectra are virtually identical.

One interpretation of these results is that we are dealing with stable ions **2a**$^{\bullet+}$ only. This implies that (i) direct ionization of 2-hydroxypyridine yields enol ions **2a**$^{\bullet+}$ only and thus the neutral molecules generated by evaporation of the solid 2-pyridone sample in the rarefied gas-phase of the ion source are 2-hydroxypyridine molecules that cannot equilibrate with their keto form ; (ii) the 2-ethoxypyridine ions do not yield the more stable keto ion via a 1,5-H shift but rather the enol ion via a β-hydrogen transfer. This is surprising since a 1,5-H shift generally is less energy demanding than a 1,3-H transfer. On the other hand, it follows from the PES study of ref. 6 that the state that would best accommodate the 1,5-H transfer to N, the n_N state, lies c. 1 eV above the ground state of the ion.

Another scenario, depicted as pathway (b) in Scheme 7.3, is that decarbonylation of the keto ions **2b**$^{\bullet+}$ into 1-H pyrrole product ions is associated with a barrier for the reverse reaction that lies considerably above the ketonization barrier **2a**$^{\bullet+}$ → **2b**$^{\bullet+}$. Considering that two bonds need to be broken and one is being formed to close the pyrrole ring, it is not without precedent that there be a high barrier associated with this dissociation. One such case is the loss of N_2 from the pyridazine radical cation which occurs via a barrier of ca. 2 eV [25]. Another example concerns the decarbonylation of 2- and 4-pyrone radical cations into ionized furan. Here too, the dissociations involve substantial reverse activation energies, 25 and 40 kcal/mol respectively, as further exemplified by the broad metastable peaks [26].

In this scenario, enol and keto ions would show the same metastable characteristics. A mixture of the two ions could perhaps also remain undetected by the CID experiments reported above. Comparison of the CID and NR/CID spectra of a given ion can be advantageously used to probe its isomeric purity but only if its recombination and ionization energies are largely different from those of the potential isomeric impurities. When dealing with ions of a conventional structure in admixture with their distonic counterparts (or vice versa) this criterion is readily fulfilled. For the present system the RE and IE values of the two isomers, see Table 7.2, are not greatly different. Moreover, isomer differentiation by this procedure is greatly facilitated if the isomers have at least one structure diagnostic peak in their respective CID spectra. This unfortunately does not pertain to this system either : loss of $^{\bullet}$OH from **2a**$^{\bullet+}$ to yield *m/z* 78 α-pyridyl cations [27] lies far too high in energy, see Scheme 7.3, to

compete with other non-structure diagnostic dissociations, as witnessed by its very low abundance in the spectra of all three hydroxypyridine isomers.

Demethylation upon collisional activation of protonated 2-methoxypyridine, as depicted in the upper part of Scheme 7.4, could provide an independent route to the generation of keto ions **2b**$^{\bullet+}$.

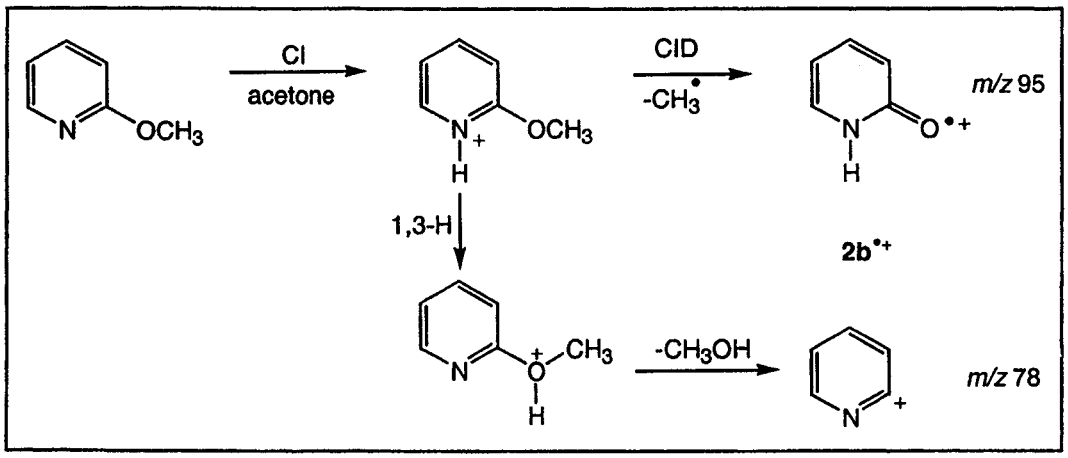

Scheme 7.4

Under chemical ionization conditions, using acetone or pyridine as the reagent gas, 2-methoxypyridine is readily protonated at the N-moiety and the resulting mass selected 10 keV *m/z* 110 ions were collisionally decomposed in the 2ffr. Similar experiments were performed with the 3- and 4-methoxypyridines. When collisionally energized, all three protonated molecules readily undergo demethylation to yield *m/z* 95 ions, see Figure 7.3. These *m/z* 95 putative keto ions were then transmitted to the 3ffr to obtain their CID mass spectra which are presented in the right hand column of Figure 7.3. From a comparison with the CID spectra of the hydroxy isomers **2a**$^{\bullet+}$, **3a**$^{\bullet+}$ and **4a**$^{\bullet+}$ in Figure 7.1, it follows that the keto isomers **3b**$^{\bullet+}$ and **4b**$^{\bullet+}$ generated by the CI-CID sequence indeed have a unique CID spectrum. This is exemplified by a low *m/z* 26 : *m/z* 28 ratio, in keeping with the fact that the keto ions **3b**$^{\bullet+}$ and **4b**$^{\bullet+}$ can readily generate HC≡NH^{+}.

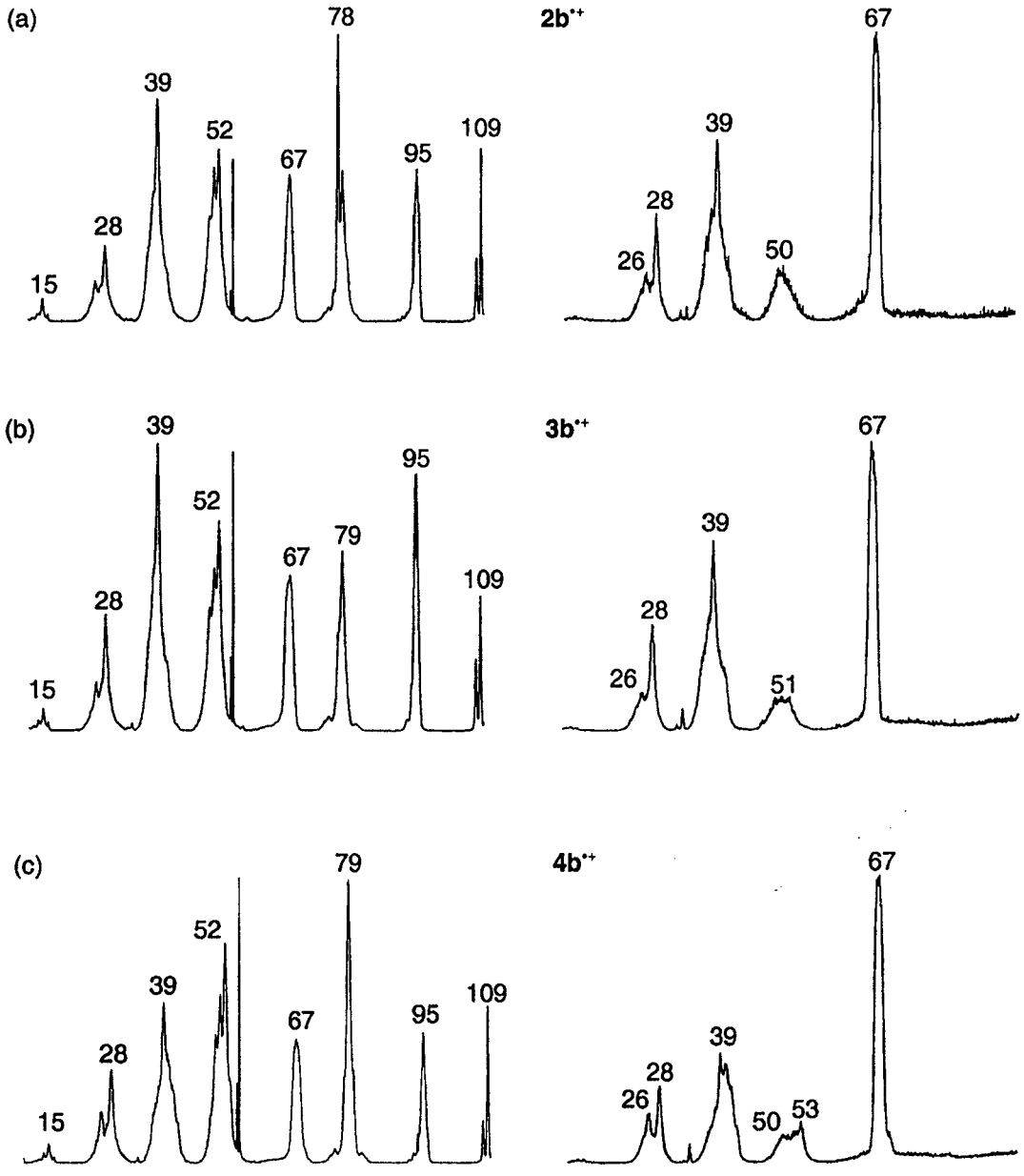

Figure 7.3. 10 keV Collision-Induced Dissociation (CID) mass spectra of the *m/z* 110 protonated 2-, 3-, and 4-methoxypyridines, items (a), (b) and (c), and the *m/z* 95 of putative structures **2b**$^{\bullet+}$, **3b**$^{\bullet+}$ and **4b**$^{\bullet+}$ ions generated therefrom.

In contrast, the CID spectrum of the keto ion **2b**$^{\bullet+}$ is indistinguishable from that shown in Figure 7.1 for the enol ion **2a**$^{\bullet+}$. It could be argued, see Scheme 7.4, that the demethylation in this case takes place from the intermediate O-protonated ion which serves as the precursor for the loss of CH_3OH, yielding the intense signal at *m/z* 78 in Figure 7.3a. However, when pyridine-d_5 is used to form the N-D isotopologue, loss of CH_3OD suffers from a pronounced isotope effect whereas the demethylation does not. Thus, it is likely that keto ions **2b**$^{\bullet+}$ are indeed generated in the CI-CID sequence and considering that their spectrum is indistinguishable from that of the enol type ions, scenario (b) in Scheme 7.3 emerges as the most likely option.

Nevertheless, we feel that this intriguing problem can only be settled when an accurate appearance energy measurement and/or an elaborate computational study at a high level of theory becomes available.

The dissociation characteristics of the distonic ions and the stability of their neutral counterparts

The MI spectrum of the α-ylide ions **1b**$^{\bullet+}$ displays a single peak at *m/z* 78, corresponding to the loss of OH$^{\bullet}$. This observation clearly differentiates these ions from their isomer of conventional structure, **1a**$^{\bullet+}$. It further follows that ions **1b**$^{\bullet+}$ do not readily communicate with 2-hydroxypyridine ions **2a**$^{\bullet+}$, via a simple 1,2-OH shift. As discussed above, loss of OH$^{\bullet}$ from **2a**$^{\bullet+}$ has a minimum energy requirement of ~ 94 kcal/mol, which greatly exceeds that associated with its decarbonylation, see Scheme 7.3. Consequently, metastable ions **2a**$^{\bullet+}$ exclusively lose CO and even upon collisional activation the loss of OH$^{\bullet}$ is of only marginal importance. Ions **1b**$^{\bullet+}$, however, lie much higher in energy than **2a**$^{\bullet+}$, by 57 kcal/mol, and are therefore closer to the threshold for the generation of the α-pyridyl cation at *m/z* 78.

The two isomers, **1a**$^{\bullet+}$ and **1b**$^{\bullet+}$, also show significant differences in their CID spectra. The signals at *m/z* 30 ($NO^{\bullet+}$), 68 (-HCN) and 79 (-O$^{\bullet}$) are tell-tale peaks in the CID spectrum of **1a**$^{\bullet+}$, whereas loss of $^{\bullet}$OH dominates the CID spectrum of **1b**$^{\bullet+}$. These observations leave little doubt that the ylide ions **1b**$^{\bullet+}$ are stable species in the gas-phase, which do not

tautomerize via a 1,3-H shift into pyridine N-oxide ions **1a**$^{\bullet+}$. For the behaviour of the neutral ylide, the NR and NR/CID spectra tell a different story. The CID and NR/CID spectra of ions **1a**$^{\bullet+}$ are virtually the same but this is clearly not the case for ions **1b**$^{\bullet+}$: the CID spectrum of the intense survivor ions in the NR spectrum of **1b**$^{\bullet+}$ is not that of ions **1b**$^{\bullet+}$, but rather that of ions **1a**$^{\bullet+}$. Thus, ions **1b**$^{\bullet+}$ which survived the neutralization step of the NR experiment have isomerized into their more stable neutral tautomer **1a** prior to collisional ionization. The presence of signature peaks for **1a**$^{\bullet+}$, *m/z* 79 and *m/z* 68, in the NR spectrum of **1b**$^{\bullet+}$ supports this proposal. Nevertheless, the NR spectrum of **1b**$^{\bullet+}$ also contains a sizeable peak at *m/z* 78, the signature peak of ions **1b**$^{\bullet+}$, which seems to suggest that part of the incipient neutrals **1b** retain their structure integrity on the μs time-frame of the NR experiment. A closer examination of the shapes of the *m/z* 78 peaks in the CID and NR spectra of **1b**$^{\bullet+}$ shows that this is not the case. The *m/z* 78 peak in the CID spectrum is considerably broader than that displayed in the NR spectrum : the width at half height of the two peaks differs by almost a factor of 2. Thus, the *m/z* 78 peak in the NR spectrum does not originate from collision-induced dissociative ionization of intact neutrals **1b**. It rather signifies dissociation of **1b** into α-pyridyl radicals which are subsequently collisionally ionized to yield *m/z* 78 ions. In this context we note that the minimum energy requirement for the dissociation **1b** → [α-pyridyl]$^{\bullet}$ + OH$^{\bullet}$, is fairly low, ~ 34 kcal/mol (from ΔH_f **1b** = 61 kcal/mol, this work and using ΔH_f **2a** = -18 kcal/mol [22], ΔH_f OH$^{\bullet}$ = 9 kcal/mol [22] and ΔH_f [α-pyridyl]$^{\bullet}$ = 86 kcal/mol [12b]).

The scenario that ions **1b**$^{\bullet+}$ upon neutralization partly remain intact but then completely isomerize into **1a** and partly decompose into α-pyridyl radicals, is fully supported by the computational results presented above : the barrier for the 1,3-H shift associated with the isomerization **1b** → **1a** is fairly low, ~ 15 kcal/mol, whereas vertical neutralization of **1b**$^{\bullet+}$ is expected to yield excited neutrals with minimum energies in the 10-20 kcal/mol range.

Structure characteristic intensity differences are also present in the CID spectra of **2a**$^{\bullet+}$ and its distonic isomers **2c**$^{\bullet+}$ and **2d**$^{\bullet+}$. Whereas the 2-hydroxypyridine ions **2a**$^{\bullet+}$ lose no H_2O, this reaction occurs in both distonic ions, as witnessed by the narrow peak at *m/z* 77. The distonic ions also lose COH$^{\bullet}$ much more readily to yield *m/z* 66 ions. They further share the

weak but clearly discernable peak at *m/z* 44, which may well be a signature peak for the common structure element [HO-C=N-H]. Differences between the individual distonic ions are also evident, particularly in the *m/z* 41 : *m/z* 28 peak intensity ratios. Assuming that these ions have the stable structures CH_2=C=N-H$^{\bullet+}$ and H-C=N-H$^+$ respectively, the large differences in these ratios correlate well with the proposed structures.

Ions **2c**$^{\bullet+}$ yield a NR spectrum with an intense survivor signal, see Figure 7.2. Its NR/CID spectrum, see Figure 7.1b, is, apart from the enhanced *m/z* 67 peak which results from the low-energy decarbonylation, virtually identical with the conventional CID spectrum. This attests to the isomeric purity of the source generated ions and moreover it leaves little doubt that the neutral ylide is a stable species in the gas-phase.

Analysis of the NR and NR/CID spectra of isomer **2d**$^{\bullet+}$ is less straightforward. The ion-molecule reactions described in the next section remove any doubt that we are dealing with ions of structure **2d**$^{\bullet+}$ but, surprisingly, their NR spectrum displays a recovery signal of only marginal intensity. Analysis of the NR spectrum gives no indication that this can be attributed to a facile decomposition of the incipient neutrals by a simple bond cleavage, as proposed for isomer **1b**. However, as pointed out in the previous computational section, the incipient neutrals **2d** are expected to be generated with at least 0.5 eV (11.5 kcal/mol) of excess energy whereas the barrier for the 1,3-H shift leading to the very stable 2-pyridone isomer **2b** is only 13 kcal/mol. It is therefore anticipated that the vertical neutralization of **2d** largely yields 2-pyridone molecules which, see Table 7.1b, contain at least 66 kcal/mol of excess energy. Such a high internal energy could suffice for their decarbonylation into 1-H pyrrole for which the minimum thermochemical energy requirement is ~ 18 kcal/mol [22]. This proposal implies that (i) the decarbonylation of *neutrals* **2b** and *ions* **2a/b**$^{\bullet+}$ is associated with the *same* large kinetic energy release, and (ii) that the NR spectrum contain a peak for CO$^{\bullet+}$ at *m/z* 28, which is as broad as the *m/z* 67 peak for ionized 1-H pyrrole. It is difficult to decide whether these conditions are met. The decarbonylation of 2-pyridone may well have a reverse activation energy, but the actual height of this barrier is not known. Further, the peaks in the *m/z* 25-29 region of the NR spectrum are not sufficiently resolved to establish whether the *m/z* 28 peak contains a broad component for CO$^{\bullet+}$.

An alternative explanation which we think is more likely, is that the incipient neutrals **2d** isomerize into pyridone molecules **2b**, which, because of their high internal energy content, readily decarbonylate as *ions* when ionized in the collisional ionization step of the NR experiment. This tentative proposal is not incompatible with the 'noisy' NR/CID spectrum of the weak survivor ions: this spectrum, see Figure 7.1b, still shows tell-tale peaks at *m/z* 77 and 44 for the presence of ions $\mathbf{2d}^{\bullet+}$ but their relative intensity has become lower and this is particularly true for the *m/z* 66 peak, compare the CID and NR/CID spectra of Figure 7.1b. From a comparison of the shapes of the *m/z* 67 peaks in narrow scans, it follows that those in the NR/CID spectra of ions $\mathbf{2d}^{\bullet+}$ and $\mathbf{2a}^{\bullet+}$ are closely similar. This supports the proposal that the weak survivor ions in the spectrum of $\mathbf{2d}^{\bullet+}$ represent a mixture of ions $\mathbf{2d}^{\bullet+}$ and $\mathbf{2b}^{\bullet+}$. However, it also suggests that the large energy release associated with the decarbonylation is an inherent property of ions $\mathbf{2b}^{\bullet+}$ rather than $\mathbf{2a}^{\bullet+}$, as suggested in the previous section. More decisive evidence in favour of this proposal would come from a careful examination of the *metastable* ion spectrum of the $\mathbf{2d}^{\bullet+}$ survivor ions, but unfortunately the signals in the NR/MI spectrum are too weak to permit a meaningful analysis.

Analysis of the spectra of the remaining distonic isomer, $\mathbf{3c}^{\bullet+}$, is straightforward. Unlike its isomer $\mathbf{3a}^{\bullet+}$, which shows a competitive loss of CO and HCN in its MI spectrum, metastable ions $\mathbf{3c}^{\bullet+}$ only undergo decarbonylation, most likely via the route $\mathbf{3c}^{\bullet+} \rightarrow$ (1,3-H) $\rightarrow$ $\mathbf{3b}^{\bullet+} \rightarrow$ [1-H pyrrole]$^{\bullet+}$ + CO. The kinetic energy release associated with this reaction is substantial, $T_{0.5} = 720$ meV, but nevertheless smaller than that for the decarbonylation of $\mathbf{3a}^{\bullet+}$, $T_{0.5} = 780$ meV. This further underlines that isomerization of the distonic ion into its more stable counterpart $\mathbf{3a}^{\bullet+}$ via a 1,2-H shift does not occur to a significant extent. This is also borne out by the CID spectra of $\mathbf{3a}^{\bullet+}$ and $\mathbf{3c}^{\bullet+}$, see Figure 7.1a. Ions $\mathbf{3a}^{\bullet+}$ have signature peaks at *m/z* 68 (loss of HCN) and *m/z* 55 (possibly hydroxy cyclopropenium ions, which also feature in the spectrum of $\mathbf{4a}^{\bullet+}$) while the distonic ion features a much more pronounced *m/z* 28 peak, indicative of the presence of the [-CH-NH-] structure element in the ion. The NR spectrum of $\mathbf{3c}^{\bullet+}$, see Figure 7.2, displays an abundant recovery signal whose CID spectrum, see Figure 7.1a, is close to that of the source generated ions. Thus, these distonic ions retain their structure

integrity in the NR experiment which signifies that their neutral counterpart is a stable species in the rarefied gas-phase.

Ion-molecule reactions with dimethyl disulfide

A complementary approach to the characterization of isomeric ions involves probing differences in their reactivity by interactions with selected neutral molecules. One such molecule is dimethyl disulfide (DMDS), $CH_3S\text{-}SCH_3$ [28]. It was successfully used in recent work [29] to differentiate the pyridine radical cation from its α-ylide isomer. The pyridine ion readily undergoes charge exchange with DMDS, because pyridine's IE (9.3 eV) is higher than that of DMDS (8.0 eV [28]). The IE of pyridine's ylide isomer (6.8 eV) is lower than that of DMDS and thus the ylide ions do not undergo charge exchange. Instead, they abstract a $CH_3S^{\bullet}$ radical from the DMDS to yield adduct ions whose structure was characterized by a subsequent high energy CID experiment.

In light of these interesting observations on the pyridine system, it seemed worthwhile to use DMDS in the present study as well. From the IE values reported in Table 7.2, it follows that the neutral counterparts of the ions of conventional structure, *viz.* $\mathbf{1a}^{\bullet+}$, $\mathbf{2a}^{\bullet+}$, $\mathbf{3a}^{\bullet+}$ and $\mathbf{4a}^{\bullet+}$ all have IEs higher than DMDS whereas the reverse obtains for the distonic ions $\mathbf{1b}^{\bullet+}$, $\mathbf{2c}^{\bullet+}$, $\mathbf{2d}^{\bullet+}$ and $\mathbf{3c}^{\bullet+}$.

The results of the ion-molecule reactions with DMDS are summarized in the left column of Table 7.3. It is seen that $\mathbf{1a}^{\bullet+}$ - $\mathbf{4a}^{\bullet+}$ all undergo charge exchange, whereas the distonic ions all yield adduct ions at *m/z* 142 resulting from $CH_3S^{\bullet}$ abstraction. That the *m/z* 94 ions in the spectra of $\mathbf{1a}^{\bullet+}$ - $\mathbf{4a}^{\bullet+}$ are $DMDS^{\bullet+}$ ions resulting from charge exchange and not $C_5H_4NO^+$ ions resulting from a $H^{\bullet}$ abstraction, readily follows from the sulfur characteristic *m/z* 94-96 peak intensity ratios observed.

Table 7.3. Product ions resulting from the interaction of various $C_5H_5NO^{\bullet+}$ ions with dimethyl disulfide (DMDS) and *tert*-butyl isocyanide molecules.

Substrate →	$CH_3S\text{-}SCH_3$		$(CH_3)_3C\text{-}NC$	
Ion	*m/z*	I [a]	*m/z*	I [a]
1a$^{\bullet+}$	94 [DMDS]$^{\bullet+}$	200	57	0.3
			79	4
2a$^{\bullet+}$	94 [DMDS]$^{\bullet+}$	200	57	7
			84	10
3a$^{\bullet+}$	94 [DMDS]$^{\bullet+}$	160	57	1
			84	20
			121	2
4a$^{\bullet+}$	94 [DMDS]$^{\bullet+}$	300	57	1
			84	40
			121	40
1b$^{\bullet+}$	142 [**1b** + $CH_3S^{\bullet}$]$^+$	20	57	0.3
			84	0.2
			105	20
			121	5
2c$^{\bullet+}$	142 [**2c** + $CH_3S^{\bullet}$]$^+$	100	57	10
			84	30
			121	70
2d$^{\bullet+}$	142 [**2d** + $CH_3S^{\bullet}$]$^+$	40	57	2
			84	2
			121	10
3c$^{\bullet+}$	142 [**3c** + $CH_3S^{\bullet}$]$^+$	60	57	10
			84	20
			121	40

[a] Intensities relative to the main beam of reactant ions which was normalized to 1000 units.

Structure proposals for the *m/z* 142 adduct ions generated from the distonic ions are presented in Scheme 7.5. That all four reactions are exothermic is supported by our B3LYP/CBSB7 calculations which yield heat of reaction values of 35, 39, 37 and 38 kcal/mol respectively. The high energy CID spectra of the four isomeric *m/z* 142 adduct ions are presented in Figure 7.4.

These CID spectra are uniquely different. The adduct ions derived from **1b**$^{\bullet+}$ show a prominent loss of H_2O (*m/z* 124) and also of $OH^{\bullet}$ (*m/z* 125). The latter ion uniquely

characterizes the **1b**$^{\bullet+}$ isomer as does the *m/z* 79 peak which may originate from the consecutive loss of CH_2=S. The losses of $CH_3^{\bullet}$, H_2S and $CH_3S^{\bullet}$ yielding *m/z* 127, 108 and 95 ions respectively, represent common dissociation pathways for the adduct ions from **2b**$^{\bullet+}$, **2c**$^{\bullet+}$ and **3c**$^{\bullet+}$. However, the relative abundance is strongly isomer dependent as are the *m/z* 124 (loss of H_2O) and *m/z* 83 (loss of CS from the ion at *m/z* 127) peaks. The adduct ions [**2c** + $CH_3S^{\bullet}$]$^+$ lose both H_2O and CS whereas [**2d** + $CH_3S^{\bullet}$]$^+$ loses no CS and loss of H_2O does not occur from [**3c** + $CH_3S^{\bullet}$]$^+$. These observations can perhaps be correlated with the position of the OH- or CH_3S- substituent but, more importantly, they fully support the conclusion derived from the dissociation characteristics in the previous section that all four distonic ions are viable species in the gas-phase.

Another potentially useful substrate for isomer differentiation by ion-molecule reactions is *tert*-butyl isocyanide [30]. Its use in this study is described in the next section.

Ion-molecule reactions of the $C_5H_5NO^{\bullet+}$ ions with tert-butyl isocyanide

Kenttämaa et al. [30] have recently investigated the reactivity of *tert*-butyl isocyanide towards various distonic radical cations. Two distinct reactivity patterns were observed, one characteristic of the electrophilic nature of the charge site of the ion, and the other characteristic of the unpaired spin of the free radical moiety. Reaction of the isocyanide with the charge site of the distonic ion involves CN^- transfer, yielding *m/z* 57 *tert*-$C_4H_9^+$ ions, while reaction at its radical site involves cyano radical transfer, yielding CN-adduct ions. The isocyanide prefers to react at the distonic ion's charge site, but if this site is coordinately saturated, "chemically inert", reaction at the radical site becomes prevalent.

When the $C_5H_5NO^{\bullet+}$ isomeric ions of this study were allowed to interact with the isocyanide, several reactions were observed. From the results presented in Table 7.3, it follows that proton-transfer from the ion to the isocyanide, yielding $(CH_3)_3C$-N=CH^+ ions at *m/z* 84, and CN^- transfer, yielding *tert*-$C_4H_9^+$ ions at *m/z* 57, are common reactions for all isomeric ions but ion **1a**$^{\bullet+}$. The pyridine N-oxide ion is not deprotonated by the isocyanide, indicating that the associated C-H bond cleavage is less favoured than the O-H or N-H

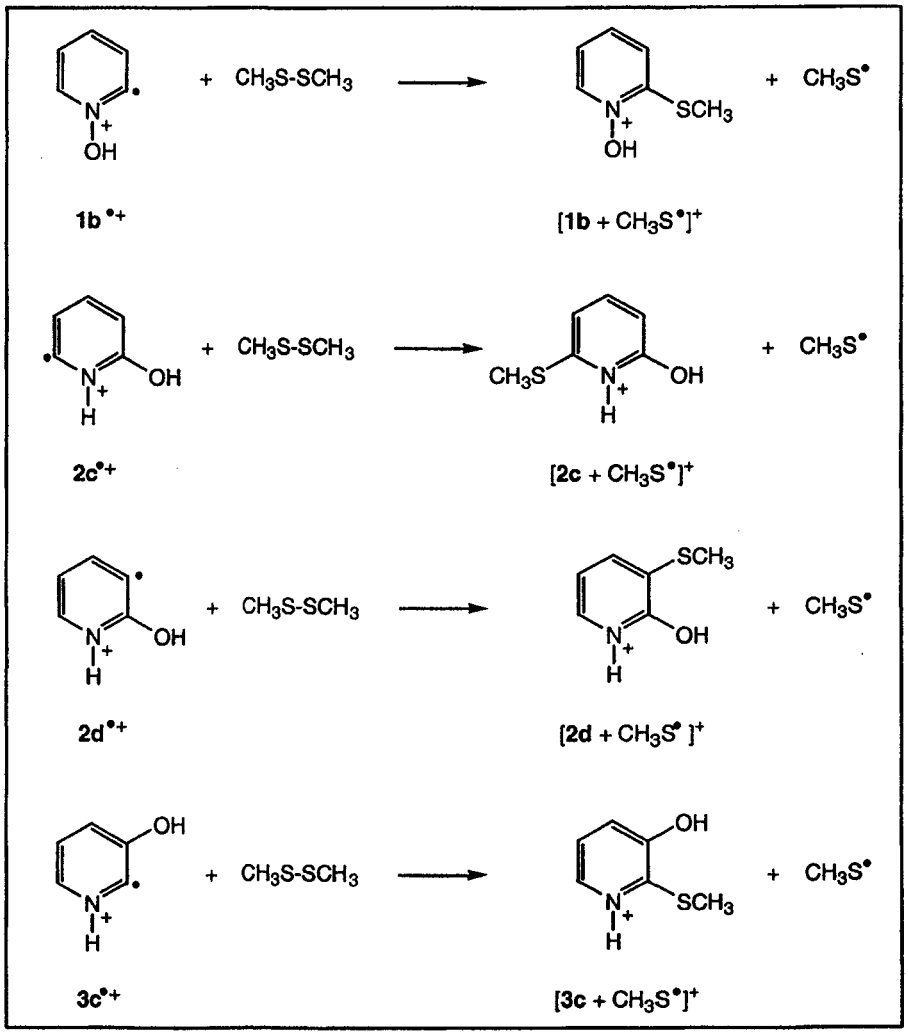

Scheme 7.5

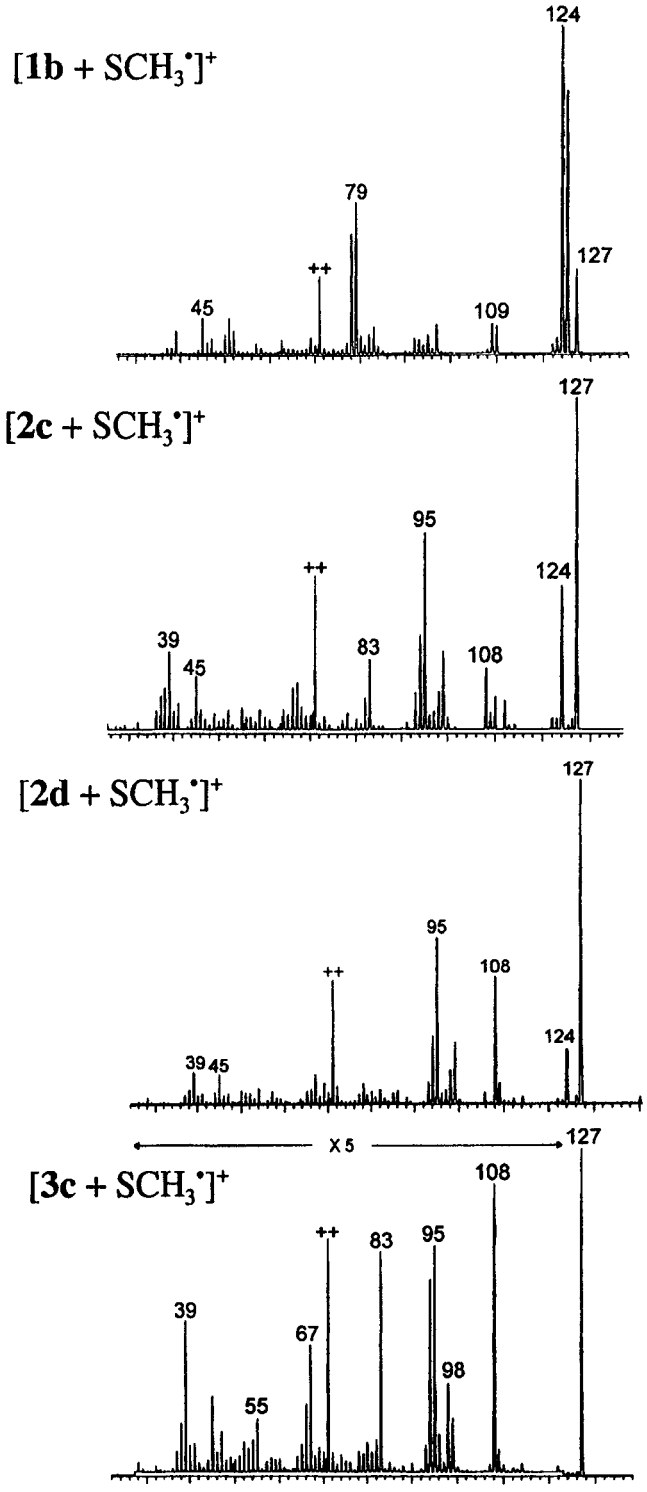

Figure 7.4. Ion-molecule reactions between $C_5H_5NO^{\bullet+}$ radical cations (*m/z* 95) and dimethyl disulfide: the collision-induced dissociation spectra of the *m/z* 142 adduct ions generated from ions **1b**$^{\bullet+}$, **2c**$^{\bullet+}$, **2d**$^{\bullet+}$ and **3c**$^{\bullet+}$.

abstraction reactions occurring from the other isomers. Instead, ions **1a**$^{\bullet+}$ show another reaction which uniquely characterizes them, *viz.* a deoxygenation reaction yielding pyridine ions and t-butyl isocyanate neutrals. That the *m/z* 79 ions generated have the pyridine structure was confirmed by the analysis of the CID spectrum. We further note that the IE of pyridine (9.3 eV) is lower than that of the isocyanate (10.1 eV [22]) and thus the charge remains on the reactant ion in the deoxygenation process. A second unique reaction, see Table 7.3, is the formation of *m/z* 105 ions from the ylide ion **1b**$^{\bullet+}$. The CID spectrum of these ions was obtained and it appeared to be virtually identical with that of the *m/z* 105 ions generated by the (ring N) protonation of 2-cyanopyridine. Having established the product ion structure, we tentatively propose that the ion is generated via the mechanism of Scheme 7.6.

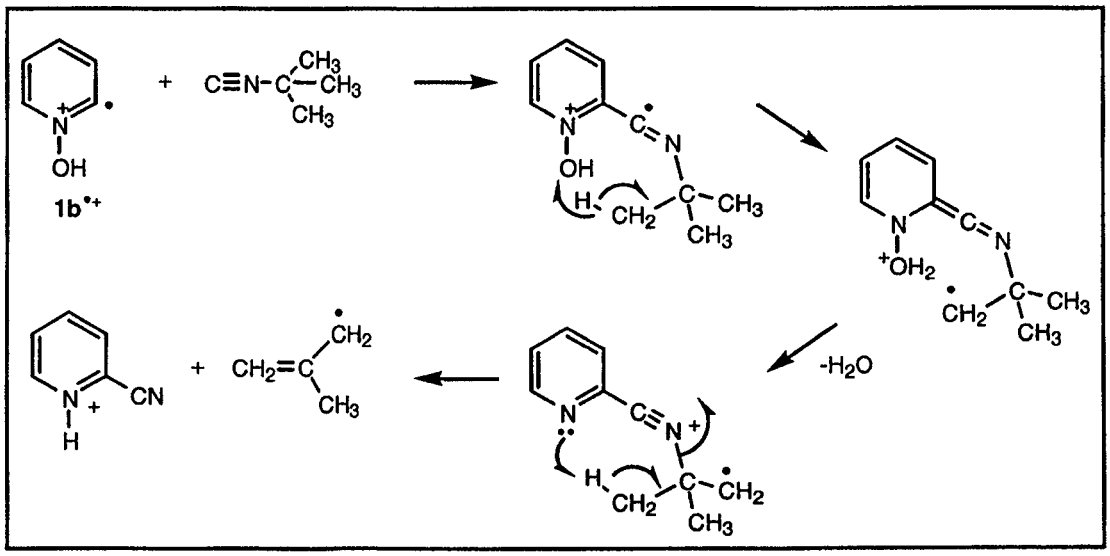

Scheme 7.6

The first step involves formation of an adduct ion of **1b**$^{\bullet+}$ and the isocyanide. Consecutive H-transfers then lead to the losses of H_2O and $C_4H_7^{\bullet}$ to yield the N-protonated 2-cyanopyridine product ion at *m/z* 105.

Another prominent reaction of ions **1b**$^{\bullet+}$ with the isocyanide involves a $CN^{\bullet}$ transfer to the radical position of the ion, yielding $[\mathbf{1b} + CN^{\bullet}]^+$ ions at *m/z* 121 and t-butyl radicals. However, this is also a prominent reaction with the distonic ions **2c**$^{\bullet+}$, **2d**$^{\bullet+}$ and **3c**$^{\bullet+}$ and the

4-hydroxypyridine radical cation **4a**$^{\bullet+}$. The reaction is also observed with the 3-hydroxy isomer **3a**$^{\bullet+}$ but it is absent for **2a**$^{\bullet+}$. The proposed *m/z* 121 product ion structures are given in Scheme 7.7 and their CID spectra are presented in Figure 7.5.

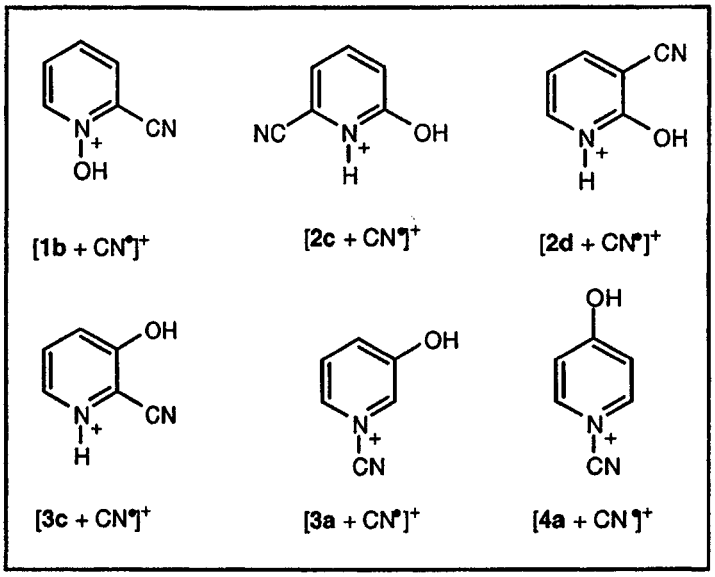

Scheme 7.7

In the absence of detailed labelling experiments and thermochemical information about the various reaction products, a detailed analysis of these spectra remains speculative. Nevertheless, it is clear that the spectra are characteristically different. The CID spectrum of the adduct ion with **1b**$^{\bullet+}$ features an abundant loss of OH$^{\bullet}$ to yield 2-cyanopyridine ions at *m/z* 104. Loss of H_2O (*m/z* 103) is also observed but this reaction is only prominent for the distonic ions **2c**$^{\bullet+}$ and **2d**$^{\bullet+}$. These two isomers however, can easily be differentiated on the basis of the *m/z* 66 and *m/z* 93 ions that dominate in the spectrum of **2d**$^{\bullet+}$. The *m/z* 66 ions are possibly HO-C≡C-C≡N$^{\bullet+}$, considering that they are also readily formed from [**3c** + CN$^{\bullet}$]$^+$, whereas those at *m/z* 93 could result from the loss of CO initiated by a 1,5-H transfer to the CN moiety of the ion.

Further, ions [**3a** + CN$^{\bullet}$]$^+$ and [**4a** + CN$^{\bullet}$]$^+$ which both contain an [NC-N=] moiety, appear to uniquely lose this structure element as NCN to yield *m/z* 81 ions, possibly having the structure of the hydroxy cyclopentenium ion [31].

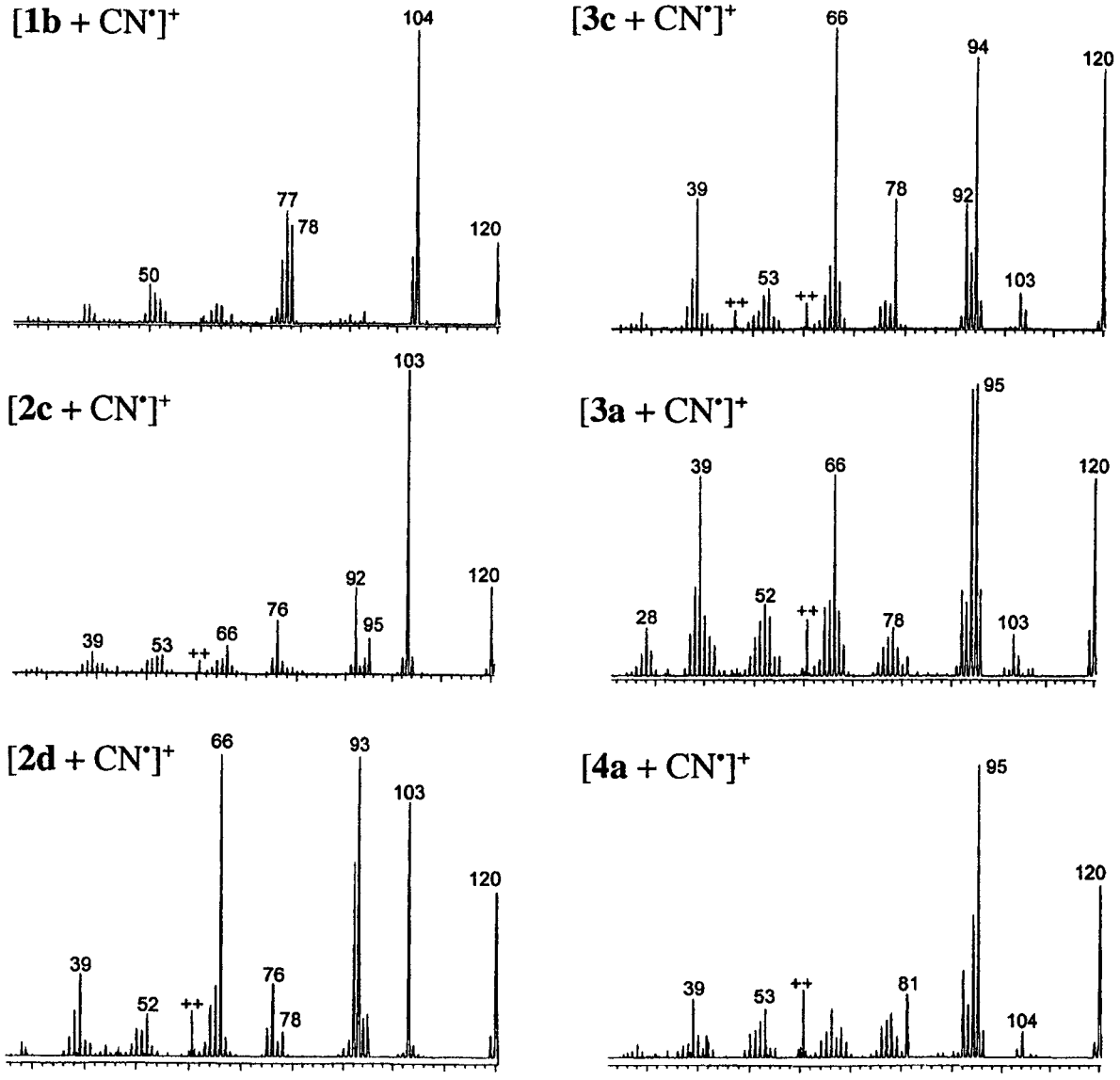

Figure 7.5. Ion-molecule reactions between $C_5H_5NO^{\bullet+}$ radical cations (*m/z* 95) and t-butyl isocyanide: the collision-induced dissociation spectra of the *m/z* 121 adduct ions generated from ions **1b**$^{\bullet+}$, **2c**$^{\bullet+}$, **2d**$^{\bullet+}$, **3c**$^{\bullet+}$, **3a**$^{\bullet+}$ and **4a**$^{\bullet+}$.

Finally, we note that, although these associative ion-molecule reactions elegantly confirm the structure identity of the distonic ions, they do not allow us to decide whether the 2-hydroxy-pyridine ions are isomerically pure or actually consist of a mixture of keto and enol ions **2a/b**$^{\bullet+}$ as discussed above.

Conclusions

The combined information from the dissociation and reactivity characteristics of the $C_5H_5NO^{\bullet+}$ ions studied, confirms our theoretical predictions that the distonic ions **1b**$^{\bullet+}$, **2c**$^{\bullet+}$, **2d**$^{\bullet+}$ and **3c**$^{\bullet+}$, depicted in Scheme 7.1, are stable species in the gas-phase. From the analysis of the recovery signals in their neutralization-reionization spectra, it follows that the neutral counterparts of **2c**$^{\bullet+}$ and **3c**$^{\bullet+}$ are also stable. In contrast, the ylide-type neutrals **1b** readily isomerize into pyridine N-oxide, **1a**, or else dissociate. The neutral counterparts of the distonic ions **2d**$^{\bullet+}$ have only a marginal stability and part of these neutrals are proposed to isomerize into energy-rich 2-pyridone molecules **2b**. This too, is in agreement with the computational results. Finally, we note that the question whether 2-hydroxypyridine yields isomerically pure ions **2a**$^{\bullet+}$ or, alternatively, a mixture of enol and keto (2-pyridone) ions, remains unresolved. Unlike the situation with the keto-enol isomeric pairs **3a**$^{\bullet+}$/**3b**$^{\bullet+}$ and **4a**$^{\bullet+}$/**4b**$^{\bullet+}$ whose CID spectra are characteristically different, enol ions **2a**$^{\bullet+}$ and keto ions **2b**$^{\bullet+}$ exhibit virtually the same dissociation characteristics.

References

[1] M. Gallant, T.P. Viet, J.D. Wuest, *J. Am. Chem. Soc.* **1991**, *113*, 721.

[2] P. Beak, *Acc. Chem. Res.* **1977**, *10*, 186.

[3] (a) U. Ohms, H. Guth, E. Hellner, H. Dannöhl, A.Z. Schwig, *Z. Kristallogr.* **1984**, *169*, 185; (b) G.L. Wheeler, H.L. Ammon, *Acta Crystallogr. Sect. B* **1974**, *B30*, 680.

[4] J. Wang, R.J. Boyd, *J. Phys. Chem.* **1996**, *100*, 1641.

[5] (a) P. Beak, F.S. Fry, J. Lee, F.J. Steele, *J. Am. Chem. Soc.* **1976**, *98*, 171 ; (b) R.S. Brown, A. Tse, J.C. Vederas, *J. Am. Chem. Soc.* **1980**, *102*, 1174 ; (c) S.S.T. King, W.L. Dilling, N.B. Tefertiller, *Tetrahedron* **1972**, *28*, 5859 ; (d) C. Guimon, G. Garrabe, G. Pfister-Buillouzo, *Tetrahedron Lett.* **1979**, *28*, 2585.

[6] M.J. Cook, S. El-Abbady, A.R. Katritzky, C. Guimon, G. Pfister-Guillouzo, *J. Chem. Soc. Perkin Trans II* **1977**, 1652.

[7] (a) J.R. Reimers, L.E. Hall, N.S. Hush, *J. Phys. Chem. A* **2000**, *104*, 5087 ; (b) A.L. Sobolewski, L. Adamowicz, *Chem. Phys.* **1996**, *213*, 193 ; (c) J.S. Kwiatkowski, J. Leszczynski, *J. Mol. Struc.* **1996**, *376*, 325 ; (d) A.L. Sobolewski, L. Adamowicz, *J. Phys. Chem.* **1996**, *100*, 3933 ; (e) R.J. Hall, N.A. Burton, I.H. Hillier, P.E. Young, *Chem. Phys. Lett.* **1994**, *220*, 129 ; (f) O.G. Parchment, N.A. Burton, I.H. Hillier, *Chem. Phys. Lett.* **1993**, *203*, 46 ; (g) M. Moreno, W.H. Miller, *Chem. Phys. Lett.* **1990**, *171*, 475 ; (h) M.J. Scanlan, I.H. Hillier, *Chem. Phys. Lett.* **1984**, *107*, 330 ; (i) M.J. Scanlan, I.H. Hillier, A.A. Macdowell, *J. Am. Chem. Soc.* **1983**, *105*, 3568; (j) J.K. Wolken, F. Tureček, *J. Phys. Chem. A.* **1999**, *103*, 6268; (k) J.K. Wolken, F. Tureček, *J. Am. Chem. Soc.* **1999**, *121*, 6010.

[8] S. Suradi, N. El-Saiad, G. Pilcher, H.A. Skinner, *J. Chem. Thermodyn.* **1982**, *14*, 45.

[9] (a) A. Maquestiau, R. Flammang, *Mass Spectrom. Rev.* **1982**, *1*, 237 ; (b) P.B. Terent'ev, A.G. Kalandarishuili, *Mass Spectrom. Rev.* **1996**, *15*, 339.

[10] (a) M.J. Cook, A.R. Katritzky, M. Taagepera, *J. Am. Chem. Soc.* **1976**, *98*, 6048 ; (b) A. Maquestiau, Y. Van Haverbeke, C. De Meyer, A.R. Katritzky, M.J. Cook, A.D. Page, *Can. J. Chem.* **1975**, *53*, 490; (c) A. Maquestiau, Y. Van Haverbeke, R. Flammang, H. Mispreuve, A.R. Katritzky, J. Ellison, J. Frank, Z. Meszarox, *Chem. Commun.* **1979**, 888 ; (d) T. Gronneberg, K. Undheim, *Tetrahedron Lett.* **1972**, 3193 ; (e) M.W.E.M. van Tilborg, J. van Thuijl, *Org. Mass Spectrom.* **1983**, *18*, 331.

[11] M.A. Baldwin, G.J. Langley, *J. Chem. Soc. Perkin Trans. II* **1988**, 347.

[12] (a)D. Lavorato, J.K. Terlouw, T.K. Dargel, W. Koch, G.A. McGibbon, H. Schwarz, *J. Am. Chem. Soc* **1996**, *118*, 11898; (b) M.A. Trikoupis, D.J. Lavorato, J.K. Terlouw, P.J.A. Ruttink, P.C. Burgers, *Eur. Mass Spectrom.* **1999**, *5*, 431; (c) D.J. Lavorato, J.K. Terlouw, G.A. McGibbon, T.K. Dargel, W. Koch, H. Schwarz, *Int. J. Mass Spectrom. Ion Proc.* **1998**, *179/180*, 7; (d) T.K. Dargel, W. Koch, D.J. Lavorato, J.K. Terlouw, H. Schwarz, *Int. J. Mass Spectrom.* **1999**, *185/186/187*, 925; (e)D.J. Lavorato, T.K. Dargel, W. Koch, G.A. McGibbon, H. Schwarz, J.K. Terlouw, *Int. J. Mass Spectrom.* **2001**, *210/211*, 43.

[13] For a recent review see : N. Goldberg, H. Schwarz, *Acc. Chem. Res.* **1994**, *27*, 34.

[14] (a) H.I. Kenttämaa, *Org. Mass Spectrom.* **1994**, *29*, 1; (b) L.A.B. Moraes, F.C. Gozzo, M.N. Eberlin, *J. Org. Chem.* **1997**, *62*, 5096 ; (c) P. Gerbaux, Y. Van Haverbeke, R. Flammang, *J. Mass Spectrom.* **1997**, *32*, 1170.

[15] H.F. van Garderen, P.J.A. Ruttink, P.C. Burgers, G.A. McGibbon, J.K. Terlouw, *Int. J. Mass Spectrom. Ion Processes* **1992**, *121*, 159.

[16] (a) R.H. Bateman, J. Brown, M. Lefevere, R. Flammang, Y. van Haverbeke, *Int. J. Mass Spectrom. Ion Processes* **1992**, *115*, 205 ; (b) R. Flammang, Y. van Haverbeke, C. Braybrook, J. Brown, *Rapid Commun. Mass Spectrom.* **1995**, *9*, 795.

[17] (a) J.A. Montgomery Jr., M.J. Frisch, J.W. Ochterski, G.A. Petersson, *J. Chem. Phys.* **2000**, *112*, 6532; (b) J.A. Montgomery Jr., M.J. Frisch, J.W. Ochterski, G.A. Petersson, *J. Chem. Phys.* **1999**, *110*, 2822.

[18] Gaussian 98, Revision A.7, M.J. Frisch, G.W. Trucks, H.B. Schlegel, G.E. Scuseria, M.A. Robb, J.R. Cheeseman, V.G. Zarzewski, J.A. Montgomery Jr., R.E. Stratmann, J.C. Burant, S. Dapprich, J.M. Millam, A.D. Daniels, K.N. Kudin, M.C. Strain, O. Farkas, J. Tomasi, V. Barone, M. Cossi, R. Cammi, B. Mennucci, C. Pomelli, C. Adamo, S. Cliffrd, J. Ochterski, G.A. Petersson, P.Y. Ayala, Q. Cui, K. Morokuma, D.K. Malick, A.D. Rabuck, K. Raghavachari, J.B. Foresman, J. Cioslowski, J.V. Ortiz, A.G. Baboul, B.B. Stefanov, G. Liu, A. Liashenko, P. Piskorz, I. Komaromi, R. Gomperts, R.L. Martin, D.J. Fox, T. Keith, M.A. Al-Laham, C.Y. Peng, A. Nanayakkara, C. Gonzalez, M. Challacombe, P.M.W. Gill, B. Johnson, W. Chen, M.W. Wong, J.L. Andres, C. Gonzalez, M. Head-Gordon, E.S. Replogle, J.A. Pople, Gaussian Inc., Pittsburgh PA, **1998**.

[19] (a) S.J. Vosko, L. Wilk and M. Nusair, *Can. J. Chem.* **1980**, *58*, 1200; (b) A.D. Becke, *Phys. Rev. A* **1988**, *38*, 5648; (c) C. Lee, W. Yang, R.G. Parr, *Phys. Rev. B* **1988**, *37*, 785; (d) A.D. Becke, *J. Chem. Phys.* **1993**, *98*, 1372; (e) A.D. Becke, *J. Chem. Phys* **1993**, *98*, 5648.

[20] H. Ozeki, M. C.R. Cockett, K. Okuyama, M. Takahashi, K. Kimura, *J. Phys. Chem.* **1995**, *99*, 8008.

[21] The height of the barrier was also calculated using the CBS-QB3 method [17]. The UMP2 and UMP4 single point calculations within this collective method suffered from large spin contamination and in place of their energies, the projected energies (PMP2 and PMP4), where the higher spin component is projected out, were used. The relative energy obtained using this strategy agreed within 2 kcal/mol with that from the B3LYP/CBSB7 procedure.

[22] S.G. Lias, J.E. Bartmess, J.F. Liebman, J.L. Holmes, R.O. Levin, W.G. Mallard, *J. Phys. Chem. Ref. Data* **1988**, *17*, Supplement 1.

[23] R. Flammang, V. Henrotte, P. Gerbaux, M.T. Nguyen, *Eur. Mass Spectrom.* **2000**, *6*, 3.

[24] (a) J.L. Holmes, J.K. Terlouw, *Org. Mass Spectrom.* **1980**, *15*, 383 ; (b) J. Laskin, C. Lifshitz, *J. Mass Spectrom.* **2001**, *36*, 459.

[25] R. Buff, J. Dannacher, *Int. J. Mass Spectrom.* **1984**, *62*, 1.

[26] J.L. Holmes, J.K. Terlouw, *J. Am. Chem. Soc.* **1979**, *101*, 4973.

[27] The 298 K enthalpy for this ion, 267 kcal/mol, was obtained from a CBS-QB3 calculation [17].

[28] D.T. Leeck, H.I. Kenttämaa, *Org. Mass Spectrom.* **1994**, *29*, 106.

[29] P. Gerbaux, M. Barbieux-Flammang, J.K. Terlouw, R. Flammang, *Int. J. Mass Spectrom* **2001**, *206*, 91.

[30] E.D. Nelson, R. Li, H.I. Kenttämaa, *Int. J. Mass Spectrom.* **1999**, *185/186/187*, 91.

[31] S.J. Blanksby, S. Dua, J.H. Bowie, D. Schröder, H. Schwarz, *J. Chem. Phys. A* **2000**, *104*, 11248.

NOTE TO USERS

Page(s) missing in number only; text follows. Page(s) were scanned as received.

48, 76, 98, 168, 196

Page(s) not included in the original manuscript and are not available from the author or university. The manuscript was scanned as received.

This reproduction is the best copy available.

Chapter 8

Generation and Characterization of Ionic and Neutral $(CH_3OBH)^{+/\bullet}$ and $(CH_3BOH)^{+/\bullet}$ in the Gas-Phase by Tandem Mass Spectrometry

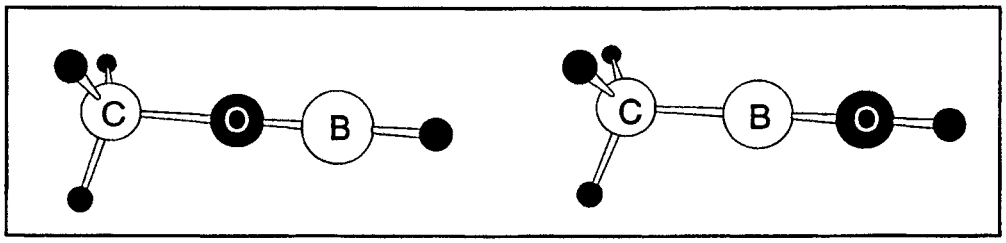

The isomeric dicoordinated borinium ions $CH_3O\text{-}B\text{-}H^+$ and $CH_3\text{-}B\text{-}OH^+$ are generated upon electron ionization of trimethylborate and methyl boronic acid, respectively. The connectivity of the ions is confirmed by collision-induced dissociation experiments on magnetic deflection type tandem mass spectrometers. Neutralization-Reionization (NR) experiments on these structurally characterized ions indicate that the neutral radicals $CH_3O\text{-}B\text{-}H^\bullet$ and $CH_3\text{-}B\text{-}OH^\bullet$ are viable species in the gas phase. Calculations at the G2 level of theory were performed to obtain thermochemical data on the title isomers and their main dissociation products. The calculations also provide a rationale for the moderate yield of the neutrals generated in the experiments : the vertical NR process for both systems is associated with particularly unfavourable Franck-Condon factors.

The work described here has been published previously in an article under the same title: R. Srinivas, S. Vivekananda, S.J. Blanksby, D. Schröder, M.A. Trikoupis, J.K. Terlouw and H. Schwarz, Int. J. Mass Spectrom. 2000, 202, 315-322.

Introduction

Dicoordinated boron molecules are important intermediates in organoboron chemistry, not least because of their role in the combustion of boron compounds in aerospace systems [1-2]. However, so far not many of such subvalent boron species have been experimentally identified. One reason is their high reactivity which has been attributed to the electrophilicity induced by the two empty p-orbitals on boron.

In contrast, their ionic counterparts, borinium ions, are readily generated as stable species in a mass spectrometer by either dissociative ionization of simple boron containing compounds or ion-molecule reactions [3]. The chemical reactivity of various borinium ions towards different organic substrates has been thoroughly investigated by Kenttamaa and co-workers using a dual cell Fourier Transform Ion Cyclotron Resonance (FT-ICR) mass spectrometer [4]. The group of Brodbelt extended these studies and has demonstrated that borinium ions are useful reagents in the analysis of drugs by chemical ionization [5].

One electron reduction of stable borinium ions in the dilute gas-phase may therefore be an attractive route to generate their highly reactive counterparts. This process represents the first step in neutralization-reionization (NR) mass spectrometry which has developed over the years into a powerful method for the study of elusive neutral species [6]. Using this technique, we have recently demonstrated that neutral $B(OH)_2^{\bullet}$ is a stable species in the gas phase [7]. Here we report on the use of the NR methodology to study the generation of $CH_3OBH^{\bullet}$ and $CH_3BOH^{\bullet}$ from their ionic counterparts.

Results and Discussion

I. Trimethylborate

The 70 eV electron ionization mass spectrum of trimethylborate (**I**) displays an intense molecular ion at *m/z* 104 (55%, ^{11}B isotope) and prominent fragment ions at *m/z* 73 (base peak, loss of $CH_3O^{\bullet}$), *m/z* 43 (27%) and *m/z* 15 (21%, CH_3^+). Early experimental work [16] suggested that the *m/z* 43 ion would correspond to $^{11}BO_2^+$ generated by loss of C_2H_6 from the *m/z* 73 ion. However, in subsequent experiments Hettich et al. [17] showed that the ion has the elemental composition $CH_4{}^{11}BO$ and that it is exclusively generated by loss of CH_2=O

from the *m/z* 73 $CH_3O^{11}BOCH_3^+$ ion. On this basis, the connectivity CH_3O-B-H^+ ($\mathbf{1}^+$) was proposed for the *m/z* 43 ions, implying that the loss of CH_2=O involves a 1,3-H shift. An alternative route for this rearrangement would involve a 1,4-H shift leading to the isomer CH_3-O(H)-B^+. However, see the computational results in Table 8.1a, this species lies c. 60 kcal/mol higher in energy than $\mathbf{1}^+$ and thus it is unlikely to be (co-)generated.

Table 8.1a. Calculated G2 energies E_{tot} (hartrees) and relative energies E_{rel} (kcal/mol) of possible fragmentation channels of the CH_3OBH^+ cation at 0K.

	E_{tot} (G2)	E_{rel}
CH_3OBH^+ ($\mathbf{1}^+$)	-140.054961	0
$CH_3O(H)B^+$ ($\mathbf{1a}^+$)	-139.958120	60.8
$CH_2O(H)BH^+$ ($\mathbf{1b}^+$)	-140.012745	26.5
$CH_2OBH^{\bullet+}$ + H$^\bullet$	-139.881234	109.0
$CH_3OB^{\bullet+}$ + H$^\bullet$	-139.867196	117.8
CH_2OB^+ + H_2	-139.890957	102.9
$HBO^{\bullet+}$ + $CH_3^\bullet$	-139.755740	188.0
$BOH^{\bullet+}$ + $CH_3^\bullet$	-139.880649	109.4
HBO + CH_3^+	-139.951958	65.0
BOH + CH_3^+	-139.880442	109.5

The difference of the total energies yields $IE_a(CH_3OBH)$ = 6.67 eV, and combined with $\Delta H_{f,0}(CH_3OBH)$ = -16.4 kcal/mol (Table 8.1b), $\Delta H_{f,0}(CH_3OBH^+)$ = 137.4 kcal/mol is predicted.

Table 8.1b. Calculated G2 energies E_{tot} (hartrees) and relative energies E_{rel} (kcal/mol) of possible fragmentation channels of the CH_3OBH radical at 0K.

	E_{tot} (G2)	E_{rel}
$CH_3OBH^\bullet$ ($\mathbf{1}^\bullet$)	-140.300013	0
$CH_3O(H)B^\bullet$ ($\mathbf{1a}^\bullet$)	-140.238254	38.8
CH_2OBH + H$^\bullet$	-140.227356	45.6
CH_3OB + H$^\bullet$	-140.201023	62.1
$CH_2OB^\bullet$ + H_2	-140.209257	57.0
HBO + $CH_3^\bullet$	-140.311472	-7.2
BOH + $CH_3^\bullet$	-140.239956	37.7

The G2 atomization method using experimental values for the heats of formation of the atoms predicts $\Delta H_{f,0}(CH_3OBH)$ = -16.4 kcal/mol, $\Delta H_{f,298}(CH_3OBH)$ = -19.9 kcal/mol is predicted using the calculated thermal corrections.

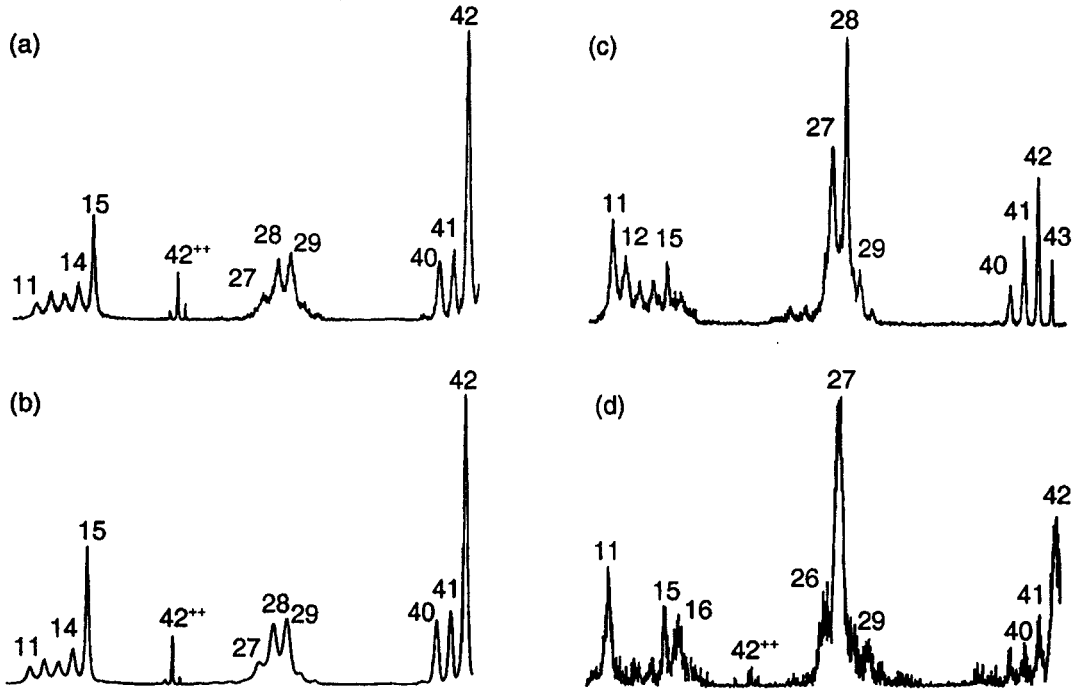

Figure 8.1. Collision-Induced Dissociation (CID) mass spectra of :(a) *m/z* 43 $CH_3O\text{-}B\text{-}H^+$ ions generated from 10 keV metastable $CH_3OBOCH_3^+$ ions, 3ffr ; (b) source generated *m/z* 43 $CH_3O\text{-}B\text{-}H^+$ ions having 6 keV translational energy, 3ffr ; (c) Neutralization-Reionization (NR) mass spectrum of 8 keV $CH_3O\text{-}B\text{-}H^+$ ions, 2ffr ; (d) CID mass spectrum of 8 keV *m/z* 43 survivor ions, 3ffr.

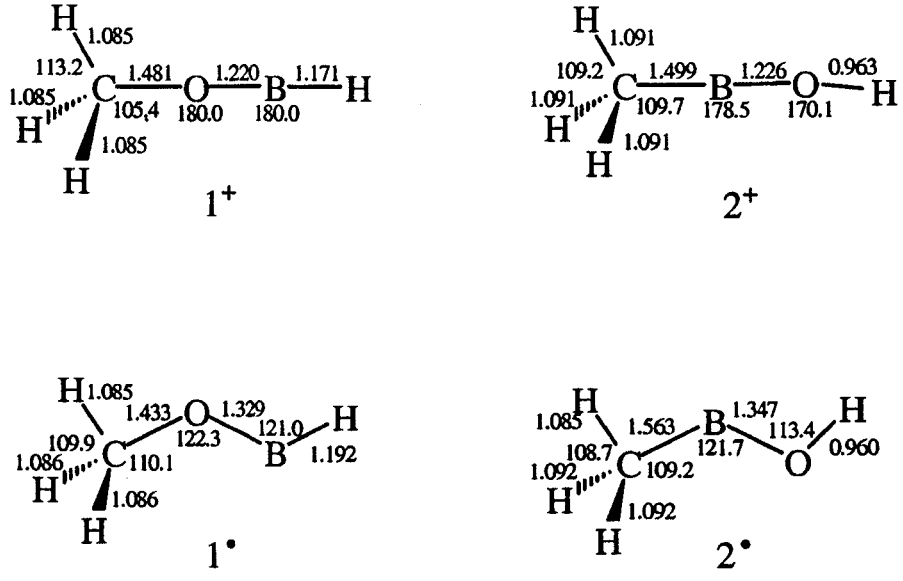

Figure 8.2. MP2/6-311+G(3df,2p) optimized geometries of CH_4BO isomers, bond lengths in Ångstrom, bond angles in degrees.

That the $CH_4{}^{11}BO$ ions represent a single structure follows from a comparison of the CID spectra of the source generated *m/z* 43 ions and the low energy ions generated from metastable *m/z* 73 precursor ions, which, see Figures 8.1a and 8.1b, are virtually identical. The (weak) metastable ion (MI) spectrum of the source generated ions is dominated by a CH_3^+ signal at *m/z* 15 and, see Table 8.1a, this is indeed the reaction of lowest energy requirement for *m/z* 43 ions having the connectivity $CH_3O\text{-}B\text{-}H^+$. The *m/z* 15 peak also features prominently in the CID spectrum. However, the spectrum is dominated by a more energy demanding, see Table 8.1a, loss of $H^\bullet$ from either the CH_3O or the BH moiety yielding stable *m/z* 42 product ions of structure $CH_3OB^{\bullet+}$ and $CH_2OBH^{\bullet+}$, respectively. The spectrum also shows an intense structure characteristic charge stripping peak at *m/z* 21 which may represent ions of structure $^+CH_2O\text{-}B\text{-}H^+$ generated by loss of $H^\bullet$ from the weak *m/z* 21.5 ions of structure $CH_3O\text{-}B\text{-}H^{++}$. Finally, a cluster of ions is observed at *m/z* 27 - 29. From a comparison with the spectrum of the ^{10}B isotopomer at *m/z* 42, it follows that these ions represent $^{11}BO^+$, $H^{11}BO^{\bullet+}$ and HCO^+ respectively, the latter ion being characteristic of the CH_3O moiety.

Collisional neutralization of $\mathbf{1}^+$ followed by reionization and mass spectrometric analysis, see Scheme 8.1, yields the NR spectrum shown in Figure 8.1c.

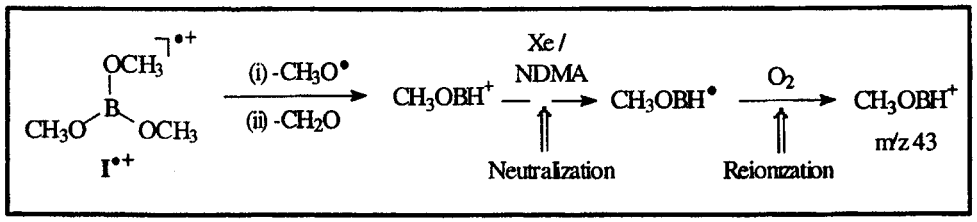

Scheme 8.1

The spectrum shows a substantial "survivor" signal at *m/z* 43 which seems to suggest that a sizeable fraction of the ions subjected to the NR process has remained intact. However, the fragment ion distribution in the NR spectrum is considerably different from that in the CID spectrum : ions at *m/z* 15 and *m/z* 42 are still present in the NR spectrum but it is dominated by *m/z* 28 ions. From the results presented in Table 8.1b, which lists calculated minimum energy requirements for various dissociations of neutral $CH_3O\text{-}B\text{-}H^\bullet$, it follows that

dissociation into H-B=O and $CH_3^{\bullet}$ may well be facile and thus the *m/z* 28 ions and (part of) the *m/z* 15 ions in the NR spectrum are likely to originate from collisional ionization. In this context we note that the slight exothermicity calculated for the dissociation of $\mathbf{1}^{\bullet}$ into H-B=O does not necessarily imply that CH_3O-B-H$^{\bullet}$ can not be a viable species in the gas phase. A case in point is the experimentally characterized CH_3O-C=O$^{\bullet}$ radical which lies 19 kcal/mol higher in energy than its dissociation products $CH_3^{\bullet}$ + CO_2 but which is prevented to dissociate by a sizeable barrier of 27 kcal/mol [18]. On the other hand, the computations discussed below indicate that, analogous to the $B(OH)_2^{+/\bullet}$ system [7], the NR process for CH_3O-B-H$^{+/\bullet}$ is associated with unfavourable Franck-Condon factors. Moreover, it is well known that neutralization-(collisional) reionization efficiencies of isobaric and even isomeric species can easily differ by a factor of 100 [6]. We therefore decided to try to verify the identity of the mass selected "survivor" ions by obtaining their CID spectra [19]. The result for the ^{11}B isotopomer is shown in Figure 8.1d. Signals at *m/z* 42, 41, 29, 21, and 15 characteristic of $\mathbf{1}^+$ are clearly present, implying that neutralization of $\mathbf{1}^+$ does yield stable species CH_3O-B-H$^{\bullet}$ that retain their structural identity. The spectrum also displays peaks of sizable intensity at *m/z* 27 (BO^+), 16 (O^+) and 11(B^+). These signals point to the contribution of an isobaric species [20] to the survivor signal, viz. $^{11}BO_2^+$. These $^{11}BO_2^+$ ions only contribute to a minor extent to the CID spectrum of the source generated *m/z* 43 ions (they could account for part of the weak *m/z* 27 signal) but apparently their neutralization-reionization efficiency is far greater than that of CH_3O-B-H$^+$. From the NR characteristics of BO_2^+, its contribution to the recovery signal at *m/z* 43 could easily be estimated. Unfortunately, however, a precursor molecule providing an intense beam of pure BO_2^+ ions was not available. We therefore decided to examine a sample of the $^{10}B/D$ labelled trimethylborate isotopomer $^{10}B(OCD_3)_3$ whose *m/z* 46 CD_3O-^{10}B-D$^+$ ions produce a NR spectrum which does not suffer from BO_2^+ interference [21]. From the intensity of the survivor ion in this spectrum (10 % of the base peak at *m/z* 28 D-^{10}B=O$^{\bullet+}$) it follows that ~ 45 % of the recovery signal in Figure 8.1c accounts for the stable CH_3O-B-H$^{\bullet}$ radical.

That the NR of the $CH_3O\text{-}B\text{-}H^{+/\bullet}$ system suffers from unfavourable Franck-Condon factors - the survivor ion yield is only $1{:}10^5$ - can be seen from the computational results presented in Figures 8.2 and 8.3. From Figure 8.2, it follows that there are large geometry differences between the ion and the neutral : the COB moiety is almost linear in the cation, but bent in the radical. To a first approximation electron transfers in neutralization-reionization (NR) experiments occur vertically and thus the vertical recombination energy (RE_v) of the cation and the vertical ionization energy (IE_v) of the neutral need to be considered as well. The G2 results presented in Table 8.2 predict that $RE_a=IE_a=6.68$ eV. Further, vertical ionization of the neutral ($IE_v=7.94$ eV) requires 1.3 eV more than the adiabatic process and it is therefore associated with unfavourable Franck-Condon factors, see Figure 8.3a. Similarly, vertical neutralization of thermalized $CH_3O\text{-}B\text{-}H^+$ differs by almost 2 eV from the adiabatic process. It yields $CH_3OBH^\bullet$ radicals with a highly non-relaxed geometry which are prone to dissociate. This effect may account for the enhanced *m/z* 28 ($H\text{-}B{=}O^{\bullet+}$) peak in the NR spectrum as well as the weak but discrete survivor signal for $CH_3O\text{-}B\text{-}H^+$.

Table 8.2. Calculated G2 energies E_{tot} (hartrees) and relative energies E_{rel} (kcal/mol) of neutral and ionic $CH_3OBH^{\bullet+}$ and $CH_3BOH^{\bullet+}$ at 0K.

Species	G2 (0K)	Rel. Energy (kcal/mol)
$CH_3BOH^\bullet$	-140.336728	0
$CH_3OBH^\bullet$	-140.300013	23
CH_3BOH^+	-140.109833	142
CH_3OBH^+	-140.054961	177
$CH_3BOH^\bullet$ (vert. neutral.)	-140.232630	65
$CH_3OBH^\bullet$ (vert. neutral.)	-140.232573	65
CH_3BOH^+ (vert. ioniz.)	-140.055023	177
CH_3OBH^+ (vert. ioniz.)	-140.007402	206

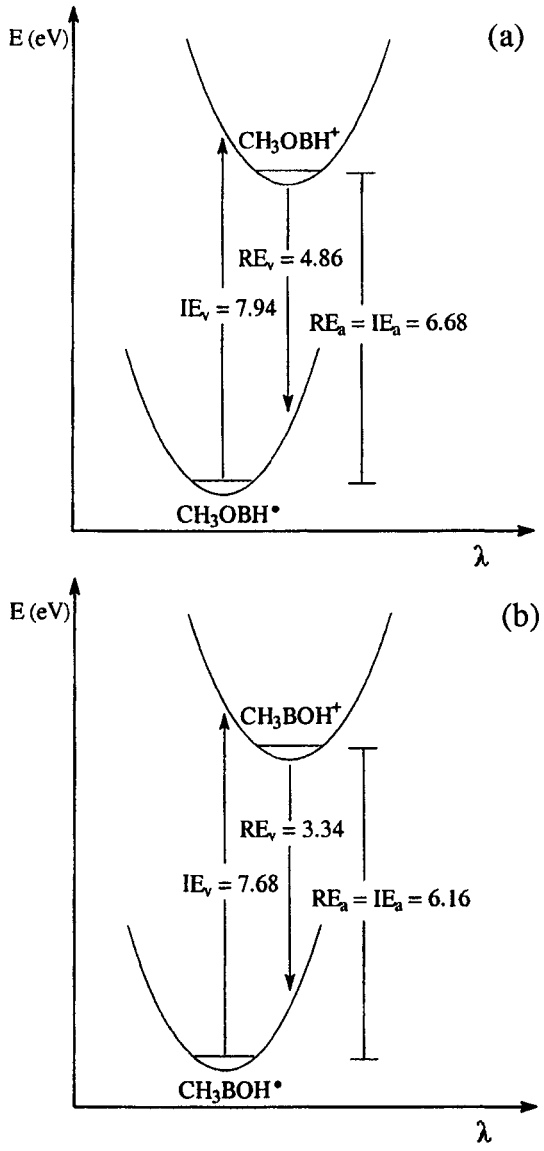

Figure 8.3. Schematic G2 potential-energy surfaces for the sequential electron transfer during the NR sequence (a) $CH_3O\text{-}B\text{-}H^+ \rightarrow CH_3O\text{-}B\text{-}H^\bullet \rightarrow CH_3O\text{-}B\text{-}H^+$ and (b) $CH_3\text{-}B\text{-}OH^+ \rightarrow CH_3\text{-}B\text{-}OH^\bullet \rightarrow CH_3\text{-}B\text{-}OH^+$.

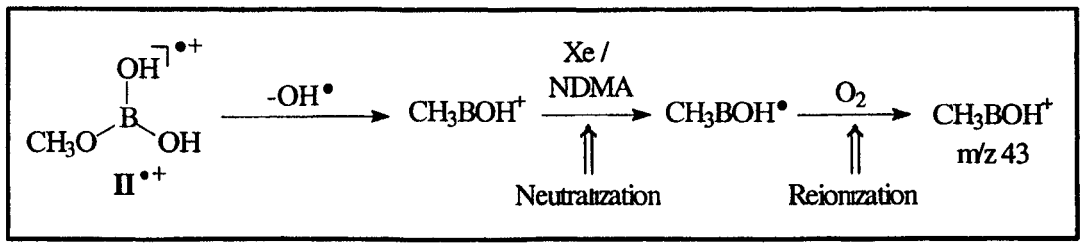

Scheme 8.2

II. Methyl boronic acid

Another interesting CH_4BO isomer is CH_3-B-OH^+ ($\mathbf{2}^+$), which can be envisaged to be generated by direct bond cleavage from ionized methyl boronic acid, (**II**), see Scheme 8.2. The 70 eV EI mass spectrum of **II** indeed yields *m/z* 43 ions which comprise 24% of the base peak at *m/z* 45, the $^{11}B(OH)_2^+$ ion generated by loss of $CH_3^\bullet$ [7]. The mass spectrum also displays a peak at *m/z* 44 (39%) which represents a mixture of $^{10}B(OH)_2^+$ and HO-^{11}B=O$^{\bullet+}$. Considering that the $^{11}B/\ ^{10}B$ natural abundance is 81 : 19, it follows that the *m/z* 43 $CH_4{}^{11}BO^+$ ions are contaminated with ~ 15% isobaric HO-^{10}B=O$^{\bullet+}$ ions. The presence of these ions does not significantly compromise the CID spectrum of the *m/z* 43 ions, but as we shall see this does not hold true for the NR spectrum and particularly the abundance of the recovery signal therein. The CID spectrum of the *m/z* 43 ions is shown in Fig.8.4a. The spectrum resembles that of isomer $\mathbf{1}^+$ as far the major dissociations leading to *m/z* 15, 28,29 and 40-42 are concerned. This is not unexpected in light of the calculated minimum energy requirements for dissociation listed in Table 8.3a. Nevertheless, tell-tale peaks at *m/z* 23-26 (BCH_n ; n = 0-3) reveal that the ions have the B-C connectivity associated with the proposed CH_3-B-OH^+ structure $\mathbf{2}^+$. In this context we further note that interconversion between $\mathbf{1}^+$ and $\mathbf{2}^+$ is unlikely since a key intermediate, $CH_3O(H)B^+$, lies 60 kcal/mol higher in energy than $\mathbf{1}^+$ (see Table 8.1a).

The NR spectrum of the *m/z* 43 ions is shown in Figure 8.4b. It is seen that the signals characteristic of CH_3-B-OH^+ are still clearly present in the NR spectrum but the peaks at *m/z* 27 and 28 have become much more prominent. Moreover, the spectrum shows an abundant recovery signal. This is surprising in view of our calculations which - analogous to the behaviour of ionic and neutral $\mathbf{1}^\bullet$ - indicate that in the neutralization step energetic neutrals are generated with distorted geometries. As shown in Figure 8.2, radical $\mathbf{2}^\bullet$ exhibits a structure with $\alpha_{CBO} = 122°$, whereas an almost linear CBO unit is found for the cation. Upon vertical neutralization of low energy ions, therefore, energy rich neutrals with bent CBO moieties may be generated and these may dissociate via the routes listed in Table 8.3b which all have fairly low energy requirements.

Table 8.3a. Calculated G2 energies E_{tot} (hartrees) and relative energies E_{rel} (kcal/mol) of possible fragmentation channels of the CH_3BOH^+ cation at 0K.

	E_{tot} (G2)	E_{rel}
CH_3BOH^+ (**2**$^+$)	-140.109833	0
CH_2BHOH^+ (**2a**$^+$)		[*]
$CH_2BOH^{\bullet+} + H^\bullet$	-139.931362	112.0
$CH_3BO^{\bullet+} + H^\bullet$	-139.791455	199.8
$CH_2BO^+ + H_2$	-139.931298	112.0
$CH_3B^{\bullet+} + OH^\bullet$	-139.806019	190.6
$BOH^{\bullet+} + CH_3^\bullet$	-139.880649	143.8
$HBO^{\bullet+} + CH_3^\bullet$	-139.755740	222.2
$BOH + CH_3^+$	-139.880442	143.9
$HBO + CH_3^+$	-139.951958	99.0

The difference of the total energies yields $IE_a(CH_3BOH)$ = 6.17 eV, and combined with $\Delta H_{f,0}(CH_3BOH)$ = -39.5 kcal/mol (Table 3b), $\Delta H_{f,0}(CH_3BOH^+)$ = 102.8 kcal/mol is predicted.

Table 8.3b. Calculated G2 energies E_{tot} (hartrees) and relative energies E_{rel} (kcal/mol) of possible fragmentation channels of the CH_3BOH radical at 0K.

	E_{tot} (G2)	E_{rel}
$CH_3BOH^\bullet$ (**2**$^\bullet$)	-140.336728	0
$CH_2BHOH^\bullet$ (**2a**$^\bullet$)		[*]
$CH_2BOH + H^\bullet$	-140.240022	60.7
$CH_3BO + H^\bullet$	-140.312888	15.0
$CH_2BO^\bullet + H_2$	-140.320945	9.9
$BOH + CH_3^\bullet$	-140.239956	60.7
$HBO + CH_3^\bullet$	-140.311472	15.8

The G2 atomization method using experimental values for the heats of formation of the atoms predicts $\Delta H_{f,0}(CH_3BOH)$ = -39.5 kcal/mol, $\Delta H_{f,298}(CH_3BOH)$ = -42.9 kcal/mol is predicted using the calculated thermal corrections.

[*] All attempts to optimize the geometry of **2a**$^+$ and **2a**$^\bullet$ failed and led to the isomeric structures **2**$^+$ and **2**$^\bullet$ respectively.

A satisfactory explanation for both the seemingly intense recovery signal and the enhanced *m/z* 27 and 28 peak intensities comes from an analysis of the *m/z* 43, 44 and 45 recovery signals in the NR spectra. Their relative intensities were found to be 30 : 100 : 21 whereas the corresponding source generated ions (see above) yield 24 : 39 : 100. Knowing the isobaric species contributing to these three peaks (see above), it becomes clear that HO-B=O ions have a much higher probability of surviving the NR process than either $B(OH)_2^+$ or CH_3-B-OH^+. As a result the estimated 15% isobaric HO-^{10}B=$O^{\bullet+}$ contamination of the *m/z* 43 ions manifests itself in the NR spectrum by contributing to ~ 85% of the survivor ion signal. Thus only ~ 15% of the survivor signal stems from CH_3-B-$OH^{\bullet}$, in line with the theoretical considerations discussed above.

That neutrals **2**$^{\bullet}$ are stable under NR conditions but only marginally so, is further confirmed by the CID spectrum of the *m/z* 43 survivor ions displayed in Figure 8.4c. The spectrum is dominated by fragment ions characteristic of HO-^{10}B=$O^{\bullet+}$, compare Figure 8.4d, including the intense peaks at *m/z* 27 (H- ^{10}B=$O^{\bullet+}$)and 26 ($^{10}BO^+$) but the weak signal at *m/z* 15 does attest to the presence of CH_3-B-OH^+.

Conclusions

High energy collision experiments on magnetic deflection type tandem mass spectrometers show that stable *m/z* 43 ions of structure CH_3O-B-H^+ and CH_3-B-OH^+ are generated by electron ionization of trimethylborate and methyl boronic acid respectively.

Neutralization-reionization experiments indicate that the neutral counterparts of both cations, CH_3O-B-$H^{\bullet}$ and CH_3-B-$OH^{\bullet}$, are viable species in the gas phase. However, when contributions from isobaric impurities to the recovery signals in the NR spectra are considered, both species appear to display survivor ion signals of only moderate intensity. Theoretical calculations at the G2 level of theory provide a rationale for these observations. The calculations show (i) that unfavourable Franck-Condon factors [7] govern the NR process of both systems and (ii) that fairly low lying dissociation channels are accessible to the incipient neutrals.

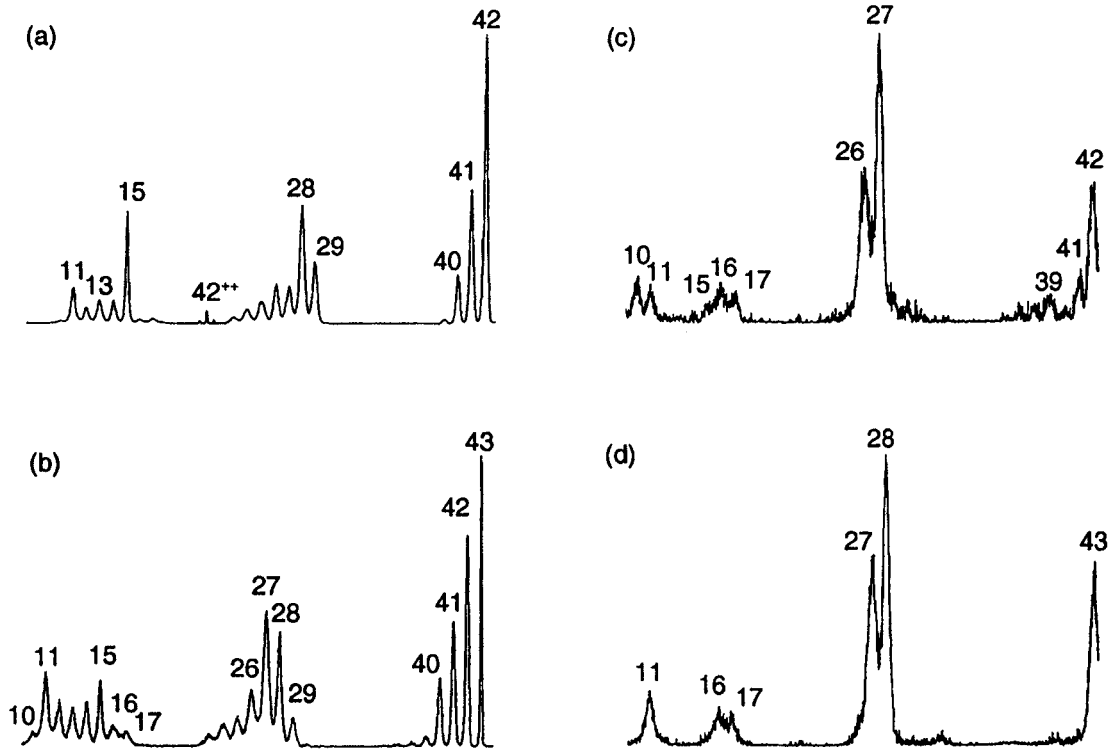

Figure 8.4. (a) Collision-Induced Dissociation (CID) mass spectrum of 8 keV *m/z* 43 CH_3-B-OH^+ ions, 2ffr; (b) Neutralization-Reionization (NR) mass spectrum of 8 keV *m/z* 43 CH_3-B-OH^+ ions, 2ffr ; (c) CID mass spectrum of the 8 keV *m/z* 43 survivor ions in the NR spectrum, 3ffr; (d) CID mass spectrum of the 8 keV *m/z* 44 survivor ions in the NR spectrum of $HO^{11}B{=}O^{+\bullet}$, 3ffr.

References

[1] H. Noth, B. Rastoger, C.H. Narula, A. Konstantinov, *Pure Appl. Chem.* **1983**, *55*, 1453.

[2] P. Kolle, H. Noth, *Chem. Rev.* **1985**, *85*, 399.

[3] R.H. Cragg, A.F. Weston, *J. Organometallic Chem.* **1974**, *67*, 161.

[4] D.T. Leeck, T.D. Ranatunga, R.L.Smith, T. Partaneu, P. Vainiotalo, H.I. Kenttamaa, *Int. J. Mass Spectrom. Ion Processes* **1995**, *141*, 229.

[5] A. Colarado, J. Brodbelt, *J. Mas Spectrom.* **1996**, *31*, 403.

[6] N. Goldberg, H. Schwarz, *Acc. Chem. Res.* **1994**, *27*, 34.

[7] R. Srinivas, S. Vivekanada, S.J. Blanksby, D. Schroder, H. Schwarz, L.M. Fell, J.K. Terlouw, *Int. J. Mass Spectrom.* **2000**, *197*, 105.

[8] (a) S. Vivekananda, R. Srinivas, J.K. Terlouw, *Int. J. Mass Spectrom. Ion Processes* **1997**, *171*, L13; (b) R. Srinivas, D. Sulzle, W. Koch, C.H. DePuy, H. Schwarz, *J. Am. Chem. Soc.* **1991**, *113*, 5970; (c) H.F. van Garderen, P.J.A. Ruttink, P.C. Burgers, G.A. McGibbon, J.K. Terlouw, *Int. J. Mass Spectrom. Ion Processes* **1992**, *121*, 159.

[9] NIST/EPA/NIH Mass Spectral Library - NIST 98, Release 1A.4, U.S. Secretary of Commerce, **1998**.

[10] Gaussian 94, Revision B.3, M.J. Frisch, G.W. Trucks, H.B. Schlegel, P.M.W. Gill, B.G. Johnson, M.A. Robb, J.R. Cheeseman, T. Keith, G.A. Petersson, J.A. Montgomery, K. Raghavachari, M.A. Al-Laham, V.G. Zakrzewski, J.V. Ortiz, J.B. Foresman, C.Y. Peng, P.Y. Ayala, W. Chen, M.W. Wong, J.L. Andres, E.S. Replogle, R. Gomperts, R.L. Martin, D.J. Fox, J.S. Binkley, D.J. Defrees, J. Baker, J.P. Stewart, M. Head-Gordon, C. Gonzalez, J.A. Pople, Gaussian Inc., Pittsburgh PA, **1995**.

[11] Gaussian 98, Revision A.7, M.J. Frisch, G.W. Trucks, H.B. Schlegel, G.E. Scuseria, M.A. Robb, J.R. Cheeseman, V.G. Zarzewski, J.A. Montgomery Jr., R.E. Stratmann, J.C. Burant, S. Dapprich, J.M. Millam, A.D. Daniels, K.N. Kudin, M.C. Strain, O. Farkas, J. Tomasi, V. Barone, M. Cossi, R. Cammi, B. Mennucci, C. Pomelli, C. Adamo, S. Cliffrd, J. Ochterski, G.A. Petersson, P.Y. Ayala, Q. Cui, K. Morokuma, D.K. Malick, A.D. Rabuck, K. Raghavachari, J.B. Foresman, J. Cioslowski, J.V. Ortiz, A.G. Baboul, B.B. Stefanov, G. Liu, A. Liashenko, P. Piskorz, I. Komaromi, R. Gomperts, R.L. Martin, D.J. Fox, T. Keith, M.A. Al-Laham, C.Y. Peng, A. Nanayakkara, C. Gonzalez, M. Challacombe, P.M.W. Gill, B. Johnson, W. Chen, M.W. Wong, J.L. Andres, C. Gonzalez, M. Head-Gordon, E.S. Replogle, J.A. Pople, Gaussian Inc., Pittsburgh PA, **1998**.

[12] L.A. Curtiss, K. Raghavachari, G.W. Trucks, J.A. Pople, *J. Chem. Phys.* **1991**, *94*, 7221.

[13] L.A. Curtiss, P.C. Redfern, K. Raghavachari, J.A. Pople, *J. Chem. Phys.* **1998**, *109*, 42.

[14] B.J. Bruke, L. Radom, *J. Chem. Phys.* **1998**, *109*, 3352.

[15] L.A. Curtiss, K. Raghavachari, P.C. Redfern, V. Rassolov, J.A. Pople, *J. Chem. Phys.* **1998**, *109*, 7764.

[16] (a) R.H. Cragg, T.F.J. Todd, A.F. Weston, *J. Chem. Soc. Dalton. Trans.* **1972**, 1373 ; (b) R.W. law, J.L. Margrave, *J. Chem. Phys.* **1956**, *25*, 1086.

[17] R.L. Hettich, T. Cole, B.S. Freiser, *Int. J. Mass Spectrom. Ion Processes* **1987**, *81*, 203.

[18] M.A. Trikoupis, J.K. Terlouw, P.C. Burgers, M. Peres, C. Lifshitz, *J. Am. Soc. Mass Spectrom.* **1999**, *10*, 869.

[19] D.J. Lavorato, L.M. Fell, G.A. McGibbon, S. Sen, J.K. Terlouw, H. Schwarz, *Int. J. Mass Spectrom.* **2000**, *195/196*, 71.

[20] The spectrum also displays weak signals at *m/z* 10 ($^{10}B^+$) and *m/z* 26 ($^{10}BO^+$) which point to the presence of HO-^{10}B=O$^{\bullet+}$ as a minor component in the initial ion beam.

[21] The *m/z* 46 ions actually consist of a 9:1 mixture of CD_3O-^{10}B-D$^+$ and DO-^{10}B-OD$^+$. However, from reference NR spectra of $B(OH)_2^+$, see ref 7, we derive that the contribution of DO-^{10}B-OD$^+$ to the recovery signal is not more than ~ 10% of the *m/z* 46 survivor ion yield.

Chapter 9

Characterization of Iminothiosulfine-type Ions $[HNCS_2]^{\bullet+/\bullet-}$ and their Neutral Counterparts by Mass Spectrometry and Computational Chemistry

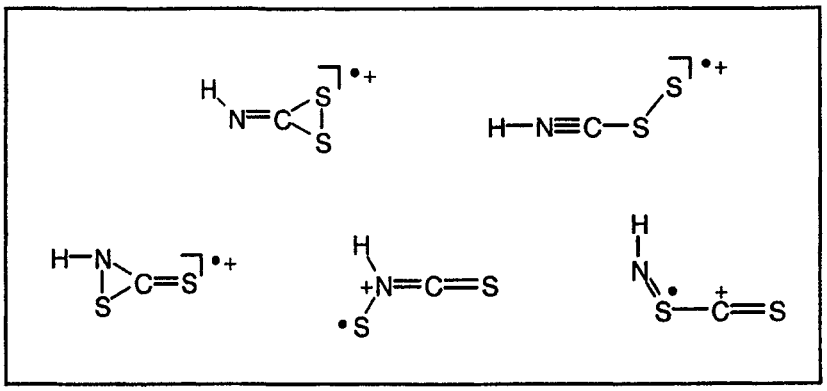

Electron ionization of rhodanine yields iminothiosulfine ions H-N≡C-S-S$^{\bullet+}$, **1b**$^{\bullet+}$, which readily communicate with the higher energy cyclic isomer H-N=$CS_2^{\bullet+}$, **1a**$^{\bullet+}$. CBS-QB3 and Gaussian-2 model chemistries predict that one electron reduction reverses the stability order but that the (singlet) neutrals remain connected via a negligible energy barrier. Neutralization-reionization (NR) experiments demonstrate that singlet **1a** and its heterocumulene isomer **1b** are stable species in the gas-phase. However, the co-generated triplet species readily dissociate into $^3S_2^{\bullet+}$ + HNC. Confirmatory experimental evidence comes from charge reversal and NR experiments on the cyclic anion H-N=$CS_2^{\bullet-}$, **1a**$^{\bullet-}$.

The work described here has been published previously in an article under the same title: S. Vivekananda, P. Raghunath, K. Bhanuprakash, R. Srinivas, M.A. Trikoupis and J.K. Terlouw, Chem. Phys. Lett. 2000, 332, 251-258.

Introduction

Over the years neutralization-reionization mass spectrometry (NRMS) has proven to be a useful technique for the generation and identification of small elusive molecules [1,2]. The technique has provided experimental evidence for an impressive range of such species which occur as key intermediates in reaction mechanisms [3], photochemical and catalytic reactions [4], flames and explosions [5], atmospheric chemistry [6] and also interstellar matter [7]. Among the reactive molecules that have been successfully "synthesized" in the gas-phase using NRMS, (hetero)cumulenes occupy an important place [8,9,10,11,12]. Some of these have been directly observed in interstellar space [13,14,15] and they are also of synthetic and theoretical importance [16].

In the present work we deal with the characterization of the heterocumulene with the HNCSS connectivity, using the NRMS methodology in conjunction with CBS-QB3 [17,18] and Gaussian-2 [19] model chemistries.

Results and Discussion

Characterization of the positive ions $HNCS_2^{\bullet+}$

The 70 eV electron-ionization mass spectra of rhodanine (**I**) and 3-ethylrhodanine (**II**) display moderately intense *m/z* 91 peaks with a relative abundance of 4 and 8 % respectively. High resolution experiments show that these ions have the elemental composition $CHNS_2$ and that isobaric ions of the composition $C_2H_3S_2$ are not (co-)generated.

As indicated in Scheme 9.1, loss of ketene from $\mathbf{I}^{\bullet+}$ and consecutive losses of CH_2CO and C_2H_4 from $\mathbf{II}^{\bullet+}$ represent the formation of the *m/z* 91 ions. For $\mathbf{II}^{\bullet+}$ the two steps represent low energy processes as witnessed by the metastable ion (MI) spectra of $\mathbf{II}^{\bullet+}$ and [**II** - CH_2CO]$^{\bullet+}$. The CID spectra of the *m/z* 91 ions from the two precursor molecules appear to be virtually identical.

Based on this information, two a priori plausible *m/z* 91 ion structures were considered *viz.* the cyclic ions $\mathbf{1a}^{\bullet+}$ and $\mathbf{1c}^{\bullet+}$, which may undergo ring opening into $\mathbf{1b}^{\bullet+}$ and $\mathbf{1d}^{\bullet+}/\mathbf{1e}^{\bullet+}$ respectively. From the computational results presented in Table 9.1 and Figure 9.1, it follows

that all five species, $\mathbf{1a}^{\bullet+}$ - $\mathbf{1e}^{\bullet+}$, are minima on the potential energy surface. There is general agreement between CBS-QB3 and G2 energies. However, whereas the B3LYP/CBSB7 algorithm (of the CBS-QB3 method) predicts that $\mathbf{1c}^{\bullet+}$ ring opens into $\mathbf{1d}^{\bullet+}$, MP2(Full)/6-31G(d) (in the G2 calculation) indicates $\mathbf{1c}^{\bullet+}$ to be a stable species, albeit of high energy.

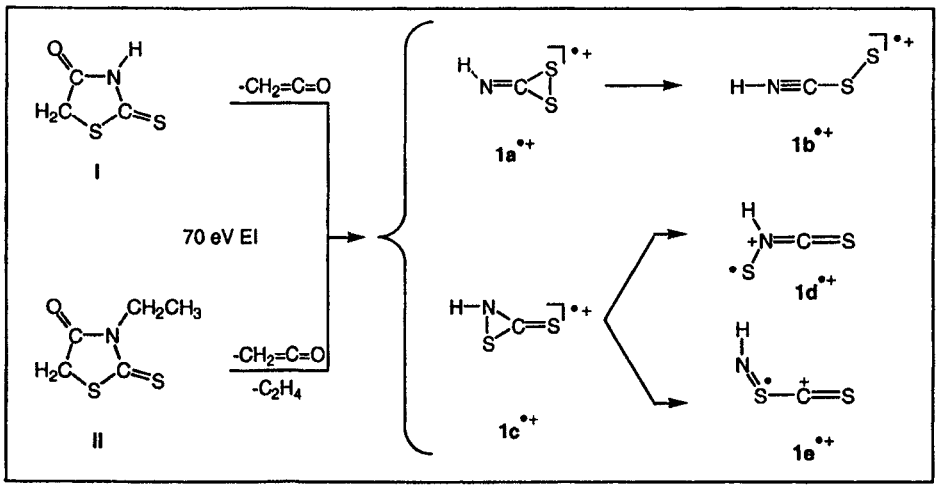

Scheme 9.1

The MI spectrum of the *m/z* 91 ions displays a single narrow Gaussian-shaped [27] peak at *m/z* 64 corresponding with the formation of $S_2^{\bullet+}$. This, see Table 9.2, suggests that we are dealing with ions $\mathbf{1a}^{\bullet+}/\mathbf{1b}^{\bullet+}$ for which direct bond cleavage into $S_2^{\bullet+}$ + HNC is expected to be the reaction of lowest energy requirement. In the CID spectrum, see Figure 9.2a, the *m/z* 64 peak still dominates, while the peaks at *m/z* 59 ($HNCS^{\bullet+}$), and 27 further support the connectivity assignment. From the energies listed in Table 9.2, it further follows that ions $\mathbf{1c}^{\bullet+}/\mathbf{1d}^{\bullet+}/\mathbf{1e}^{\bullet+}$ can reasonably be expected to dissociate into $HNS^{\bullet+}$ + CS upon collisional activation. However, the CID spectrum displays *m/z* 47 ($HNS^{\bullet+}$) and *m/z* 46 (NS^{+}) peaks of only marginal intensity and this effectively rules out a significant contribution of ions $\mathbf{1c}^{\bullet+}/\mathbf{1d}^{\bullet+}/\mathbf{1e}^{\bullet+}$ to the *m/z* 91 ion population.

The interconversion barrier $\mathbf{1a}^{\bullet+} \rightarrow \mathbf{1b}^{\bullet+}$ is calculated to be small (~ 2 kcal/mol) and lies well below the dissociation threshold for loss of HNC. Therefore, the scenario emerging from the computations, see top part of Figure 9.3, is that the CID represents a mixture of

interconverting ions $\mathbf{1a}^{\bullet+}/\mathbf{1b}^{\bullet+}$. For energetic and entropic reasons most of the ions will have the iminothiosulfine structure $\mathbf{1b}^{\bullet+}$.

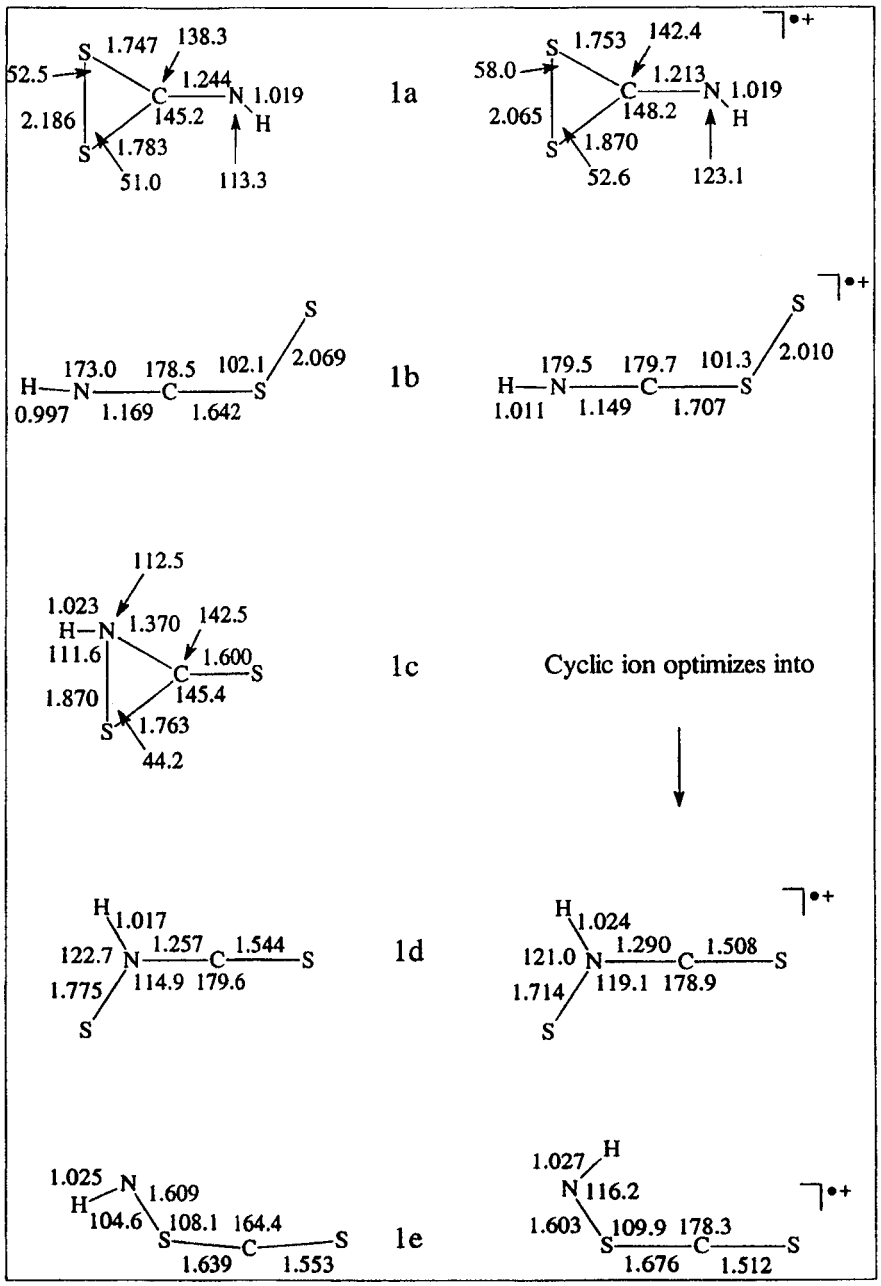

Figure 9.1. Selected optimized geometries of ionic and neutral [C,H,N,S_2] isomers from B3LYP/CBSB7 (CBS-QB3) calculations.

Table 9.1. Energies (kcal/mol) derived from CBS-QB3 and G2 calculations on the various $CHNS_2$ ionic and neutral species.

Species		ΔH_f CBS-QB3 298 K (0 K), kcal/mol		ΔH_f G2 298 K (0 K), kcal/mol	
	cation	266.9	(267.9)	270.7	(272.2)**
1a	neutral	57.7	(59.0)	60.1	(61.8)
	anion	8.1	(9.3)	12.4	(14.1)
	cation	253.9	(254.6)	260.2	(261.2)
1b	neutral	75.5	(76.3)	79.8	(80.4)
	anion	31.0	(31.7)	36.2	(37.4)
	cation	OPEN*		291.0	(292.4)
1c	neutral	73.4	(74.7)	75.0	(76.7)
	anion	OPEN*		OPEN*	
	cation	264.2	(265.3)	265.6	(267.5)
1d	neutral	82.4	(83.3)	83.9	(85.3)
	anion	36.4	(37.3)	40.8	(42.1)
	cation	261.9	(262.6)	--	--
1e	neutral	54.7	(55.4)	--	--

* All attempts to optimize the structure led to the connectivity of **1d**.

** This calculation suffers from a spin contamination, $\langle s^2 \rangle = 0.83$.

Table 9.2. Energies (kcal/mol) derived from CBS-QB3 and G2 calculations on various dissociation reactions of $CHNS_2^{\bullet+}$ ions relative to the dissociation into $S_2^{\bullet+}$ + HNC.

Dissociation Products / Precursor Ion	*m/z*	CBS-QB3 (0K)	G2 (0K)
$S_2^{\bullet+}$ + HNC	64	0	0
$HNCS^{\bullet+}$ + ^3S	59	32	33
$HNS^{\bullet+}$ + CS	47	37	36
$HNCS^{\bullet+}$ + ^1S	59	60	60
$HNC^{\bullet+}$ + $^3S_2$	27	61	64
$HNC^{\bullet+}$ + $^1S_2$	27	77	78
$S^{\bullet+}$ + HNCS	32	87	86
$1a^{\bullet+}$	91	-23	-21
TS ($1a^{\bullet+} \rightarrow 1b^{\bullet+}$)	--	-21	-18
$1b^{\bullet+}$	91	-36	-35

Table 9.3. Ionization (IE) and Recombination (RE) Energies (eV) from CBS-QB3 (0K) and G2 (0K) (values in brackets) calculations.

Species	IE (adiabatic)	IE (vertical)	RE (vertical)	RE (vertical) (→ triplet)
1a	9.06 (9.12)	9.37 (9.28)	8.82 (8.80)	6.45 (6.29)
1b	7.73 (7.71)	7.84 (7.90)	7.66 (7.63)	5.81 (5.78)

Table 9.4. Energies (kcal/mol) derived from CBS-QB3 and G2 calculations on various dissociation reactions of $CHNS_2$ neutrals relative to the dissociation into $^3S_2$ + HNC.

Dissociation Products / Precursor Ion	CBS-QB3 (0K)	G2 (0K)
$^3S_2$ + HNC	0	0
$^1S_2$ + HNC	17	14
^3S + HNCS	22	18
HNS + CS	47	43
^1S + HNCS	50	46
1a	-15	-17
TS (1a → 1b)	2	2
1b	2	2
1a (triplet)	14	--
1b (triplet)	-0.5	--

Characterization of the neutral species $HNCS_2$

The neutralization-reionization (NR) mass spectrum of the ions $\mathbf{1b^{\bullet+}}$ ($\mathbf{1a^{\bullet+}}$) is shown in Figure 9.2b. The spectrum displays a fairly abundant recovery signal at *m/z* 91 (30% of the base peak at *m/z* 64) and resembles the CID spectrum of Figure 9.2a. This suggests that vertical neutralization of ions $\mathbf{1b^{\bullet+}}$ ($\mathbf{1a^{\bullet+}}$) yields neutral species that are stable on the μs time scale and have retained the $HNCS_2$ connectivity. This is further supported by the spectrum of Figure 9.2c which represents CID of the *m/z* 91 survivor ions in Figure 9.2b. It clearly shows, compare Figure 9.2a, that most of the survivor ions have retained their structure integrity.

The computational findings presented in the bottom part of Figure 9.3 are in line with this proposal: singlet neutrals **1a/1b** are not prone to dissociate and moreover the vertical recombination energies - RE_v(s) in Figure 9.3 - are close to the adiabatic values and the same applies to the ionization energies (see Table 9.3). The computations further indicate that whereas most of the neutralized ions are open species $\mathbf{1b}^{\bullet+}$, the incipient neutrals **1b** are only marginally stable - TS[^{1}**1b** → ^{1}**1a**] is ~ 0.5 kcal/mol - towards ring-closure into **1a** which is more stable by 17 kcal/mol. Consequently, most of the stable neutrals generated will reach the potential well of **1a** during their μs lifetime.

Most of the differences between the CID and NR spectra can readily be rationalized, including the presence of a narrow component in the *m/z* 27 signal and the absence of a *m/z* 45.5 charge-stripping peak in the NR spectrum. The narrow component of the *m/z* 27 NR peak derives from the collision induced dissociative ionization (CIDI) of HNC neutrals generated by the dissociation of ions $\mathbf{1b}^{\bullet+}$ ($\mathbf{1a}^{\bullet+}$) in the neutralization chamber. However, it is not immediately clear why the *m/z* 64 ($S_2^{\bullet+}$) peak in the NR spectrum is considerably broader than the corresponding CID peak. A close inspection of the shapes of these peaks reveals that the NR peak consists of a poorly resolved 1:1 composite of a narrow and a broad component. The width of the narrow component matches that of the CID peak and is thus readily assigned to CIDI of intact neutrals **1a/1b**. The broad component, whose kinetic energy release is ~ 0.4 eV (as measured from its half-height width [27]), will then reflect the dissociation of neutral species into S_2 + HNC. In line with this [28], the broad component of the *m/z* 27 ($HNC^{\bullet+}$) peak is associated with the same large kinetic energy release.

The energy diagram Figure 9.3b, indicates that dissociation of *singlet* neutrals **1a/1b** into $^1S_2$ + HNC is unfavourable and what is more, this reaction is not expected to be associated with a significant energy release. However, the NR experiment involves (vertical) neutralization of a doublet species, and thus triplet neutrals can also conceivably be generated. We have computationally identified a stable triplet isomer of **1a** whereas that of **1b** was found to be marginally stable towards dissociation into $^3S_2$ + HNC, see Figure 9.3 and Table 9.4. Unlike the situation with the singlet species, the vertical recombination energies leading to

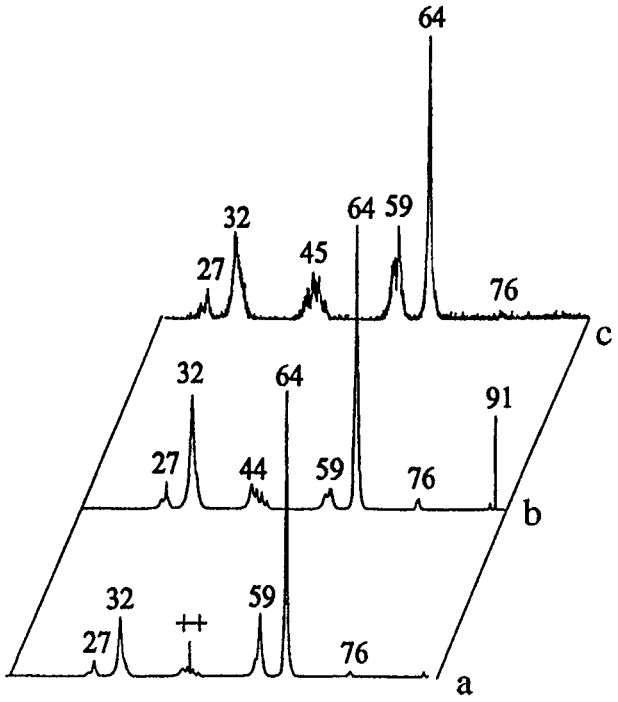

Figure 9.2. Collision induced dissociation (CID) spectrum, item (a), and neutralization-reionization (NR) spectrum, item (b), of the *m/z* 91 ions from 3-ethylrhodanine. Item (c) represents the CID spectrum of the *m/z* 91 survivor ions in Figure 2b.

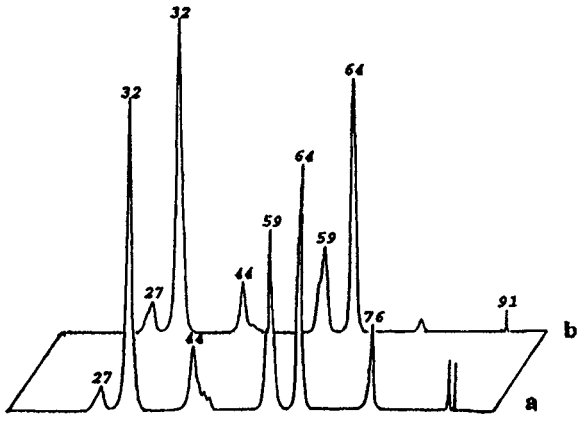

Figure 9.4. Charge reversal (CR) spectrum, item (a), and neutralizaiton-reionization ($^{-}NR^{+}$) spectrum, item (b), of the negative *m/z* 91 ions from rhodanine.

these triplet species are calculated to be considerably lower than the adiabatic values, see the arrows labelled $RE_v(t)$ in Figure 9.3 and also Table 9.3. The energy levels of the resulting excited triplet species lie far above the energy level for $^3S_2$ + HNC and thus a fast exothermic dissociation may occur in which part of the internal energy is converted into kinetic energy of the products. The broad component comprising the *m/z* 64 ion signal in Figure 9.2b, we thus attribute to the reaction $[^3\mathbf{1b}]^* \rightarrow {}^3S_2$ + HNC.

Summarizing, we propose that a mixture of neutral species **1a/1b** is generated upon neutralization. Formation of ^{1}**1a**/^{1}**1b** accounts for the observed survivor ions which upon collisional activation dissociate into $^1S_2^{\bullet+}$ + HNC as represented by the narrow component of the *m/z* 64 peak in the NR spectrum. Vertical neutralization to ^{3}**1b** (^{3}**1a**), on the other hand, leads to the formation of $^3S_2$ in a reaction associated with a substantial kinetic energy release and accounts for the broad component of the *m/z* 64 and 27 NR peaks.

Characterization of the negative ions $HNCS_2^{\bullet-}$

To further probe the behaviour of the $HNCS_2$ species, we have generated the radical anion $HNCS_2^{\bullet-}$ by the procedure described in the Experimental. Our computations indicate, see Table 9.1, that these ions adopt the cyclic structure **1a**$^{\bullet-}$ which is considerably lower in energy than its ring-opened counterpart **1b**$^{\bullet-}$, by 22 kcal/mol. Upon charge reversal, which involves a vertical two electron transfer in a high energy collision with O_2, the incipient positive ions are expected to be cyclic ions **1a**$^{\bullet+}$ having the geometry of the anion. If the cation is frozen in the anionic geometry and its energy is then calculated, it is found to lie as much as 50 kcal/mol above the ground state cationic conformer. Thus, highly excited cyclic ions **1a**$^{\bullet+}$ are expected to be formed upon charge reversal and this is borne out by the CR spectrum shown in Figure 9.4a. Apart from the peaks at *m/z* 64, 59, 58 and 32, which attest to the connectivity of the ion, the spectrum displays a very weak survivor signal. In addition, it shows a prominent signature peak of the cyclic structure, at *m/z* 76 ($CS_2^{\bullet+}$). Not unexpectedly, this high energy reaction features less prominently in the CID spectrum of the long-lived, low energy positive ions generated by dissociative electron ionization.

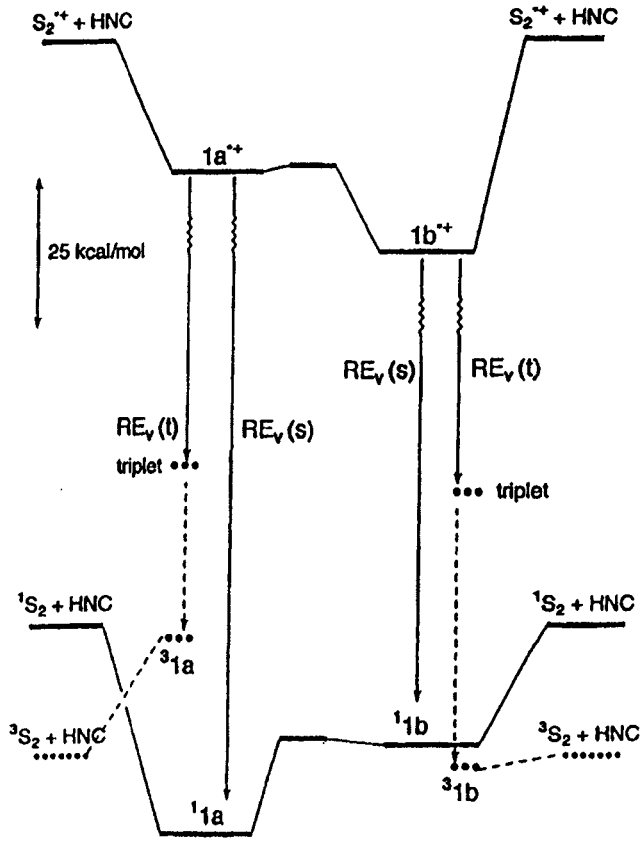

Figure 9.3. Energy level diagram for the rearrangement and dissociation reactions of ions $\mathbf{1a^{\bullet+}/1b^{\bullet+}}$ (top part) and their neutral counterparts (bottom part).

Finally we subjected $\mathbf{1a}^{\bullet-}$ to the reaction sequence $\mathbf{1a}^{\bullet-} - (He) \rightarrow \mathbf{1a} - (O_2) \rightarrow \mathbf{1a}^{\bullet+}$ of a $^{-}NR^{+}$ experiment. In agreement with the NR spectrum of $\mathbf{1a}^{\bullet+}/\mathbf{1b}^{+}$, the $^{-}NR^{+}$ spectrum, shown in Figure 9.4b, displays a significant recovery signal along with fragmentations characteristic of **1a/1b**.

Conclusions

From the combined results of mass spectrometric experiments and CBS-QB3/Gaussian-2 based computations, it is proposed that dissociative electron ionization of rhodanine and 3-ethylrhodanine yields $[C,H,N,S_2]^{\bullet+}$ ions of the connectivity $HNCS_2$. The initially generated cyclic ions $H\text{-}N{=}CS_2^{\bullet+}$, $\mathbf{1a}^{\bullet+}$, face a minimal energy barrier towards ring opening into iminothiosulfinic ions $H\text{-}N{\equiv}C\text{-}S\text{-}S^{\bullet+}$, $\mathbf{1b}^{\bullet+}$, which are thermodynamically more stable by 13 kcal/mol. In their neutral counterparts the stability order is reversed; the cyclic species **1a**, is now more stable, by 15 kcal/mol, but the (singlet) neutrals **1a/1b** remain connected via a negligible barrier. As pointed out by a reviewer, a similar situation obtains for the related $CS_3^{\bullet+}$ system [29,30]. Neutralization-reionization (NR) experiments confirm the theoretical prediction that **1a/1b** are stable species in the gas-phase. A substantial survivor ion signal is observed and a CID spectrum of these ions attests to the structure assignment of the neutral species. Energy-rich triplet species $^3\mathbf{1b}$ ($^3\mathbf{1a}$) with non-relaxed geometries may also be generated in the NR experiment. These are predicted to readily dissociate into $^3S_2$ + HNC and this, we propose, accounts for the observed broadening of the *m/z* 64 $S_2^{\bullet+}$ peak in the NR spectrum. Negative chemical ionization on rhodanine produces the cyclic anion $H\text{-}N{=}CS_2^{\bullet-}$, $\mathbf{1a}^{\bullet-}$ which is calculated to be 22 kcal/mol more stable than its ring opened counterpart $\mathbf{1b}^{\bullet-}$. Upon charge reversal (CR) most of the incipient positive ions decompose producing a spectrum characteristic of highly excited ions $\mathbf{1a}^{\bullet+}$. Subjected to a $^{-}NR^{+}$ experiment, again a mixture of interconverting neutrals **1a/1b** is generated.

References

[1] F. W. McLafferty, *Science* **1990**, *247*, 925.

[2] C. A. Schalley, G. Hornung, D. Schröder and H. Schwarz, *Chem. Soc. Rev.* **1998**, *27*, 91.

[3] C. Wentrup, *Reactive Molecules : The Neutral Reactive Intermediates in Organic Chemistry* (Wiley, New York, **1984**).

[4] J. C. Scaiano, L. J. Johnston, W. G. McGimspey, D. Weir, *Acc. Chem. Res.* **1988**, *21*, 22.

[5] H. Bock and R. Dammel, *Angew. Chem. Int. Ed. Engl.* **1987**, *26*, 504.

[6] J. S. Levine, Ed. *Photochemistry of Atmospheres* (Academic Press, Orlando, FL, 1987).

[7] H. Kroto, *Science* **1988**, *242*, 119.

[8] D. Sülzle and H. Schwarz, *Fundamentals of Gas phase Ion Chemistry*, K. R. Jennings (Ed.), (Kluwer, Dordrecht, **1991**).

[9] R. Flammang and C. Wentrup, *Sulfur Reports* **1997**, *20*, 255.

[10] R. Flammang and C. Wentrup, *Sulfur Reports* **1999**, *22*, 357.

[11] C. Wentrup and R. Flammang, *J. Phys. Org. Chem.* **1998**, *11*, 350.

[12] S.J. Blanksby and J.H. Bowie, *Mass Spectrom. Rev.* **1999**, *18*, 1.

[13] D. Smith, N. G. Adams, *J. Chem. Soc. Faraday Trans 2* **1989**, *85*, 1613.

[14] D. A. Williams, *Chem. Eur. J.* **1997**, *3*, 1929.

[15] C. R. Crowley, *An Introduction to Cosmochemistry*, (Cambridge University Press, Cambridge, **1995**).

[16] Houben-Weyl, *Methoden der Organischen Chemie*; E. Schaumann and H. Kroff, Eds., (Thieme: Stuttgart, **1993**) Vol. *E15*.

[17] J.A. Montgomery Jr., M.J. Frisch, J.W. Ochterski, G.A. Petersson, *J. Chem. Phys.* **2000**, *112*, 6532.

[18] J.A. Montgomery Jr., M.J. Frisch, J.W. Ochterski, G.A. Petersson, *J. Chem. Phys.* **1999**, *110*, 2822.

[19] L.A. Curtiss, K. Raghavachari, G.W. Trucks, J.A. Pople, *J. Chem. Phys.* **1991**, *94*, 7221.

[20] S. Vivekananda, R. Srinivas, J.K. Terlouw, *Int. J. Mass Spectrom. Ion Processes* **1997**, *171*, L13.

[21] H.F. van Garderen, P.J.A. Ruttink, P.C. Burgers, G.A. McGibbon, J.K. Terlouw, *Int. J. Mass Spectrom. Ion Processes* **1992**, *121*, 159.

[22] D. Lavorato, J.K. Terlouw, T.K. Dargel, G.A. McGibbon, W.Koch, and H. Schwarz, *Int. J. Mass Spectrom.* **1998**, *179/180*, 7.

[23] K. Levsen. and H. Schwarz, *Angew. Chem. Int. Ed. Engl.* **1976**, *15*, 509.

[24] N. Goldberg, H. Schwarz, *Acc. Chem. Res.* **1994**, *27*, 34.

[25] M. M. Bursey, *Mass Spectrom. Rev.* **1990**, *9*, 555.

[26] Gaussian 98, Revision A.7, M.J. Frisch, G.W. Trucks, H.B. Schlegel, G.E. Scuseria, M.A. Robb, J.R. Cheeseman, V.G. Zarzewski, J.A. Montgomery Jr., R.E. Stratmann, J.C. Burant, S. Dapprich, J.M. Millam, A.D. Daniels, K.N. Kudin, M.C. Strain, O. Farkas, J. Tomasi, V. Barone, M. Cossi, R. Cammi, B. Mennucci, C. Pomelli, C. Adamo, S. Clifford, J. Ochterski, G.A. Petersson, P.Y. Ayala, Q. Cui, K. Morokuma, D.K. Malick, A.D. Rabuck, K. Raghavachari, J.B. Foresman, J. Cioslowski, J.V. Ortiz, A.G. Baboul, B.B. Stefanov, G. Liu, A. Liashenko, P. Piskorz, I. Komaromi, R. Gomperts, R.L. Martin, D.J. Fox, T. Keith, M.A. Al-Laham, C.Y. Peng, A. Nanayakkara, C. Gonzalez, M. Challacombe, P.M.W. Gill, B. Johnson, W. Chen, M.W. Wong, J.L. Andres, C. Gonzalez, M. Head-Gordon, E.S. Replogle, J.A. Pople, Gaussian Inc., Pittsburgh PA, **1998**.

[27] J.L. Holmes and J.K. Terlouw, *Org. Mass Spectrom* **1980**, *15*, 383.

[28] The broad component of the *m/z* 27 NR peak has a much lower intensity than its *m/z* 64 counterpart. This is not unexpected, considering that the collisional ionization of S_2 benefits from the combination of a relatively high translational energy and a relatively low ionization energy.

[29] D. Sülzle, H. Egsgaard, L. Carlsen, and H. Schwarz, *J. Am. Chem. Soc.* **1990**, *112*, 3750.

[30] P. Gerbaux, Y. van Haverbeke, R. Flammang, M.W. Wong, and C. Wentrup, *J. Phys. Chem. A* **1997**, *101*, 6970.

NOTE TO USERS

Page(s) missing in number only; text follows. Page(s) were scanned as received.

48, 76, 98, 168, 196

Page(s) not included in the original manuscript and are not available from the author or university. The manuscript was scanned as received.

This reproduction is the best copy available.

Chapter 10

The heat of formation of sulfine, CH_2=S=O, revisited : a CBS-QB3 study

The heat of formation (ΔH_f) of sulfine, CH_2=S=O, has been determined by the CBS-QB3 quantum chemical method, using ten reactions, including the isodesmic reaction $CH_2SO + SO_2 \quad CH_2S + SO_3$. The derived ΔH_f at 298 K of sulfine, - 30 ± 6 kJ/mol, lies midway between two previously calculated values : -9 ± 14 and –52 ± 10 kJ/mol. The CBS-QB3 derived ΔH_f at 0 K was very recently validated against the very accurate W1 (Weizmann-1) method and there is excellent agreement between the two methods (within 3 kJ/mol). Our recommended value is evaluated against experimental observables, such as the measured proton affinity of CH_2=S=O and the appearance energy of CH_2=S^+-OH from dimethyl sulfoxide ions, $CH_3S(=O)CH_3^{\bullet+}$.

The work described here has been published previously in an article under the same title: P.J.A. Ruttink, P.C. Burgers, M.A. Trikoupis, J.K. Terlouw, Chem. Phys. Lett. 2001, *342*, 447-451.

Sulfines are four-centered heterocumulenes with general formula $R_1R_2C=S=O$ [1]. Although sulfines derived from ketones are generally stable compounds, simple aldehydic sulfines are relatively unstable and do not survive for a long time at room temperature [2]. A notable exception is ethylsulfine, $CH_3CH_2CH=S=O$ which plays a key role in allium chemistry and which is responsible for the well-known lachrymatory effect of onions [3]. Other, non-natural sulfines have been prepared in the laboratory [1], but it was not until 1976 that the parent molecule, sulfine itself, $CH_2=S=O$, **1**, was prepared in the gas-phase [4] and identified [4,5,6]. Sulfine has also been implicated as an intermediate in solution [7,8].

Sulfine has a planar, but bent geometry [4]; it is a relatively short-lived molecule ($t_{1/2}$ ~ 30 – 60 min.) and this is probably the reason why so little is known about its thermochemical properties, such as its heat of formation (ΔH_f) and bond strengths, although an estimate of its ΔH_f at 298 K, -51 ± 22 kJ/mol, has been available for some time [9]. It was this lack of experimental data on this transient species that drove us, some six years ago, to assess sulfine's ΔH_f by the increasingly attractive technique of computational chemistry [10]. We used *ab initio* calculations executed at the CAS-SDCI/CASSCF/DZ/(2df,2d,p) + f(S) level of theory to determine ΔH_f (**1**). Our strategy was to calculate the energy of **1** relative to those of the well-known products H_2S + CO, H_2O + CS, H_2 + SCO and $CH_2^{\bullet\bullet}$ + $SO^{\bullet\bullet}$ and to that of its isomer HC(=O)SH for which a reliable experimental estimate was available [9]. Averaging yielded a value of ΔH_f (**1**) = - 9 ± 14 kJ/mol at 298 K which represented a significant revision upwards of the original estimate, -51 ± 22 kJ/mol.

Since our original study was published, two other calculations for ΔH_f (**1**) have appeared, but only recently so [11, 12]. The first one, by Ventura et al. was critical not of our level of theory, but rather of our chosen strategy. They argue that because our dissociation reactions involve the making and breaking of very different chemical bonds, there would be no cancellation of errors in these calculations. One could rebut that this is precisely the reason for choosing *several* dissociation channels. Ventura et al. propose to calculate ΔH_f (**1**) from the enthalpy change of the isodesmic reaction, Eq. 9 in Table 10.1:

$$CH_2=S=O + S=O \rightleftharpoons CH_2=S + O=S=O \qquad \text{Eq. 9}$$

where cancellation of errors would be more complete than in our reactions. At their highest level of theory, by using the experimentally well-established ΔH_f's of SO, CH_2S and SO_2, they obtain ΔH_f (298 K) values for **1** of - 62.4 kJ/mol (B3PW91 level of theory [13-15]) and - 42.4 kJ/mol (CCSD(T,FC) level of theory[16]), both with Pople's basis set 6-311++G(3df, 2pd) [17], and they recommend a value of - 52 ± 10 kJ/mol, precisely the value originally estimated by Benson [9].

Table 10.1. CBS-QB3 reaction enthalpies in kJ/mol at 298 K for the reactions studied in this Letter and enthalpies of formation in kJ/mol at 298 K deduced for CH_2SO.

	Reaction	ΔH_f (products / exp)	ΔH (reaction / CBS)	ΔH_f (CH_2SO)
1	$CH_2SO \leftrightarrow C + S + O + 2H$	1679	1714	-35
2	$CH_2SO \leftrightarrow C + S + (1/2)O_2 + H_2$	994	1023	-29
3	$CH_2SO \leftrightarrow CH_2S + (1/2)O_2$	118	147	-29
4	$CH_2SO \leftrightarrow CH_2 + SO$	391	433	-42
5	$CH_2SO \leftrightarrow H_2O + CS$	39	70	-31
6	$CH_2SO \leftrightarrow H_2S + CO$	-131	-101	-30
7	$CH_2SO \leftrightarrow SCO + H_2$	-138	-121	-17
8	$CH_2SO \leftrightarrow HCOSH$	-121	-96	-25
9	$CH_2SO + SO \leftrightarrow CH_2S + SO_2$	-184	-151	-33
10	$CH_2SO + SO_2 \leftrightarrow CH_2S + SO_3$	19	52	-33

However, and as hinted by Ventura et al., one could argue that Eq. 9 is not truly isodesmic, because SO" is a triplet whereas the other molecules are singlets. Recently a hybrid empirical correction / pair correlation energy extrapolation scheme known as CBS-QB3 became available [18]. Briefly, the method involves a combination of a CCSD(T) calculation using a fairly small basis set with perturbation theory calculations in larger basis sets. With CBS-QB3 it is possible to calculate, to within 4-8 kJ/mol, the total atomization energy (TAE) of a molecule, i.e. the energy needed to disintegrate the molecule into its solitary atoms. Very recently [12], in the context of a study on the dissociation of dimethyl phosphonate ions, Martin et al. obtained the CBS-QB3 TAE of **1** from which they derived ΔH_f (**1**) = -26.86

kJ/mol at 0 K. This value includes an atomic spin-orbit correction of magnitude -3.64 kJ/mol; without this correction ΔH_f (1) becomes -30.50 at 0 K. The corresponding 298 K value was derived using the method of Nicolaides et al. [19], -36.6 kJ/mol, and this value lies midway between our earlier value (-9 ± 4 kJ/mol) and the recommended value of Ventura et al. (-52 ± 10 kJ/mol). In the same study [12], both CH_2=S=O and H_3PO were used to validate the CBS-QB3 method against the very accurate, but computationally much more demanding Weizmann-1 method (W1) of Martin and de Oliveira [20] (specifically, the recently proposed W1′ variant [21] was used, which exhibits greatly improved performance for second-row molecules at no additional cost). For CH_2=S=O it was found that the TAE's derived from CBS-QB3 and W1′ (both without spin-orbit and scalar relativistic corrections), were equal to within 3 kJ/mol, and so the CBS-QB3 method does lead to target accuracy for this kind of molecules.

We therefore decided to use our original strategy [10] to calculate ΔH_f (1) at 298 K, but now by employing the CBS-QB3 method. The reactions are listed in Table 10.1 and they are those used in our original study [10] and those of Ventura et al. [11] plus an additional reaction, namely the true isodesmic reaction of Eq. 10 :

$$CH_2=S=O + O=S=O \rightleftharpoons CH_2=S + SO_3 \qquad \text{Eq. 10}$$

The CBS-QB3 (298 K) enthalpies of all species are given in Table 10.2, together with the experimental heats of formation from Ref. 22. The CBS-QB3 products' enthalpy of the reactions 1 – 10 is given in the second column of Table 10.1 in kJ/mol. The third column gives the reaction enthalpy, using the CBS-QB3 value for CH_2=S=O and the final column gives the derived ΔH_f (1). For the average value we find : ΔH_f (1) = - 30 ± 6 kJ/mol at 298 K. The r.m.s error can be taken as a measure for the reliability of the CBS-QB3 method. The derived value for ΔH_f (1) lies almost exactly midway between our previous value (- 9 ± 14 kJ/mol [10]) and that recommended by Ventura et al. (- 52 10 kJ/mol [11]). Again, considering the above validation with W1′, we are confident that our new value is accurate. We also note that in the B3PW91 calculations of Ventura et al., ΔH_f of SO_2, which features in their isodesmic reaction of Eq. 9, is rather poorly reproduced, namely at -279 kJ/mol,

compared to the experimental value of -297 kJ/mol. By contrast, the CBS-QB3 method gives ΔH_f (SO_2) = -298 kJ/mol, which is almost identical to experiment, again attesting to the reliability of CBS-QB3. In this respect it is of interest to note that the average value of Ventura et al. for reactions 1-8, that is excluding the very reaction which features the above SO_2, becomes −31.2 ± 5.7 kJ/mol (B3PW91) which is virtually identical to our CBS-QB3 value.

We now evaluate ΔH_f (**1**) with respect to (i) the Proton Affinity (PA) of CH_2=S=O, derived from the deprotonation of CH_2=S^+-OH, $\mathbf{2}^+$ [23] and (ii) the TPEPICO Appearance Energy (AE) for the generation of $\mathbf{2}^+$ from ionised dimethyl sulfoxide, CH_3-S(=O)-$CH_3^{\bullet+}$ (DMSO) [24]. We do this because one way to experimentally determine ΔH_f (**1**) is to measure the PA of **1** provided that ΔH_f of the protonated form is known. Mass spectrometry based experiments [25] as well as *ab initio* calculations [26,27] leave no doubt that the protonated form of sulfine is CH_2=S^+-OH, $\mathbf{2}^+$, and not CH_3-S^+=O, $\mathbf{3}^+$. First, the calculations indicate that $\mathbf{2}^+$ is the more stable form, by c. 100 kJ/mol. It had previously been thought that ions $\mathbf{3}^+$ are generated by the loss of $CH_3^\bullet$ from the DMSO molecular ion, CH_3-S(=O)-$CH_3^{\bullet+}$, by direct bond cleavage. However, collision induced dissociation experiments [25] clearly indicated that the product ions are $\mathbf{2}^+$, rather than the less stable species $\mathbf{3}^+$. This dissociation must proceed via a 1,3-hydrogen shift within the DMSO molecular ion, i.e. via the sequence CH_3-S(=O)-$CH_3^{\bullet+}$ → CH_2=S(OH)-$CH_3^{\bullet+}$ → CH_2=S^+-OH + $CH_3^\bullet$. The AE for loss of $CH_3^\bullet$ from DMSO ions was subsequently used to derive ΔH_f ($\mathbf{2}^+$) at 298 K = 736 kJ/mol [24]. Using this value and the three values for ΔH_f (**1**) listed above : - 9 ± 14 kJ/mol [10], − 30 ± 6 kJ/mol [this work] and - 52 ± 10 kJ/mol [11], we calculate sulfine's PA as: 786, 765 and 743 kJ/mol respectively. If we compare the latter values with the experimentally derived PA by Bouchoux et al.[23], 787.6 ± 2.6 kJ/mol, then it would seem that our earlier value for ΔH_f (**1**) perfectly matches the experiment.

However, the concern may be expressed, as Ventura et al. did [11], that the AE for CH_2=S^+-OH may be too high. This is a valid concern because, as shown above, this reaction must proceed via a rearrangement process and so the AE for this reaction will be too high if the barrier for the associated 1,3-H shift lies higher than the energy of the products. In fact, the

AE would then correspond to this very barrier and not to the dissociation products at threshold. A first indication that this may be so, comes from the CBS-QB3 ΔH_f (2^+) at 298 K, 707 kJ/mol, which is 29 kJ/mol *lower* than the experimental value, see Table 10.3. Further, calculations at the MP2/6-31G(d,p)//6-31G(d,p) level of theory [27] indicate that a barrier does exist and that it lies c. 35 kJ/mol above the threshold for formation of CH_2=S^+-OH + $CH_3^{\cdot}$. With CBS-QB3, see Table 10.3, we derive a barrier height of 10 - 15 kJ/mol. More importantly, the DMSO radical cation undergoes a competing dissociation ; this is not loss of $H^{\cdot}$ as claimed by Ventura et al., but loss of $OH^{\cdot}$ to produce $^+CH_2$-S-CH_3 which is a well-characterized product ion, having ΔH_f = 816 kJ/mol at 0 K [28]. Our 0 K CBS-QB3 value is virtually the same and the corresponding 298 K value, see Table 10.3, is 803 kJ/mol. This dissociation too proceeds via the above 1,3-H shift. Now, from its AE (10.55 ± 0.07 eV, virtually identical to that for the loss of $CH_3^{\cdot}$, 10.64 ± 0.07 eV), an apparent ΔH_f ($^+CH_2$-S-CH_3) of 828 kJ/mol at 298 K was derived [24], which is 25 kJ/mol higher than the true value. This elevated value is due, we argue, to the barrier associated with the above 1,3-H shift and so not only theory, but also experiment indicates that a barrier exists for the formation of CH_2=S^+-OH. Thus the AE measurement for the formation of CH_2=S^+-OH from ionised DMSO only provides an upper limit to its ΔH_f, calculated to be 736 kJ/mol. Using the experimental PA of CH_2=S=O, 787.6 ± 2.6 kJ/mol [23], ΔH_f (H^+) = 1531 kJ/mol [22] and our CBS-QB3 derived ΔH_f (2^+), 707 kJ/mol, we derive ΔH_f (**1**) is -36 kJ/mol at 298 K. This value is gratifyingly close to that derived from the above CBS-QB3 calculations on the various isodesmic reactions, –30 ± 6 kJ/mol. Considering the reliability of the CBS-QB3 method for determining the gas phase thermochemical properties of species containing second-row elements, as verified with the very accurate W1′ method [20,21], we propose to adopt -30 ± 6 kJ/mol as the recommended value for the ΔH_f of CH_2=S=O.

Table 10.2. CBS-QB3 enthalpies in Hartrees at 298 K and experimental enthalpies of formation in kJ/mol at 298 K of the atoms and molecules studied in this Letter.

Molecule	H(CBS-QB3)	ΔH_f (exp) [a]	Molecule	H(CBS-QB3)	ΔH_f (exp) [a]
C	-37.78302	717	O	-74.98527	249
CH_2	-39.06601	386	O_2	-150.16139	0
CH_2S	-436.9346	118	S	-397.655	277
CO	-113.17895	-111	SCO	-510.95461	-138
CS	-435.71085	280	SO	-472.84038	5
H	-0.49746	218	SO_2	-548.03457	-297
H_2	-1.16277	0	SO_3	-623.15143	-396
H_2O	-76.33382	-242	HC(=O)SH	-512.10783	-121 [b]
H_2S	-398.9308	-21	CH_2SO	-512.07116	

[a] ref. 21 ; [b] ref. 9

Table 10.3. CBS-QB3 derived enthalpies (kJ/mol) for selected ions and neutrals associated with the isomerization and dissociation of the dimethyl sulfoxide radical cation.

Species	ΔH_f (CBS-QB3)	
	298 K	0 K
$CH_3S(=O)CH_3^{\bullet+}$ (**I**$^{\bullet+}$)	704	722
$CH_2=S(OH)CH_3^{\bullet+}$ (**II**$^{\bullet+}$)	721	738
TS (**I**$^{\bullet+}$ → **II**$^{\bullet+}$)	868	888
CH_3-S^+=O	793	802
CH_2=S^+-OH	707	715
CH_3-S-CH_2^+	803	816
$OH^{\bullet}$	38	38
$CH_3^{\bullet}$	148	151

References

[1] B. Zwanenburg, Recl. Trav. *Chim. Pays-Bas* **1982**, *101*, 1.

[2] N. Pelloux-Leon, Y. Vallee, *Gas-Phase Reactions in Organic Synthesis*; Y. Vallee, Ed.; Gordon and Breach, Amsterdam pp 275 -303.

[3] E. Block, Ang. Chem., *Int. Ed. Engl.* **1992**, *31*, 1135.

[4] E. Block, R.E. Penn, R.J. Olson, P.F. Sherwin, *J. Am. Chem. Soc.* **1976**, *98*, 1264.

[5] E. Block, H. Boch, S. Mohmand, P. Rosmus, B. Solouki, *Angew. Chem.* **1976**, *88*, 380.

[6] E. Block, E.R. Corey, R.E. Penn, T.L. Renken, P.F. Sherwin, H. Bock, T. Hirabayashi, S. Mohmand, B. Solouki, *J. Am. Chem. Soc.* **1982**, *104*, 3119.

[7] E. Block, A. Wall, *Tetrahedron Lett.* **1985**, *26*, 1425.

[8] F. Freeman, M.C. Keindl, *J. Chem. Soc., Chem. Commun.* **1984**, 138.

[9] S.W. Benson, *Chem. Rev.* **1978**, *78*, 23.

[10] P.J.A. Ruttink, P.C. Burgers, J.T. Francis and J.K. Terlouw, *J. Phys. Chem.* **1996**, *100*, 9694.

[11] O. N. Ventura, M. Kieninger, R. E. Cachau and S. Suhai, *Chem. Phys. Lett.* **2000**, *329*, 145.

[12] L.N. Heydorn, Y. Ling, G. de Oliveira, J.M.L. Martin, C. Lifshitz, J.K. Terlouw, *Z. Phys. Chem.* **2001**, *215*, 141.

[13] A.D. Becke, *J. Chem. Phys.* **1993**, *98*, 5648.

[14] A.D. Becke, *Phys. Rev. B* **1988**, *38*, 3098.

[15] J.P. Perdew, Y. Wang, *Phys. Rev. B* **1992**, *45*, 13244.

[16] K. Raghavachari, G.W. Trucks, J.A. Pople, M. Headgordon, *Chem. Phys. Lett.* **1989**, *157*, 479.

[17] W.J. Hehre, L. Radom, P.v.R. Schleyer, J.A. Pople, *Ab Initio Molecular Orbital Theory*, Wiley, New York, **1986**.

[18] (a) J.A. Montgomery Jr, M.J. Frisch, J. W. Ochterski, G.A. Petersson, *J. Chem. Phys.* **1999**, *110*, 2822 ; (b) ibid. **2000**, *112*, 6532.

[19] A. Nicolaides, A. Rauk, M.N. Glukhovtsev, L. Radom, *J. Phys. Chem.* **1996**, *100*, 17460.

[20] J.M.L. Martin, G. de Oliveira, *J. Chem. Phys.* **1999**, *111*, 1843.

[21] J.M.L. Martin, *Chem. Phys. Lett.* **1999**, *310*, 271.

[22] M.W. Chase Jr., NIST-JANAF Thermochemical Tables, 4th edn., *J. Chem. Ref. Data* **1998**, *9*, 1.

[23] G. Bouchoux, J.-Y. Salpin, *Rapid. Commun. Mass Spectrom.* **1999**, *13*, 932.

[24] Q. Zha, T. Nishimura, G.G. Meissels, *Int. J. Mass Spectrom. Ion Processes* **1988**, *83*, 1.

[25] G.A. McGibbon, P.C. Burgers, J.K. Terlouw, *Chem. Phys. Lett.* **1994**, *218*, 499.

[26] P.J.A. Ruttink, P.C. Burgers, J.K. Terlouw, *Chem. Phys. Lett.* **1994**, *229*, 495.

[27] F.C. Gozzo, M.N. Eberlin, *J. Mass Spectrom.* **1995**, *30*, 1553.

[28] Z.-X. Ma, C-L. Liao, H.-M. Yin, C.Y. Ng, S-W. Chiu, N.L. Ma, W-K. Li, *Chem. Phys. Lett.* **1993**, *213*, 250.

Chapter 11

Dissociation Reactions of Low-Energy Pentenyl Methyl Ether Radical Cations $C_5H_9OCH_3^{\bullet+}$

The dissociation chemistry of the low-energy $C_5H_9OCH_3^{\bullet+}$ ions generated from the thirteen isomeric pentenyl methyl ethers derived from stable alkenols has been studied. This was done by examining their metastable ion (MI) characteristics, in conjunction with ^2H and ^{13}C-labelling as well as collision-induced dissociation (CID) and neutralisation-reionisation (NR) experiments.

The influence of the position and substitution pattern of the double bond on the chemistry of these $C_6H_{12}O^{\bullet+}$ species is considered. The closely similar reactions of $C_2H_5CH{=}CHCH_2OCH_3^{\bullet+}$, **3**$^{\bullet+}$, $CH_2{=}CH\text{-}CH(C_2H_5)OCH_3^{\bullet+}$, **4**$^{\bullet+}$, and $CH_2{=}C(C_2H_5)CH_2OCH_3^{\bullet+}$, **13**$^{\bullet+}$, point to a common chemistry, which is rationalised in terms of facile 1,2-H and 1,2-C_2H_5 shifts via distonic ions. Each of the other isomers displays a distinct, though often related, chemistry. The eight allylic ionised ethers easily lose $CH_3^{\bullet}$ to produce $C_5H_9O^+$ oxonium ions, whose structure was established by CID experiments ; ions **3**$^{\bullet+}$/**4**$^{\bullet+}$/**13**$^{\bullet+}$ also readily expel $C_2H_5^{\bullet}$ to give $C_4H_7O^+$ ions of structure $CH_2{=}CH\text{-}C^+(H)OCH_3$. Elimination of CH_3OH is also significant for **3**$^{\bullet+}$/**4**$^{\bullet+}$/**13**$^{\bullet+}$ and for $(CH_3)_2C{=}CHCH_2OCH_3^{\bullet+}$, **8**$^{\bullet+}$, and $CH_3CH{=}C(CH_3)CH_2OCH_3^{\bullet+}$, **11**$^{\bullet+}$.

Besides expelling $CH_3^{\bullet}$ and/or $C_2H_5^{\bullet}$ and CH_3OH, the three homoallylic isomers undergo dissociations which are (almost) absent for their allylic counterparts : thus, both $CH_3CH{=}CH(CH_2)_2OCH_3^{\bullet+}$, **2**$^{\bullet+}$ and $CH_2{=}CH\text{-}CH(CH_3)CH_2OCH_3^{\bullet+}$, **10**$^{\bullet+}$ lose $H^{\bullet}$ and H_2O, whereas $CH_2{=}C(CH_3)CH_2CH_2OCH_3^{\bullet+}$, **7**$^{\bullet+}$, are unique in predominantly losing CH_2O. For the losses of CH_2O and H_2O mechanisms are proposed in which ion-neutral complexes of the type $[C_5H_{10}^{\bullet+} / CH_2O]$ and $[C_6H_{10}^{\bullet+} / H_2O]$ are key intermediates.

The behaviour of the non (homo)allylic isomer, $CH_2{=}CH(CH_2)_3OCH_3^{\bullet+}$, **1**$^{\bullet+}$, is similar to that of **2**$^{\bullet+}$ but the reactions occur in different proportions. A mechanism for the facile loss of an alkyl radical from **1**$^{\bullet+}$ is proposed in which 1,4-H shifts and distonic ions as well as communication with ionised cyclopentyl methyl ether, **14**$^{\bullet+}$, play an important role.

The work described here has been accepted for publication in an article under the same title: R.D. Bowen, M.A. Trikoupis and J.K. Terlouw, Eur. Mass Spectrom. 2001, in press.

Introduction

Most classes of $C_nH_{2n}O^{\bullet+}$ radical cations have been investigated in great deal by mass spectrometry. Various reviews [1-5] summarise the intriguing chemistry that has been reported for a wide range of ionised $C_nH_{2n}O$ species, including aldehydes and ketones [6-12], alkenols and cycloalkanols [13-15] and cyclic ethers [16-19].

Many $C_nH_{2n}O^{\bullet+}$ species undergo hydrogen transfer and even skeletal isomerisation before dissociating. Distonic ions [20,21] and ion-neutral complexes (INCs) [22-28] frequently are of crucial importance in the rearrangements which precede fragmentation of these ions [4,5]. Thus, the hydrogen transfer steps resulting in tautomerism are readily interpreted in terms of interconversion of distonic ions and the skeletal rearrangements of some $C_nH_{2n}O^{\bullet+}$ species may be explained by postulating the intermediacy of INCs [18,19].

In contrast to most categories of $C_nH_{2n}O^{\bullet+}$ ions, ionised alkenyl methyl ethers have received only a little attention until quite recently. A comparatively early study of ionised 5-hexenyl methyl ether revealed that $C_2H_5^{\bullet}$ loss from this $C_7H_{14}O^{\bullet+}$ isomer occurs by at least two mechanisms, one of which involves rearrangement to structures accessible to ionised cyclohexyl methyl ether [29]. A subsequent survey of the 70 and 12 eV electron ionization mass spectra of a great many alkenyl ethers $C_nH_{2n-1}OCH_3^{\bullet+}$ (n = 3 - 6) showed that alkyl radical elimination from some of these $C_nH_{2n}O^{\bullet+}$ species also occurs by more than one mechanism [30]. Further insight into the mechanisms of these reactions was obtained by establishing the structure of the $[M - alkyl]^+$ fragment ions formed from a large number of $C_nH_{2n-1}OCH_3^{\bullet+}$ species (n = 3 - 6) by analysing their high energy collision-induced dissociation (CID) mass spectra [31,32].

Important conclusions from these studies include the following. First, for ionised ethers derived from secondary and tertiary alcohols, $C_2H_5^{\bullet}$ and larger alkyl groups are lost readily by α-cleavage without prior rearrangement. In contrast, $CH_3^{\bullet}$ loss from ionised secondary allylic ethers is more complex : α-cleavage frequently occurs in competition with apparent β- or γ-cleavage. Thus, $CH_3^{\bullet}$ is lost at a similar or greater rate than $CD_3^{\bullet}$ from both $CH_3CH{=}CH\text{-}CH(CD_3)OCH_3^{\bullet+}$ and $CH_2{=}C(CH_3)\text{-}CH(CD_3)OCH_3^{\bullet+}$; moreover, the tendency to lose $CH_3^{\bullet}$

increases as the internal energy decreases. In each case, $CH_3^{\bullet}$ loss produces CH_2=CH-$C^+(CD_3)$-OCH_3 as the ionic fragment [31].

Secondly, ionised ethers of primary allylic alcohols also expel an alkyl group attached to the β- or γ-carbon atom. These reactions do not proceed by simple bond cleavage of the initial structure, even at high internal energies; instead, isomerisation occurs to give an ionised enol ether, which then dissociates by γ-cleavage. Expulsion of a γ-substituent merely requires two consecutive hydrogen shifts, followed by C-C cleavage. However, a skeletal rearrangement, which may be considered to proceed via an ionised substituted methoxycyclopropane, is also needed before a β-alkyl group may be lost. Similar rearrangements explain the loss of a δ-alkyl substituent from ionised ethers of primary allylic alcohols with a relatively long alkenyl chain [32,33].

Studies of **metastable** ionised allyl methyl ethers [34,35] and the four isomeric butenyl methyl ethers [36] shed further light on the chemistry of these radical cations. From experiments with ^{2}H-labelled analogues of $C_3H_5OCH_3^{\bullet+}$ and $C_4H_7OCH_3^{\bullet+}$, it became apparent that extensive hydrogen exchange precedes dissociation. Moreover, ^{13}C-labelling revealed that $CH_3^{\bullet}$ loss from ionised allyl methyl ether differs substantially from that of its higher homologues. Whereas CH_2=$CHCH_2O^{13}CH_3^{\bullet+}$ expels $^{13}CH_3^{\bullet}$ with a large and relatively specific kinetic energy release (KER), the ions CH_3CH=$CHCH_2O^{13}CH_3^{\bullet+}$ and CH_2=$C(CH_3)$-$CH_2O^{13}CH_3^{\bullet+}$ expel $CH_3^{\bullet}$, with a small KER. The third allylic isomer, CH_2=CH-$CH(CH_3)O^{13}CH_3^{\bullet+}$, also loses mainly $CH_3^{\bullet}$ (~ 94 %) with a small KER; however, a minor contribution from $^{13}CH_3^{\bullet}$ elimination occurs with a large KER, analogous to that found for CH_2=$CHCH_2O^{13}CH_3^{\bullet+}$.

These investigations focusing on the reactions of metastable ions $C_3H_5OCH_3^{\bullet+}$ and $C_4H_7OCH_3^{\bullet+}$ refined the conclusions derived from the CID studies. Alkyl radical elimination from ionised allylic alkenyl methyl ethers generally occurs by C-C fission to give (alkyl substituted) ions of the type CH_2=CH-C^+(H)-OCH_3, which can be viewed as conjugated oxonium ions CH_2=CH-C(H)=O^+CH_3. The atypical $CH_3^{\bullet}$ expulsion by C-O cleavage of CH_2=$CHCH_2OCH_3^{\bullet+}$ and, to a lesser extent, CH_2=CH-$CH(CH_3)OCH_3^{\bullet+}$, yields ions of the type CH_2=CH-C^+(H)-OH with a hydroxy substituent in place of the methoxy group. However, $CH_3^{\bullet}$

loss from ionised homoallyl methyl ether occurs by a distinct mechanism to give a cyclic oxonium ion.

In view of the strong contrast between the reactions of metastable $C_3H_5OCH_3^{\bullet+}$ and $C_4H_7OCH_3^{\bullet+}$, further work on this class of $C_nH_{2n}O^{\bullet+}$ species seemed desirable. This paper presents an overview of the reactions of the thirteen isomeric ionised methyl pentenyl ethers derived from stable alkenols, shown in Scheme 11.1.

CH_2=$CH(CH_2)_3OCH_3$		**1**	$(CH_3)_2C$=$CHCH_2OCH_3$		**8**
CH_3CH=$CH(CH_2)_2OCH_3$	(trans)	**2**	CH_2=$CHC(CH_3)_2OCH_3$		**9**
C_2H_5CH=$CHCH_2OCH_3$	(trans)	**3a**	CH_2=$CHCH(CH_3)CH_2OCH_3$		**10**
C_2H_5CH=$CHCH_2OCH_3$	(cis)	**3b**	CH_3CH=$C(CH_3)CH_2OCH_3$	(trans)	**11**
CH_2=$CHCH(C_2H_5)OCH_3$		**4**	CH_2=$C(CH_3)CH(CH_3)OCH_3$		**12**
CH_2=$CHCH_2CH(CH_3)OCH_3$		**5**	CH_2=$C(C_2H_5)CH_2OCH_3$		**13**
CH_3CH=$CHCH(CH_3)OCH_3$	(trans)	**6**	c-$C_5H_9OCH_3$		**14**
CH_2=$C(CH_3)(CH_2)_2OCH_3$		**7**			

Scheme 11.1

Results and Discussion

The Metastable Ion (MI) spectra of the isomeric radical cations $\mathbf{1}^{\bullet+}$-$\mathbf{13}^{\bullet+}$ are reported in Table 11.1 ; the corresponding data for ionised cyclopentyl methyl ether, $\mathbf{14}^{\bullet+}$, are also included for purposes of comparison. For selected members of the set of isomeric ions, the Collision-Induced Dissociation (CID) and Neutralisation-Reionisation (NR) [37] spectra are presented in Figure 11.1. It is clear from the contrasting behaviour of the metastable $C_5H_9OCH_3^{\bullet+}$ species, see Table 11.1, that the chemistry of these radical cations is rich and varied.

Correlations between the structure and reactivity of the $C_5H_9OCH_3^{\bullet+}$ species

Several trends in the reactivity of the isomeric $C_5H_9OCH_3^{\bullet+}$ radical cations are apparent. These correlations are also evident in faster reactions occurring in the ion source, but they are more clearly seen in the reactions of metastable species.

Table 11.1. Relative abundances [a] and kinetic energy releases [b] for the main dissociations of metastable ions $C_5H_9OCH_3^{\bullet+}$ generated by ionisation of methyl pentenyl ethers.

Ion/Loss →	$CH_3^\bullet$		$C_2H_5^\bullet$		CH_3OH		$H^\bullet$	H_2O	CH_2O
1$^{\bullet+}$	90	[2.1]	100	[1.9]	70	[0.4]	15	20	2
2$^{\bullet+}$	8	[2.9]	90	[1.3]	95	[0.2]	45	100	5
3a$^{\bullet+}$	70	[2.3]	100	[1.3]	30	[2.2]	14	4	1
3b$^{\bullet+}$	85	[2.3]	100	[1.3]	30	[1.7]	3	1	1
4$^{\bullet+}$	80	[2.5]	100	[1.3]	30	[1.7]	5	--	1
5$^{\bullet+}$	100	[2.4]	--		2	[2.7]	--	--	1
6$^{\bullet+}$	100	[2.6]	--		0.5		--	--	0.5
7$^{\bullet+}$	15	[c]	2		0.5		--	9	100
8$^{\bullet+}$	100	[2.5]	--		40	[1.1]	--	--	1
9$^{\bullet+}$	100	[2.8]	--		0.5		--	--	--
10$^{\bullet+}$	45	[2.5]	50	[1.5]	80	[0.3]	100	85	20
11$^{\bullet+}$	100	[2.4]	2	[1.9]	20	[1.6]	--	--	0.5
12$^{\bullet+}$	100	[2.3]	--	--	0.5		--	--	--
13$^{\bullet+}$	90	[2.3]	100	[1.5]	30	[2.3]	3	0.5	0.5
14$^{\bullet+}$	60	[2.1]	100	[1.4]	35	[1.7]	< 4	--	--

[a] Relative abundance measured by peak height and normalised to a total of 100 units for the base peak in the metastable ion spectrum for ions dissociating in the second field-free region. The MI spectra also contain weak signals (< 5) for the losses of C_2H_4, $C_3H_5^\bullet$ and C_3H_6 which are not presented.

[b] Numbers in square brackets represent kinetic energy releases, $T_{0.5}$, in kJ/mol as obtained from the width at half height of the peak ; the peaks had a Gaussian or approximately Gaussian profile. For loss of $H^\bullet$ the KER could not reliably be estimated because of overlap with the tail of the parent ion signal. For loss of H_2O from **1**$^{\bullet+}$, **2**$^{\bullet+}$ and **10**$^{\bullet+}$ the KERs are 2.8, 2.1 and 4.1 kJ/mol, respectively, while loss of CH_2O from **7**$^{\bullet+}$ and **10**$^{\bullet+}$ yields 0.8 and 1.3 kJ/mol, respectively.

[c] Composite metastable peak, see text for discussion.

Alkyl radical loss is important for each of the ionised ethers, but it is more strongly favoured for allylic species. Thus, an extremely high proportion of metastable ions **5**$^{\bullet+}$, **6**$^{\bullet+}$, **8**$^{\bullet+}$, **9**$^{\bullet+}$, **11**$^{\bullet+}$ and **12**$^{\bullet+}$ expels $CH_3^\bullet$. Indeed, apart from **2**$^{\bullet+}$ and **7**$^{\bullet+}$, all of the isomers show a pronounced loss of $CH_3^\bullet$. In addition, ions **3**$^{\bullet+}$, **4**$^{\bullet+}$ and **13**$^{\bullet+}$ eliminate large proportions of both $CH_3^\bullet$ and $C_2H_5^\bullet$.

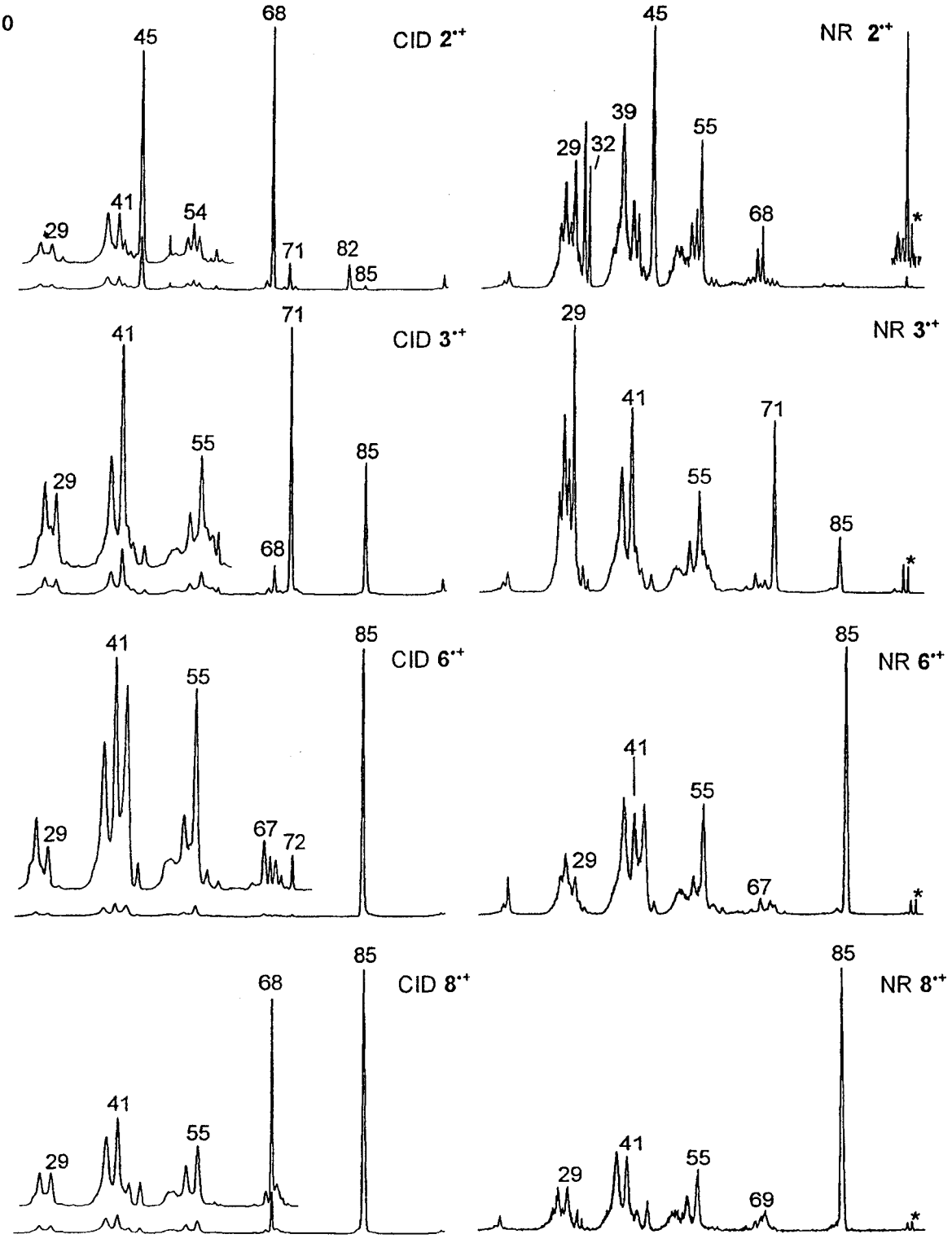

Figure 11.1.: CID mass spectra (2ffr, 8 keV ions) of $C_5H_9OCH_3^{\bullet+}$ ions **1**$^{\bullet+}$-**3**$^{\bullet+}$, **5**$^{\bullet+}$-**8**$^{\bullet+}$, **10**$^{\bullet+}$, **11**$^{\bullet+}$ and **14**$^{\bullet+}$ and a selection of the corresponding NR mass spectra (2ffr, 8 keV ions). The *m/z* 100 survivor ion peaks in the NR spectra are denoted by an asterisk.

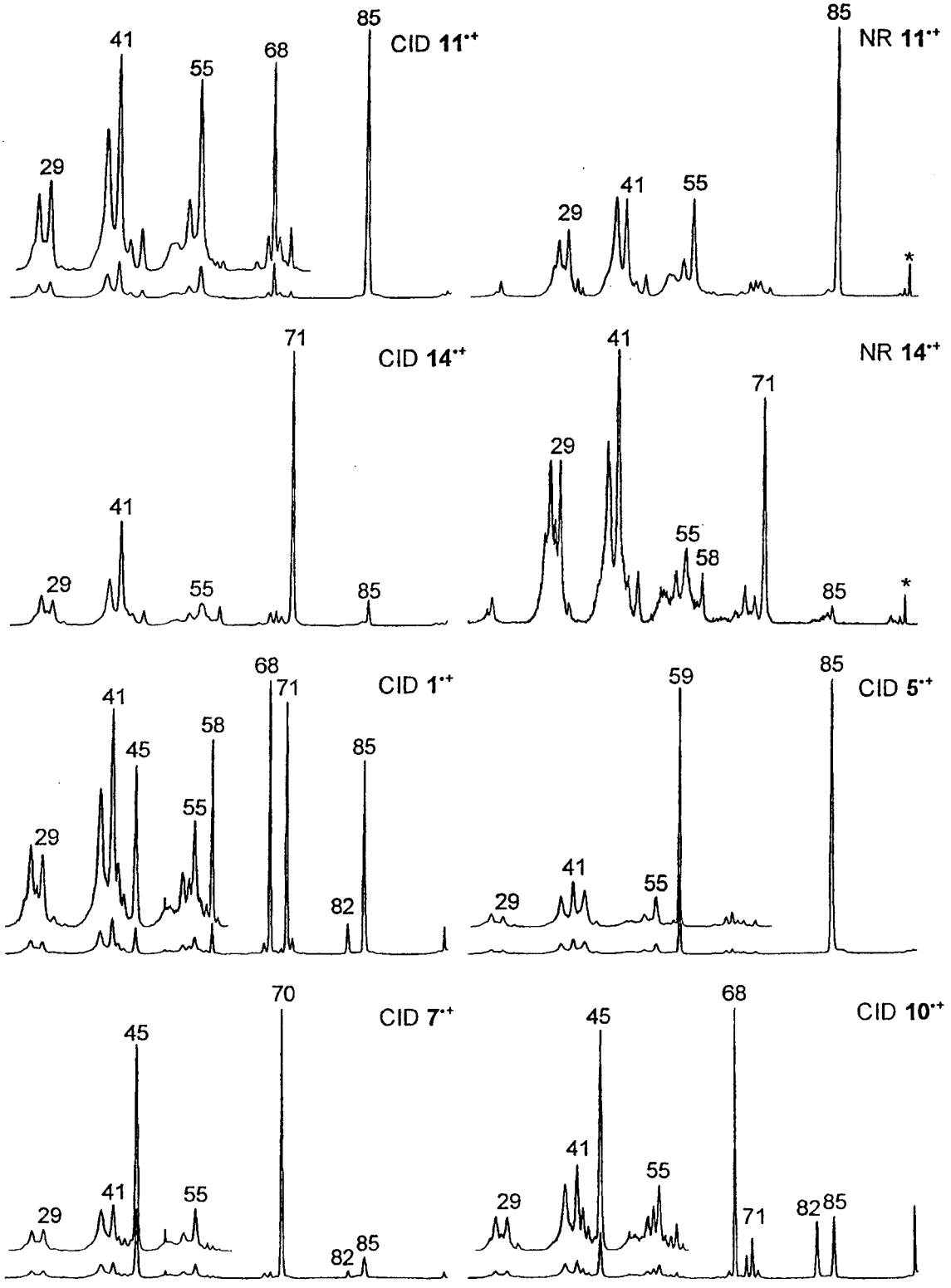

Figure 11.1 cont.

Elimination of CH_3OH is also of general importance, occurring prominently for **1**$^{\bullet+}$-**4**$^{\bullet+}$, **8**$^{\bullet+}$, **10**$^{\bullet+}$, **11**$^{\bullet+}$ and **13**$^{\bullet+}$; however, it is of minor importance for the other five isomers. In contrast to $CH_3^{\bullet}$ and $C_2H_5^{\bullet}$ elimination, CH_3OH loss is less favoured for *allylic* $C_5H_9OCH_3^{\bullet+}$ species.

Loss of $H^{\bullet}$ is of occasional importance : it features in the spectra of **2**$^{\bullet+}$ and **10**$^{\bullet+}$, but it does not occur for either of the other two homoallylic isomers, **5**$^{\bullet+}$ and **7**$^{\bullet+}$. Of the allylic isomers, only **3**$^{\bullet+}$, **4**$^{\bullet+}$ and **13**$^{\bullet+}$ lose $H^{\bullet}$ and that to a minor extent, see Table 11.1. For the homoallylic isomers there may be a correlation between the elimination of $H^{\bullet}$ and H_2O, both of which are prominent in the reactions of **2**$^{\bullet+}$ and **10**$^{\bullet+}$, see Table 11.1. In contrast, **5**$^{\bullet+}$ undergoes neither reaction and **7**$^{\bullet+}$ loses only a little H_2O. The only other metastable species to lose both $H^{\bullet}$ and H_2O is **1**$^{\bullet+}$, where the OCH_3 substituent and the double bond are separated by three CH_2 groups. Elimination of $H^{\bullet}$ and H_2O resemble CH_3OH loss in apparently being preferentially associated with $C_5H_9OCH_3^{\bullet+}$ species that are not allylic.

Other reactions involving the loss of C_2H_4, C_3H_6, $C_3H_5^{\bullet}$ and CH_2O occur to only a minor extent with one notable exception : CH_2O loss is the main reaction of metastable ions **7**$^{\bullet+}$.

Structure of the $C_5H_9OCH_3^{\bullet+}$ species, CID and NR spectra

Although tentative deductions about the structure of isomeric species are possible on the basis of the behaviour of metastable ions, more secure conclusions may be made when their CID and NR spectra are also considered. These spectra were obtained for the complete set of isomers, see Figure 11.1 for a selection, and they indicate that most of the isomeric $C_5H_9OCH_3^{\bullet+}$ species retain independent structures, rather than isomerising to common intermediates. However, this generalisation is not true for the three isomers, **3**$^{\bullet+}$, **4**$^{\bullet+}$ and **13**$^{\bullet+}$, whose CID and NR spectra are even more closely similar than their MI spectra. These results suggest strongly that these ions react via closely related mechanisms, probably involving the same intermediates and low lying transition states. This behaviour may be rationalised in terms of a mechanism involving 1,2-H and 1,2-C_2H_5 shifts as depicted in Scheme 11.2.

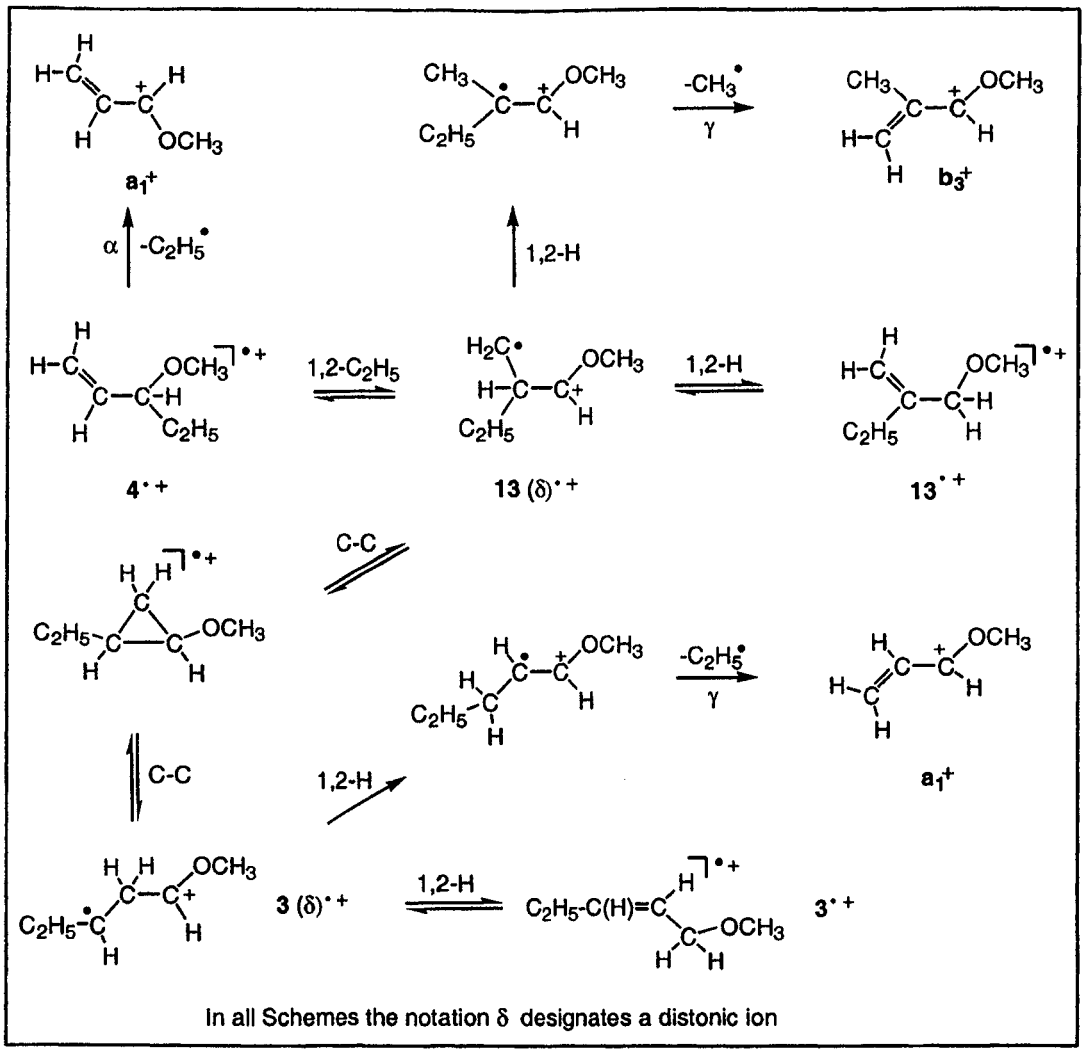

Scheme 11.2

It is noteworthy that the analogous process for the corresponding isomeric $C_5H_9OCH_3^{\bullet+}$ species, which could interconvert via 1,2-H and 1,2-CH_3 shifts, does not occur so easily, if at all. The superior aptitude for migration of a $C_2H_5^{\bullet}$ group may be responsible for this contrast. It is well-known that the rate of detachment of a $CH_3^{\bullet}$ by α- or γ-cleavage is much less than that of $C_2H_5^{\bullet}$, even though the former process often produces more stable products [38-40]. Moreover, the relative rate for elimination of a primary alkyl radical by α- or γ-cleavage of a variety of radical cations is greatest for $C_2H_5^{\bullet}$ loss [39-42]. Similar effects may make the 1,2-C_2H_5 shifts of Scheme 11.2 more facile than the corresponding 1,2-CH_3 shifts in the homologous $C_4H_7OCH_3^{\bullet+}$ system.

Not unexpectedly, the CID spectra of many of the $C_5H_9OCH_3^{\bullet+}$ species are dominated by peaks which also appear in the MI spectra. This is particularly true for ions **6**$^{\bullet+}$, **9**$^{\bullet+}$ and **12**$^{\bullet+}$ whose closely similar CID spectra are dominated by $CH_3^{\bullet}$ loss (*m/z* 85), see Figure 11.1 for a representative spectrum. The NR spectra of this set of isomers are also very close as are the KERs for the preponderant loss of $CH_3^{\bullet}$ in their MI spectra. Nevertheless, these ions do not interconvert to a major extent since, in agreement with earlier CID results [31,32], the $[M - CH_3]^+$ ions formed from **6**$^{\bullet+}$, **9**$^{\bullet+}$ and **12**$^{\bullet+}$ have different structures.

In the majority of these spectra, the most intense peak which contains no contribution for decomposition of unactivated metastable ions is *m/z* 41. The formation of this fragment $C_3H_5^+$ ion is typical of precursor ions in which there are saturated or slightly unsaturated alkyl chains. In contrast, for **2**$^{\bullet+}$, **7**$^{\bullet+}$ and **10**$^{\bullet+}$, the strongest signal associated specifically with collision-induced dissociation is at *m/z* 45. This peak corresponds to $C_2H_5O^+$ ions of structure $^+CH_2OCH_3$ arising by allylic cleavage of these ionised homoallylic ethers. A similar signal, though marginally less pronounced, see Figure 11.1, is present in the CID spectrum of **1**$^{\bullet+}$, in which $^+CH_2OCH_3$ may be formed by homoallylic cleavage. Similarly, the CID spectrum of the ionised secondary homoallylic ether, **5**$^{\bullet+}$, also contains a prominent signal arising by allylic fission, but this time at *m/z* 59 corresponding to $C_3H_7O^+$ ions of structure $CH_3C^+(H)OCH_3$. The absence of an appreciable signal at *m/z* 59 in the spectrum of **6**$^{\bullet+}$ is good evidence that **5**$^{\bullet+}$ and **6**$^{\bullet+}$ do not rapidly interconvert or isomerise to a common structure and that $C_3H_5^{\bullet}$ elimination is associated specifically with **5**$^{\bullet+}$. The peaks at *m/z* 45 and 59 arising by allylic cleavage of the ionised ethers are analytically useful because they allow homoallylic and allylic ethers to be distinguished from their allylic counterparts.

Secondly, the CID spectra reveal that skeletal isomerisation of $C_5H_9OCH_3^{\bullet+}$ species by allylic rearrangement is not facile. Two pairs of isomeric ions which might be expected to interconvert by an allylic rearrangement show distinct reactivities. Thus, **8**$^{\bullet+}$ and **9**$^{\bullet+}$ have different CID spectra, as do **11**$^{\bullet+}$ and **12**$^{\bullet+}$. Parallel conclusions follow from the different NR (and also MI) spectra of the members of these pairs of ions. Only in the case of **3**$^{\bullet+}$ and **4**$^{\bullet+}$ are similar spectra found for $C_5H_9OCH_3^{\bullet+}$ species which could isomerise by allylic rearrangement.

However, this similarity reflects the ease of the 1,2-H and 1,2-C_2H_5 shifts depicted in Scheme 11.2, rather than an allylic rearrangement.

There are superficial similarities in the MI spectra of $\mathbf{1}^{\bullet+}$ and the cyclic species $\mathbf{14}^{\bullet+}$, but H_2O is not lost from metastable ions $\mathbf{14}^{\bullet+}$ at a significant rate, whereas it is an important reaction of $\mathbf{1}^{\bullet+}$. Consequently, at least part of the population of the dissociating ions generated as $\mathbf{1}^{\bullet+}$ does not isomerise to $\mathbf{14}^{\bullet+}$. This conclusion is clearly borne out by their different CID spectra. In a recent detailed labelling study [42] it is proposed that $C_2H_5^{\bullet}$ and $CH_3^{\bullet}$ loss from $\mathbf{1}^{\bullet+}$ may involve rearrangement to $\mathbf{14}^{\bullet+}$ or species accessible to $\mathbf{14}^{\bullet+}$, but expulsion of H_2O and CH_3OH occur by routes that do not entail isomerisation to $\mathbf{14}^{\bullet+}$.

The CID spectra of the $C_5H_9OCH_3^{\bullet+}$ species are further evidence against the proposal that ionised phytyl methyl ether $C_{16}H_{33}(CH_3)C{=}CHCH_2OCH_3^{\bullet+}$ rearranges to ionised isophytyl methyl ether $CH_2{=}CH\text{-}C(CH_3)(C_{16}H_{33})OCH_3^{\bullet+}$ prior to loss of a γ-alkyl substituent [43]. This suggestion is inconsistent with CID studies [44] which established that the structure of the resultant $[M\text{-}(C_{16}H_{33})]^+$ ion is $CH_3CH{=}CH\text{-}C^+(H)\text{-}OCH_3$, $\mathbf{b_1}^+$. The isomeric oxonium ion, $CH_2{=}CHC^+(CH_3)OCH_3$, $\mathbf{b_2}^+$, would be formed if allylic rearrangement to ionised isophytyl methyl ether preceded $C_{16}H_{33}^{\bullet}$ loss. Later CID investigations showed that a range of ionised alkenyl methyl ethers with two γ-alkyl substituents, $R^1R^2C{=}CHCH_2OCH_3^{\bullet+}$, expel an alkyl radical without undergoing allylic rearrangement [44].

The NR spectra underline the conclusions from the CID spectra and bear further evidence that most of the ionised pentenyl methyl ethers have distinct structures.

Two further aspects of the NR spectra deserve consideration:

(i) The NR spectra presented in Figure 11.1 are those of ethers that display sizeable molecular ions in their mass spectra : 15 % of base peak for $\mathbf{2}^{\bullet+}$ and $\mathbf{3}^{\bullet+}$, 35 % for $\mathbf{6}^{\bullet+}$ and $\mathbf{8}^{\bullet+}$, 60 % for $\mathbf{11}^{\bullet+}$ and 20 % for $\mathbf{14}^{\bullet+}$. The relative intensity of the survivor ion signals in the NR spectra is much lower, particularly for $\mathbf{2}^{\bullet+}$, $\mathbf{6}^{\bullet+}$ and $\mathbf{8}^{\bullet+}$. This suggests that a sizeable fraction of the stable ions has undergone extensive rearrangement into distonic ions and other structures that have no neutral counterpart and which dissociate upon neutralisation. For $\mathbf{11}^{\bullet+}$, the survivor ion abundance was sufficiently high to subject the mass selected beam of these ions

to a CID experiment in the third field-free region (3ffr). The resulting NR/CID spectrum is shown in Figure 11.2a. This spectrum is closely similar to the 3ffr CID spectrum of the source generated ions, see Figure 11.2b, which demonstrates that the NR survivor ions have (largely) retained their structure integrity.

(ii) All NR spectra contain a significant contribution of collision-induced dissociative ionisation (CIDI) [37b] of neutral species generated in the decomposition of the metastable ions and, to a lesser extent, collision-induced dissociation promoted by the neutralisation gas. Thus, for example, the narrow peaks at *m/z* 32 and *m/z* 29 in the NR spectra of $\mathbf{2}^{\bullet+}$ and $\mathbf{3}^{\bullet+}$, largely stem from CIDI of the abundant CH_3OH and $C_2H_5^{\bullet}$ neutral losses that characterise their MI spectra. The CIDI efficiency of a given neutral strongly depends on its translational energy and this may explain why the *m/z* 15 CIDI peak in e.g. the NR spectrum of $\mathbf{6}^{\bullet+}$ is of only moderate intensity.

From the foregoing discussion it follows that, with the exception of $\mathbf{3}^{\bullet+}$, $\mathbf{4}^{\bullet+}$ and $\mathbf{13}^{\bullet+}$, each of the metastable $C_5H_9OCH_3^{\bullet+}$ species has a unique reactivity. In the next sections, the reactions of selected labelled isotopologues are presented to assist in the formulation of mechanistic proposals for the major dissociations of the low-energy ether ions.

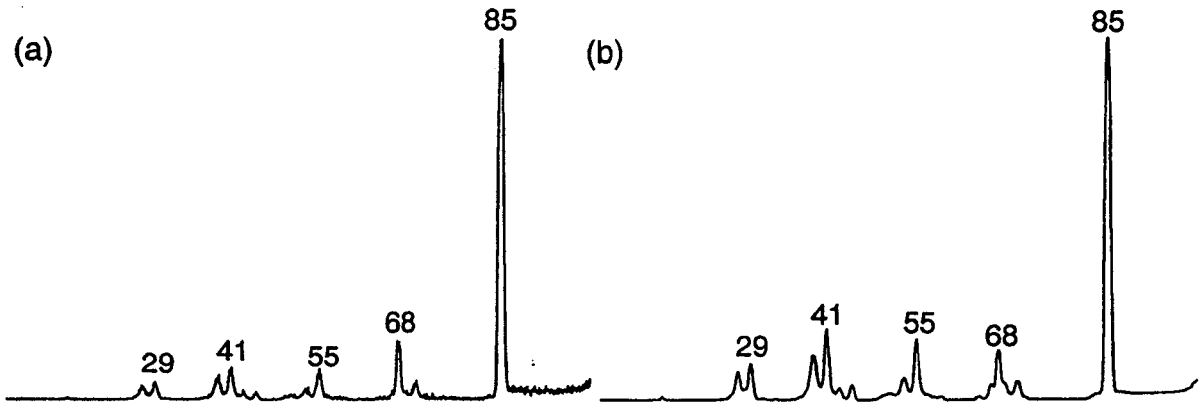

Figure 11.2. NR/CID and comparative CID mass spectra (3ffr, 8 keV ions) of $C_5H_9OCH_3^{\bullet+}$ ions $\mathbf{11}^{\bullet+}$, $CH_3CH{=}C(CH_3)CH_2OCH_3^{\bullet+}$.

Alkyl radical loss from $C_5H_9OCH_3^{\bullet+}$ species

Since alkyl radical elimination at high internal energies is one of the few aspects of the chemistry of ionised pentenyl and hexenyl methyl ethers to have received a fair amount of attention [31,32], this discussion focuses on new information pertaining to the behaviour of the low-energy $C_5H_9OCH_3^{\bullet+}$ ions. The $C_5H_9O^+$ and $C_4H_7O^+$ product ion structures for the $CH_3^\bullet$ and $C_2H_5^\bullet$ losses were determined from their CID spectra (not shown) which are in good qualitative agreement with those reported previously under somewhat different experimental conditions [31,32]. A metastable ion study of various $C_5H_9O^+$ ions, which also addresses a criterion to establish the isomeric purity of the ions pertinent to this study ($\mathbf{b_1}^+$ - $\mathbf{b_3}^+$), is presented elsewhere [33].

*Loss of $CH_3^\bullet$ from $CH_3CH{=}CHCH(CH_3)OCH_3^{\bullet+}$, **6**$^{\bullet+}$, $CH_2{=}CHC(CH_3)_2OCH_3^{\bullet+}$, **9**$^{\bullet+}$ and $CH_2{=}C(CH_3)CH(CH_3)OCH_3^{\bullet+}$, **12**$^{\bullet+}$*

Elimination of $CH_3^\bullet$ dominates the MI spectra of these species. Formation of product ion $\mathbf{b_2}^+$ by simple cleavage of the tertiary species, **12**$^{\bullet+}$, has been shown to be a satisfactory explanation for $CH_3^\bullet$ loss at high internal energies [31,32]. However, the secondary isomers, **6**$^{\bullet+}$ and **9**$^{\bullet+}$, expel $CH_3^\bullet$ by two mechanisms, to give a mixture of $\mathbf{b_2}^+$ with a less stable oxonium ion, $\mathbf{b_1}^+$, and $CH_2{=}C(CH_3)CHOCH_3^+$, $\mathbf{b_3}^+$ respectively [31,32]. Moreover, the proportion of $\mathbf{b_1}^+$ increases as the internal energy of the dissociating population of radical cations decreases [30]. Our CID spectra confirm these conclusions. In addition, the behaviour of the labelled analogues of **6**$^{\bullet+}$ and **9**$^{\bullet+}$, see Table 11.2, reveals that loss of $CH_3^\bullet$ near threshold occurs by the routes involving skeletal isomerisation with over 90 % selectivity. There is a negligible contribution for expulsion of methyl radicals containing both protium (H) and deuterium (D) atoms from metastable ions **6**$^{\bullet+}$ [1-CD_3] and **9**$^{\bullet+}$ [1-CD_3]. Thus, the positional integrity of the labelled methyl group is not eroded during the steps leading to rearrangement. All these observations are consistent with the mechanism of Scheme 11.3.

However, the picture is complicated by the loss of both $CD_3^\bullet$ and $CH_3^\bullet$ from metastable ions **9**$^{\bullet+}$ [1-1'-$(CD_3)_2$]. One possible explanation is that a proportion (~ 25 %) of ions generated

Table 11.2. Methyl radical loss [a] from metastable ionised labelled methyl pentenyl ethers.

Ion Loss →	$CH_3^{\bullet}$ [$^{13}CH_3^{\bullet}$]	$CH_2D^{\bullet}$	$CHD_2^{\bullet}$	$CD_3^{\bullet}$
$\mathbf{1}^{\bullet+}$ [OCD_3]	100	--	--	< 3[b]
$\mathbf{1}^{\bullet+}$ [1,1-D_2]	100	35	--	--
$\mathbf{2}^{\bullet+}$ [OCD_3]	100	20	30	[b]
$\mathbf{2}^{\bullet+}$ [1,1-D_2]	100	< 50	55	--
$\mathbf{2}^{\bullet+}$ [1,1-D_2-OCD_3]	100	65	65	[b]
$\mathbf{3}^{\bullet+}$ [OCD_3] [**3a** & **3b**]	100	< 0.5	--	--
$\mathbf{4}^{\bullet+}$ [OCD_3]	100	< 0.5	--	--
$\mathbf{4}^{\bullet+}$ [4,4-D_2]	100	4	5	--
$\mathbf{4}^{\bullet+}$ [5-CD_3]	100	17	19	95
$\mathbf{5}^{\bullet+}$ [OCD_3]	100	~ 1	--	--
$\mathbf{6}^{\bullet+}$ [OCD_3]	100	~ 1	--	--
$\mathbf{6}^{\bullet+}$ [1-CD_3]	100	--	--	7
$\mathbf{7}^{\bullet+}$ [OCD_3]	100	30	10	9
$\mathbf{7}^{\bullet+}$ [$O^{13}CH_3$]	100 [0]	--	--	--
$\mathbf{8}^{\bullet+}$ [OCD_3]	100	--	--	--
$\mathbf{9}^{\bullet+}$ [OCD_3]	100	< 0.5	--	--
$\mathbf{9}^{\bullet+}$ [1-1'-$(CD_3)_2$]	25	~ 3	--	100
$\mathbf{9}^{\bullet+}$ [$O^{13}CH_3$]	100 [< 2]	--	--	--
$\mathbf{10}^{\bullet+}$ [OCD_3]	100	~ 1	--	< 13 [b]
$\mathbf{11}^{\bullet+}$ [OCD_3]	100	< 0.5	--	--
$\mathbf{12}^{\bullet+}$ [OCD_3]	100	1	--	--
$\mathbf{12}^{\bullet+}$ [1-CD_3]	100	--	--	5
$\mathbf{13}^{\bullet+}$ [OCD_3]	100	0.5	--	--
$\mathbf{14}^{\bullet+}$ [OCD_3]	100	< 0.5	--	--

[a] Relative abundance measured by peak height and normalised to a total of 100 units for the base peak in the metastable ion spectrum for ions dissociating in the second field-free region. The KER values for these processes were unexceptional for all of the isomers but $\mathbf{7}^{\bullet+}$ which displays composite peaks, see text for discussion.

[b] Part or all of the signal may arise from loss of H_2O rather than $CD_3^{\bullet}$; for the isotopologues of $\mathbf{2}^{\bullet+}$ these signals have intensities of ~ 500.

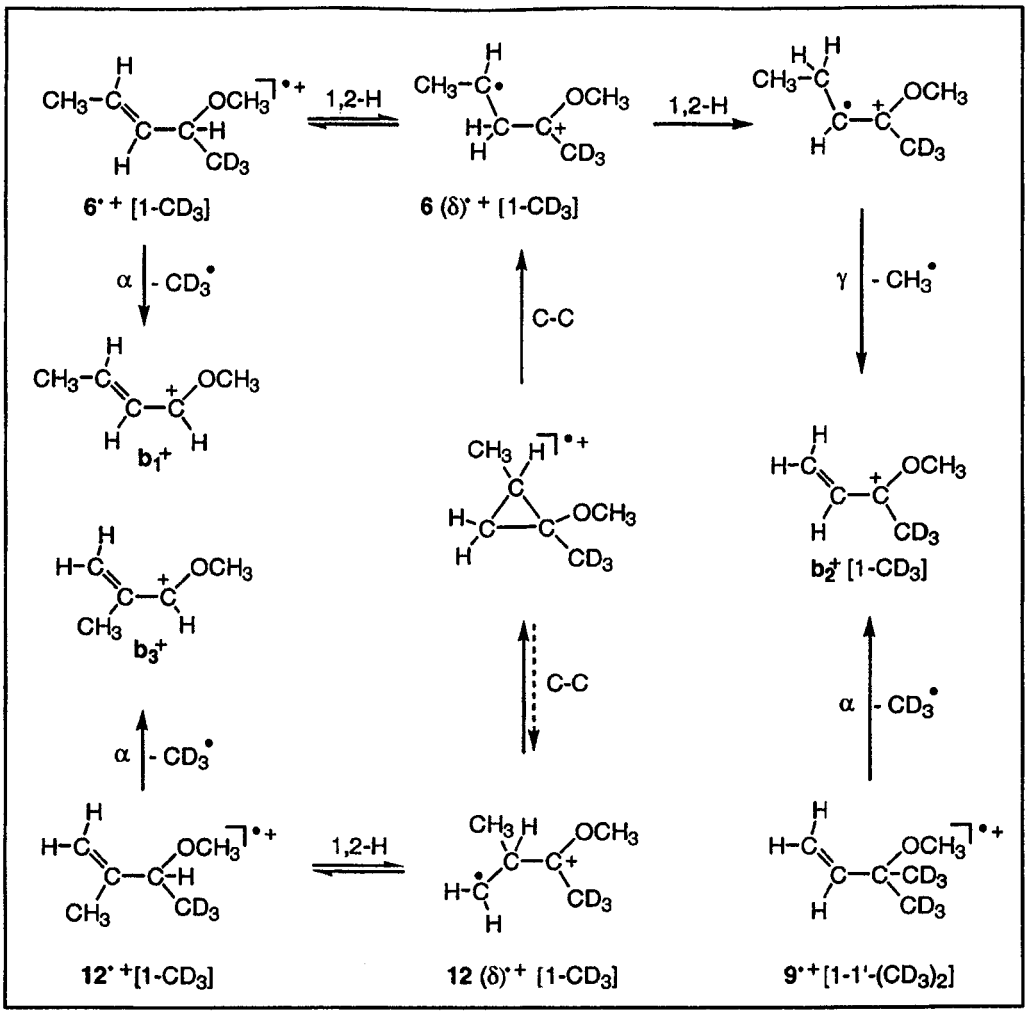

Scheme 11.3

as $\mathbf{9}^{\bullet+}$ undergo an additional rearrangement at low internal energies to give species in which a new methyl group is formed from the hydrogen atoms of the original vinyl group, as shown in Scheme 11.4. This route competes poorly with simple fission because it entails 1,2-H/D shifts to the radical centre of a distonic ion; such 1,2-H shifts to radical centres are known to be slow and often rate-limiting [14,39,46-48].

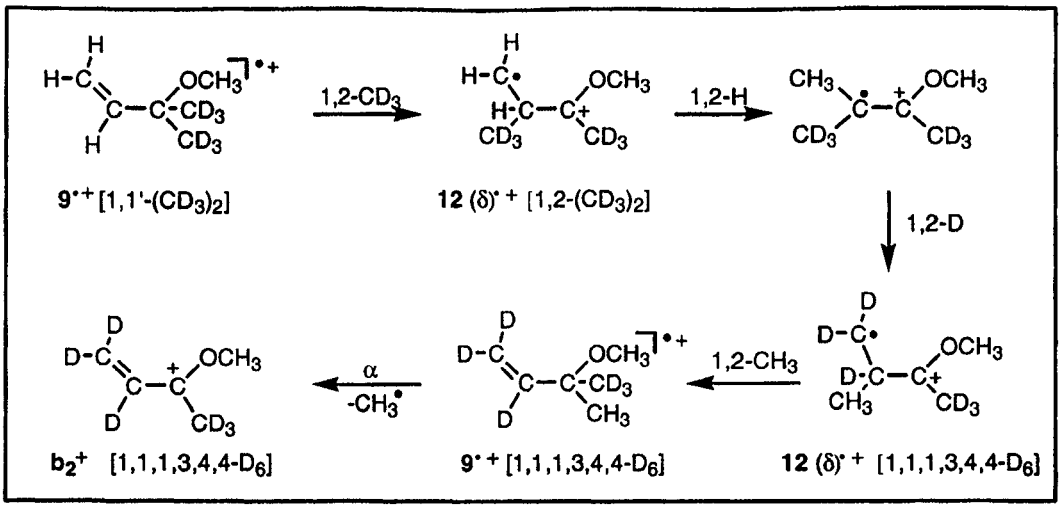

Scheme 11.4

Loss of $CH_3^\bullet$ from $CH_2{=}CHCH_2CH(CH_3)OCH_3^{\bullet+}$, $5^{\bullet+}$

Previous studies did not resolve the question of the structure of the $[M - CH_3]^+$ ion formed from $\mathbf{5}^{\bullet+}$. Our new CID data are consistent with formation of a mixture of $\mathbf{b}_1^+$ and $\mathbf{b}_2^+$, as is produced by loss $CH_3^\bullet$ from $\mathbf{6}^{\bullet+}$.

If this interpretation is correct, it is likely that $\mathbf{5}^{\bullet+}$ rearranges to its allylic isomer $\mathbf{6}^{\bullet+}$, or species accessible to $\mathbf{6}^{\bullet+}$ by a sequence of H-shifts involving one or more distonic ions. A plausible possibility is a direct 1,4-H shift to give the same distonic ion, $\mathbf{6}(\delta)^{\bullet+}$, as is accessible to $\mathbf{6}^{\bullet+}$ by a 1,2-H shift, see Scheme 11.5. This rearrangement must be irreversible because $\mathbf{6}^{\bullet+}$ does not show the side reaction, $C_3H_5^\bullet$ elimination, which is uniquely associated with $\mathbf{5}^{\bullet+}$. This minor process in the MI spectrum - which becomes prominent upon collisional activation - may be attributed to direct α-cleavage of $\mathbf{5}^{\bullet+}$, with formation of $CH_3C^+(H)OCH_3$. Apart from this additional dissociation channel, metastable ions $\mathbf{5}^{\bullet+}$ resemble $\mathbf{6}^{\bullet+}$ in losing predominantly $CH_3^\bullet$ (~95 %), apparently to give the same ionic products.

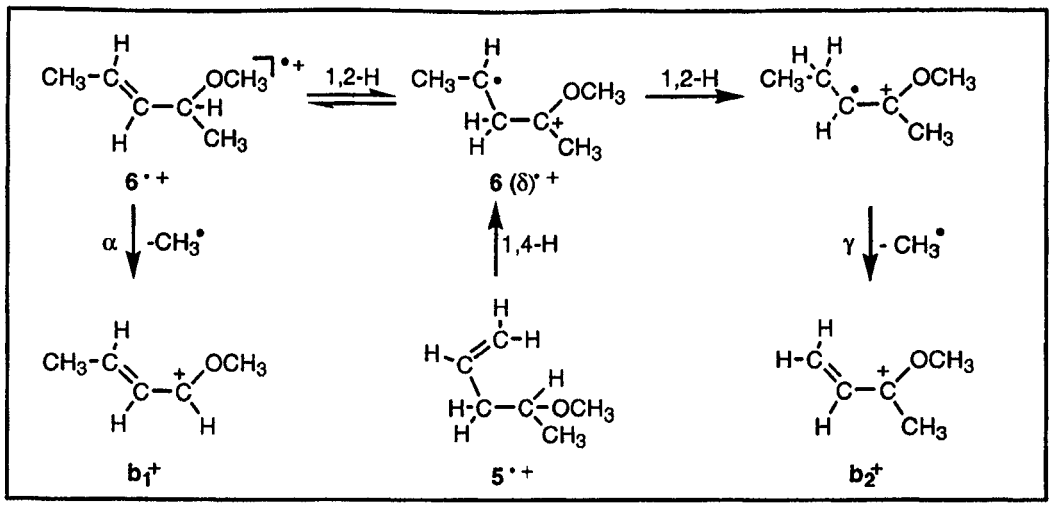

Scheme 11.5

Loss of $CH_3^{\bullet}$ from $CH_2{=}C(CH_3)(CH_2)_2OCH_3^{\bullet+}$, *7*$^{\bullet+}$ *and* $(CH_3)_2C{=}CHCH_2OCH_3^{\bullet+}$, *8*$^{\bullet+}$

The structure of the $[M - CH_3]^+$ product ion in the normal EI spectra of **7** and **8** has been shown to be $\mathbf{b_2}^+$ [31,32]. A sequence of H-shifts converts **7**$^{\bullet+}$ and **8**$^{\bullet+}$ into the ionised enol ether, $(CH_3)_2CHCH{=}CHOCH_3^{\bullet+}$, which fragments by γ-cleavage, see Scheme 11.6. Our CID product ion spectra confirm these findings. In addition, the behaviour of the labelled analogues of **7**$^{\bullet+}$ and **8**$^{\bullet+}$ supports this broad interpretation and establishes that the chemistries of these isomeric species, though related, differ substantially from each other.

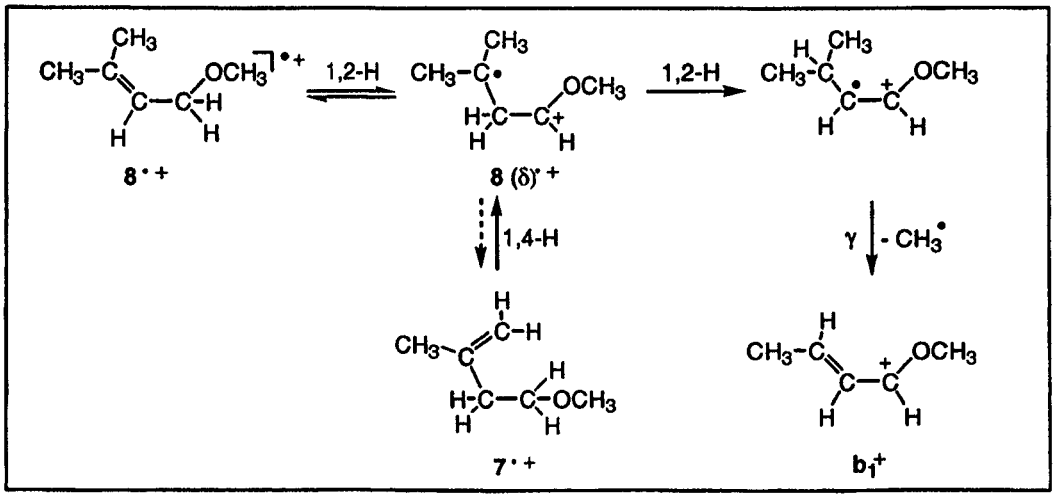

Scheme 11.6

Thus, the OCD_3 group of **8**$^{\bullet+}$ [OCD_3] is exclusively retained in the fragment ion arising by loss of $CH_3^{\bullet}$; furthermore, this group is incorporated in the expelled molecule of methanol in the other main fragmentation of this allylic species. Consequently, H-shifts between the O-CH_3 substituent and the pentenyl group do not precede dissociation of **8**$^{\bullet+}$.

In contrast, although **7**$^{\bullet+}$ [OCD_3] does expel $CH_3^{\bullet}$ with comparatively high selectivity (~ 70%), there are appreciable contributions from $CH_2D^{\bullet}$ and $CHD_2^{\bullet}$ loss, both of which give rise to a composite metastable peak containing a very broad component (overall $T_{0.5}$ = 15-17 kJ/mol). These data show that a second channel in which the final step has a substantial reverse critical energy operates to a minor extent in $CH_3^{\bullet}$ loss from metastable **7**$^{\bullet+}$. This route is preceded by exchange of hydrogen atoms initially located in the pentenyl chain with those of the methoxy group. Some parallel effects have been reported for the lower homologue, CH_2=$CHCHCH_2OCD_3^{\bullet+}$, which also loses partially labelled methyl radicals, but this species differs from its allylic isomer, CH_3CH=$CHCH_2OCD_3^{\bullet+}$, in forming a 5-membered ring oxonium ion [35]. However, $CH_3^{\bullet}$ loss from **7**$^{\bullet+}$ and **8**$^{\bullet+}$ normally produces the same conjugated oxonium ion $\mathbf{b_1}^+$. A detailed mechanism for the alternative minor route for $CH_3^{\bullet}$ loss from **7**$^{\bullet+}$ cannot be deduced from the available data, but facile H transfers may occur by several steps, including those shown in Scheme 11.6.

Moreover, CH_2O loss, which is actually the main fragmentation of **7**$^{\bullet+}$, also is preceded by hydrogen migration between the methoxy group and the pentenyl chain. Thus, **7**$^{\bullet+}$ [OCD_3] loses more CHDO than CD_2O (55 vs 40 %) and there is even a sizeable contribution from CH_2O elimination (15 %). Further discussion of this reaction is presented below.

*Loss of $CH_3^{\bullet}$ from CH_2=$CHCH(CH_3)CH_2OCH_3^{\bullet+}$, **10**$^{\bullet+}$ and CH_3CH=$C(CH_3)CH_2OCH_3^{\bullet+}$, **11**$^{\bullet+}$*

Previous research [32,33] established that $CH_3^{\bullet}$ elimination from **11**$^{\bullet+}$ yields $\mathbf{b_3}^+$, but could not determine the structure of the product ion formed when $CH_3^{\bullet}$ is lost from **10**$^{\bullet+}$. Our product ion CID spectra suggest that the ionic fragment produced by this fragmentation of **10**$^{\bullet+}$ is predominantly $\mathbf{b_3}^+$.

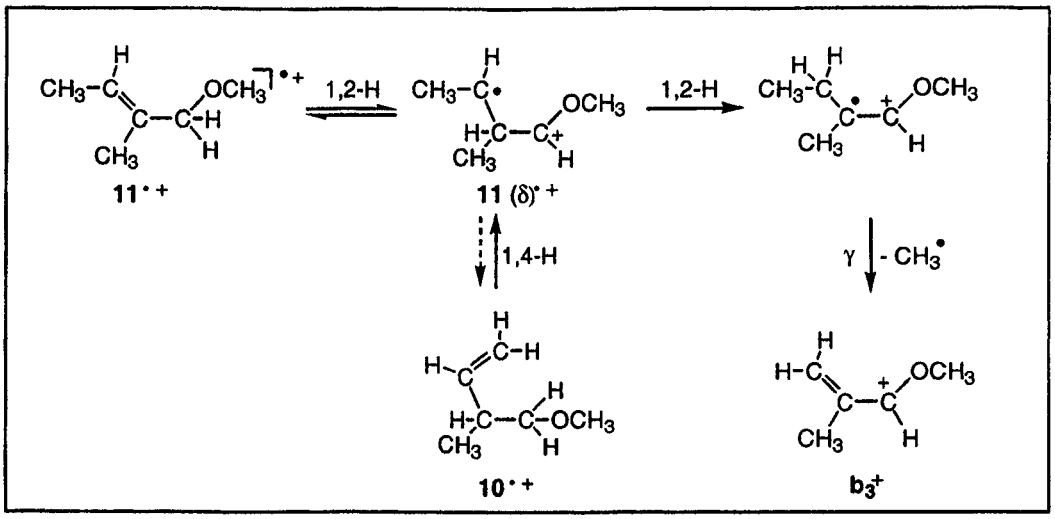

Scheme 11.7

The behaviour of metastable ions $\mathbf{10}^{\bullet+}$ [OCD_3], which expel $CH_3^\bullet$ with high selectivity, is consistent with the mechanism proposed previously, in which consecutive 1,2-H shifts, the second of which is slow because it terminates at a radical site, leads to an ionised enol ether, which then fragments via γ-cleavage, see Scheme 11.7. Isomerisation of $\mathbf{10}^{\bullet+}$ to the same ionised enol ether via successive 1,4- and 1,2-H shifts offers a plausible explanation for $CH_3^\bullet$ elimination, but other route(s) leading to isomeric oxonium ions may compete to a limited extent. The competition of other reactions, particularly loss of $H^\bullet$, H_2O, $C_2H_5^\bullet$, and CH_2O, in the dissociation of $\mathbf{10}^{\bullet+}$ but not $\mathbf{11}^{\bullet+}$ shows that any rearrangement of $\mathbf{10}^{\bullet+}$ to $\mathbf{11}^{\bullet+}$ (or structures accessible to $\mathbf{11}^{\bullet+}$) prior to $CH_3^\bullet$ expulsion is irreversible. The marginally greater $T_{0.5}$ value for $CH_3^\bullet$ loss from $\mathbf{10}^{\bullet+}$ compared to that starting from $\mathbf{11}^{\bullet+}$ is in accord with this view.

Loss of $CH_3^\bullet$ and $C_2H_5^\bullet$ from $C_2H_5CH{=}CHCH_2OCH_3^{\bullet+}$, $\mathbf{3}^{\bullet+}$, $CH_2{=}CHCH(C_2H_5)OCH_3^{\bullet+}$, $\mathbf{4}^{\bullet+}$ and $CH_2{=}C(C_2H_5)CH_2OCH_3^{\bullet+}$, $\mathbf{13}^{\bullet+}$

Our new CID spectra indicate that the common $[M - CH_3]^+$ ion formed from these isomers is $\mathbf{b_3}^+$. Formation of this branched structure, rather than the linear isomer $\mathbf{b_1}^+$, is at first sight surprising, but it may be explained as shown in Scheme 11.2 : a 1,2-H shift in the appropriate distonic ion, $\mathbf{3}(\delta)^{\bullet+}$, gives an ionised enol ether which may expel $CH_3^\bullet$ by γ-cleavage [33,34]. Loss of $C_2H_5^\bullet$ may be explained by similar routes, including direct α-

cleavage of $\mathbf{4}^{\bullet+}$ and consecutive 1,2-H shifts in $\mathbf{3}^{\bullet+}$, followed by γ-cleavage, as postulated previously; both these routes give $CH_2{=}CHCHOCH_3^+$, $\mathbf{a}_1^+$ [32,33]. A more complete analysis of this system will be presented separately [49].

Loss of $CH_3^\bullet$ and $C_2H_5^\bullet$ from $CH_2{=}CH(CH_2)_3OCH_3^{\bullet+}$, $\mathbf{1}^{\bullet+}$ and $CH_3CH{=}CH(CH_2)_2OCH_3^{\bullet+}$, $\mathbf{2}^{\bullet+}$

Both the non-allylic ether ions, $\mathbf{1}^{\bullet+}$ and $\mathbf{2}^{\bullet+}$, with a methoxy group at one end of a linear pentenyl chain, eliminate a considerable proportion of $C_2H_5^\bullet$, see Table 11.1 ; ions $\mathbf{1}^{\bullet+}$ also expel a similar amount of $CH_3^\bullet$, but $\mathbf{2}^{\bullet+}$ undergoes this fragmentation to only a very limited extent.

Product ion analysis based on CID indicates that $CH_3^\bullet$ loss from $\mathbf{1}^{\bullet+}$ and $\mathbf{2}^{\bullet+}$ yields the same branched conjugated oxonium ion, $\mathbf{b}_3^+$, as is formed from $\mathbf{3}^{\bullet+}$, $\mathbf{4}^{\bullet+}$, $\mathbf{10}^{\bullet+}$, $\mathbf{11}^{\bullet+}$ and $\mathbf{13}^{\bullet+}$. A logical interpretation is that $\mathbf{1}^{\bullet+}$ and $\mathbf{2}^{\bullet+}$ are able to isomerise onto the same part of the $C_5H_9OCH_3^{\bullet+}$ manifold as is involved in the dissociation of $\mathbf{3}^{\bullet+}$, $\mathbf{6}^{\bullet+}$ and $\mathbf{13}^{\bullet+}$, thereby giving access to the 2-ethyl-1-methoxycyclopropane ion and the branched distonic ion $\mathbf{13}(\delta)^{\bullet+}$. The required rearrangement may be accomplished by various sequences of 1,2-, 1,4- and 1,5-H shifts, including that shown for $\mathbf{1}^{\bullet+}$, see Scheme 11.8. The behaviour of ^{2}H-labelled analogues of $\mathbf{1}^{\bullet+}$ is consistent with rearrangement to $\mathbf{14}^{\bullet+}$ (or species accessible to $\mathbf{14}^{\bullet+}$) prior to ethyl or methyl radical loss. These reactions are analysed in more detail elsewhere [42].

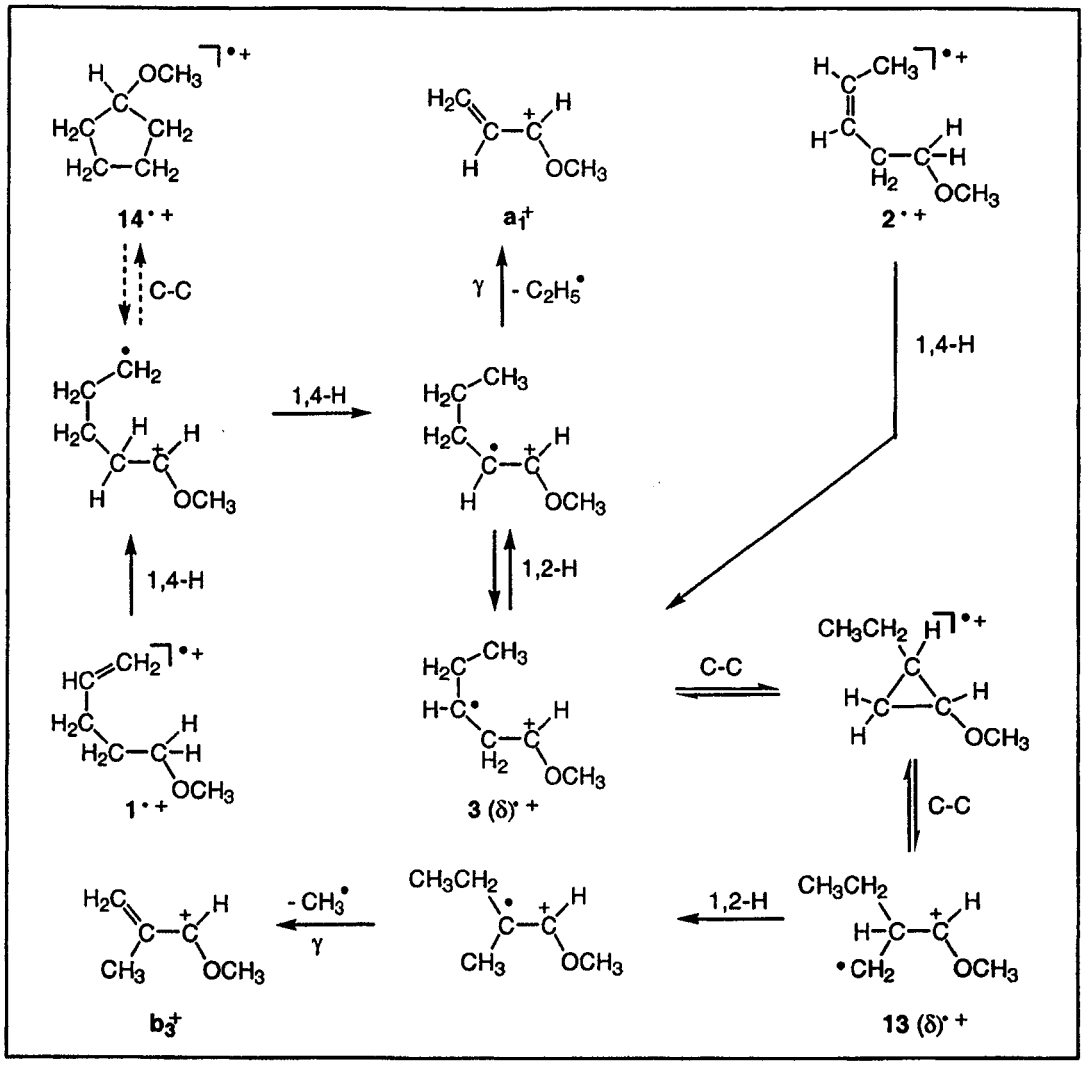

Scheme 11.8

Table 11.3. Ethyl radical loss [a] from metastable ionised labelled pentenyl methyl ethers.

Ion	Loss →	$C_2D_5^{\bullet}$	$C_2HD_4^{\bullet}$	$C_2H_2D_3^{\bullet}$	$C_2H_3D_2^{\bullet}$	$C_2H_4D^{\bullet}$	$C_2H_5^{\bullet}$
$\mathbf{1}^{\bullet+}$	$[OCD_3]$	--	--	1	8	2	100
$\mathbf{1}^{\bullet+}$	$[1,1\text{-}D_2]$	--	--	--	13	100	90
$\mathbf{2a}^{\bullet+}$	$[OCD_3]$	--	< 2	100	8	6	--
$\mathbf{2a}^{\bullet+}$	$[1,1\text{-}D_2]$	6	20	35	100	40	17
$\mathbf{2}^{\bullet+}$	$[1,1\text{-}D_2\text{-}OCD_3]$	55 [b]	< 2	5	100	15	5
$\mathbf{3b}^{\bullet+}$	$[OCD_3]$	--	--	0.5	1	1	100
$\mathbf{4}^{\bullet+}$	$[OCD_3]$	--	--	2	11	13	100
$\mathbf{4}^{\bullet+}$	$[4,4\text{-}D_2]$	--	--	--	100	30	70
$\mathbf{4}^{\bullet+}$	$[5\text{-}CD_3]$	--	--	85 [c]	100	35	16
$\mathbf{10}^{\bullet+}$	$[OCD_3]$	--	--	10	100	11	12
$\mathbf{13}^{\bullet+}$	$[OCD_3]$	--	--	1	1	1	100
$\mathbf{14}^{\bullet+}$	$[OCD_3]$	--	--	--	--	< 0.5	100

[a] Relative abundance measured by peak height and normalised to a total of 100 units for the base peak in the metastable ion spectrum for ions dissociating in the second field-free region.

[b] Most or all of this signal arises from loss of CHD_2OH, rather than $C_2D_5^{\bullet}$.

[c] After allowance for the contribution from CH_3OH loss.

Loss of CH_3OH from $C_5H_9OCH_3^{\bullet+}$ species

Elimination of CH_3OH is the second most important reaction for many of the ionised pentenyl methyl ethers, see Table 11.1.

The labelling data of Table 11.4 show that the methoxy group is usually retained intact in the eliminated methanol, especially for allylic species. Thus, the OCD_3 isotopologues of $\mathbf{3}^{\bullet+}$, $\mathbf{4}^{\bullet+}$, $\mathbf{8}^{\bullet+}$, $\mathbf{11}^{\bullet+}$ and $\mathbf{13}^{\bullet+}$ all lose CD_3OH with a ≥ 99.5 % selectivity. Lower selectivities (90 and 75 %, respectively) are shown by the non-allylic species, $\mathbf{1}^{\bullet+}$ $[OCD_3]$, and the homoallylic radical cation $\mathbf{10}^{\bullet+}$ $[OCD_3]$, which expel appreciable amounts of CHD_2OH. However, labelled analogues of another homoallylic species, $\mathbf{7}^{\bullet+}$ $[OCD_3]$ and $\mathbf{7}^{\bullet+}$ $[O^{13}CH_3]$, lose CH_3OH and $^{13}CH_3OH$ with at least 97 and 99 % selectivities, respectively.

For most of the allylic isomers a simple cycloreversion of their cis-geometrical configuration as depicted in Eq. 1 could account for the CH_3OH loss. A facile cis-trans isomerisation is not unexpected and indeed, see Table 11.1, the trans-isomer, $\mathbf{3a}^{\bullet+}$, loses

Table 11.4. Methanol loss [a] from metastable ionised labelled pentenyl methyl ethers.

Ion Loss →	CD_3OH	CHD_2OH	CH_3OD	CH_3OH	$^{13}CH_3OH$
$\mathbf{1}^{\bullet+}$ $[OCD_3]$	100	11	--	--	--
$\mathbf{1}^{\bullet+}$ $[1,1\text{-}D_2]$	--	< 1	4	100	--
$\mathbf{2}^{\bullet+}$ $[OCD_3]$	100	30	< 1	~ 1	--
$\mathbf{2}^{\bullet+}$ $[1,1\text{-}D_2]$	--	--	--	100	--
$\mathbf{3}^{\bullet+}$ $[OCD_3]$	100	< 0.5	--	--	--
$\mathbf{4}^{\bullet+}$ $[OCD_3]$	100	< 0.5	--	--	--
$\mathbf{4}^{\bullet+}$ $[4,4\text{-}D_2]$	--	--	30	100	--
$\mathbf{4}^{\bullet+}$ $[5\text{-}CD_3]$	--	--	8	100 [b]	--
$\mathbf{7}^{\bullet+}$ $[OCD_3]$	100	< 3	--	--	--
$\mathbf{7}^{\bullet+}$ $[O^{13}CH_3]$	--	--	--	< 0.5	100
$\mathbf{8}^{\bullet+}$ $[OCD_3]$	100	< 0.5	--	--	--
$\mathbf{10}^{\bullet+}$ $[OCD_3]$	100	30	2 [c]	--	--
$\mathbf{13}^{\bullet+}$ $[OCD_3]$	100	2	--	--	--
$\mathbf{14}^{\bullet+}$ $[OCD_3]$	100	< 0.5	--	--	--

[a] Relative abundance measured by peak height and normalised to a total of 100 units for the base peak in the metastable ion spectrum for ions dissociating in the second field-free region.
[b] After allowance for the contribution from $C_2H_2D_3^{\bullet}$ loss.
[c] More likely to be CH_2DOH loss.

CH_3OH just as readily as the cis-isomer, $\mathbf{3b}^{\bullet+}$. Isomers $\mathbf{4}^{\bullet+}$ and $\mathbf{13}^{\bullet+}$ do not possess the δ-hydrogen atom required for the cycloreversion but, as argued above, see also Scheme 11.2, these isomers readily communicate with $\mathbf{3}^{\bullet+}$.

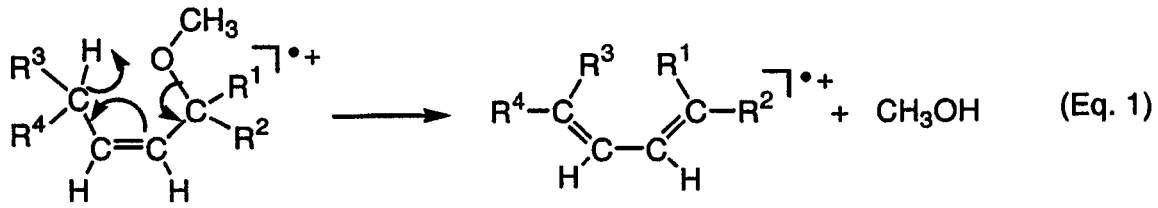

(Eq. 1)

Nevertheless, no definitive conclusions about the mechanism(s) of CH_3OH loss may be made because it is not possible to establish the structure of the $C_5H_8^{\bullet+}$ product ion. The CID spectra of the most likely candidates, *viz.* cyclopentene$^{\bullet+}$, $CH_2{=}C(CH_3)CH{=}CH_2^{\bullet+}$, isoprene$^{\bullet+}$

and $CH_3CH=CHCH=CH_2^{\bullet+}$, piperylene$^{\bullet+}$ are virtually identical while the associated charge-stripping (CS) spectra - which display distinctive differences when O_2 is used as collision gas- are too weak to permit a meaningful analysis.

Similarly, the selectivity of H-transfer to oxygen in methanol loss from ionised ^{2}H-labelled ethers contains little unequivocal mechanistic information. Complications arise from the likelihood that rearrangements precede fragmentation, the possibility of the intervention of isotope effects, and the overlap between signals for elimination of labelled methanol molecules and ethyl radicals, especially CH_3OH and $C_2H_2D_3^{\bullet}$.

On the other hand, expulsion of CH_3OH from most of the non-allylic isomers is characterised by an extremely small KER. Thus, see Table 11.1, the $T_{0.5}$ values for methanol loss from **1**$^{\bullet+}$, **2**$^{\bullet+}$ and **10**$^{\bullet+}$ are 0.4, 0.2 and 0.2 kJ/mol, respectively. In contrast, the $T_{0.5}$ values for CH_3OH expulsion from the allylic species typically lie in the range 1.6 - 2.3 kJ/mol, although a somewhat smaller value is found for **8**$^{\bullet+}$ (1.1 kJ/mol). Very small KER values are frequently found for the dissociation of metastable ions via INCs [22-28]. Consequently, the facile CH_3OH loss from **1**$^{\bullet+}$, **2**$^{\bullet+}$ and **10**$^{\bullet+}$ and the associated very low KER values may indicate that these processes are initiated by a H-transfer from carbon to oxygen, to form a distonic ion which could isomerise to an INC. However, only an outline mechanism, as illustrated in Scheme 11.9 for **1**$^{\bullet+}$ and **2**$^{\bullet+}$, may be proposed at this stage.

Loss of CH_2O from $C_5H_9OCH_3^{\bullet+}$ species

Elimination of CH_2O is of negligible importance for the majority of the isomeric ions, see Table 11.1. However, it occurs to some extent from metastable ions **2**$^{\bullet+}$ and **10**$^{\bullet+}$, and it dominates the dissociation of metastable ions **7**$^{\bullet+}$. A simple cycloreversion involving a 1,5-H shift from the OCH_3 group to the more distant end of the C=C bond, see Eq. 2, cannot explain CH_2O loss.

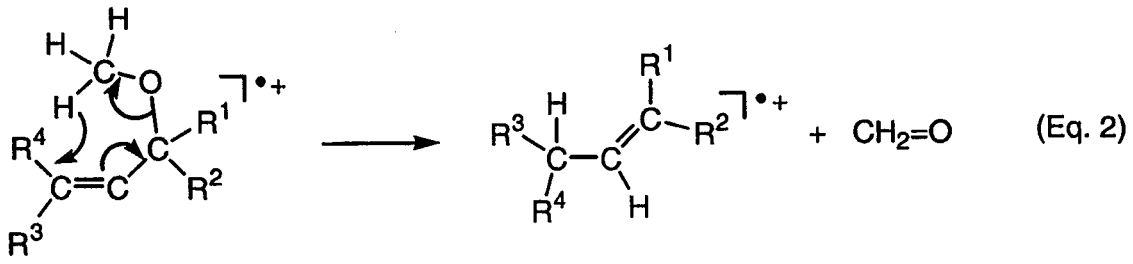

Such a mechanism could elegantly rationalise formaldehyde loss from the ionised allylic ethers, but these do not expel CH_2O to any appreciable extent. In contrast, no comparable simple mechanism may be devised for CH_2O elimination from the homoallylic radical cations, which do react in this manner. A similar unexpected correlation is found for the four isomeric ionised butenyl methyl ethers: expulsion of CH_2O occurs to an appreciable extent only from ionised homoallyl methyl ether [36]. The only ionised allylic alkenyl methyl ether to expel CH_2O is metastable $CH_2{=}CHCH_2OCH_3^{\bullet+}$ [34,35], which is atypical.

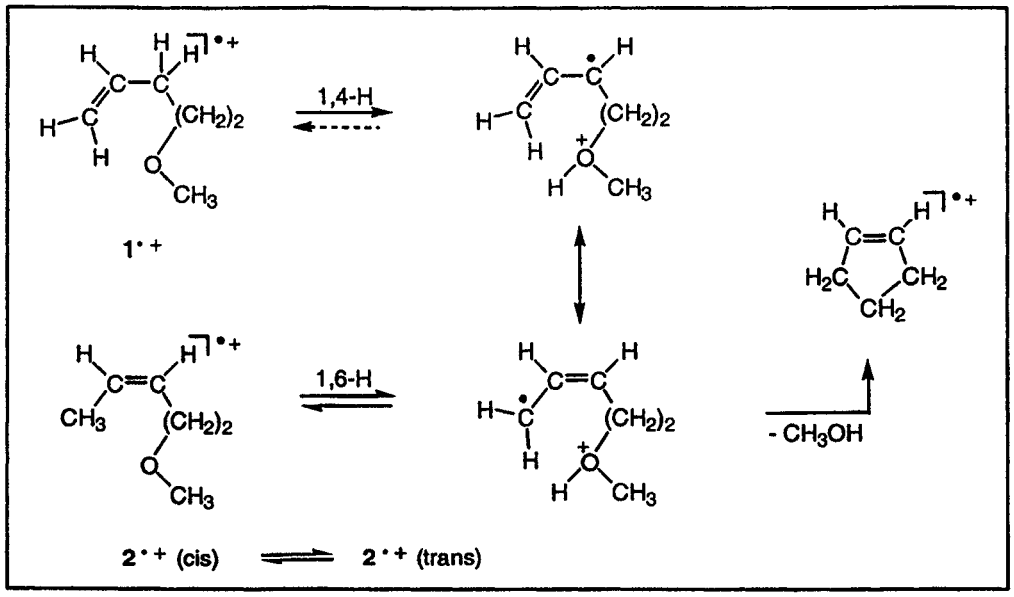

Scheme 11.9

Here, too, problems in establishing the structure of the ($C_5H_{10}^{\bullet+}$) alkene type product ions hamper the study of the mechanism, as does the overlap of signals for loss of CH_2O and $C_2H_5^{\bullet}$ from labelled analogues of $\mathbf{2}^{\bullet+}$ and $\mathbf{10}^{\bullet+}$. Nevertheless, some progress is possible in the case of $\mathbf{7}^{\bullet+}$, which loses CH_2O so readily that interference from the minor competing channel for $C_2H_5^{\bullet}$ elimination may be neglected. The loss of $^{13}CH_2O$ with very high selectivity from $\mathbf{7}^{\bullet+}$ [$O^{13}CH_3$] shows that the carbon atom of the formaldehyde originates from the methoxy group. However, $\mathbf{7}^{\bullet+}$ [OCD_3] eliminates mainly CHDO (~ 52 %) with smaller contributions for expulsion of CD_2O (~ 12 %) and CH_2O (~ 36 %).

Therefore, quite extensive exchange of the H atoms of the OCH_3 group precedes loss of CH_2O. These results may be understood if a reversible 1,6-H shift in $\mathbf{7}^{\bullet+}$ allows the three H atoms of the OCH_3 group to exchange with those of the terminal CH_2 and CH_3 groups, as proposed in Scheme 11.10.

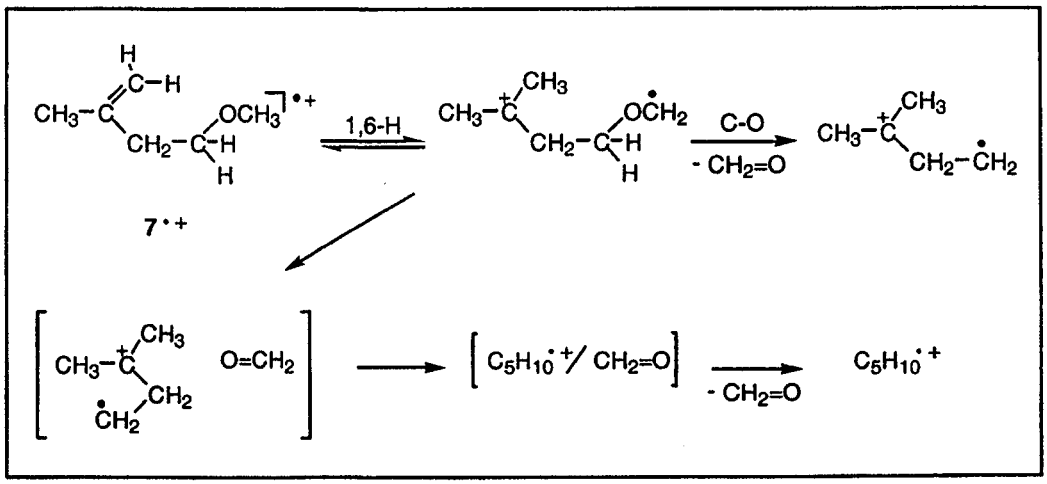

Scheme 11.10

The ratios of CH_2O, CHDO and CD_2O which would be expected to be lost from ions $\mathbf{7}^{\bullet+}$ [OCD_3] if any two of these eight H atoms were incorporated in the formaldehyde are 38 : 58 : 4, which is in reasonable agreement with the experimental data. The deviation is greatest for CD_2O loss, which occurs roughly three times more than would be expected; this discrepancy is not unreasonable because it could merely represent a slight residual preference for expelling the D atoms which are initially part of the OCD_3 group. Parallel effects operate for the lower

homologue, CH_2=$CHCH_2CH_2OCD_3^{\bullet+}$, which also eliminates significant amounts of CHDO and CH_2O, as well as CD_2O. Consequently, this 1,6-H/D shift appears to be of general significance in the reactions of low-energy ionised homoallylic ethers.

Direct dissociation of the distonic ion **7**(δ)$^{\bullet+}$ would afford the distonic ion $(CH_3)_2C^+CH_2CH_2^{\bullet}$. More stable isomers of $C_5H_{10}^{\bullet+}$ would be accessible if this distonic ion isomerised within INCs of general structure [$C_5H_{10}^{\bullet+}$/ CH_2O]. Any such isomerisation does not release enough energy to promote rapid separation of the components because the $T_{0.5}$ value (~ 0.8 kJ/mol) is very small. This small KER is consistent with facile isomerisation to a distonic ion or INC containing an intact CH_2O entity. These possibilities are also included in the tentative proposal of Scheme 11.10. Parallel conclusions may be made for the much less facile elimination of CH_2O from **2**$^{\bullet+}$ and **10**$^{\bullet+}$.

Loss of H_2O from $C_5H_9OCH_3^{\bullet+}$ species

As with CH_2O elimination, H_2O loss appears to be favoured for non-allylic species. Thus, both **1**$^{\bullet+}$ and **7**$^{\bullet+}$ lose ~ 7% H_2O. Moreover, this remarkable process is a major fragmentation of **2**$^{\bullet+}$ and **10**$^{\bullet+}$, see Table 11.1, but the fourth homoallylic isomer, **5**$^{\bullet+}$, does not eliminate H_2O to a significant extent.

Table 11.5. Water loss [a] from metastable ionised labelled pentenyl methyl ethers.

Ion	Loss →	H_2O	HDO	D_2O
1$^{\bullet+}$	[OCD_3]	70	100	19
1$^{\bullet+}$	[1,1-D_2]	100	4	--
2a$^{\bullet+}$	[OCD_3]	85	100	18
2a$^{\bullet+}$	[1,1-D_2]	100	4	< 1
2$^{\bullet+}$	[1,1-D_2-OCD_3]	65	100	20
10$^{\bullet+}$	[OCD_3]	70	100	15

[a] Relative abundance measured by peak height and normalised to a total of 100 units for the base peak in the metastable ion spectrum for ions dissociating in the second field-free region.

The behaviour of labelled analogues, see Table 11.5, reveals that the hydrogen atoms of the methoxy group are sometimes selected in the eliminated water : **10**$^{\bullet+}$ [OCD_3] loses H_2O, HOD and D_2O in the ratio 70 : 100 : 15; both **1**$^{\bullet+}$ [OCD_3] and **2**$^{\bullet+}$ [OCD_3] show a similar selectivity, but the results for **1**$^{\bullet+}$ [OCD_3] are less accurate because the peaks are much weaker. Only loss of H_2O would occur if the hydrogen atoms of the eliminated water molecule were selected solely from those of the pentenyl chain. Random selection of any two of the nine H and three D atoms in $C_5H_9OCD_3^{\bullet+}$ would result in elimination of H_2O, HOD and D_2O in the ratio 100 : 32 : 3 ; this model seriously overestimates the importance of the loss of H_2O. A reasonable approximation to the experimental data is obtained if the three D atoms exchange with an average of five H atoms, followed by selection of any two of these H atoms : H_2O, HOD and D_2O loss would then be expected in the ratio 68 : 100 : 21. The H atoms on the α-carbon atom are rarely lost in the expelled water molecule, as indicated by the minor contribution from HOD elimination from **1**$^{\bullet+}$ [1,1-D_2] and **2**$^{\bullet+}$ [1,1-D_2].

Only tentative mechanistic conclusions about H_2O loss are possible. It seems likely that the reaction is initiated by H-transfer from the OCH_3 group to the pentenyl chain. A second H-transfer from the C_5H_{10} entity to the oxygen atom in the resultant distonic ion gives an α-distonic ion in which the charge and radical site are located on the oxygen and carbon atoms derived from the original OCH_3 group.

Fission of the bond connecting the oxygen atom to the pentenyl chain in this α-distonic ion then leads to an INC comprising protonated formaldehyde and a pentenyl radical. Rotation of the protonated formaldehyde with respect to the pentenyl radical then allows recombination of these components to form a new C-C bond. This ability of the components to undergo mutual rotation is a characteristic property of INCs and it is often called the Longevialle criterion. A final hydrogen transfer to oxygen in the resultant ionised hexenol, followed by C-O cleavage, perhaps with rearrangement of the developing $C_5H_{10}^{\bullet+}$ radical cation, then results in H_2O expulsion, see Scheme 11.11.

There is precedent for the key step of this mechanism, in which an unsaturated hydrocarbon entity adds to protonated formaldehyde within an INC, in detailed studies of H_2O

loss from $C_nH_{2n+1}O^+$ oxonium ions containing a non-terminal oxygen atom [50]. A slightly modified mechanism may operate for H_2O elimination from **7**$^{\bullet+}$ and a more detailed discussion of H_2O loss from **1**$^{\bullet+}$ and **2**$^{\bullet+}$ is presented elsewhere [42].

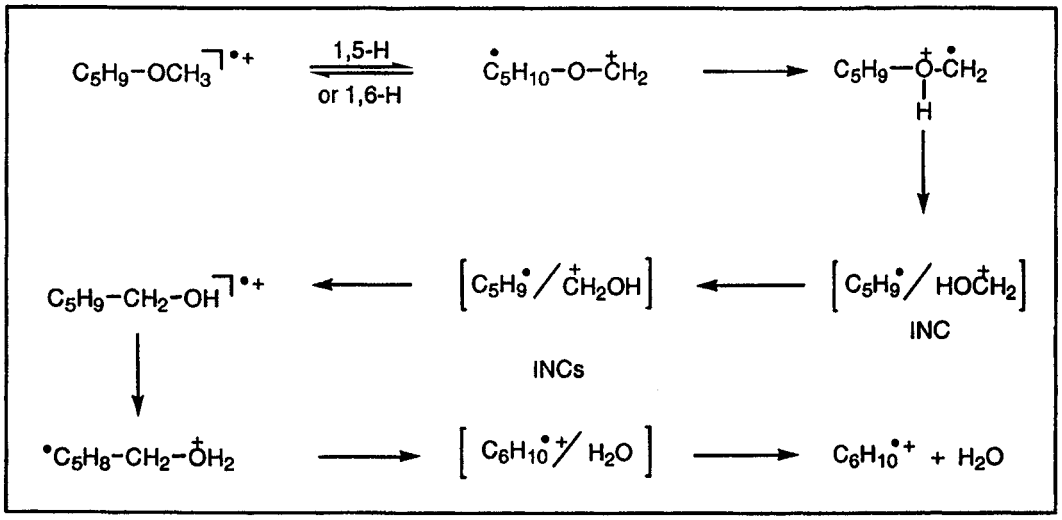

Scheme 11.11

Conclusions

The reactivities of ten of the thirteen isomeric ionised pentenyl methyl ethers are distinct, though sometimes subtly related. Only three isomers, $C_2H_5CH{=}CHCH_2OCH_3^{\bullet+}$, **3**$^{\bullet+}$, $CH_2{=}CHCH(C_2H_5)OCH_3^{\bullet+}$, **4**$^{\bullet+}$, and $CH_2{=}C(C_2H_5)CH_2OCH_3^{\bullet+}$, **13**$^{\bullet+}$, have a common chemistry, as indicated by their closely similar MI, CID and NR spectra. Metastable ionised pentenyl methyl ethers show an impressive array of reactions, of which elimination of $CH_3^{\bullet}$ or $C_2H_5^{\bullet}$ are of the greatest general importance, especially for allylic species. These reactions produce acyclic conjugated oxonium ions, usually by α-cleavage of an ionised allylic ether or by γ-cleavage of an ionised enol ether formed by a series of hydrogen shifts involving distonic ions. Skeletal rearrangements occasionally occur, at least some of which may be interpreted by mechanisms involving ionised alkylmethoxycyclopropanes. Methyl radical elimination sometimes proceeds by more than one route, as is illustrated by the loss of either methyl group of the pentenyl chain in $CH_3CH{=}CHCH(CH_3)OCH_3^{\bullet+}$, **6**$^{\bullet+}$, or $CH_2{=}C(CH_3)CH(CH_3)OCH_3^{\bullet+}$, **12**$^{\bullet+}$, to give the isomeric oxonium ions $\mathbf{b}_1^+$ and $\mathbf{b}_2^+$, or $\mathbf{b}_3^+$ and $\mathbf{b}_2^+$, respectively, see Scheme

11.3. Labelling experiments confirm that hydrogen shifts often precede alkyl radical loss, but these shifts rarely involve the hydrogens of the methoxy group, except for some ionised homoallylic ethers, particularly $CH_2=C(CH_3)(CH_2)_2OCH_3^{\bullet+}$, $\mathbf{7}^{\bullet+}$.

Loss of CH_3OH is also common, and may be formulated as a cycloreversion, although skeletal isomerisation is necessary before it may occur from ionised allylic ethers without the required δ-hydrogen atom. This reaction is probably initiated by hydrogen transfer from the pentenyl chain to the oxygen atom.

Other reactions of significance include elimination of H_2O or CH_2O. These processes are favoured for ionised non-allylic ethers and they may occur via related mechanisms involving ion-neutral complexes. It is possible that water loss begins with hydrogen transfer from the methoxy group to the pentenyl chain, followed by a second hydrogen transfer from the hydrocarbon chain to the oxygen atom.

References

[1] D.G.I. Kingston, J.T. Bursey and M. M. Bursey, *Chem. Rev.* **7**, 215 (1974).

[2] C. Lifshitz, *J. Phys. Chem.* **1983**, *87*, 2304.

[3] H. Schwarz in *Advances in Mass Spectrometry*, J.F.J. Todd (Ed.), Wiley, New York (**1986**).

[4] G. Bouchoux, *Mass Spectrom. Rev.* **1988**, *7*, 203.

[5] F. Turecek in *The Chemistry of Enols*, Z. Rappoport (Ed.), Wiley, New York (**1990**).

[6] F. McLafferty, *Anal. Chem.* **1956**, *28*, 306.

[7] D.J. McAdoo, D.N. Witiak, F.W. McLafferty and J.D. Dill, *J. Am. Chem. Soc.* **1978**, *100*, 215

.

[8] D.J. McAdoo, C.E. Hudson, M. Skyiepal, E. Broido and L.L. Griffin, *J. Am. Chem. Soc.* **1987**, *109*, 7648.

[9] B.L.M. van Baar, J.K. Terlouw, S. Akkok, W. Zummack and H. Schwarz, *Int. J. Mass Spectrom. Ion Processes* **1987**, *81*, 217.

[10] N. Heinrich and H. Schwarz in *Ion and Cluster Ion Spectroscopy*, J.P. Maier (Ed.), Elsevier, Amsterdam (**1988**).

[11] G. Bouchoux, J. Tortajada, J. Dagaut and J. Fillaux, *Org. Mass Spectrom.* **1987**, *22*, 451.

[12] G. Bouchoux, F. Bidault, F. Djazi, B. Nicod and J. Fillaux, *Org. Mass Spectrom.* **1987**, *22*, 748.

[13] D.J. McAdoo, C.E. Hudson and D.N. Witiak, *Org. Mass Spectrom.* **1979**, *14*, 350.

[14] C.E. Hudson and D.J. McAdoo, *Tetrahedron* **1986**, *46*, 331, and references therein.

[15] R.D. Bowen and A.G. Harrison, *J. Chem. Soc. Perkin 2*, **1989**, 1483, and references therein.

[16] F. Turecek and F.W. McLafferty, *J. Am. Chem. Soc.* **1984**, *106*, 2528.

[17] C. Lifshitz, T. Peres, N. Ohmichi and I. Pri-Bar, *Int. J. Mass Spectrom. Ion Processes* **1986**, *72*, 253.

[18] G. Bouchoux, Y. Hoppilliard and P. Jaudon, *Org. Mass Spectrom.* **1987**, *22*, 98.

[19] G. Bouchoux, F. Djazi, Y. Hoppilliard, P. Jaudon and N. Nouts, *Org. Mass Spectrom.* **1988**, *23*, 33.

[20] B.F. Yates, W.J. Bouma and L. Radom, *J. Am. Chem. Soc.* **1984**, *106*, 5805.

[21] S. Hammerum, *Mass Spectrom. Rev.* **1988**, *7*, 123.

[22] T.H. Morton, *Tetrahedron* **1982**, *38*, 3195.

[23] D.J. McAdoo, *Mass Spectrom. Rev.* **1988**, *7*, 363.

[24] S. Meyerson, *Org. Mass Spectrom.* **1989**, *24*, 267.

[25] S. Hammerum in *Fundamentals of Gas-Phase Ion Chemistry*, K.R. Jennings (Ed.), Kluwer, Dordrecht, (**1990**).

[26] R.D. Bowen, *Acc. Chem. Res.* **1991**, *24*, 364.

[27] P. Longevialle, *Mass Spectrom. Rev.* **1992**, *11*, 157.

[28] D.J. McAdoo and T.H. Morton, *Acc. Chem. Res.* **1993**, *26*, 295.

[29] T.A. Molenaar-Langeveld, R.H. Fokken and N.M.M. Nibbering, *Org. Mass Spectrom.* **1988**, *23*, 364.

[30] R.D. Bowen, A.D. Wright, S.R. Thomas, K.R. Jennings and A. Maccoll, *Org. Mass Spectrom.* **1991**, *26*, 421.

[31] (a) R.D. Bowen and A.D. Wright, *J. Chem. Soc., Chem. Commun.* **1991**, 1055 ; (b) R.D. Bowen and A.D. Wright, *J. Chem. Soc., Chem. Commun.* **1992**, 96.

[32] A.D. Wright and R.D. Bowen, *Can. J. Chem.* **1993**, *71*, 1073.

[33] R.D. Bowen, L.N. Heydorn and J.K. Terlouw, *Int. J. Mass Spectrom.*, in press.

[34] J.R. Cao, M. George and J.L. Holmes, *J. Am. Soc. Mass Spectrom.* **1992**, *3*, 99.

[35] R.D. Bowen, A.D. Wright and P.J. Derrick, *Org. Mass Spectrom.* **1992**, *27*, 905.

[36] R.D. Bowen, A.D. Wright, A.W. Colburn and P.J. Derrick, *Int. J. Mass Spectrom. Ion Processes* **1992**, *116*, 193.

[37] (a) C.A. Schalley, G. Hornung, D. Schröder and H. Schwarz, *Chem. Soc. Rev.* **1998**, *27*, 91; (b) J.K. Terlouw and H. Schwarz, *Angew. Chem. Int. Ed. Engl.* **1987**, *26*, 805.

[38] F.W. McLafferty and F. Turecek, *Interpretation of Mass Spectra*, 4th ed., University Science Books, Mill Valley, California (**1993**).

[39] T.Weiske and H. Schwarz, *Tetrahedron* **1986**, *42*, 6245 and references therein.

[40] (a) R.D. Bowen, P. Clifford, J.T. Francis and J.K. Terlouw, *Int. J. Mass Spectrom. Ion Processes* **1997**, *165/166*, 155 ; (b) S.J. Mandeville, R.D. Bowen, M.A. Trikoupis and J.K. Terlouw, *Eur. Mass Spectrom.* **1999**, *5*, 339.

[41] S. Hammerum, unpublished results.

[42] R.D. Bowen, S.J. Mandeville, M.A. Trikoupis and J.K. Terlouw, *Int. J. Mass Spectrom.*, **2001**, *210/211*, 447-457.

[43] J.-F. Rontani, *Org. Mass Spectrom* **1994**, *29*, 808.

[44] R.D. Bowen, R.T. Gallagher and S. Meyerson, *J. Am. Soc. Mass Spectrom.* **1996**, *7*, 205.

[45] R.D. Bowen, P. Clifford and R.T. Gallagher, *Eur. Mass Spectrom.* **1996**, *2*, 233.

[46] D.C. Nonhebel, J.M. Tedder and J.C. Walton, *Radicals*, Cambridge University Press (**1979**).

[47] A.L.J. Beckwith, *Tetrahedron* **1981**, *37*, 3073.

[48] S. Hammerum, *Acta. Chem. Scand. Ser. B* **1984**, *38*, 707.

[49] R.D. Bowen, S.J. Mandeville, M.A. Trikoupis and J.K. Terlouw, in preparation.

[50] (a) R.D. Bowen and D.H. Williams, *J. Am. Chem. Soc.* **1978**, *100*, 7454 ; (b) R.D. Bowen, A.W. Colburn and P.J. Derrick, *J. Chem. Soc. Perkin Trans. 2* **1990**, 147.

[51] (a) R.D. Bowen, H.G.M. Edwards, D.W. Farwell, I. Rusike and D.M. Saunders, *J. Chem. Res. (S)* **1998**, 426 ; (b) R.D. Bowen, H.G.M. Edwards, D.W. Farwell, I. Rusike and D.M. Saunders, *J. Chem. Res. (M)* **1998**, 1901.

[52] H.F. van Garderen, P.J.A. Ruttink, P.C. Burgers, G.A. McGibbon and J.K. Terlouw, *Int. J. Mass Spectrom. Ion Processes* **1992**, *121*, 159.

[53] J.L. Holmes and J.K. Terlouw, *Org. Mass Spectrom.* **1980**, *15*, 383.

Chapter 12

Experimental

The VG Analytical ZAB-R Mass Spectrometer

All tandem mass spectrometry-based experiments were performed at McMaster University using the VG Analytical ZAB-R instrument of $B(\perp Q)E_1E_2$ geometry (B = magnet, Q = quadrupole, E = electrostatic analyzer). This custom built mass spectrometer is three sector instrument whose design is based on the standard, non-extended geometry of its predecessor the ZAB-2f [1].

The ion source, which is kept under high vacuum using a 160/170 Diffstak, is equipped with four inlet systems for sample introduction : i) a septum inlet used for compounds having very high vapour pressures, ii) an all glass heated inlet system (AGHIS), which can also be used as a very low pressure (VLVP) inlet, used for volatile compounds, iii) an all quartz direct insertion probe used for less volatile compounds and iv) a direct solid insertion probe used for solid samples which have very low vapour pressures. For involatile liquid samples, it is often useful to smear a sample on the tip of the quartz probe to obtain greater sensitivity. Both the AGHIS and quartz probe possess reservoirs from which the sample steadily evaporates/sublimes, consequently the temperature of bulk sample can easily be varied to obtain a desired source pressure.

Located in the first field free region (1ffr) of the instrument, there is a collision cell (cell 1). An Autospec magnet precedes the second field free region (ffr) housing which has the form of a rectangular box. This box [79 x 23 x 23 cm] has easily removable top and side panels. The box may be quickly isolated from its two 160/170 Diffstaks and the other sectors by using four valves. This enables rapid access to the collision chambers and lens assemblies which are mounted to its "optical bench" type of internal base. The box contains three collision gas chambers, i.e. cells 2, 3 and 4, whose locations are shown in Figure 1.1. Cell 2

[30(1) x 3(w)x 14(h) mm] is a home-built chamber used for neutralization with organic vapours, such as N,N-dimethylaniline. Cell 3 [20(1) x 1(w) x 10(h) mm], which is also electrically isolated and equipped with a y-focus/deflection lens assembly, is used for "standard" reionization and collision-induced dissociation (CID) experiments. These collision chambers are situated at distances of 240, 44 and 10 mm, respectively, from the focal point at the intermediate slit located next to the glass window which is situated on the top of the box. Immediately following the first electrostatic analyzer (E_1), there is a box type collector housing in which the 3ffr collision gas chamber is located in front of a small Autospec ESA (E_2, 5" radius, 72.5°). This housing contains two photomultiplier type detectors and a fifth 160/700 Diffstak is used to pump this region.

A Quadrupole mass analyzer (200 amu), with a channeltron electron multiplier detector, is mounted on one side of cell 3 - perpendicular to the flight path of the fast moving ion beam. The quadrupole is used to acquire spectra of ionized target molecules and their dissociation products resulting from the neutralization process of a mass selected ion beam [2]. This technique was not used in the context of the work described in the thesis.

Experimental Conditions

Unless otherwise stated, all mass spectra were obtained using electron ionization and were acquired under the following conditions : electron energy, 70 eV; emission current, 0.5 mA; source temperature 100-120 °C. The accelerating potential used in individual experiments is given in the Chapters. Source pressures, monitored by a remote ionization gauge, of 10^{-5} to 10^{-6} Torr were used.

The chemical ionization experiments carried out in this work were carried out at pressures of approximately 10^{-4} Torr. All other parameters were as indicated above.

The metastable ion (MI) mass spectra were obtained in the 2ffr of the instrument unless otherwise indicated. The kinetic energy release (KER) values were estimated from the width at half hight ($T_{0.5}$) of the appropriate metastable peak, by means of a standard equation (see Chapter 1) and corrected for the width at half height of the main beam [3].

The collision-induced dissociation (CID) spectra were obtained in either the second or third ffr using O_2 (main beam transmittance - 80 %) as the collision target. The MS/MS/MS experiments, i.e. the MI/CID, CID/CID and NR/CID, were all obtained in the 3ffr again using O_2 (main beam transmittance - 80 %) to collisionally activate the ions.

The neutralization-reionization (NR) mass spectra were obtained in the 2ffr using either N,N-dimethylaniline (cell 2) or cyclopropane (cell 3) as the neutralization target (main beam transmittance - 70 %) and O_2 (cell 4, main beam transmittance - 80 %) as the reionization agent. For all NR experiments, a total analyzer pressure of 2-3 x 10^{-5} Torr was used. A positive deflector electrode is located between cells 3 and 4 to remove any remaining ions from the beam.

All spectra were recorded using a PC-based data system with ZABCAT software developed by Mommers Technologies Inc. (Ottawa, Canada). The quoted MI, CID and MS/MS/MS spectra represent an accumulation of 25-35 individual scans.

The ionization and appearance energy measurements reported in Chapter 6, were performed in Israel by Prof. C. Lifshitz, using the technique of vacuum ultraviolet (VUV) photoionization mass spectrometry (PIMS) as described in detail in [4]. Briefly, photoionization is induced by a pulsed vacuum UV light source, a Hinteregger discharge in hydrogen producing the many-line spectrum. Photoions are ejected from the ion source into a quadrupole mass filter by a drawout pulse. The ion lifetime sampled prior to dissociation in the present experiments is about 24 μs. The outcomes of the PIMS experiment are photoionization efficiency (PIE) curves, from which ionization energies (IES) and AEs can be deduced. The effective wavelength resolution employed is 5.0 Å. This corresponds to an energy resolution of about 0.04 eV near the ionization threshold of DMO (10.0 eV) and of about 0.05 eV near the fragmentation onsets.

The experiments on the *m/z* 91 negative ions in Chapter 9, were performed on the Autospec M in Berlin by the Schwarz group. The ions were generated from rhodanine in the negative chemical ionization (NCI) mode with CH_4 as electron moderating gas. Subsequent charge reversal (CR) [5] experiments involved collision of the mass selected negative ions with O_2 and recording the positively charged precursor ions and fragments. In the $^-NR^+$

experiments He was used for neutralization and O_2 for reionization. The spectra shown are accumulations of 25-50 scans.

The ion-molecule reaction spectra of Chapter 7, were recorded on a six sector tandem mass spectrometer (Micromass Autospec 6F, Manchester) of $c_1E_1B_1c_2E_2c_3c_4E_3B_2c_5E_4$ geometry (E = electric sector, B = magnetic sector, c = collision cell) [6a] at the University of Mons. General conditions were 8 kV accelerating voltage, 200 μA trap current (in the electron ionization mode, EI), 1 mA (in the chemical ionization mode, CI), 70 eV ionizing electron energy and 200 °C ion source temperature. The solid samples were introduced with a direct insertion probe, while the liquid samples were injected into the ion source via a heated (180 °C) septum inlet.

The instrument has been modified with an rf-only quadrupole collision cell (Q cell) between E_2 and E_3 as has been reported elsewhere [6b]. This modification allows the study of associative ion-molecule reactions and the study of collision induced dissociation of decelerated ions having 20-30 eV kinetic energy. Briefly, the experiments utilizing the quadrupole consist of the selection of a beam of fast moving ions (8 keV) with the three first sectors ($E_1B_1E_2$), the deceleration of these ions to approximately 5 eV (to maximize ion-molecule reactions) or 20-30 eV (to maximize collision-induced dissociations). The interaction between the ions and the reagent gas (the pressure of the gas is estimated to be ca. 10^{-3} Torr) is thereafter realized in the Q cell and, after reacceleration to 8 keV, all the ions generated in the quadrupole are separated and mass measured by scanning the field of the second magnet. The high-energy CID spectra of mass-selected ions generated in the Q cell can be recorded by a linked scanning of the fields of the three last sectors. The pressure of the neutral reagent in the quadrupole collision cell cannot be reliably measured as it is estimated using an ionization gauge situated quite far away from the quadrupole cell. For the sake of consistency, an ion transmission of 50 % was used in all experiments.

Preparation of Precursor Molecules

Unless otherwise indicated, all precursor molecules were commercially available (Aldrich, Milwaukee, USA) and were used without further purification. The procedure for all synthesized precursor molecules is given below and is presented by Chapter. High resolution measurements were performed on all precursor molecules to verify the identity of the compound.

Chapter 3

Acetamide-d_3 was synthesized on a small scale by reacting $CD_3C(=O)Cl$ with NH_3. In the first step, a three neck round bottom flask fitted with a dry ice condenser, was filled with NH_3 gas. Slowly (as the reaction is very vigorous), $CD_3C(=O)Cl$ was admitted dropwise into the round bottom flask. After the reaction was complete, the dry ice condenser was replaced with a cold water condenser and left standing for 30 minutes. The sample was then dried on a rotary pump.

Chapter 4

The 2,6-d_2 labelled analogue of pyridine was synthesized on a small scale using the procedure described in ref. 7. Three grams of pyridine 1-oxide was dissolved in 15 mL of 2% NaOH-D_2O and heated under reflux for 4 hours. The reaction mixture was concentrated to c. 7 mL, to which 15 mL of fresh D_2O was added. The reaction mixture was heated under reflux for another 4 hours. After most of the solvent was removed at room temperature, the residue was extracted throughly with $CHCl_3$. The extract was dried over anhydrous Na_2SO_4 and concentrated to 35 mL in volume. Then, 8 mL of PBr_3 was added to this solution under ice-cooling and the reaction mixture was warmed under gentle reflux for 1 hour. After an excess of $PBr_3$was decomposed by addition of 10 mL of H_2O, $CHCl_3$ was evaporated. The residual aqueous solution was made alkaline with Na_2CO_3 and saturated with $(NH_4)_2SO_4$ for the salting out. The dideuterated pyridine was extracted with ether.

Chapter 6

The D-labeled isotopomers $CD_3O_2CCO_2CH_3$ and $CD_3O_2CCO_2CD_3$ were prepared on a mg scale by reacting 90 μL of oxalyl chloride (Aldrich) with 200 μL of a 1:1 CD_3OD/CH_3OH mixture and pure CD_3OD, respectively, at room temperature for ~ 30 min., followed by removal of the excess methanol with a rotary pump.

Methylpyruvate-OCD_3 was synthesized from pyruvic acid and CD_3OH using a standard exchange procedure.

Chapter 8

The D-labelled isotopomer of trimethylborate $^{10}B(OCD_3)_3$ was prepared on a mg scale by reacting 50mg of $^{10}B(OH)_3$ with 150μL of CD_3OD at room temperature for ~ 15 min. The resulting solution was introduced without further purification. Methyl boronic acid has a tendency to trimerize during the introduction of the sample. The mass spectrum of the resulting trimethylboroxine is characterized by signals at *m/z* 126, 111, 69 and 41 but does not show a peak at *m/z* 43 and thus the trimerization does not cause interference in this study.

Chapter 11

The ethers used in this work were prepared by methylating the alkoxide of the corresponding pentenol with a slight deficiency of CH_3I. The alkoxides were made by treatment of the alcohols with a slight excess of a NaH dispersion in triethylene glycol dimethyl ether (triglyme). In the methylation procedure, after stirring for 24-72 hours at ambient temperature, the ether was carefully distilled from the reaction flask, washed with water, dried with $MgSO_4$ and redistilled. Methylation with CD_3I or $^{13}CH_3I$ under the same conditions gave the analogous $C_5H_9OCD_3$ and $C_5H_9O^{13}CH_3$ ethers.

Most of the pentenols were commercial samples of high purity. The three pentenols that were not commercially available were synthesised as follows : $CH_3CH=(CH_3)CCH_2OH$ and $CH_3CH=CHCH_2CH_2OH$ were prepared by reduction of $CH_3CH=(CH_3)CCO_2CH_3$ and $CH_3CH=CHCH_2CO_2H$, respectively, with $LiAlH_4$ in ethereal solution/suspension at reduced temperature (-78 to -50°C); $CH_2=(CH_3CH_2)CCH_2OH$ was prepared by reduction of

CH_2=C(CH_2CH_3)C(H)=O with $NaBH_4$ in methanol at 5°C. Ethers labelled in the pentenyl chain were prepared by the routes shown in Scheme 13.1. Full descriptions of representative examples of these synthetic procedures have been published elsewhere [8].

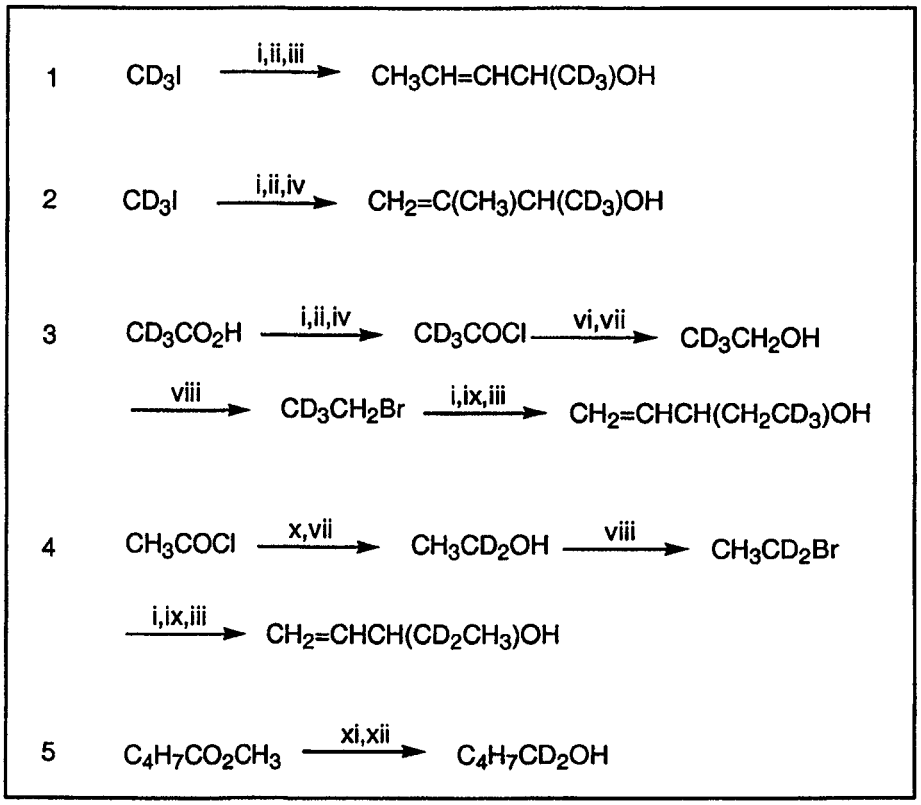

Reagents and conditions : i, 1.2 moles Mg, $(C_2H_5)_2O$; ii, 0.8 moles CH_3CH=CHCH=O;-78° C; iii, saturated aqueous $NH_4^+Cl^-$ solution; iv,ii 0.8 moles CH_2=C(CH_3)CH=O; -78° C; v, excess $(PhCO)_2O$, distil; vi, 1.8 moles $LiAlH_4$, $CH_3O(CH_2CH_2O)_3CH_3$; vii, excess $HO(CH_2CH_2O)_4H$, distill; viii, conc. HBr/H_2SO_4, distil slowly; ix, 0.8 moles CH_2=CHCH=O; -78° C; x, 1.2 moles $LiAlD_4$, $CH_3O(CH_2CH_2O)_3CH_3$; xi, 0.3 moles $LiAlD_4$, $(C_2H_5)_2O$; xii, $NaOH/H_2O$.

Scheme 12.1

References

[1] R.P. Morgan, J.H. Beynon, R.H. Bateman and B.N. Green, Int. J. Mass Spectrom. Ion Phys. (1978), 28, 171.

[2] T. Wong, J.K. Terlouw, T. Weiske, H. Schwarz, Int. J. Mass Spectrom. Ion Processes, 1992, 113, R23.

[3] M.A. Baldwin, P.J. Derrick, R.P. Morgan, Org. Mass Spectrom. 1976, 11, 400.

[4] C. Lifshitz, *Int. J. Mass Spectrom. Ion Processes* **1991**, *106*, 159.

[5] M. M. Bursey, *Mass Spectrom. Rev.* **1990**, *9*, 555.

[6] (a) R.H. Bateman, J. Brown, M. Lefevere, R. Flammang, Y. van Haverbeke, Int. J. Mass Spectrom. Ion Processes 115 (1992) 205 ; (b) R. Flammang, Y. van Haverbeke, C. Braybrook, J. Brown, Rapid Commun. Mass Spectrom. 9 (1995) 795.

[7] M. Tsuda and Y. Kawazoe, *Chem. Pharm. Bull.* **1968**, *16*, 702

[8] (a) R.D. Bowen, H.G.M. Edwards, D.W. Farwell, I. Rusike and D.M. Saunders, *J. Chem. Res. (S)* **1998**, 426 ; (b) R.D. Bowen, H.G.M. Edwards, D.W. Farwell, I. Rusike and D.M. Saunders, *J. Chem. Res. (M)* **1998**, 1901.

Summary

The research presented in this thesis is focused on a unified mass spectrometric and computational chemistry approach to problems of gas-phase ion chemistry. The reactivity, including structure, stability and isomerization behaviour of intermediates, and thermochemical properties of various reactive organic radical cations in the gas phase were studied.

The radical cations of acetone $[CH_3C(=O)CH_3]^{\bullet+}$, acetamide $[CH_3C(=O)NH_2]^{\bullet+}$ and pyridine $[C_5H_5N]^{\bullet+}$ are separated from their more stable counterparts $[CH_2=C(OH)CH_3]^{\bullet+}$, $[CH_2=C(OH)NH_2]^{\bullet+}$ and the α-ylide isomer $[C_5H_4N\text{-}H]^{\bullet+}$ by a large barrier and thus, these ions do not interconvert. However, when the ions encounter a suitable base, the barrier can be significantly reduced (for example for pyridine the barrier is reduced from 71 kcal/mol to a mere 9 kcal/mol), by proton transport catalysis. In general, successful catalysis is achieved when the base B satisfies the following criteria : (i) the PA of the base should lie between the PA of conjugate base $[X\text{-}Y]^{\bullet}$ at X and at Y, see eq (1) ; (ii) the IE of the base should not be much lower than that of the substrate and (iii) the base should not readily undergo self protonation. Under these conditions, the dimer radical cation $B\bullet\bullet\bullet H^+\bullet\bullet\bullet[X\text{-}Y]^{\bullet}$ may be formed. This species can be isolated and its unimolecular chemistry may provide evidence for the isomerization of the substrate. For the keto ions, ionized acetone and acetamide, and the heterocyclic pyridine ion, the bases benzonitrile (BN) and 2-cyanopyridine (2-CP), respectively, fulfill the above criteria. For acetone this isomerization also occurs in the dimer radical cation $[CH_3C(=O)CH_3]_2^{\bullet+}$. *Ab initio* calculations on these systems yield valuable pictures of the transformations occurring during the proton transport catalyses

The dissociative behaviour of dimethyl oxalate was probed using both MI and CID mass spectrometry. DMO ions fragment step-wise by first losing CO_2 to generate the ionized carbene $CH_3O\text{-}C\text{-}OCH_3^{\bullet+}$ and this species then releases a $CH_3^{\bullet}$ group. Dissociation by the consecutive loss of CO_2 and $CH_3^{\bullet}$ is possible because $CH_3O\text{-}C{=}O^{\bullet}$ is thermodynamically *less*

stable. At higher energies direct dissociation to intact CH_3O-C=O$^{\bullet}$ takes place. The competitive loss of CO generates via a rate determining 1,5-H shift, the HBRC CH_2=O•••H•••O=$COCH_3^{\bullet+}$. Neutralization of DMO ions too is completely dissociative, the major product being CH_3O-C=O$^{\bullet}$ radicals. Half of these radicals are formed in the ground state and these survive reionization. Thus, despite its thermodynamic instability, CH_3O-C=O$^{\bullet}$ is a kinetically stable species. Neutralization of DMO ions too is completely dissociative, the major product being CH_3O-C=O$^{\bullet}$ radicals. Half of these radicals are formed in an excited state and rapidly dissociate to $CH_3^{\bullet}$ + CO_2 and the remaining half are formed in the ground state and these survive reionization. Thus, despite its thermodynamic instability, CH_3O-C=O$^{\bullet}$ is a kinetically stable species.

Computational chemistry and MI and CID experiments reveal that the ionic hydrogen shift isomers of pyridine N-oxide and the three hydroxypyridines are thermodynamically as stable as their parent isomer of conventional structure. They are accessible by dissociative electron ionization of carefully chosen molecules, i.e. precursors capable of 1,4- or 1,5-hydrogen migrations to the heteroatom are excellent candidates. NR experiments showed that, despite their elevated enthalpies of formation the neutral ions 2-hydroxy-6-ylidene and 3-hydroxy-2-ylidene are stable species on the microsecond timescale. In contrast the ylide neutrals of pyridne N-oxide readily isomerize into their conventional structure, or else dissociate. The neutral counterpart of the distonic ions, 2-hydroxy-3-ylidene, have only a marginal stability and part of these neutrals are proposed to isomerize into energy-rich 2-pyridone molecules. The question whether 2-hydroxypyridine yields isomerically pure enol ions or alternatively, a mixture of enol and keto (2-pyridone) ions, remains unresolved : the enol ions and keto ions exhibit virtually the same dissociation characteristics.

Stable *m/z* 43 ions of structure CH_3O-B-H$^+$ and CH_3-B-OH$^+$ are generated by electron ionization of trimethylborate and methyl boronic acid respectively. NR experiments indicate that their neutral counterparts are also viable species in the gas phase. Theoretical calculations on this system show that unfavourable Franck-Condon factors govern the NR process of both systems and that fairly low lying dissociation channels are accessible to the incipient neutrals.

Dissociative electron ionization of rhodanine and 3-ethylrhodanine yields $[C,H,N,S_2]^{\bullet+}$ ions of the connectivity $HNCS_2$. The combined results of mass spectrometric experiments and CBS-QB3/Gaussian-2 based computations indicate that the initially generated cyclic ions H-N=$CS_2^{\bullet+}$ face a minimal energy barrier towards ring opening into iminothiosulfinic ions H-N≡C-S-$S^{\bullet+}$ which are thermodynamically more stable. In their neutral counterparts the stability order is reversed; the cyclic species, is now more stable, but the (singlet) neutral counterparts of both ions remain connected via a negligible barrier.

The CBS-QB3 method was also used to re-evaluate the heat of formation of CH_2=S=O. The recommended value now lies at -30 ± 6 kJ/mol.

The reactivities of ten of the thirteen isomeric ionized pentenyl methyl ethers are distinct, though sometimes subtly related. Metastable ionized pentenyl methyl ethers show an impressive array of reactions, of which elimination of $CH_3^{\bullet}$ or $C_2H_5^{\bullet}$ are of the greatest general importance, especially for allylic species. These reactions produce acyclic conjugated oxonium ions, usually by α-cleavage of an ionized allylic ether or by γ-cleavage of an ionized enol ether formed by a series of hydrogen shifts involving distonic ions. Skeletal rearrangements occasionally occur, at least some of which may be interpreted by mechanisms involving ionized alkylmethoxycyclopropanes. Methyl radical elimination sometimes proceeds by more than one route. Labelling experiments confirm that hydrogen shifts often precede alkyl radical loss, but these shifts rarely involve the hydrogens of the methoxy group. Loss of CH_3OH is also common, and may be formulated as a cycloreversion, although skeletal isomerization is necessary before it may occur from ionized allylic ethers without the required δ-hydrogen atom. This reaction is probably initiated by hydrogen transfer from the pentenyl chain to the oxygen atom. Other reactions of significance include elimination of H_2O or CH_2O. These processes are favoured for ionized non-allylic ethers and they may occur via related mechanisms involving ion-neutral complexes. It is possible that water loss begins with hydrogen transfer from the methoxy group to the pentenyl chain, followed by a second hydrogen transfer from the hydrocarbon chain to the oxygen atom.